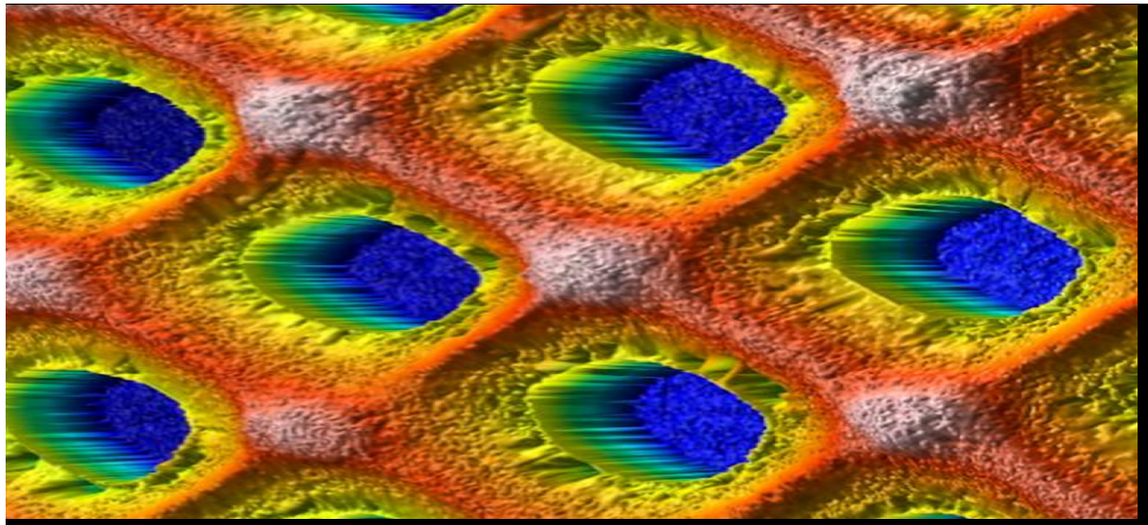

NanoBioCel

Nanocellulose-alginate-based bioinks for 3D bioprinting and osteochondral regeneration

Markel Lafuente Merchan

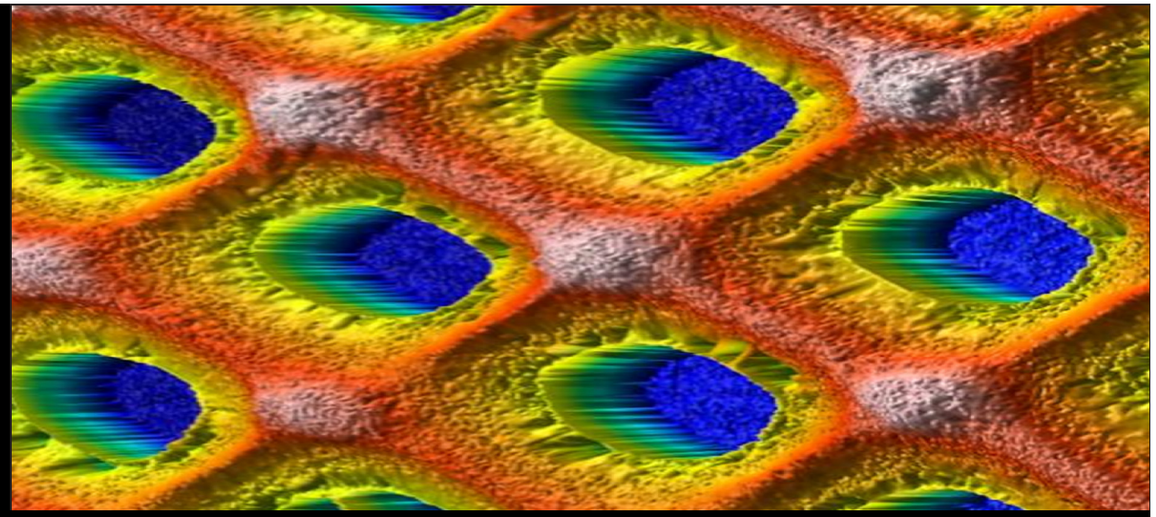

Nanocellulose-alginate-based bioinks for 3D bioprinting and osteochondral regeneration

Markel Lafuente Merchan

Vitoria-Gasteiz, 2023

eman ta zabal zazu

Universidad del País Vasco

Euskal Herriko Unibertsitatea

eman ta zabal zazu
Universidad del País Vasco
Euskal Herriko Unibertsitatea
NAZIOARTEKO BIKAINTASUN CAMPUSA
CAMPUS DE EXCELENCIA INTERNACIONAL

Nanocellulose-alginate-based bioinks for 3D bioprinting and osteochondral regeneration

Markel Lafuente Merchan

Vitoria-Gasteiz, 2023

NanoBioCel group
Laboratory of Pharmaceutics, School of Pharmacy
University of the Basque Country UPV/EHU

Acknowledgements for the financial support

This doctoral thesis has been supported by the Department of Education of the Basque Country Government (Consolidated Groups IT907-16); the Ministerio de Economía, Industria y Competitividad (FEDER funds, project RTC-2016-5451-1); the intellectual and technical assistance from the ICTS "NANBIOSIS", more specifically the Drug Formulation Unit (U10) of the Networking Research Centre of Bioengineering, Biomaterials and Nanomedicine (CIBER-BBN).

Acknowledgments to research groups

Authors would like to thank the Surface Technologies group at the University of Mondragon, Bioibérica S.A.U., the department of Human Anatomy and Embryology at the University of Granada, the Institute of Polymer Science and Technology at the ICTP-CSIC and the Organic Chemistry department at the University of the Basque Country, UPV-EHU for their contribution in this thesis.

Authors also acknowledge the Duffy Lab research group at the University of Galway for the intellectual and technical support to Markel Lafuente Merchan during his stay in their lab.

Acknowledgements to the editorials

Authors thank the editorials for granting permission to reuse the published articles. The published versions can be accessed at the following links:

Lafuente-Merchan M et al. Pharmaceutics. 2022, 14:15788. https://doi.org/10.3390/pharmaceutics14081578. (Appendix 1)

Lafuente-Merchan M et al. Mater. Sci. Eng. C, 2021, 126:112160. https://doi.org/10.1016/j.msec.2021.112160. (Appendix 2)

Lafuente-Merchan M et al. Macromol. Biosci. 2022, 22:2100435. https://doi.org/10.1002/mabi.202100435. (Appendix 3)

Lafuente-Merchan M et al. Macromol. Biosci. 2022, 11:2200236. https://doi.org/10.1002/mabi.202200236. (Appendix 4)

Agradecimientos

Y llego el final de la tesis y con ello el final de una etapa. Un final al que no hubiera llegado sin el apoyo ni ayuda de muchas personas.

Me gustaría empezar agradeciendo a todo el personal que comprende el grupo NanoBioCel y al departamento de Farmacia y Tecnología Farmacéutica. En especial a mis directores de tesis Jose Luis y Laura, por su ayuda, consejos y enseñanzas. Gracias por vuestra constante dedicación y por guiarme en todo momento. Quería extender el agradecimiento a Idoia por su ayuda y aportaciones durante las reuniones.

A mis compañer@s de laboratorio por esos momentos de desconexión en el café, las comidas y los planes fuera del laboratorio. En especial quería agradecer a las personas con las que he compartido más momentos tanto dentro como fuera del laboratorio. A Sandra, mi compañera de batallas, mil gracias por todo, sin duda esta tesis no hubiera sido lo mismo sin ti. Myriam gracias por tu apoyo incondicional y por estar ahí siempre que te he necesitado. A Tania por amenizar todos los experimentos interminables y por los momentos fuera del labo.

Quisiera extender mi agradecimiento a Bea por recibirme con los brazos abierto en los comienzos, a Kaoutar e Itsasne por todas las risas y a Fátima por su total predisposición a echarme una mano. A Susi por revolucionar y alegrar el laboratorio, a Matteo por los planes de finde y a Fouad y Jorge por el apoyo en los lab meetings. En general, gracias a tod@s!

No podían faltar aquí los de siempre. A Ander, Aingeru, Raquel, Koldo e Iris por esos findes de locura que te ayudan a desconectar de todo. Por qué se sigan repitiendo esas barbacoas, cenas y planes que siempre sientan bien.

Finalmente quería agradecer a mi familia. A mis padres, Mª Angeles y Enrique, por enseñarme que con esfuerzo y dedicación se pueden alcanzar tus objetivos. A Julen por su ejemplarizante ilusión en cumplir sus metas. Sin

vosotros esto no hubiera sido posible.

A Sergio, por ser de los pocos que ha vivido de cerca todo el proceso, por aconsejarme, aguantarme, seguirme y por celebrar conmigo los logros. Gracias de corazón.

Any sufficiently advanced technology is indistinguishable from magic

- Arthur C. Clarke -

Glossary

3D: three-dimensional
AB: alamar blue
ACI: autologous chondrocyte implantation
ACPC: articular cartilage progenitor cells
Alg: alginate
ALP: alkaline phosphatase
ASCs: adipose-derived stromal cells
ATR: attenuated total reflectance
BMSCs: bone marrow stem cells
CAD: computer-aided-design
cDNA: complementary deoxyribonucleic acid
CH: chitosan
COL: collagen
CPC: calcium phosphate cement
CS: chondroitin sulfate
dECM: decellularized extracellular matrix
DS: dermatan sulfate
DMEM: dulbecco´s modified wagle´s medium
DPBS: dulbecco's phosphate buffered saline
D1-MSCs: D1 mouse mesenchymal stem cells
D1-MSCs-EPO: D1 mouse mesenchymal stem cells to express erythropoietin hormone
ECM: extracellular matrix
EMA: european medicines agency
EPO: erythropoietin hormone
FBS: fetal bovine serum
FCS: fetal calf serum
FDA: food and drug administration
FDM: fused deposition modelling
FGN: fibrinogen
FT-IR: fourier transform infrared
GADPH: glyceraldehyde-3-phosphate dehydrogenase

GAGs: glycosaminoglycans
Gel: gelatin.
GelMA: gelatin methacrylate
GG: gellan gum
GO: graphene oxide
G': elastic modulus
G'': viscous modulus
HA: hyaluronic acid
HAMA: hyaluronic methacrylate
HAP: hydroxyapatite
hiPSCs: human-derived induced pluripotent stem cells
HPMC: hydroxypropyl-methylcellulose
LAP: laponite
MC: methylcellulose
mRNA: messenger ribonucleic acid
MSCs: mesenchymal stem cells
MTT: 3-(4,5-dimethylthiazol-2-yl)-2,5-diphenyltetrazoliumbromid
NC: nanofibrillated cellulose
NSAIDs: nonsteroidal anti-inflammatory drugs
OA: osteoarthritis
P/S: penicillin/streptomycin
PBS: phosphate buffered saline
PCL: polycaprolactone
PEG: polyethylene glycol
PEGDA: polyethylene glycol diacrylate
PLA: polylactic acid
PLGA: poly-lactic-co-glycolic acid
PRP: platelet-rich plasma
PTH: parathyroid hormone
PVA: polyvinyl alcohol
qRT-PCR: qualitative real-time polymerase chain reaction
SEM: scanning electron microscopy
SF: silk fibroin
SLA: stereolithography

SYSADOA: symptomatic slow-acting drugs in osteoarthritis
TE: tissue engineering
TCP: β-tricalcium phosphate
UV: ultraviolet
W/V: weight/volume

Index

Chapter 1

INTRODUCTION

1. State of the art

3D manufacturing techniques emerged in the earlies 80s when stereolithography (SLA), the first three-dimensional (3D) technology, was invented. SLA consisted in focusing a laser, mainly ultraviolet (UV) light, towards a bath composed of a photocurable material and sacrificial non-photocurable material. Thus, sacrificial material remained unchanged inside the bath while photocurable material became harder to create patterns [1]. The patterns formed a 3D structure which was similar to a computer-aided design (CAD). Hence, CAD software programs expanded to develop layered structures which were compatible not only with SLA, but also with the following 3D additive manufacturing techniques [1,2].

However, it was not until the following decade that the first 3D printing technology was invented [1,3]. It was based on fused deposition modelling (FDM) technology which consisted of extruding layer by layer a viscous semi-liquid material to create 3D objects according to CAD [1,3]. The extruded materials were termed inks and were principally based on amorphous thermoplastics. During the 2000s, this technology became popular and visible in the media since the first printed bladder was successfully implanted in one human [3]. Furthermore, these collagen-polyglycolic acid bladders printed by Athala et al. were functional after 5 years of implantation [4]. Later, the first functional leg prosthesis manufactured through 3D printing was patented [5]. This was a revolutionary advance in orthopaedics since the prosthesis was fabricated to real size and without the need for any later assembly.

The next decades brought the extinction of FDM patents, which resulted in the appearance of more accessible and cheaper prototypes [6]. Consequently, this manufacturing technology extended to diverse fields such as architecture, mechanics, engineering, food industry and biomedicine. It was there when bioprinting technology was invented. 3D bioprinters enable the addition of living cells or biological components into the ink which was renamed as bioink [2]. In the succeeding decades, 3D printing and bioprinting have been evolving and expanding. Bioprinting companies have been founded, more affor-

dable prototypes have been released and research based on bioprinting has been increased.

The history of the 3D manufacturing techniques is reflected in Fig. 1

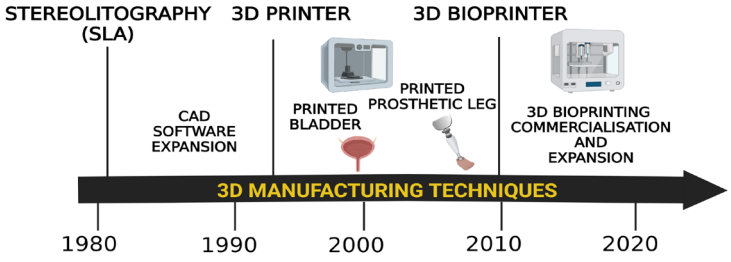

Figure 1. History of 3D manufacturing techniques.

Conventional manufacturing techniques have been displaced by 3D manufacturing techniques since they have the advantage of creating precisely structured objects. Thus, anatomically functional structures have successfully reached clinics. 3D printing, in particular, has proven to be a useful technology when it comes to fabricating diverse organs such as skin, liver, heart or kidney (Fig. 2) [7-13]. Furthermore, the United States Food and Drug Administration (FDA) has approved different 3D printed devices for clinical use, including dental objects, orthopaedic devices, restorative devices and patient-specific implants [13].

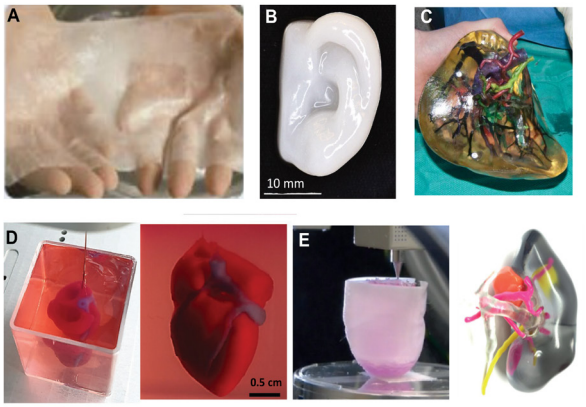

Figure 2. Examples of organs fabricated with 3D printing technique. A) Skin substitute [13]. B) Nanocellulose-alginate based human-scale ear [9]. C) Printed liver with hepatic vasculature using acrylic materials [11]. D) Small-scaled heart made of alginate, xanthan gum, gelatin and decellularized human omenta [12]. E) A kidney fabricated with photocurable materials [10].

On the other hand, after the 3D bioprinting emergence, it has been sought that the manufacturing structures not only would be anatomically functional, but also physiologically viable. However, due to high complexity, the fabrication of a viable organ from scratch is far to complete. However, in an initial state, 3D bioprinting has demonstrated to be an excellent tool to regenerate damaged tissues [2].

Furthermore, apart from its uses in organ fabrication and tissue engineering field, 3D bioprinting has proven to be a versatile technique (Fig. 3). In fact, it has been applied for drug screening, surgical approaches, personalised medicine, the fabrication of drug delivery systems and medical devices [14]

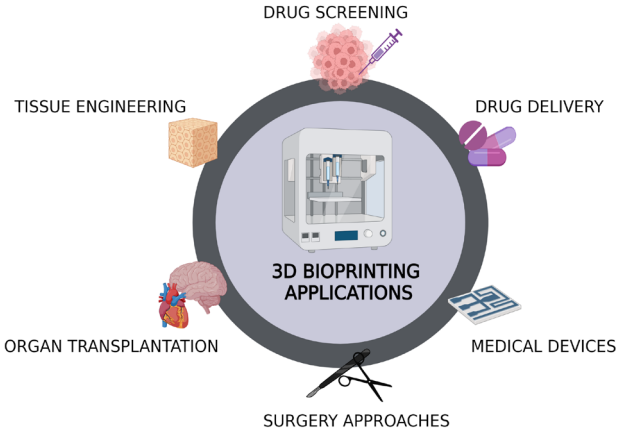

Figure 3. 3D bioprinting applications.

Focusing on the tissue engineering application, 3D bioprinting has gained popularity over other manufacturing techniques since it takes advantage of being a rapid prototyping, reproducible and automatic machine [15]. Furthermore, it accepts a wide range of materials and cells [15,16]. Depending on the method that bioink is extruded and deposited, three different 3D bioprinting types can be differentiated; extrusion-based, inkjet-based and laser-assisted bioprinting (Fig. 4).

Extrusion-based bioprinting consists of the continuous deposition of the bioink through a needle. Extrusion occurs via the application of pressure which can be either mechanical or pneumatic. As a result, the obtained 3D structures usually have high resolution. It is the most common bioprinting technique since it allows the use of high cell densities as well as very viscous materials [2,17]. Inkjet-based bioprinting is based on droplet deposition of the bioink after the application of an electrostatic or piezoelectric source [2,18]. It takes advantage of its simplicity and low costs, but it may be limiting when using highly viscous materials as well as high cell densities [2,18]. Finally, laser-assisted bioprinting is characterised by the application of a laser energy beam for the deposition of the bioink. Contrary to previous techniques, this bioprinting method does not expose the cells to shear stress which may damage them [2,17]. Nevertheless, it is highly expensive and it has limitations when using high cell densities as well as non-photocrosslinkable materials [2,17].

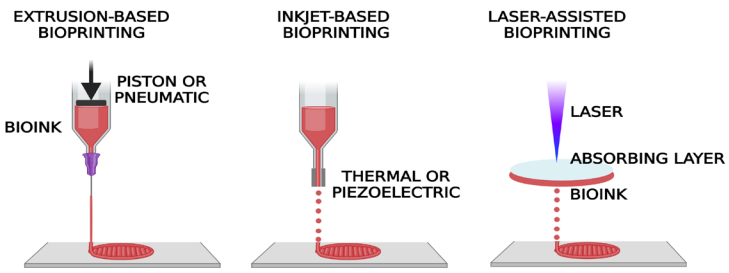

Figure 4. 3D bioprinting techniques: extrusion-based, inkjet-based and laser-assisted 3D bioprinting.

Regardless of the bioprinting technique, one of the main points for successful bioprinting is the bioink. In this regard, bioinks should present excellent mechanical and biological properties [15]. Mechanical properties are related to printability, which evidences the suitability of the bioink to manufacture 3D scaffolds. Moreover, these properties are connected with the stability of printed structures as well as with scaffold shape fidelity to CAD design [13]. Conversely, biological properties refer to being biocompatible and non-toxic. In addition, the bioink should support the adhesion, proliferation and maturation of living cells [13,16]. Since the 3D manufacturing techniques were inven-

ted, several polymer-based materials have been demonstrated to be desirable candidates to be considered as inks or bioinks (Fig. 5).

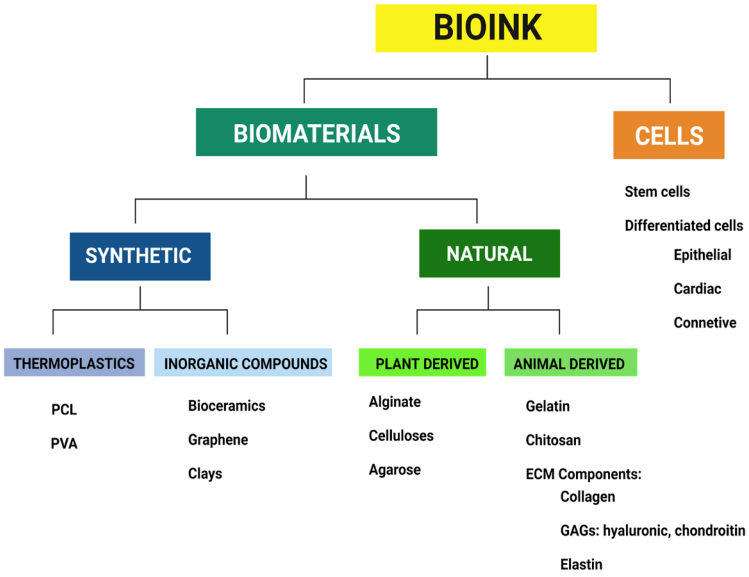

Figure 5. Bioink components. Cells and the most used biomaterials classification.
Acronyms; PCL: polycaprolactone, PVA: polyvinyl alcohol, ECM: extracellular matrix, GAG: glycosaminoglycans.

Synthetic biomaterials such as thermoplastics are the preferred option for 3D printing due to their ability to transform into an easily extrudable viscous liquid at high temperatures [19]. Among them, polycaprolactone (PCL), polyvinyl alcohol (PVA) and polylactic acid (PLA) have stood out since they are biocompatible and biodegradable [19].

With the appearance of 3D bioprinting, the biological component began to be included inside the ink to form the bioink. The biological component is composed of living cells that may be undifferentiated such as mesenchymal stem cells (MSCs) or differentiated cells such as epithelial, cardiac and connective cells [20]. In this regard, the use of natural biomaterials has been gaining ground over synthetic ones. In fact, natural biopolymers tend to form highly watered hydrogels which increase the viability of living cells and bioac-

tive molecules [21]. Furthermore, they are able to create gels after crosslinkers exposure which favours 3D construct fabrication [22]. An example of crosslinkable biopolymers are ion-sensitive such as alginate, thermosensitive such as gelatin, photosensitive such as hyaluronic methacrylate, pH-responsive such as chitosan or enzyme-sensitive such as fibrinogen [13,23].

Although natural polymers tend to enhance bioink biological properties, they are devoid of the great mechanical properties that synthetic materials display. Additionally, these properties can be further reduced by a key step such as sterilisation, since natural polymers tend to be more sensitive to physical and mechanical processes [24]. For instance, it is often challenging to use common sterilisation methods, including heat, radiation, filtration and chemicals, on bioinks. Thereby, their implications should be addressed on a case-by-case basis depending on the bioink components.

Taking into account that a good bioink aims to achieve a balance between mechanical and biological properties, alginate (Alg) has become one of the most widely used biomaterials. Its excellent biocompatibility together with its simple gelation procedure with divalent cations makes it ideal for 3D bioprinting [25,26]. Good mechanical properties are shown in Fig. 6A. Likewise, gelatin-based bioinks are also extensive due to their good mechanical properties as well as their exceptional support to the cells [27]. Another example of having balanced mechanical and biological properties is chitosan, which has been also used to form bioinks [28]. For instance, Fig. 6B shows excellent mechanical properties on the chitosan-based scaffold in terms of stability and elasticity.

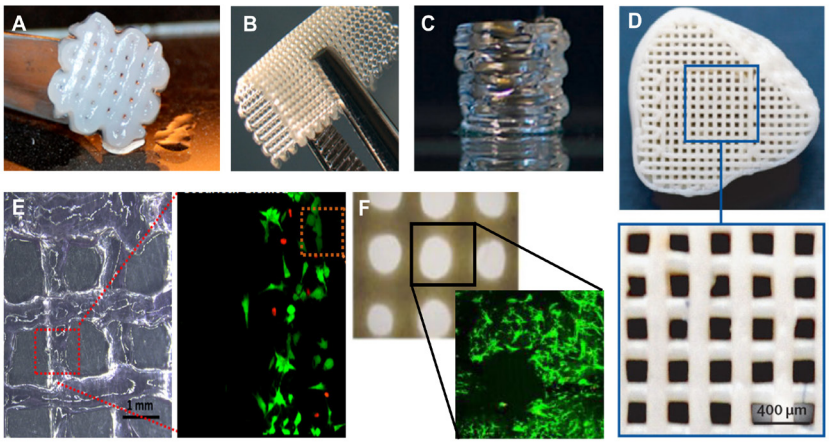

Figure 6. Examples of 3D bioprinted structures with diverse materials. A) Alginate-nanocellulose-human chondrocytes [9]. B) Chitosan scaffold showing good elasticity/stability [33]. C) Elastin-based scaffold for vessel reconstruction [33]. D) PCL-hydroxyapatite scaffold for bone repair [41]. E) Hyaluronic scaffold showing good biological properties [36]. F) Graphene-alginate scaffold showing excellent biocompatibility [40].

However, these plant or animal-derived polymers are not naturally found in human native tissues and taking into account that one of the main purposes of 3D bioprinting is biomimicry, extracellular matrix (ECM) components-based bioinks have been proposed [29]. Thus, hyaluronic acid (HA) and collagen have been gaining notoriety since they are found in almost all connective tissues and they have demonstrated excellent biological properties [29,30]. Similar to HA, other glycosaminoglycans (GAGs) such as chondroitin sulfate (CS) and dermatan sulfate (DS) have shown to be an excellent choice to fabricate more tissue-specific scaffolds such as cartilage, since they are components that are naturally found in the cartilage ECM [31,32]. In this regard, fibrin and elastin may be also considered tissue-specific biomaterials. In fact, elastin has been used to develop bioprinted blood vessels (Fig. 6C) since arteries are rich in this protein [33,34].

One of the main disadvantages of ECM-based bioinks is that they fail in having adequate mechanical properties in terms of viscosity (poor) and ge-

lation kinetics (slow) [35]. Therefore, in order to increase these properties, they have been chemically modified to make them photocrosslinkable by UV. In this sense, HA methacrylate or collagen methacrylate have been used as bioinks obtaining interesting results [29]. As Fig 6E shows, HA methacrylate scaffolds presented good printability together with biocompatibility since embedded cells demonstrated high cell viability together with elongated shape [36]. Despite this approach, bioinks composed of different biomaterials have been shown to be more successful. Thus, the lack of mechanical properties of ECM-based bioinks has been supplied by adding Alg or gelatin [29,35,37]. Furthermore, to extol even more the mechanical properties, cellulose derivatives such as nanocellulose (NC) or methylcellulose have been also applied in bioink development [38,39]. An example of this bioink combination is shown in Fig. 6A, in which scaffolds were made with Alg-NC to support human chondrocytes [9].

Another important factor when selecting the biomaterials that integrate the bioink is the target tissue. The aforementioned natural biomaterial-based bioinks are useful for soft tissues, but they fail in obtaining the intrinsic biomechanics of much harder tissues such as bone [35]. Consequently, apart from adding the synthetic material PCL, it has been proposed the addition of inorganic elements. One of the most widely used materials are bioceramics. Among them, hydroxyapatite (HAP) has gained notoriety since it is the main component of native bones. It has been usually applied in combination with natural biomaterials or, as shown in Fig. 6D, in combination with PCL to improve not only the printability, but also the biological properties such as osteoinduction [41]. In addition, bioglasses or multifunctional components such as graphene oxide (GO) have also been utilised [40,42,43]. GO, apart from its exceptional physicochemical and mechanical properties, has shown to be biocompatible when it was added at low concentrations to Alg bioinks [40] (Fig. 6F).

3D bioprinting has been applied to develop diverse tissues, from skin, bone, and cartilage to apparently more complex ones such as cornea, pancreas or circulatory system [44]. This technology has the advantage of ma-

nufacturing structures with different sizes, geometrics and porosity which may be very useful to treat patient-specific bone defects [45]. Likewise, its ability to deposit bioinks with precise spatial control may be very beneficial to mimic the compositional and structural heterogeneity of tissues such as cartilage.

In fact, osteochondral injuries are very common in the overall population due to the increase in risk factors such as obesity, age and intense sport practising [46]. Furthermore, osteochondral injury can lead to most serious diseases such as osteoarthritis (OA) which is characterised by joint pain, inflammation, stiffness and dysfunction [46]. OA pathology and symptomatology are shown in Fig 7. Despite the seriousness together with the high prevalence of the disease, current pharmacological treatments become ineffective over time and the surgical approach has its limitations in terms of high bone and cartilage graft demand [47,48]. In this regard, 3D bioprinting provides a potential solution since bone and cartilage grafts could be supplied with 3D bioprinted constructs.

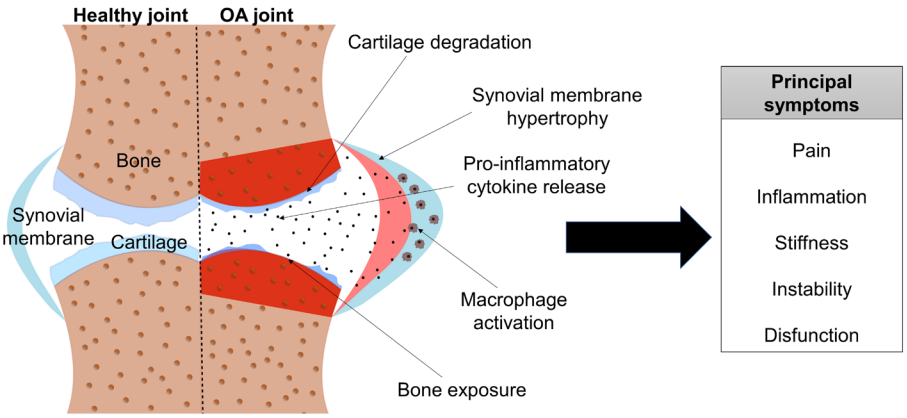

Figure 7. OA disease. Pathology and symptoms.

In conclusion, 3D bioprinting has emerged to be an effective scaffolding tool for the fields of tissue engineering and regenerative medicine. The importance of bioink composition is essential because it has to be not only printable to make highly precise structures in a previously designed manner, but also compatible with the embedded living cells as well as with the implantation tissues. Consequently, scaffolds may fabricate to be very similar to native tissues

which could represent a great therapeutic advance in diseases such as OA.

2. Methodology

The methodology of this thesis was divided into different phases called pre-bioprinting, bioprinting and post-bioprinting. As shown in Fig. 8, the pre-bioprinting phase was focused on bioink development and characterisation. Then, the bioprinting phase entailed designing the scaffold and establishing the bioprinting process. Finally, the post-bioprinting phase encompassed the characterisation of the bioprinted scaffold as well as the evaluation of embedded cells.

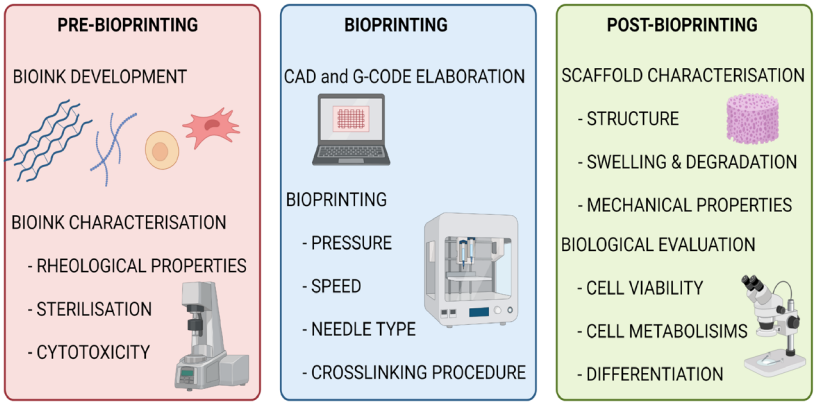

Figure 8. The bioprinting methodology is divided into phases: pre-bioprinting, bioprinting and post-bioprinting.

2.1 Pre-bioprinting phase

In the pre-bioprinting phase, the biomaterials, as well as cells type, were selected. In this sense, Alg was the chosen biomaterial to be a component of the bioink since it forms viscous hydrogels with an easy crosslinking process with divalent ions such as calcium [25]. Moreover, it has been widely applied for different applications such as drug delivery, cell encapsulation and cell therapy due to its excellent biocompatibility and non-toxic properties [49,50]. However, the former hydrogel had not the adequate rheological properties to manufacture high-precision scaffolds through bioprinting. Therefore, NC was added as a rheological modifier. Furthermore, NC is biocompatible as well

as biodegradable and it has also been applied in diverse biomedical fields [51,52].

After obtaining the NC-Alg base bioink, different elements were added. First, in order to enhance the biological properties of the base bioink, HA was added to form the hyaluronic bioink. HA was reported to be biodegradable as well as biocompatible [23]. It has been shown to enhance cell adhesion, proliferation and growth [30][53]. Consequently, it has been used in different fields such as cell therapy, drug delivery and 3D bioprinting [30,54].

Then, CS and DS were separately added to NC-Alg bioink to develop the cartilage bioinks due to the fact that they can be naturally found in the cartilage ECM. They have got high stability together with low immunogenicity in comparison with other ECM components [55]. CS promotes cell differentiation and regulates cartilage metabolism. Furthermore, CS has been used as a treatment for chondral diseases such as OA due to its therapeutic properties [56]. Hence, it has been used to fabricate hydrogels for tissue engineering [57] as well as to develop bioinks in combination with chitosan [32]. On the other side, DS has been poorly studied as a bioink component. However, DS has been shown to modulate chondrogenesis, promote the differentiation of MSCs and improve the maturation of cartilage cells [58].

Finally, bone bioinks were fabricated by adding separately HAP and GO into NC-Alg bioink. HAP is the main component of bone tissue. It has been widely applied in the tissue engineering field to create structures for bone regeneration. In addition, its use in 3D printing in combination with thermoplastics has shown to be osteoinductive and bioactive [41]. In 3D bioprinting, it has been combined with Alg or collagen to improve scaffold porosity as well as mechanical properties [59]. Likewise, GO has been applied as a bioink component in combination with Alg or gelatin [40,60]. GO has been shown to enhance scaffold mechanical properties. Furthermore, it has been reported to improve the proliferation and osteogenic differentiation ability of MSCs [60,61].

Once the biomaterials that form the bioinks were selected, cell inclusion

had to be carried out. However, prior to biological component addition, some vitally important bioink characteristics had to be addressed such as rheology, cytotoxicity and sterilisation process.

2.1.1 Rheological characterisation

Rheology is a part of mechanics that studies the deformation and flow of matter. Rheological properties are of key importance since they are related to bioink printability and scaffold fabrication. In this thesis, rheological properties were evaluated on the AR100 TA rheometer by performing two different measurements; steady flow and oscillatory shear measurements.

In the first assay, the flow behaviour of all bioinks was evaluated by performing shear rate sweeps from 0.1 to 100 s^{-1} and *vice versa*. The flow behaviour curve permitted us to know whether the bioinks are printable or not, since the viscosity of bioinks must decrease under stress as it occurs in the bioprinting process to pass through the needle. This flow behaviour is known as shear-thinning. In addition, when the stress is finished after bioprinting, the bioinks must recover their viscosity to achieve scaffolds with high structural fidelity. This property is considered thixotropy.

On the other side, oscillatory shear measurements offered to know the bioink viscoelasticity properties in terms of elastic modulus (G') and viscous modulus (G''). For a good bioprinting procedure, the bioinks must present high enough viscoelasticity values to prevent the bioink from leaking out of the bioprinting needle. In addition, these properties are related to cell protection against bioprinting pressures. From the G''/G' relation, Tan δ values were calculated that are related to bioprinting filament form and bioprinting pressures to apply.

2.1.2 Sterilisation

Before cell incorporation into the bioinks, pathogen elimination must be ensured. Among the most common sterilisation techniques, filtration, UV ra-

diation and ethylene oxide sterilisation were discarded due to incompatibilities, low sterilisation ability with UV and safety issues in the case of ethylene oxide [24]. Consequently, short and long-cycle autoclave, β-radiation and γ-radiation techniques were selected to sterilise the NC-Alg and NC-Alg-HA bioinks.

An autoclave is a technique that uses high pressures and temperatures to eliminate microorganisms. The sterilisation process in a long-cycle autoclave occurred at 121 ºC temperature and 2 bar pressure for 30 min. However, glycoproteins and polysaccharides such as Alg and HA could be affected by high temperatures. Thus, a short-cycle autoclave was tested in which the sterilisation process was set at 3.60-3.70 bar pressure and 123-124 ºC temperature for 3.04 min.

As an alternative to avoid high temperatures, ionising radiations were explored. Although both, β-radiation and γ-radiation sterilisations are based on the disruption of the DNA of microorganisms, they differ in penetration ability. β-radiation is less penetrant, therefore, NC-Alg and NC-Alg-HA bioinks were irradiated twice to guarantee a homogeneous dose of 25 kGy in a Rhodotron TT200 following the ISO 11137 standards [62]. On the other side, γ-radiation sterilisation was performed in a Mark I–30137Cs irradiator applying the required total dose of 25 kGy.

After the sterilisation, NC-Alg and NC-Alg-HA bioink were characterised by rheology.

Cartilage and bone bioinks were sterilised using the short-cycle autoclave method and, after that, they were evaluated by rheology. NC-Alg-GO bioink was further evaluated after sterilisation.

2.1.3 FT-IR study of graphene bioink

NC-Alg-GO bioink was analysed with a Fourier Transform Infrared (FT-IR) technique to determine the chemical functional groups inside the bioink after autoclave sterilisation. The spectra were acquired with a Nicolet iS10 spectrometer applying an attenuated total reflectance (ATR) technique. The results

were in the range of 4000-500 cm^{-1} with a resolution of 4 cm^{-1} and 32 scans. The study was performed at room temperature.

2.1.4 Cytotoxicity assay

The potential cytotoxicity effect of all sterilised bioinks was assayed using mouse L929 fibroblasts following the ISO 10993-5-2009 standards [63]. Three different assays were conducted: adhesion, indirect contact and direct contact assays.

With the adhesion assay, the ability of the cells to adhere to the bioinks was measured by seeding them directly onto the bioinks. In the indirect contact assay, the bioinks were kept in culture media to evaluate any possible cytotoxic product release in the culture media. Afterwards, the obtained conditionate media was used to culture the cells. On the other hand, in the direct contact assay, the bioinks were directly put in contact with previously seeded cells to analyse any cytotoxic effect.

In all the assays, 3-(4,5-dimethylthiazol-2-yl)-2,5-diphenyltetrazoliumbromid (MTT) *in vitro* toxicology assay was used to measure cell metabolic activity as an indicator of cell cytotoxicity, viability and proliferation. The absorbance at 570 nm with a reference wavelength set at 650 nm was read in an infinitive M200 microplate reader. Cell viability was calculated by applying the following equation (1):

$$\text{Cell viability (\%)} = \frac{\text{Testing sample OD570}}{\text{Untreated blank OD570}} \times 100 \qquad (1)$$

Six independent samples were evaluated with three replicates per study. Cell viability above 70% was considered non-toxic.

2.1.5 D1-MSCs culture and cell-laden bioinks fabrication

After bioink characterisation, sterilisation evaluation and cytotoxicity measurement, cells to include inside the bioink were selected.

Murine D1-MSCs from ATCC® were used to fabricate the bioinks since they have the ability to differentiate into different cell types such as chondrocytes and osteoblasts [64]. Furthermore, MSCs have the potential to secrete anti-inflammatory and immunomodulatory molecules for which they have been used as cell therapy in OA disease [65]. D1-MSCs were cultured in T-flasks in a complete culture media at 37 ºC and in a humidified atmosphere containing 5% CO_2.

In the first experimental work, three different cell densities were proposed to fabricate NC-Alg and NC-Alg-HA bioinks; 1 x 10^6, 2.5 x 10^6 and 5 x 10^6 cells/mL.

The same cell type was used for the second experimental research paper focused on cartilage bioinks (NC-Alg-CS and NC-Alg-DS). However, D1-MSCs genetically engineered to secrete the erythropoietin hormone (D1-MSCs-EPO) were also used for a deeper study of the bioinks biological properties. For this study, the cell density was set at 5 x 10^6 cells/mL.

In the third experimental work, bone bioinks (NC-Alg-HAP and NC-Alg-GO) were studied. Similar to cartilage bioinks, D1-MSCs, as well as D1-MSCs-EPO at 5 x 10^6 cells/mL were embedded to fabricate the bioinks.

All the bioink composition is summarised in Table 1.

Table 1. Developed bioink types and their components

BIOINK	BIOMATERIALS % (w/v)	CELLS
Base bioink	NC: Alg 2% (80:20)	1 x 10^6 D1-MSCs /mL
		2.5 x 10^6 D1-MSCs/mL
		5 x 10^6 D1-MSCs /mL
Hyaluronic bioink	NC: Alg 2%, HA 1% (80:20)	1 x 10^6 D1-MSCs /mL
		2.5 x 10^6 D1-MSCs /mL
		5 x 10^6 D1-MSCs /mL
Cartilage bioinks	NC: Alg 2%, CS 5% (80:20)	5 x 10^6 D1-MSCs-(EPO)/mL
	NC: Alg 2%, DS 5% (80:20)	
Bone bioinks	NC: Alg 2%, HAP 1% (80:20)	5 x 10^6 D1-MSCs-(EPO)/mL
	NC: Alg 2%, GO 50 µg/mL (80:20)	

Acronyms: NC: nanocellulose; Alg: alginate; HA: hyaluronic acid; CS: chondroitin sulfate; DS: dermatan sulfate; HAP: hydroxyapatite; GO: graphene oxide; MSCs: mesenchymal stem cells; EPO: erythropoietin.

2.2 3D bioprinting phase

A pneumatic extrusion-based bioprinter Bio X from Cellink® was used to manufacture all the scaffolds. Extrusion-based bioprinting was selected since it accepts a wide range of cells together with highly viscous materials such as our bioinks. Before bioprinting, CAD was created using the AutoCAD® software and the G-code of the design was generated and revised to avoid any unwanted movement of the bioprinter. To evaluate scaffold characteristics in

terms of printability, internal and external structure, swelling, degradation and mechanical properties acellular scaffolds were bioprinted. Conversely, cells containing bioinks were used to analyse biological properties such as embedded cells' viability, functionality or differentiation ability.

2.2.1 Acellular 3D bioprinting

For all the bioink types, circular grid-like scaffolds with a diameter of 15 mm and 4 layers were designed and bioprinted.

In the first experimental work, to make NC-Alg constructs, bioprinting parameters were set to 20-22 kPa extrusion pressure and 4 mm/s speed. On the other hand, NC-Alg-HA bioink required an extrusion pressure of 24-26 kPa and 4 mm/s bioprinting speed. Both types of scaffolds were bioprinted through a 27 G conical needle.

In the second experimental work, cartilage scaffolds were manufactured. In this case, for both, NC-Alg-CS and NC-Alg-DS bioinks, the same bioprinting parameters of 25-30 kPa pressure and 4-5 mm/s speed were established using a 27 G conical needle.

Finally, bone bioinks NC-Alg-HAP and NC-Alg-GO were created. NC-Alg-HAP constructs were fabricated using a 22 G conical needle and by applying 15-18 kPa extrusion pressure and 4-5 mm/s bioprinting speed. In contrast, NC-Alg-GO bioink was extruded through a 27 G conical needle with 22-25 kPa pressure and 4-5 mm/s speed.

Bioprinting conditions are summarised in Table 2.

Table 2. 3D bioprinting conditions for each bioink

BIOINK		PRESSURE (kPa)	SPEED (mm/s)	NEEDLE TYPE
Base bioink		20-22	4-5	27 G conical
Hyaluronic bioink		24-26	4-5	27 G conical
Cartilage bioinks		25-30	4-5	27 G conical
Bone bioinks	NC-Alg-HAP	15-18	4-5	22 G conical
	NC-Alg-GO	22-25	4-5	27 G conical

Acronyms: NC: nanocellulose; Alg: alginate; HAP: hydroxyapatite; GO: graphene oxide.

All bioprinted scaffolds were crosslinked by submerging them in a 100 mM calcium chloride solution for 5 min. The entire bioprinting procedure was performed at room temperature.

2.2.2 3D bioprinting with cells

NC-Alg and NC-Alg-HA scaffold fabrication was conducted following the same design and bioprinting parameters as acellular bioprinting.

For the case of cartilage and bone scaffold manufacturing, the CAD was modified to facilitate the cell differentiation assays. Thus, the layers of 15 mm diameter circular grid-like constructs were reduced from 4 to 2. The same bioprinting parameters as acellular bioprinting were maintained.

In all the cases, the entire bioprinting procedure was performed in aseptic conditions and after crosslinking, all the scaffolds were placed in a complete media for their culture.

2.3 Post-bioprinting phase

2.3.1 Acellular scaffold characterisation

2.3.1.1 Structure and surface

After bioprinting, the scaffolds' external and internal structure and architecture were characterised.

First, macroscopic appearance was evaluated by observing them under a Nikon AZ100 microscope. Captured pictures were used to determine the bioinks printability by comparing them with the CAD.

Then, the internal structure was characterised with a Scanning Electron Microscope (SEM). It was wanted to examine the porosity of the scaffold which is important for good cell viability and proliferation inside the scaffolds. Two SEM types were utilised to avoid any structure change after drying the scaffolds by freeze-drying. Thus, the Hitachi S-3400 SEM was used to observe dried and gold-coated scaffolds and Hitachi TM-4000 Cryo-SEM to analyse hydrated scaffolds.

Finally, the optical profilometry technique was used to characterised all the scaffolds. This technique is used to extract topographical data from the scaffold's surface by performing full 3D scans. An optical profilometer from Sensofar S-NEOX through a focus variation method was conducted by acquiring 3 different areas of the scaffolds. 3D topographical images were obtained and the Sdr parameter which measured the uniformity of the surface texture was calculated. All the measurements were post-process with the metrological software SensoMAP Premium 7.4.

2.3.1.2 Swelling and degradation

The swelling behaviour was studied since it is related to nutrient diffusion to the cells inside the scaffold. The swelling study was carried out with freeze-

dried scaffolds that were submerged in Dulbecco´s phosphate-buffered saline (DPBS) with calcium and magnesium at 37 ºC to determine their water uptake capacity. The swelling % was calculated by weighting them at different time points and applying the following equation (2).

$$\text{Swelling (\%)} = \frac{W_{wet} - W_{dried}}{W_{dried}} \times 100 \qquad (2)$$

Where W_{wet} and W_{dried} are wet and dried weight, respectively.

The degradation study was performed to evaluate its implication on the scaffold stability *in vivo* as well as on the cell behaviour. It was conducted by placing the scaffolds in culture media at 37 ºC and by measuring the scaffold's area at different time points. The area loss in % was calculated by using the following equation (3):

$$\text{Area loss (\%)} = \frac{A_{before} - A_{after}}{A_{before}} \times 100 \qquad (3)$$

Where A_{before} and A_{after} correspond to the scaffold area before placing itin DMEM and after passing the selected time in DMEM.

2.3.1.3 Mechanical properties

Cartilage and bone scaffolds required the evaluation of their mechanical properties because both tissues are subjected to high compression and torsion forces. The study was performed by a TA.XT.plusC Texture Analyser in a compression test form. From the slope of the stress/strain curve, the compression Young´s modulus was computed, which is an intrinsic material property related to the material´s stiffness and elasticity.

2.3.2 Biological evaluation

2.3.2.1 Cell viability, metabolism and functionality

Cell viability of embedded D1-MSCs was qualitatively analysed with the

Live/Dead™ Viability/Cytotoxicity kit at 21 days after bioprinting. Cell status was tracked by staining the viable cells in green and the damaged cells in red. Images were captured in an inverted Nikon TMS microscope with an accessory for fluorescence observation.

Cell metabolic activity of the cells inside the scaffolds was assayed on days 1,7,14 and 21 after bioprinting using the AlamarBlue® reagent as an indirect indicator of cell viability and proliferation. Fluorescence was read in a Tecan Trading AG Infinitive M200 microplate reader establishing an excitation wavelength of 560 nm and an emission wavelength of 590 nm.

Finally, cell functionality was evaluated in cartilage (NC-Alg-CS and NC-Alg-DS) and bone (NC-Alg-HAP and NC-Alg-GO) scaffolds by assaying the EPO secretion of embedded D1-MSCs-EPO. A Quantikine IVD Human EPO ELISA Kit was used to quantify the EPO secretion of supernatants on days 1, 7,14 and 21 after bioprinting.

2.3.2.2 Cartilage differentiation

D1-MSCs embedded in NC-Alg-CS and NC-Alg-DS scaffolds were differentiated into chondrocytes. Cells inside NC-Alg scaffolds were used as controls. The chondrogenic differentiation was conducted by culturing the bioprinted scaffolds in a chondrogenic differentiation medium for 21 days. Afterwards, Alcian blue and Safranin-O stainings were used to observe GAGs and collagen depositions, respectively, which are naturally produced by the chondrocytes in the cartilage tissue. Pictures were captured in a Nikon AZ100 microscope. Next, the total collagen production by chondrocytes was computed by the hydroxyproline assay kit on days 1 and 21 of culture. The absorbance was measured at 550 nm. Finally, a qualitative real-time PCR (qRT-PCR) assay was used to determine the expression of chondrogenic gene markers such as *SOX9*, *ACAN*, *COL1* and *COL2*. The assay was performed by disaggregating the scaffolds, extracting the RNA from cells and converting it into cDNA. Glyceraldehyde-3-phosphate dehydrogenase (*GAPDH*) was used as a housekeeping gene. Gene expression was normalized to *GAPDH* and undifferentiated nega-

tive controls. Relative expression was calculated with the $2^{-\Delta\Delta CT}$ method.

2.3.2.2 Bone differentiation

NC-Alg-HAP and NC-Alg-GO scaffolds were cultured in an osteogenic culture medium to promote osteogenic differentiation of embedded D1-MSCs for 21 days. NC-Alg bioprinted scaffolds were used as controls. First, the mineralization capacity of embedded cells was evaluated by utilising the Alizarin Red S stain, which marks calcium deposits. Then, alkaline phosphatase (ALP) enzyme activity which is naturally released by osteoblasts, was quantified on days 1 and 21 of the osteogenic culture. The Alkaline Phosphatase Assay Kit (fluorometric) was applied and fluorescence was read at an excitation wavelength of 360 nm and an emission wavelength of 440 nm. Finally, the osteogenic gene expression was determined by quantifying osteogenic markers *RUNX2*, *ALP*, osteocalcin (*OSTC*) and osteopontin (*SPP1*). The qRT-PCR technique was applied following the same procedure as the aforementioned chondrogenic differentiation. Gene expression was normalized to housekeeping gene *GAPDH* and undifferentiated negative controls. Relative expression was calculated with the $2^{-\Delta\Delta CT}$ method.

2.4 Statistics

The experimental results were statistically analysed with IBM® SPSS® software. Normal distribution was assessed by the Shapiro-Wilk test. Student´s test was applied to determine significant differences between the two groups, whereas ANOVA was used to evaluate multiple groups. Lavene test of homogeneity of variances was utilised to apply the Tamhane post-hoc or Bonferroni tests. Nonparametric data were assessed with the Mann-Whitney test. Significant differences were considered when $p < 0.05$.

3. Hypothesis and objectives

3D bioprinting has emerged to become a feasible tool for scaffold manufacturing purposes since it is automatic, reproducible and enables the fabrication of patient-specific structures. However, the technology is in its infancy and the development of proper bioinks is still challenging. An adequate bioink should possess a balance between mechanical and biological properties to not only be printable, but also to support the embedded cells.

Taking into account these goals, Alg has proven to fulfil both purposes in its extensive use in the field of tissue engineering. However, as bioink component requires an improvement in its rheological properties, NC is added. NC-Alg blend has been shown to allow the fabrication of good shape fidelity structures through 3D bioprinting. Moreover, as the final objective of these scaffolds is to regenerate native tissues, their biological properties must be enhanced. In this regard, HA, which is naturally found in almost all the connective tissues, is added to achieve this goal.

A further step is to target the bioprinted scaffolds to regenerate specific tissues such as cartilage or bone. In fact, osteochondral defects and injuries are common among the population and may lead to very prevalent diseases such as OA which may be really limiting and has no effective treatment. For this purpose, cartilage ECM-specific components, such as CS and DS, would be a good option to add to the NC-Alg bioink. On the other hand, bone regeneration may be facilitated due to the addition of HAP, which is abundant in native bones, or GO that has shown to be a compound with diverse functionalities.

Taking into account this information, the objectives of this thesis were as below:

1. To understand osteochondral tissue and defects as well as to evaluate the advantages of bioprinting technique for OA disease. (Appendix 1).

2. To develop NC and Alg-based bioink and evaluate its suitability for being processed through 3D bioprinting which would allow us to manufacture scaffolds to support cells. (Appendix 2).

3. To include HA into the NC-Alg-based bioink and evaluate its effects on the rheological properties as well as on printability to make scaffolds. To assess the biological impact of adding HA on bioprinted scaffolds containing D1-MSCs cells. (Appendix 2).

4. To add cartilage ECM components, such as CS or DS, to the NC-Alg bioink with the objective of manufacturing cartilage-like scaffolds to regenerate chondral injuries. (Appendix 3).

4.1. To study the impact of adding CS and DS on bioink properties and printability as well as the scaffolds properties trough 3D bioprinting.

4.2. To evaluate the biological properties of bioprinted scaffolds after adding CS and DS and analyse their ability to induce embedded cells to differentiate into cartilage.

5. To add HAP and GO to the NC-Alg bioink in order to fabricate bone-like scaffolds trough 3D bioprinting to regenerate bone injuries. (Appendix 4).

5.1. To study the impact of adding HAP and GO on bioink properties and printability as well as the scaffolds properties.

5.2. To evaluate the biological properties of bioprinted scaffolds after adding HAP and GO and analyse the osteogenic differentiation ability of the embedded cells.

4. Results and discussion

4.1. Pre-bioprinting evaluation

Once the bioinks were fabricated, it was essential to demonstrate excellent mechanical properties, specifically the rheological ones which are related to bioinks printability, scaffold fabrication and embedded cell viability [66].

4.1.1 Rheological characterisation

First, the rheological behaviour of the NC-Alg bioink was evaluated. Steady flow measurement results in Fig. 9A showed that the NC-Alg bioink behaved as a shear-thinning fluid since viscosity decreased under stress. This suggested that the base bioink would be properly extruded considering that it has to reduce its viscosity to pass under pressure through the bioprinter needle. In addition, when stress finished the NC-Alg bioink viscosity returned to initial values showing a thixotropic behaviour. Therefore, after extrusion, the bioink would recover its viscosity and the bioprinted scaffold pattern would be precise. These results were in accordance with the literature in which a shear-thinning behaviour was achieved after adding NC to an Alg bioink [9,67]. In addition, these authors suggested that this rheological behaviour was dominated by the NC since plain Alg bioinks showed poor viscosity together with a Newtonian flow behaviour. Thus, the obtained scaffolds showed a bad shape fidelity [9,67].

On the other hand, viscoelasticity properties in terms of elastic modulus (G') and viscous modulus (G'') were analysed (Fig. 9B). Results showed that the NC-Alg bioink had an elastic solid-like behaviour since G' was higher than G''. Bioinks with viscoelasticity values higher than 5000 Pa showed embedded cell viability damage due to the fact that they needed high printing pressures to be extruded [68]. Moreover, very high G' values are related to dense gel-like bioinks in which cell proliferation and migration is difficulted. The NC-Alg bioink reached the 3000 Pa G' value which, according to the literature, is sufficient to hold the cells in place as well as to allow them to proliferate and

migrate [69]. Consequently, taking into account the viscoelasticity study, it was expected to apply no harmful printing pressures to the cells when manufacturing NC-Alg scaffolds.

Interestingly, Tan δ was calculated with the G''/G' relation. According to the literature, Tan δ values around 1 indicate that bioinks extrude uniformly and require low extrusion pressures, however, printed scaffolds exhibit low shape fidelity. Conversely, Tan δ values close to 0 suggest that bioinks are robust, but extrusion is uneven and requires higher bioprinting pressures [70]. As shown in Fig. 9C, the NC-Alg bioink exhibited a Tan δ value of 0.37 ± 0.06 which has been proved to be optimal to fabricate scaffolds with a uniform extrusion and good shape fidelity as well as high cell viability [70].

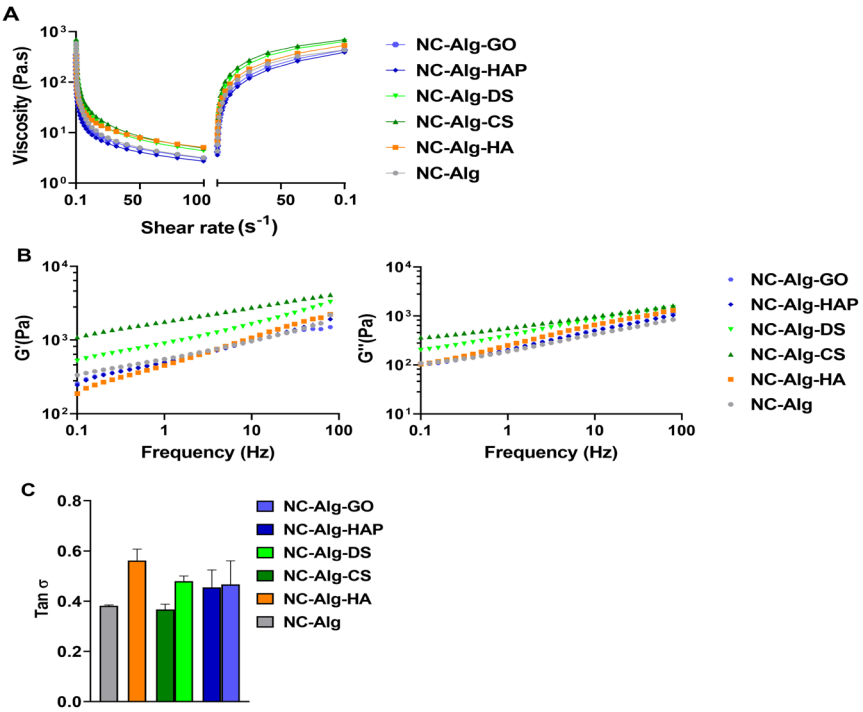

Figure 9. Rheological measurement of all the bioinks. A) Steady flow behaviour evaluation. B) Analysis of viscoelastic properties. C) Tan δ quantification.

After concluding that the NC-Alg bioink had excellent rheological properties to fabricate scaffolds through extrusion bioprinting, the other components were added and their effect on rheological properties was evaluated. In general, despite the fact that different elements such as HA, CS, DS, HAP and GO were separately added, all the bioinks demonstrated the same rheological behaviour as the NC-Alg bioink Fig. 9A-B. In fact, all of them showed a shear-thinning, thixotropic as well as elastic solid-like behaviour which would suggest good printability. However, slight differences among them were observed.

The NC-Alg-HA bioink showed an increase in viscosity values together with an improvement of the viscous modulus G" in comparison with the NC-Alg bioink. This rheological enhancement due to the HA has been previously reported in studies that blended HA with diverse biomaterials such as gelatin or alginate [71,72].

Similarly, both cartilage bioinks demonstrated much higher rheological properties than the NC-Alg bioink, being the NC-Alg-CS bioink the one in which the increase was higher. Similar rheological behaviour has been shown in other studies that have combined CS with gelatin or HA [73]. The use of DS as bioink has been little studied and there was not any research to compare the obtained rheological improvement. However, similar rheological behaviour can be assumed with the NC-Alg-DS bioink compared to the NC-Alg-CS bioink due to their close chemical composition. In fact, both are GAGs which have naturally excellent viscoelastic properties to support the joints since they protect the chondral tissue from mechanical damage together with providing it with good lubrication [74,75].

These results indicated that the printing fidelity would be enhanced since the formation of the extrusion filament would be better on the NC-Alg-HA, NC-Alg-CS and NC-Alg-DS bioinks than on the NC-Alg bioink with lower rheological properties [16]. On the other hand, as Fig. 9A-B shows, bone bioinks showed no rheological differences after the addition of HAP and GO to the NC-Alg bioink. It was expected due to the fact that these inorganic components are

not known as rheological modifiers.

Despite these differences, the G' values were adequate in all the bioinks to permit good cell migration and proliferation. Moreover, as shown in Fig. 9C, the Tan δ parameter values of all the bioinks were between the optimal values of 0.3-0.6 which suggested that the printing pressures would be soft for cell survival and the scaffolds would be manufactured with good shape fidelity.

4.1.2 Sterilisation evaluation

Once the bioinks were characterised, the sterilisation method was studied. Although sterilisation is an important aspect prior to cell inclusion in order to avoid the growth of any pathogenic microorganisms, little has been studied on bioinks. Three sterilisation techniques, such as short and long-cycle autoclave, β-radiation and γ-radiation, were proposed to sterilise the NC-Alg bioink. Afterwards, the bioink was characterised again.

Results in Fig. 10A showed a sharp decrease in rheological properties after ionic radiation sterilisations, being the γ-radiation the most destructive sterilisation technique. Despite the fact that both β-radiation and γ-radiation are very accurate sterilisation techniques, it has been published a viscosity decrease in gelatin and methylcellulose bioinks due to polymer chain disruption [76]. Furthermore, β-radiation was reported to provoke a molecular weight loss in cellulose hydrogels which affects the viscosity [77]. Likewise, γ-radiation was related to alginate crosslinking failure as well as to cellulose chain scission [76,78].

In a similar manner, autoclave sterilisation demonstrated a reduction in the viscosity values of the base bioink compared to non-sterilised one. Nevertheless, this decrease was lower than the rheological decrease caused by β-radiation and γ-radiation, suggesting better printability and scaffold fabrication after autoclaving. Between the two autoclave methods, long-cycle autoclave sterilisation showed to be more destructive than short-cycle autoclave, probably because with short-cycle autoclave the NC-Alg bioink was not subjected

to high temperatures for a long time as with long-cycle autoclave. Thus, the short-cycle autoclave seemed to be the best option to sterilise the NC-Alg bioink.

The same procedure was carried out with the NC-Alg-HA bioink resulting in a similar conclusion (Fig. 10B). Both β-radiation and γ-radiation techniques caused a sharp reduction in the rheological properties of the hyaluronic bioink. Although we did not find any study in which HA bioinks were exposed to both radiation types, it has been reported a molecular weight loss in HA nanoparticles when they were radiated with ionising radiations [79]. In addition, the hyaluronic bioink was composed of NC and Alg which was demonstrated to be damaged by both radiations. Conversely, autoclave sterilisation showed a slight decrease in rheological properties, being the short-cycle autoclave the less harmful technique. These results were in concordance with the literature which has demonstrated a viscosity reduction in HA solutions after exposing them to high temperatures [80].

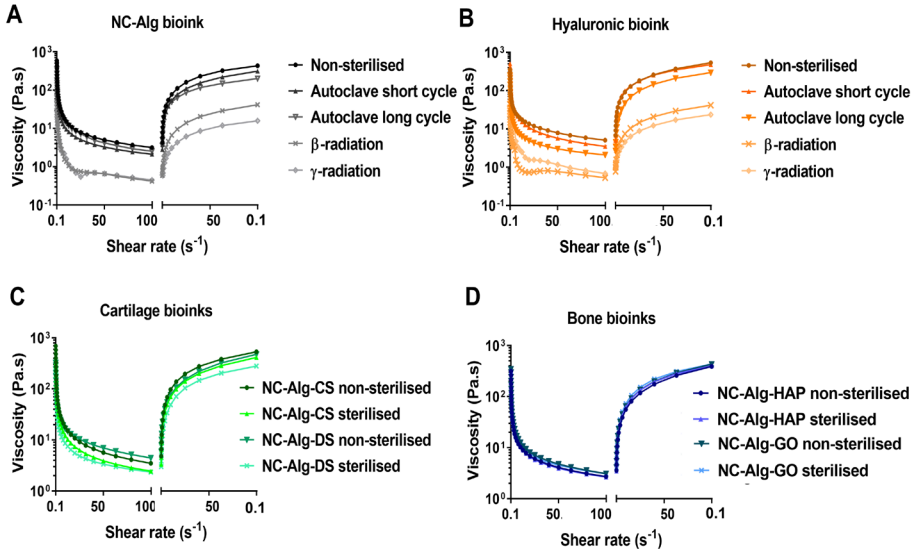

Figure 10. Sterilisation evaluation. A) Rheological steady flow behaviour after autoclave short and long-cycles, β-radiation and γ-radiation on the NC-Alg bioink. B) A Rheological steady flow behaviour after autoclave (short and long-cycles), β-radiation and γ-radiation on the NC-Alg-HA bioink. C) Rheological steady flow behaviour of the NC-Alg-CS and NC-Alg-DS bioinks after short-cycle sterilisation. D) Rheological steady flow behaviour of NC-Alg-HAP and NC-Alg-GO-bioinks after short-cycle sterilisation.

In conclusion, ionic radiation techniques were discarded to sterilise NC-Alg-based bioinks and, between the autoclave sterilisation methods, the short-cycle one was selected to sterilise NC-Alg, NC-Alg-HA as well as cartilage and bone bioinks.

To ensure that the short-cycle autoclave would not cause unexpected results on cartilage and bone bioinks, the rheological study was carried out after the sterilisation process.

Both NC-Alg-CS and NC-Alg-DS showed the same pattern as previous bioinks in terms of a reduction in viscosity values in comparison with their non-sterilised pairs (Fig. 10C). This was expected because as HA, both, CS and DS are glycoproteins that may be affected by high temperatures [81]. Nevertheless, the viscosity decrease was slight and the flow behaviour did not change, suggesting good printability and scaffold fabrication after sterilisation.

On the other side, this rheological reduction was not shown on bone bioinks due to HAP and GO properties (Fig. 10D). In fact, HAP has been shown to prevent Alg-based hydrogel from temperature damage [82] and GO has been reported to reinforce the stiffness and strength of polymeric inks [83], suggesting that both, HAP and GO, provided the NC-Alg bioink with excellent mechanical properties. However, the NC-Alg-GO bioink demonstrated a colour change, which led to conducting an FT-IR assay to evaluate any chemical alteration.

FT-IR results showed a bond loss between carbon and oxygen molecules in the sterilised NC-Alg-GO bioink compared to the non-sterilised one, indicating a GO reduction (Fig. 11). The reduced GO is related to cell toxicity and death as well as to genotoxicity [84,85]. Consequently, to sterilise the NC-Alg-GO bioink, GO was sterilised under UV radiation and then, it was mixed with the short-cycle autoclave sterilised NC-Alg part.

A

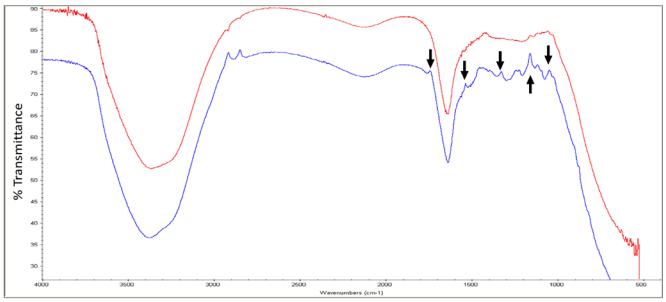

B

Sample	C=O cm^{-1}	C-O cm^{-1}	C-OH cm^{-1}	C-O-C cm^{-1}
Non-sterilised NC-Alg-GO	1763	1204	1299 1131	1077
Sterilised NC-Alg-GO	-	-	-	-

Figure 11. Short-cycle autoclave evaluation on NC-Alg-GO bioink. A) FT-IR spectra showing non-sterilised bioink in blue and sterilised bioink in red. B) Signalled results are reflected in the table.

4.1.3 Cytotoxicity assay

In order to finish the pre-bioprinting evaluation, a cytotoxicity study was performed using L929 fibroblasts. Results in Fig. 12 indicated that all the bioinks were non-toxic since cell viabilities above 70% were achieved in the three assays. Interestingly, the HA addition to the base bioink showed a statistically significant cell viability enhancement in the indirect contact assay ($p < 0.001$) compared to the NC-Alg bioink. HA-supplemented media was reported to promote cell viability which may explain these results [86]. Cartilage bioinks showed no statistical differences compared to the base bioink, nevertheless, the NC-Alg-CS bioink demonstrated statistically higher cell viability than NC-Alg-DS in the direct contact assay ($p < 0.001$). According to the literature, DS was not reported to be cytotoxic [58,87], therefore, it was suggested that the ability of the cells to adhere to the NC-Alg-DS bioink may have resulted in lower cell viability, since there were fewer cells remained in the well plate in comparison with the NC-Alg-CS bioink. Finally, bone bioinks results highlighted statistical differences in cell viability between the NC-Alg-GO and the NC-Alg

bioink in the adhesion assay ($p < 0.01$). GO was described to have excellent adhesive properties [88]. For instance, good adherence of L929 fibroblasts to a GO monolayer was reported in another research [89]. However, this study applied longer cell incubation times than in our case, which may explain the lower cell viability shown on the NC-Alg-GO bioink.

Despite these cell viability differences, all the bioinks were considered non-toxic and to deeply evaluate the biological impact of each bioink, assays with embedded D1-MSCs were conducted later.

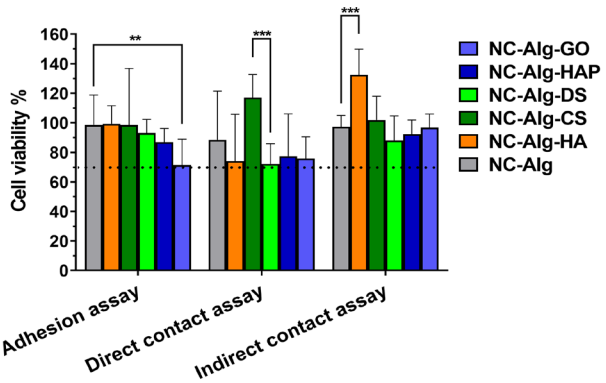

Figure 12. Cytotoxicity study of all the developed bioinks in adhesion, direct contact and indirect contact assays. Values represent means ± SD. ***: $p < 0.001$, **: $p < 0.01$.

4.2. 3D Bioprinting

NC-Alg scaffolds were manufactured through an extrusion bioprinter under the pressure of 20-25 kPa. The addition of HA, CS and DS led to an increase in the bioprinting pressure to 25-30 kPa to make NC-Alg-HA, NC-Alg-CS and NC-Alg-DS scaffolds. Both, hyaluronic and cartilage bioinks demonstrated higher viscoelastic behaviour on rheology than the NC-Alg bioink which resulted in applying higher bioprinting pressures to extrude the bioinks. Bioprinting pressures are related to cell damage due to shear stress that may provoke cell membrane breakdown as well as alterations in gene expression profile [90]. In addition, this cell damage is proportional to pressure since the higher the bioprinting pressure to apply, the higher the percentage of dead cells according to a study with embedded fibroblast into gelatin bioink [91].

In consonance with another study in which chondrocytes were included in a bioink based on gelatin, carboxymethylated nanocellulose and Alg, bioprinting pressures above 55 kPa might critically increase the shear stress and cell damage [92]. Consequently, the bioprinting pressures used in this thesis were adequate for reducing cell damage during the bioprinting process.

When it comes to bone scaffolds, the NC-Alg-GO scaffolds were obtained by applying the same pressures than to the NC-Alg scaffolds, which, as aforementioned, were good for cell survival. However, bioprinting parameters were changed to obtain the NC-Alg-HAP scaffolds due to particle size. HAP particle size was around 200-300 μm which obstructed the 27 G (200 μm inner diameter) needle. This type of HAP was selected based on previous experience in which we proved good osteoinductive and biocompatibility results *in vivo* by using gelatin-HAP hydrogels [93]. Therefore, to fabricate the NC-Alg-HAP scaffolds a 22 G (410 μm inner diameter) needle was used and pressures were adjusted to 15-20 kPa to maintain a constant extrusion flow, which in turn, would be better for cell viability.

4.3. Post-bioprinting evaluation

4.3.1 Acellular scaffold characterisation

After bioprinting, scaffolds were evaluated to study their internal and external structure and surface.

Macroscopic images showed that all the bioprinted scaffolds resembled CAD, indicating good printability (Fig. 13A). However, differences were observed among them. The higher resolution was detected in hyaluronic scaffolds as well as in cartilage scaffolds compared to the NC-Alg or bone scaffolds, which was a consequence of the addition of GAGs to the base bioink. As shown in the rheological study (Fig. 9), HA, CS and DS improved the rheological properties of the base bioink resulting in better printability. In contrast, NC-Alg-HAP and NC-Alg-GO scaffolds demonstrated a slight improvement in shape fidelity in comparison with NC-Alg scaffolds, probably owing to the

maintenance of viscosity and viscoelasticity properties after sterilisation.

Upon closer examination, almost all the scaffolds presented an oblong grid structure, being the NC-Alg-HA and NC-Alg-CS scaffolds the ones in which the grid structure was squatter and, therefore, a signal of better scaffold shape fidelity as there are more similar to CAD grid structure. In fact, as shown in Fig. 13B, when a grid area measurement was made, the NC-Alg-CS scaffolds were closer to the theoretical CAD grid area of 0.6 mm^2, suggesting that the CS was among all compounds the one that gave better printability.

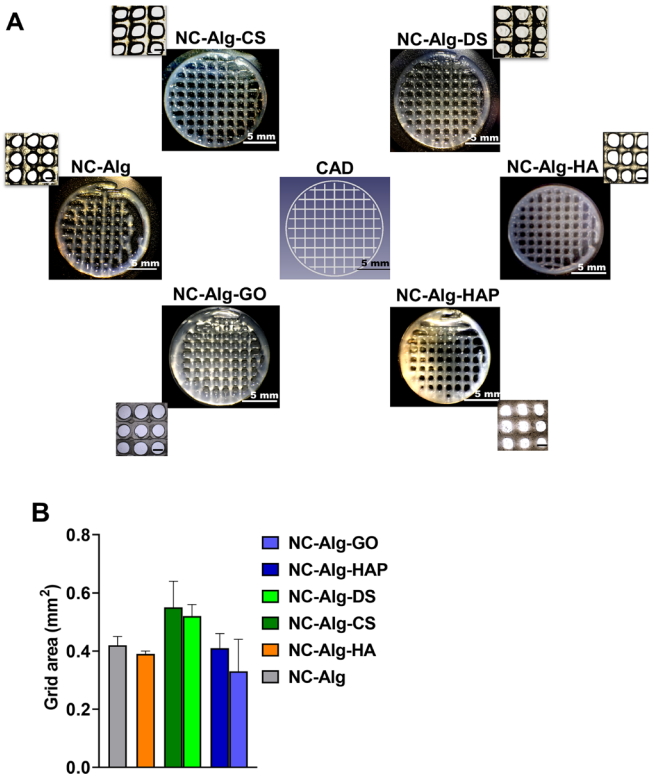

Figure 13. Printability evaluation of all types of scaffolds. A) CAD design compared to macroscopic images of the scaffolds. Scale bars 5 mm and 500 µm. B) Grid area quantification. Values represent means ± SD.

The internal structure of scaffolds was observed by SEM (Fig. 14A). First, the crosscuts of NC-Alg scaffolds were analysed. Results showed a porous internal structure indicating that nutrients, as well as oxygen exchange, may be ensured to support the embedded living cells. These results were in accordance with the literature since it was observed a porous internal structure in Alg hydrogels [94]. In addition, similar porous structures were achieved when NC was added. Importantly, this study indicated that the porosity of printed NC-Alg scaffolds was due to NC, suggesting that scaffold porosity could be modified by variating the concentration of NC [95].

The addition of GAGs resulted in a similar porous internal structure since no optical differences were observed in the pictures taken by SEM. In fact, porous internal structures were detected in other studies with scaffolds containing HA, CS, and DS [32,37,57]. Likewise, bone scaffolds showed porosity which has been reported in many studies with HAP and GO [93,96]. Porous structures are very important in fabricating tissues such as bone since porosity is related to tissue good functionality as well as to their mechanical properties.

Interestingly enough, surface differences were detected among the scaffold types while performing SEM. For instance, it seems to be higher fibrous-like structures on the hyaluronic, cartilage and GO-containing scaffolds than on the surface of the NC-Alg scaffolds. In contrast, the NC-Alg-HAP scaffolds' surface was granulose, probably due to HAP particles.

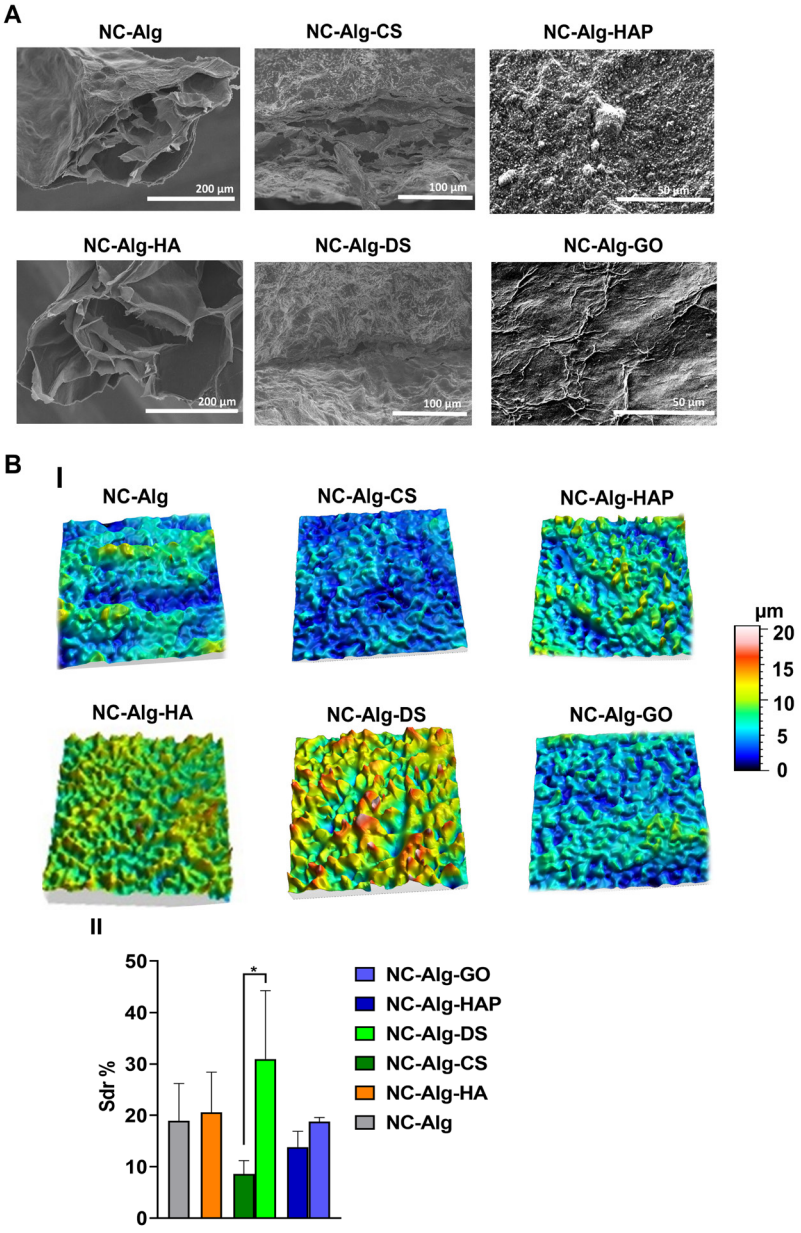

Figure 14. Scaffold internal structure and surface characterisation. A) Representative SEM images of all the scaffolds. Scale bar 200 µm for NC-Alg and NC-Alg-HA scaffolds, 100 µm for cartilage scaffolds and 50 µm for bone scaffolds. B) Optical profilometry study. I) 3D topographical images of all the scaffolds. II) Sdr parameter quantification. Values represent means ± SD. *: $p < 0.05$.

These surface differences may result in dissimilar roughness. It has been demonstrated that scaffolds with a rougher surface are related to higher success in terms of better cell adhesion compared to smooth scaffolds [97]. In addition, implantation success was also affected by the roughness according to other studies, being the smooth scaffolds the ones that demonstrated higher implantation failure rates [98]. Consequently, an in-depth study of scaffold roughness was carried out with the optical profilometry technique. Results showed in Fig. 14BI that the NC-Alg scaffolds had a considerable roughness surface between 0 and 10 μm. Notably, the addition of HA resulted in a higher roughness surface achieving a roughness surface between 5 and 10 μm. More differences were observed between cartilage scaffolds, the NC-Alg-CS scaffolds showed the smoothest surface among all the scaffold types, while the DS-containing scaffold showed the highest roughness surface.

Regarding the bone scaffolds, roughness has a greater importance due to its implications on osteogenic differentiation. It has been reported that rougher scaffolds are more osteogenic than smooth ones [98]. Similar surface roughness was observed in optical profilometry images on NC-Alg-HAP and NC-Alg-GO scaffolds, which in turn, was similar to the NC-Alg surface. However, the surface roughness may be increased by adding concentrations of HAP above 5% (w/v) or by chemically modifying the GO [99,100].

When the Sdr parameter which measured the uniformity of the surface texture was calculated, it confirmed the previous results, showing no statistical differences among bone, hyaluronic and base scaffolds (Fig. 14BII). However, the Sdr parameter of the NC-Alg-DS scaffolds was statistically higher than the value of the NC-Alg-CS scaffolds ($p < 0.05$), suggesting higher cell adhesion and implantation success with DS-containing scaffolds.

Next, scaffold water uptake capacity was assayed since it indicates the diffusion of nutrients and signalling molecules [101].

As Fig. 15A shows, the water uptake of all the scaffolds increased over time until the equilibrium was reached. Moreover, the equilibrium was achieved within the first 4-8 h suggesting excellent swelling properties. This water

uptake easiness may be related to the hydrophilicity properties of both polymeric compounds, NC and Alg, which has been described before in the literature [102]. When a comparison was made, NC-Alg scaffolds showed a higher swelling behaviour that decreased as HA, DS, CS and HAP were added, being statistically lower in NC-Alg-DS, NC-Alg-DS and NC-Alg-HAP scaffolds. The swelling degree is related to the crosslinking density as well as to the bioink inner density [103]. The addition of GAGs increased the bioink density as has been shown in the rheological study. In addition, the differences in GAGs % could explain the lower water uptake capacity of the NC-Alg-CS and NC-Alg-DS scaffolds, since HA was added at 1% concentration and CS or DS at 5%.

Likewise, a less swelling degree in NC-Alg-HAP scaffolds was related to the HAP particle size. In fact, it has been reported that HAP particles can displace water molecules as shown in other studies [104]. Interestingly, this pattern was not reflected in the NC-Alg-GO scaffolds in which the swelling behaviour was similar to the base scaffolds. It has been reported the capacity of graphene molecules to develop strong hydrogen bonds with water molecules [105], which may explain the reason why the swelling properties of the NC-Alg-GO scaffolds were high.

Despite these differences, all scaffolds showed high swelling properties (> 90%), which indicated excellent nutrient transport into the scaffolds to nourish the embedded cells.

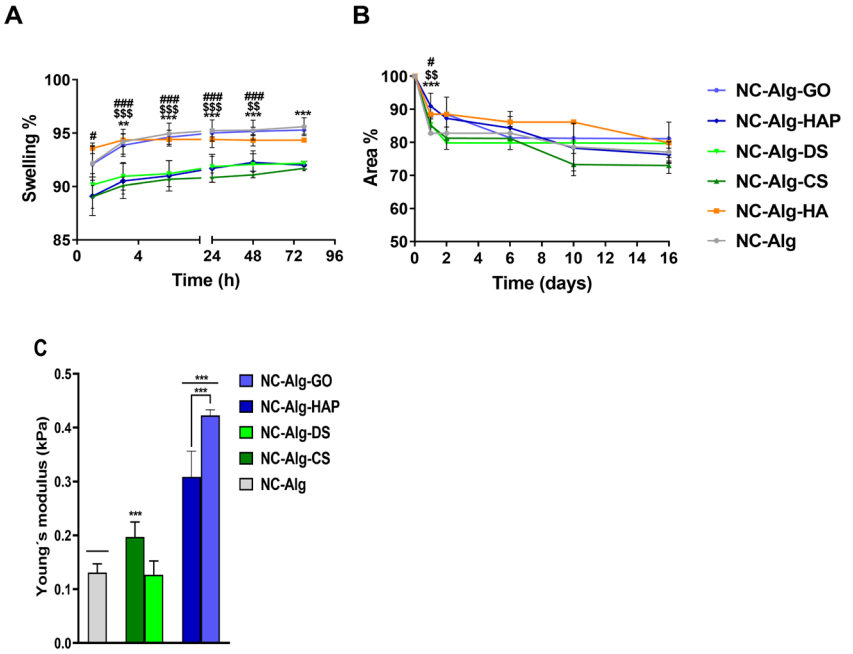

Figure 15. Scaffold characterisation. A) Swelling assay ###: $p < 0.001$, #: $p < 0.05$ NC-Alg-CS compared to NC-Alg. $$$: $p < 0.01$, $$: $p < 0.01$ NC-Alg-DS compared to NC-Alg. *** $p < 0.001$, **: $p < 0.01$, *: $p < 0.05$ NC-Alg-HAP compared to NC-Alg. B) Degradation study ***: $p < 0.001$ NC-Alg-HA compared to NC-Alg, $$: $p < 0.01$ NC-Alg-HAP compared to NC-Alg and #: $p < 0.05$ NC-Alg-GO compared to NC-Alg. Young´s modulus measurements on cartilage and bone scaffolds. ***: $p < 0.001$. Values represent means ± SD.

The degradation study was conducted due to its importance in medical applicability. NC-Alg-based scaffolds showed similar degradation kinetics, being an area loss of around 20% at the end of the study (Fig. 15B). The main area loss occurred within the first 24 h for all the scaffold types. Nevertheless, this degradation was statistically lower in scaffolds containing HA ($p < 0.001$), HAP ($p < 0.01$) and GO ($p < 0.05$) in comparison with NC-Alg scaffolds. A good degradation kinetic is important to regenerate the damaged tissue while the scaffold is being degraded [106]. For instance, cartilage regeneration depends on injury type and location together with the cartilage function, thus, it is complex to estimate de optimal scaffold degradation rate [107].

On the other hand, scaffolds targeted for bone must be stable with controlled degradation kinetics [107]. In this study, all the scaffolds demonstrated a

controlled degradation rate. Furthermore, the degradation may be adjusted by modifying chemically the bioink compounds such as Alg [108]. Interestingly, the combination of different elements may be another approach. In fact, adding HA to either cartilage or bone scaffolds could reduce the degradation.

Finally, mechanical properties were analysed in the scaffolds targeted to cartilage and bone. Cartilage requires high biomechanics since it is exposed to great forces of compression and tension [109]. Likewise, mechanical properties in bone tissue are essential for organ protection and motion support [110]. Mechanical properties were represented by Young´s modulus parameter since indicates the resistance of the material to deformation under load. As shown in Fig. 15C, in cartilage scaffolds, the biomechanics were statistically significantly improved with the presence of CS compared to NC-Alg and NC-Alg-DS scaffolds ($p < 0.001$). As reported in other studies, CS is related to the mechanical resistance of tissues such as cartilage due to its chemical composition [111,112]. In contrast and according to this study, it has been insinuated that mechanical properties are not affected by the DS [113]. On the other hand, higher Young´s modulus values were obtained in NC-Alg-HAP and NC-Alg-GO scaffolds which were statistically higher than NC-Alg values ($p < 0.001$). Between them, GO seemed to enhance scaffold mechanical properties more than HAP ($p < 0.001$). This biomechanical improvement after inorganic compound addition has been extensively described in the literature, particularly in the case of GO which has been described to possess superior mechanical properties [114].

Despite the fact that CS or HAP and GO increased the mechanical properties of the base scaffold, the values of the native tissues were not achieved. For instance, cartilage has a compression Young´s modulus of 0.2-2 MPa [115] and bone tissue values reached the 10-20 GPa [116]. For this reason, this kind of scaffold made of hydrogels should be applied to repair local injuries in conjunction with native tissue instead of substitutes for the entire tissue. In order to enhance scaffold biomechanics, other approaches should be conducted such as including HA which has been shown to promote mechanical properties [117], incorporating CS into bone scaffolds or adding other

reinforcing polymers as the PCL [118].

4.3.2 Post-bioprinting biological evaluation

Base and hyaluronic scaffolds

Biological properties were evaluated on D1-MSCs which have the ability to differentiate into diverse cell types such as chondrocytes and osteocytes [64,119].

First, the optimal cell density to include in NC-Alg and NC-Alg-HA bioinks was studied. Hence, three different concentrations of 1 x 10^6, 2.5 x 10^6 and 5 x 10^6 cells/mL were proposed. After bioprinting, cell viability, as well as metabolism, were assayed for 21 days. The cell density of 1 x 10^6 cell/mL, resulted in very low viability which hindered a good quantification; therefore, it was discarded for future studies (data not shown).

High cell viability together with uniform distribution was detected after bioprinting on NC-Alg scaffolds by using both 2.5 x 10^6 and 5 x 10^6 D1-MSCs/mL densities, since Live/Dead™ pictures showed almost all the cells alive in green. However, cell aggregates were observed inside the construct with 5 x 10^6 cells/mL (Fig. 16A). It has been published that cell aggregates are related to the induction of MSCs to differentiate [120,121]. Importantly, the addition of HA improved the biological properties of the bioink considering that there were more cells alive in green inside NC-Alg-HA scaffolds than inside the NC-Alg ones (Fig. 16A). This optical appreciation was corroborated by quantifying the Live/Dead™ images.

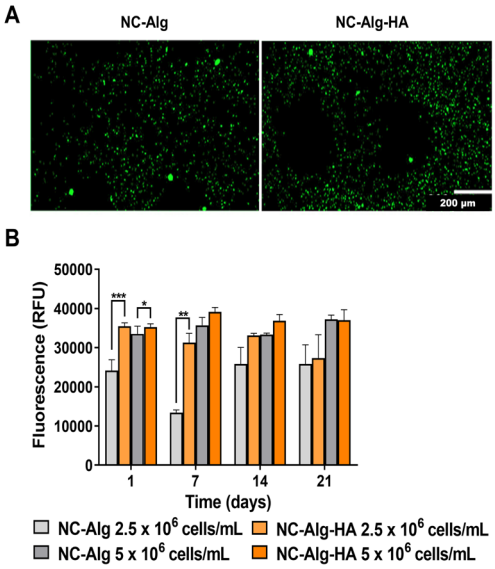

Figure 16. Biological evaluation of embedded D1-MSCs on base and hyaluronic scaffolds. A) Representative fluorescence micrographs of Live/Dead ™ stained scaffolds at day 21 after bioprinting with 5x10^6 cells/mL density. Scale bar 200 µm. B) D1-MSCs metabolic activity measurements on NC-Alg and NC-Alg-HA scaffolds. Values represent means ± SD. *** $p < 0.001$, **: $p < 0.01$, *: $p < 0.05$.

On the other side, as expected, cell metabolism was higher on both scaffolds with 5 x 10^6 cell/mL densities (Fig. 16B). However, hyaluronic scaffolds displayed an increase in cell metabolism, which with 2.5 10^6 cell/mL was statistically significant at day 1 ($p < 0.001$) and 7 ($p < 0.01$) after bioprinting as well as with 5 x 10^6 cell/mL at day 1 ($p < 0.05$) after bioprinting. These results suggested that the addition of HA to the base bioink improved its biological properties. The improvement may be related to the enhancement of the rheological properties of hyaluronic bioink, since higher viscoelastic properties protect the cells against the damage caused by shear stress during the bioprinting process [90]. Additionally, other works have shown that the viability and the functionality of MSCs were promoted after adding HA to Alg or NC hydrogels [37,122]. Therefore, the developed NC-Alg-HA bioink may become a feasible tissue engineering approach to regenerate diverse tissues.

Taking into account this preliminary study to develop both cartilage and

bone bioinks a cell density of 5 x 10^6 was selected. Moreover, D1-MSCs were genetically modified to secrete EPO, which could give us a better understanding of the cell's functionality inside the scaffold as well as assess the release of bioactive molecules through it. In addition, bioprinted scaffold layers were reduced from 4 to 2 to facilitate the scaffold degradation and thus be able to extract easily the cells to carry out the differentiation study.

Cartilage scaffolds

The biological study on cartilage scaffolds showed that both CS and DS improved the biological properties of NC-Alg scaffolds. First, Live/Dead™ images demonstrated higher cell viability inside NC-Alg-CS and NC-Alg-DS scaffolds after 21 days of bioprinting compared to NC-Alg scaffolds (Fig. 17A). In fact, the percentage of live cells was higher inside DS scaffolds in comparison with NC-Alg-CS scaffolds (NC-Alg-DS scaffolds showed 88.14 ± 2.62% cell viability and NC-Alg-CS scaffolds demonstrated 80.11 ± 1.85% cell viability). Furthermore, cell aggregations were observed in both cartilage scaffolds that was related to the promotion of the chondrogenic differentiation of MSCs [120].

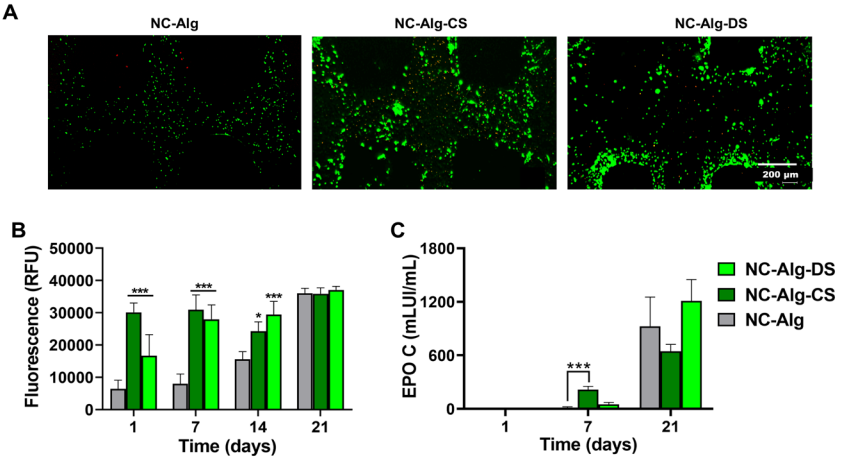

Figure 17. Biological evaluation of embedded D1-MSCs on cartilage scaffolds. A) Representative fluorescence micrographs of Live/Dead™ stained scaffolds at day 21 after bioprinting. Scale bar 200 µm. B) D1-MSCs metabolic activity measurements on NC-Alg-CS and NC-Alg-DS scaffolds. C) EPO release quantification on NC-Alg-CS and NC-Alg-DS scaffolds. Values represent means ± SD. *** $p < 0.001$, *: $p < 0.05$.

Then, as shown in Fig. 17B, the cell metabolism increased within the days after bioprinting in both scaffold types, indicating good proliferation. Furthermore, cells embedded into scaffolds containing both CS and DS presented an elevated metabolic activity compared to the base scaffolds at day 1, 7 and 14 after bioprinting, which was statistically relevant (at day 1 and 7 $p < 0.001$ for both CS and DS-containing scaffolds compared to NC-Alg ones; at day 14, NC-Alg-DS $p < 0.001$ and NC-Alg-CS $p < 0.05$ in comparison with NC-Alg scaffolds). As occurred with the hyaluronic bioink, both cartilage bioinks showed excellent rheological properties that may reduce cell damage during bioprinting. Moreover, both CS and DS have been reported to be involved in diverse biological processes resulting in higher cell viability, proliferation and metabolism when they were used in other works [57,111].

Finally, as Fig. 17C shows, EPO release was detected in all the scaffolds after 7 days of bioprinting, but was significantly higher in the NC-Alg-CS scaffolds ($p < 0.001$) than in the NC-Alg ones. At the end of the study, the highest EPO release was determined in NC-Alg-DS scaffolds. Results indicated that cells were functional inside the scaffolds after bioprinting. Furthermore, the controlled release of EPO thought scaffolds suggested that they may be used as carriers to release diverse therapeutic agents. For instance, other works have used Alg or HA hydrogels for the release of EPO to develop drug carrier systems [123].

In conclusion, the previous study corroborated that the addition of CS and DS into NC-Alg bioink promoted its biological properties since D1-MSCs cells embedded in NC-Alg-CS and NC-Alg-DS bioinks were more alive, metabolically more active and functional to secrete EPO hormone. However, the next important step would be to evaluate if these scaffolds could regenerate cartilage tissue. To do so, *in vitro* differentiation study was conducted.

First, scaffolds were stained with Safranin-O (red) to detect cartilage and Alcian blue (blue) to detect GAGs. Darker zones were observed in the NC-Alg-CS and NC-Alg-DS scaffolds than in the NC-Alg ones, suggesting a chondrogenic differentiation (Fig. 18A).

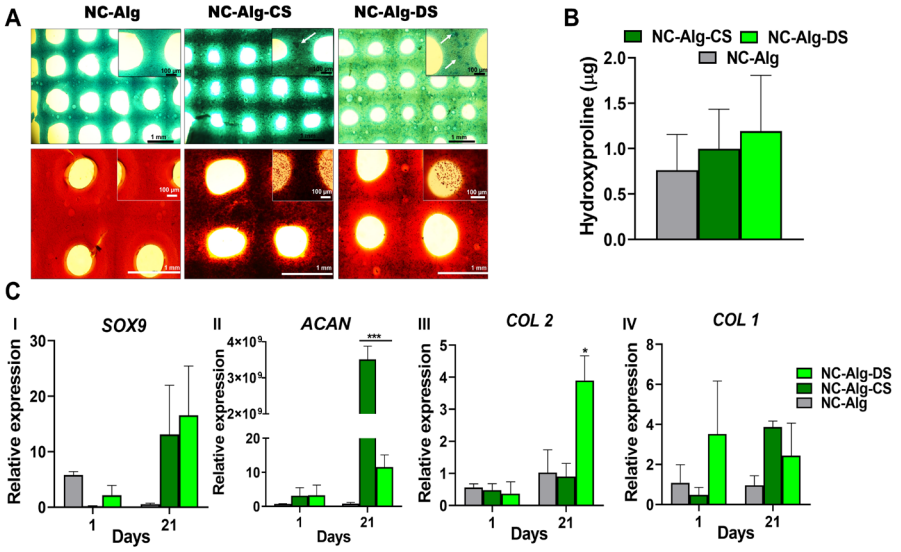

Figure 18. Evaluation of chondrogenic differentiation on embedded D1-MSCs. A) Representative images of Alcian blue and Safranin-O stained NC-Alg, NC-Alg-CS and NC-Alg-DS scaffolds. Scale bars 1 mm and 100 µm. B) Hydroxyproline quantification. C) Chondrogenic gene expression at day 1 and 21 after bioprinting. Values represent means ± SD. *** $p < 0.001$, *: $p < 0.01$.

Then, hydroxyproline quantification was performed which was related to collagen production. In Fig. 18B, results showed that hydroxyproline amount was higher on the NC-Alg-DS and NC-Alg-CS scaffolds than on the NC-Alg ones, suggesting cartilage-like ECM production. Among them, DS seemed to promote higher collagen production of embedded D1-MSCs, indicating better chondrogenic differentiation inside these scaffolds.

For an in deep evaluation, the genetic expression of chondrogenic markers was measured by RT-PCR (Fig. 18C).

Results showed that at day 21 after bioprinting *SOX9*, which is a chondrogenic transcription factor that regulates chondrogenic differentiation and cartilage ECM production [124], was overexpressed by the D1-MSCs embedded into the NC-Alg-DS and NC-Alg-CS scaffolds compared to the NC-Alg ones (Fig. 18CI). Likewise, as shown in Fig. 18CII, *ACAN* expression was statistically higher on the NC-Alg-DS and NC-Alg-CS scaffolds than on the NC-Alg ones ($p < 0.001$). Notably, the expression of this marker by cells inside CS scaffolds

was more significant than the expression inside DS scaffolds ($p < 0.001$). *ACAN* is a chondrogenic differentiation marker since transcribes the major structural protein of the cartilage tissue [115].

Additionally, collagen type 2 is another important cartilage protein which indicates cartilage regeneration as well as cartilage-specific ECM production [32]. This protein is encoded by the *COL2* gene which was significantly expressed by the cells inside the NC-Alg-DS scaffolds in comparison with the CS and the base scaffolds ($p < 0.05$) (Fig. 18CIII).

Finally, *COL1* gene expression was assayed considering that is expressed by undifferentiated chondrocytes or other intermediate cells [125]. As shown in Fig. 18CIV, *COL1* expression decreased on the NC-Alg-DS at day 21 after bioprinting suggesting that D1-MSCs were differentiated into chondrocytes inside the DS scaffolds. On the other hand, *COL1* was increased on CS constructs indicating the presence of undifferentiated cells. Nevertheless, the expression of *SOX9* together with the remarkably high *ACAN* expression suggested that there was a chondrogenic differentiation pathway inside the NC-Alg-CS scaffolds. It has been demonstrated that chondrogenic differentiation of hMSCs was accelerated on CS scaffolds [32]. Likewise, DS has been related to the promotion of MSCs to chondrocytes [58], which would corroborate the obtained results.

In conclusion, both CS and DS scaffolds showed chondrogenic differentiation *in vitro* which could be a promising treatment approach for chondral defects.

Bone scaffolds

Finally, the biological properties of scaffolds targeted to bone were evaluated. Live/Dead™ assay demonstrated that D1-MSCs were mostly alive in green and uniformly distributed inside NC-Alg-HAP and NC-Alg-GO scaffolds after 21 of bioprinting (Fig. 19A). Notably, it could be appreciated higher green intensity on these scaffolds compared to the NC-Alg ones, suggesting greater cell viability with the presence of HAP and GO. In addition, cell aggregates were observed inside HAP scaffolds while no cell aggregation signals were found inside GO scaffolds. According to the literature, cell aggregation may favour

osteogenic differentiation [121].

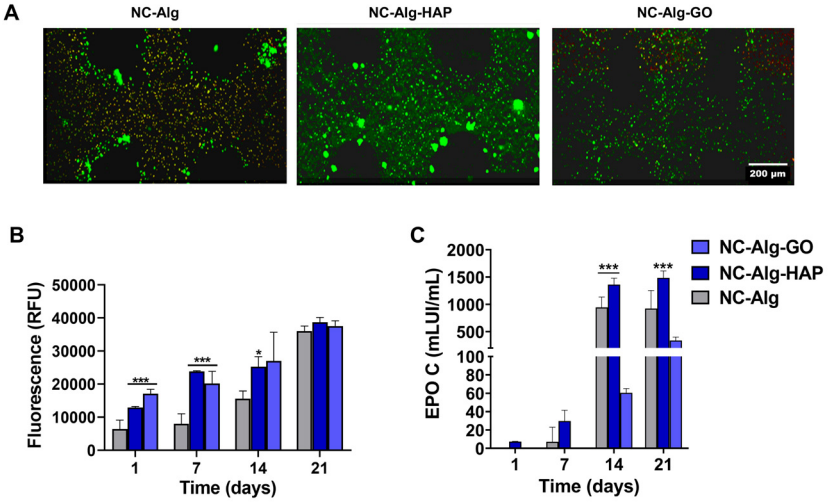

Figure 19. Biological evaluation of embedded D1-MSCs on bone scaffolds. A) Representative fluorescence micrographs of Live/Dead ™ stained scaffolds at day 21 after bioprinting. Scale bar 200 µm. B) D1-MSCs metabolic activity measurements on NC-Alg-HAP and NC-Alg-GO scaffolds. C) EPO release quantification on NC-Alg-HAP and NC-Alg-GO scaffolds. Values represent means ± SD. *** $p < 0.001$, *: $p < 0.05$.

Moreover, as (Fig. 19B) shows, the metabolic activity of embedded cells was increased along the days after bioprinting indicating good cell proliferation. Interestingly, scaffolds containing HAP and GO demonstrated higher cell metabolism than in NC-Alg scaffolds, being this increase statistically relevant on days 1 and 7 after bioprinting ($p < 0.001$). At day 14 after bioprinting, only the NC-Alg-HAP scaffold showed a statistically significant increase compared to the base scaffolds ($p < 0.05$). These results were in concordance with the literature in which it has been reported that HAP scaffolds promoted cell viability and migration, as well as that GO enhanced the metabolism of stem cells [126]. In addition, the improvement in mechanical properties after both HAP and GO addition may prevent the cells from damage caused by the bioprinting process.

Finally, EPO secretion was analysed. The hormone release increased over time in all the scaffolds suggesting excellent cell functionality (Fig. 19C). Ipor-

tantly, EPO release was higher from NC-Alg-HAP scaffolds in all the measured time points, being significant on days 14 and 21 in comparison with GO-containing scaffolds ($p < 0.001$). Likewise, cells inside NC-Alg scaffolds released a higher amount of EPO than the cells inside NC-Alg-GO which was significant on day 14 ($p < 0.001$). It was expected higher EPO production inside GO scaffolds than inside the NC-Alg ones as in the first one's higher cell viability and metabolic activity was detected. However, GO has been described to possess remarkable adhesion properties with diverse molecules [127]. Thus, EPO could bind to GO instead of releasing to the medium. In fact, this phenomenon was also shown in a study where EPO-producing cells were encapsulated in Alg-GO microcapsules [128]. According to another study by the same authors, EPO attachment to GO could be avoided by covering the microcapsules with fetal bovine serum or bovine serum albumin [129].

Taking into account these results, it may be concluded that both HAP and GO enhanced the biological properties of the NC-Alg scaffolds, being HAP the most adequate compound to add to the bioink. Nevertheless, their ability to regenerate bone should be addressed.

Alizarin red staining pictures showed in (Fig. 20A) that in all the three types of scaffolds were calcium deposits suggesting osteogenic differentiation. For further evaluation, ALP enzyme activity which is produced by osteoblast, was quantified. As shown in Fig. 20B, ALP production increased along the days in all types of scaffolds after bioprinting indicating an osteogenic pathway. However, this increase was more relevant in the NC-Alg-HAP ($p < 0.001$) and NC-Alg-GO scaffolds ($p < 0.05$). Remarkably, ALP enzyme activity was significantly higher in HAP-containing scaffolds than in GO-containing scaffolds as well as in base scaffolds ($p < 0.05$). This suggested a greater osteogenic induction of embedded cells by the presence of HAP in comparison to GO. Although the osteoinductive properties of HAP have been widely described [130], GO has also been reported to promote osteogenic differentiation [131], which has not been demonstrated according to the ALP activity measurement.

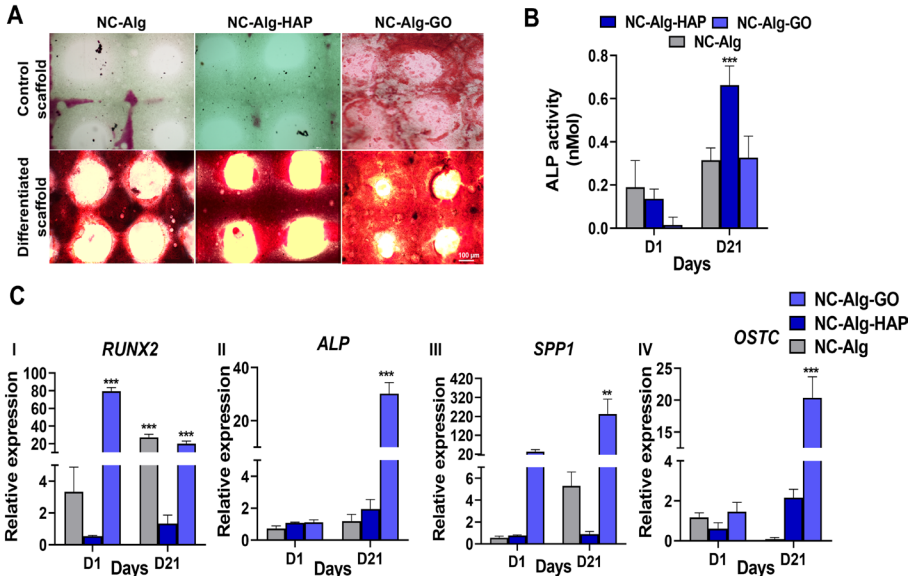

Figure 20. Evaluation of osteogenic differentiation on embedded D1-MSCs. A) Representative images of Alizarin Red stained NC-Alg, NC-Alg-HAP and NC-Alg-GO scaffolds. Scale bar 100 μm. B) ALP enzyme activity quantification at day 1 and 21 after bioprinting. C) Osteogenic gene expression at day 1 and 21 after bioprinting. Values represent means ± SD. *** $p < 0.001$, *: $p < 0.01$.

Finally, the RT-PCR technique was applied to quantify osteogenic gene expression (Fig. 20C).

RUNX2 is a key transcription factor in the creation of osteoblast [132] which was significantly overexpressed by the D1-MSCs embedded in the NC-Alg-GO scaffolds compared to NC-Alg-HAP and NC-Alg at day 1 and to NC-Alg-HAP at day 21 ($p < 0.001$) (Fig. 20CI). Likewise, as Fig. 20CII shows, *ALP* gene expression was higher in GO-containing constructs after 21 days of bioprinting than in the other types of scaffolds ($p < 0.001$). Thus, the previously analysis of ALP enzyme activity measurement did not match with *ALP* gene expression. Consequently, we suggested that the ALP enzyme was under quantification in GO scaffolds due to its adherent properties. In fact, GO has been used to immobilize enzymes as they adhered to it [133].

The bone-specific ECM protein osteopontin is regulated by the *SPP1* gene [134], and its expression was significantly higher by the cells inside the NC-Alg-GO scaffolds than by the ones inside the NC-Alg-HAP scaffolds ($p < 0.01$)

(Fig. 20CII). Furthermore, cells expressed more *SSP1* gene in NC-Alg than in HAP-containing scaffolds.

Finally, as shown in Fig. 20CIV, the *OSTC* gene which is related to mature bone [134] was also significantly overexpressed in GO scaffolds than in the HAP and base scaffolds ($p < 0.001$).

Taking into account the gene expression results, it can be concluded that the addition of GO induced a clear osteogenic differentiation of embedded D1-MSCs. On the other hand, NC-Alg-HAP scaffolds also showed a slight osteogenic pathway induction since the *ALP* gene expression and the enzyme activity as well as the *OSTC* gene expression was higher than in the NC-Alg scaffolds. Considering that both mechanical and biological properties were enhanced by the addition of HAP and GO, it can be concluded that the use of NC-Alg-HAP scaffolds tand, in particular, even more, the NC-Alg-GO scaffolds may be a feasible tissue engineering approach for the treatment of bone injuries.

5. Bibliography

1. Roopavath UK, Kalaskar DM, Introduction to 3D Printing in Medicine, Woodhead Publishing 2017;1-20.

2. Heinrich MA, Liu W, Jimenez A, Yang J, Akpek A, Liu X, et al. 3D Bioprinting: from Benches to Translational Applications. Small 2019;23:e1805510.

3. Karzyński K, Kosowska K, Ambrożkiewicz F, Berman A, Cichoń J, Klak M, et al. Use of 3D bioprinting in biomedical engineering for clinical application. Studia medyczne 2018;34:93-97.

4. Atala A, Bauer SB, Soker S, Yoo JJ, Retik AB. Tissue-engineered autologous bladders for patients needing cystoplasty. Lancet 2006;367:1241-6.

5. Summit S, Prosthetic limb with replaceable earing. US7797072B2. 2010.

6. Su A, Al'Aref SJ. History of 3D printing. 3D Printing Applications in Cardiovascular Medicine 2018:1.

7. Zhang YS, Yue K, Aleman J, Mollazadeh-Moghaddam K, Bakht SM, Yang J, et al. 3D Bioprinting for Tissue and Organ Fabrication. Ann Biomed Eng 2016;45:148.

8. Munoz-Abraham AS, Rodriguez-Davalos MI, Bertacco A, Wengerter B, Geibel JP, Mulligan DC. 3D Printing of Organs for Transplantation: Where Are We and Where Are We Heading? Curr Transpl Rep 2016;3:93-99.

9. Markstedt K, Mantas A, Tournier I, Martínez Ávila H, Hägg D, Gatenholm P. 3D Bioprinting Human Chondrocytes with Nanocellulose–Alginate Bioink for Cartilage Tissue Engineering Applications. Biomacromolecules 1900;16:1489-1496.

10. Colaco M, Igel DA, Atala A. The potential of 3D printing in urological research and patient care. Nat Rev Urol 2018;15:213.

11. Zein NN, Hanouneh IA, Bishop PD, Samaan M, Eghtesad B, Quintini C, et al. Three-dimensional print of a liver for preoperative planning in living donor liver transplantation. Liver transplantation 2013;19:1304-1310.

12. Noor N, Shapira A, Edri R, Gal I, Wertheim L, Dvir T. 3D Printing of Personalized Thick and Perfusable Cardiac Patches and Hearts. Adv Sci 2019;6:1900344.

13. Murphy SV, Atala A. 3D bioprinting of tissues and organs. Nature biotechnology 2014;32:773-785.

14. Pavan Kalyan BG, Kumar L. 3D Printing: Applications in Tissue Engineering, Medical Devices, and Drug Delivery. AAPS PharmSciTech 2022;23:92.

15. Gungor-Ozkerim PS, Inci I, Zhang YS, Khademhosseini A, Dokmeci MR. Bioinks for 3D bioprinting: an overview. Biomaterials science 2018;6:915-946.

16. Hölzl K, Lin S, Tytgat L, Van Vlierberghe S, Gu L, Ovsianikov A. Bioink properties before, during and after 3D bioprinting. Biofabrication 2016;8:032002.

17. Vanaei S, Parizi MS, Vanaei S, Salemizadehparizi F, Vanaei HR. An Overview on Materials and Techniques in 3D Bioprinting Toward Biomedical Application. Engineered Regeneration 2021;2:1.

18. Ruiz-Alonso S, Villate-Beitia I, Gallego I, Lafuente-Merchan M, Puras G, Saenz-Del-Burgo L, et al. Current Insights into 3D Bioprinting: An Advanced Approach for Eye Tissue Regeneration. Pharmaceutics 2021;13:308.

19. Kim BS, Jang J, Chae S, Gao G, Kong J, Ahn M, et al. Three-dimensional bioprinting of cell-laden constructs with polycaprolactone protective layers for using various thermoplastic polymers. BF 2016;8:035013.

20. Persaud A, Maus A, Strait L, Zhu D. 3D Bioprinting with Live Cells. Engineered Regeneration 2022;3:292-309.

21. Abdollahiyan P, Oroojalian F, Mokhtarzadeh A, Guardia M. Hydrogel-Based 3D Bioprinting for Bone and Cartilage Tissue Engineering. Biotechnology journal 2020;15:e2000095-n/a.

22. Derakhshanfar S, Mbeleck R, Xu K, Zhang X, Zhong W, Xing M. 3D bioprinting for biomedical devices and tissue engineering: A review of recent trends and advances. Bioactive Materials 2018;3:144-156.

23. Valot L, Martinez J, Mehdi A, Subra G. Chemical insights into bioinks for 3D printing. Chemical Society Reviews 2019; 48: 4049–4086.

24. Galante R, Pinto TJA, Colaço R, Serro AP. Sterilization of hydrogels for biomedical applications: A review. J Biomed Mater Res 2017;106:2472.

25. Axpe E, Oyen ML. Applications of Alginate-Based Bioinks in 3D Bioprinting. International journal of molecular sciences 2016;17:1976.

26. Nguyen D, Hägg DA, Forsman A, Ekholm J, Nimkingratana P, Brantsing C, et al. Cartilage Tissue Engineering by the 3D Bioprinting of iPS Cells in a Nanocellulose/Alginate Bioink. Sci Rep 2017;7: 658-10.

27. Wang X, Ao Q, Tian X, Fan J, Tong H, Hou W, et al. Gelatin-Based Hydrogels for Organ 3D Bioprinting. Polymers 2017;9:401.

28. Xu J, Zhang M, Du W, Zhao J, Ling G, Zhang P. Chitosan-based high-strength supramolecular hydrogels for 3D bioprinting. International journal of biological macromolecules 2022;219:545-557.

29. Wang H, Yu H, Zhou X, Zhang J, Zhou H, Hao H, et al. An Overview of Extracellular Matrix-Based Bioinks for 3D Bioprinting. Front Bioeng Biotechnol 2022;10: 905438.

30. López-Ruiz E, Jiménez G, Álvarez de Cienfuegos L, Antic C, Sabata R, Marcha JA, et al. Advances of hyaluronic acid in stem cell therapy and tissue engineering, including current clinical trials. European cells & materials 2019;37:186-213.

31. Neves MI, Araújo M, Moroni L, da Silva, Ricardo M P, Barrias CC. Glycosaminoglycan-Inspired Biomaterials for the Development of Bioactive Hydrogel Networks. Molecules 2020;25:978.

32. Agrawal P, Pramanik K, Vishwanath V, Biswas A, Bissoyi A, Patra PK. Enhanced chondrogenesis of mesenchymal stem cells over silk fibroin/chitosan-chondroitin sulfate three dimensional scaffold in dynamic culture condition. Journal of Biomedical Materials Research Part B: Applied Biomaterials 2018;106:2576-2587.

33. Farhat W, Chatelain F, Marret A, Faivre L, Arakelian L, Cattan P, Fuchs A. Trends in 3D bioprinting for esophageal tissue repair and reconstruction. Biomaterials 2021;267:120465.

34. Cocciolone AJ, Hawes JZ, Staiculescu MC, Johnson EO, Murshed M, Wagenseil JE. Elastin, arterial mechanics, and cardiovascular disease. American journal of physiology. Heart and circulatory physiology 2018;315:H189-H205.

35. Noh I. Biomimetic Medical Materials: From Nanotechnology to 3D Bioprinting. Springer Singapore 2018; 978-981-13-0445-3.

36. Noh I, Kim N, Tran HN, Lee J, Lee C. 3D printable hyaluronic acid-based hydrogel for its potential application as a bioink in tissue engineering. Biomater Res 2019;23.

37. Ansari S, Diniz I, Chen C, Aghaloo T, Wu B, Shi S, et al. Alginate/hyaluronic acid hydrogel delivery system characteristics regulate the differentiation of periodontal ligament stem cells toward chondrogenic lineage. J Mater Sci: Mater Med 2017;28:1-12.

38. Law N, Doney B, Glover H, Qin Y, Aman ZM, Sercombe TB, et al. Characterisation of hyaluronic acid methylcellulose hydrogels for 3D bioprinting. Journal of the Mechanical Behavior of Biomedical Materials 2018;77:389-399.

39. Siqueira P, Siqueira É, de Lima AE, Siqueira G, Pinzón-Garcia AD, Lopes AP, et al. Three-Dimensional Stable Alginate-Nanocellulose Gels for Biomedical Applications: Towards Tunable Mechanical Properties and Cell Growing. Nanomaterials 2019;9:78.

40. Choe G, Oh S, Seok JM, Park SA, Lee JY. Graphene oxide/alginate composites as novel bioinks for three-dimensional mesenchymal stem cell printing and bone regeneration applications. Nanoscale 2019;11:23275-23285.

41. Lee CH, Cook JL, Mendelson A, Moioli EK, Yao H, Mao JJ. Regeneration of the articular surface of the rabbit synovial joint by cell homing: a proof of concept study. Lancet. 2010 7;376(9739):440-8.

42. Bendtsen ST, Quinnell SP, Wei M. Development of a novel alginate-polyvinyl alcohol-hydroxyapatite hydrogel for 3D bioprinting bone tissue engineered scaffolds. J Biomed Mater Res 2017;105:1457.

43. Bai X, Gao M, Syed S, Zhuang J, Xu X, Zhang X. Bioactive hydrogels for bone regeneration. Bioactive Materials 2018;3:401-417.

44. Matai I, Kaur G, Seyedsalehi A, McClinton A, Laurencin CT. Progress in 3D bioprinting technology for tissue/organ regenerative engineering. Biomaterials 2020;226:119536.

45. Yazdanpanah Z, Johnston JD, Cooper DML, Chen X. 3D Bioprinted Scaffolds for Bone Tissue Engineering: State-Of-The-Art and Emerging Technologies. Front Bioeng Biotechnol 2022;10:824156.

46. S, Hawker GA, Gillian A, Hawker. OA serious disease. Clin Exp Rheumatol 2019;37:3.

47. Anandacoomarasamy A, March L. Current evidence for osteoarthritis treatments. Therapeutic Advances in Musculoskeletal Disease 2010;2:17-28.

48. Delplace V, Boutet M, Le Visage C, Maugars Y, Guicheux J, Vinatier C. Osteoarthritis: From upcoming treatments to treatments yet to come. Joint, bone, spine : revue du rhumatisme 2021;88:105206.

49. Dhamecha D, Movsas R, Sano U, Menon JU. Applications of alginate microspheres in therapeutics delivery and cell culture: Past, present and future. International journal of pharmaceutics 2019;569:118627.

50. Hariyadi DM, Islam N. Current Status of Alginate in Drug Delivery. Advances in pharmacological and pharmaceutical sciences 2020;2020:1-16.

51. Salimi S, Sotudeh-Gharebagh R, Zarghami R, Chan SY, Yuen KH. Production of Nanocellulose and Its Applications in Drug Delivery: A Critical Review. ACS sustainable chemistry & engineering 2019;7:15800-15827.

52. Sheikhi A, Hayashi J, Eichenbaum J, Gutin M, Kuntjoro N, Khorsandi D, et al. Recent advances in nanoengineering cellulose for cargo delivery. Journal of Controlled Release 2019;294:53-76.

53. Cañibano-Hernández A, Saenz del Burgo L, Espona-Noguera A, Orive G, Hernández RM, Ciriza J, et al. Hyaluronic Acid Promotes Differentiation of Mesenchymal Stem Cells from Different Sources toward Pancreatic Progenitors within Three-Dimensional Alginate Matrixes. Molecular Pharmaceutics 2019;16:834-845.

54. Cañibano-Hernández A, Saenz del Burgo L, Espona-Noguera A, Orive G, Hernández RM, Ciriza J, et al. Alginate Microcapsules Incorporating Hyaluronic Acid Recreate Closer in Vivo Environment for Mesenchymal Stem Cells. Molecular Pharmaceutics 2017;14:2390-2399.

55. Aamodt JM, Grainger DW. Extracellular matrix-based biomaterial scaffolds and the host response. Biomaterials 2016;86:68-82.

56. Bishnoi M, Jain A, Hurkat P, Jain S. Chondroitin sulphate: a focus on osteoarthritis. Glycoconj J 2016;33:693-705.

57. Chen Y, Lee H, Chan H, Sung L, Chen H, Hu Y. Composite chondroitin-6-sulfate/dermatan sulfate/chitosan scaffolds for cartilage tissue engineering. Biomaterials 2007;28:2294-2305.

58. Uygun BE, Stojsih SE, Matthew HWT. Effects of Immobilized Glycosaminoglycans on the Proliferation and Differentiation of Mesenchymal Stem Cells. Tissue engineering. Part A 2009;15:3499-3512.

59. Genova T, Roato I, Carossa M, Motta C, Cavagnetto D, Mussano F. Advances on Bone Substitutes through 3D Bioprinting. Int J Mol Sci 2020;21.7012.

60. Zhang J, Eyisoylu H, Qin X, Rubert M, Müller R. 3D bioprinting of graphene oxide-incorporated cell-laden bone mimicking scaffolds for promoting scaffold fidelity, osteogenic differentiation and mineralization. Acta biomaterialia 2021;121:637-652.

61. Boga JC, Miguel SP, de Melo-Diogo D, Mendonça AG, Louro RO, Correia IJ. In vitro characterization of 3D printed scaffolds aimed at bone tissue regeneration. Colloids and surfaces, B, Biointerfaces 2018;165:207-218.

62. ISO 1137-3-2018 sterilization of health care products- radiation-part 1: requirements for development, validation and routine control of a sterilization process for medical devices — amendment 2: revision to 4.3.4 and 11.2.

63. ISO 10993-5:2009 Biological Evaluation of Medical Devices. Part 5: Tests for in Vitro Cytotoxicity, International Organization for Standardization, Geneva, Switzerland, 2009.

64. Juffroy O, Noël D, Delanoye A, Viltart O, Wolowczuk I, Verwaerde C. Subcutaneous graft of D1 mouse mesenchymal stem cells leads to the formation of a bone-like structure. Differentiation (London) 2009;78:223-231.

65. Jevotovsky DS, Alfonso AR, Einhorn TA, Chiu ES. Osteoarthritis and stem cell therapy in humans: a systematic review. Osteoarthritis and cartilage 2018;26:711-729.

66. Amorim PA, d'Ávila MA, Anand R, Moldenaers P, Van Puyvelde P, Bloemen V. Insights on shear rheology of inks for extrusion-based 3D bioprinting. Bioprinting 2021;22:e00129.

67. Müller M, Öztürk E, Arlov Ø, Gatenholm P, Zenobi-Wong M. Alginate Sulfate–Nanocellulose Bioinks for Cartilage Bioprinting Applications. Ann Biomed Eng 2017;45:210-223.

68. Shin YJ, Shafranek RT, Tsui JH, Walcott J, Nelson A, Kim D. 3D bioprinting of mechanically tuned bioinks derived from cardiac decellularized extracellular matrix. Acta biomaterialia 2021;119:75-88.

69. Park H, Lee HJ, An H, Lee KY. Alginate hydrogels modified with low molecular weight hyaluronate for cartilage regeneration. Carbohydrate polymers 2017;162:100-107.

70. Gao T, Gillispie GJ, Copus JS, Pr AK, Seol Y, Atala A, et al. Optimization of gelatin–alginate composite bioink printability using rheological parameters: a systematic approach. Biofabrication 2018;10: 034106.

71. Antich C, de Vicente J, Jiménez G, Chocarro C, Carrillo E, Montañez E, et al. Bio-inspired hydrogel composed of hyaluronic acid and alginate as a potential bioink for 3D bioprinting of articular cartilage engineering constructs. Acta Biomaterialia 2020;106:114-123.

72. Sakai S, Ohi H, Taya M. Gelatin/Hyaluronic Acid Content in Hydrogels Obtained through Blue Light-Induced Gelation Affects Hydrogel Properties and Adipose Stem Cell Behaviors. Biomolecules 2019;9:342.

73. Mihajlovic M, Rikkers M, Mihajlovic M, Viola M, Schuiringa G, Ilochonwu BC, et al. Viscoelastic Chondroitin Sulfate and Hyaluronic Acid Double-Network Hydrogels with Reversible Cross-Links. Biomacromolecules 2022;23:1350.

74. Lujan TJ, Underwood CJ, Jacobs NT, Weiss JA. Contribution of glycosaminoglycans to viscoelastic tensile behavior of human ligament. Journal of Applied Physiology 2009;106:423-431.

75. Silipo A, Zhang Z, Cañada FJ, Molinaro A, Linhardt RJ, Jiménez-Barbero J. Conformational Analysis of a Dermatan Sulfate-Derived Tetrasaccharide by NMR, Molecular Modeling, and Residual Dipolar Couplings. Chembiochem: a European journal of chemical biology 2008;9:240-252.

76. Hodder E, Duin S, Kilian D, Ahlfeld T, Seidel J, Nachtigall C, et al. Investigating the effect of sterilisation methods on the physical properties and cytocompatibility of methyl cellulose used in combination with alginate for 3D-bioplotting of chondrocytes. J Mater Sci: Mater Med 2019;30:1-16.

77. Driscoll M, Stipanovic A, Winter W, Cheng K, Manning M, Spiese J, et al. Electron beam irradiation of cellulose. Radiation physics and chemistry 2009;78:539-542.

78. EL-Ashhab F, Sheha L, Abdalkhalek M, Khalaf HA. The influence of gamma irradiation on the intrinsic properties of cellulose acetate polymers. Journal of the Association of Arab Universities for Basic and Applied Sciences 2013;14:46-50.

79. Lierova A, Kasparova J, Pejchal J, Kubelkova K, Jelicova M, Palarcik J, et al. Attenuation of Radiation-Induced Lung Injury by Hyaluronic Acid Nanoparticles. Frontiers in pharmacology 2020;11:1199.

80. Prieto JG, Pulido MM, Zapico J, Molina AJ, Gimeno M, Coronel P, et al. Comparative study of hyaluronic derivatives: rheological behaviour, mechanical and chemical degradation. International Journal of Biological Macromolecules 2005;35:63-69.

81. O'Connell CD, Onofrillo C, Duchi S, Li X, Zhang Y, Tian P, et al. Evaluation of sterilisation methods for bio-ink components: gelatin, gelatin methacryloyl, hyaluronic acid and hyaluronic acid methacryloyl. Biofabrication 2019;11:035003.

82. Sánchez-Fernández JA, Presbítero-Espinosa G, Peña-Parás L, Pizaña EIR, Galván KPV, Vopálenský M, et al. Characterization of Sodium Alginate Hydrogels Reinforced with Nanoparticles of Hydroxyapatite for Biomedical Applications. Polymers 2021;13:2927.

83. Compton BG, Hmeidat NS, Pack RC, Heres MF, Sangoro JR. Electrical and Mechanical Properties of 3D-Printed Graphene-Reinforced Epoxy. JOM 2017;70:292-297.

84. Mittal S, Kumar V, Dhiman N, Chauhan LKS, Pasricha R, Pandey AK. Physico-chemical properties based differential toxicity of graphene oxide/reduced graphene oxide in human lung cells mediated through oxidative stress. Sci Rep 2016;6: 39548.

85. Zhang J, Cao H, Wang J, Wu G, Wang L. Graphene Oxide and Reduced Graphene Oxide Exhibit Cardiotoxicity Through the Regulation of Lipid Peroxidation, Oxidative Stress, and Mitochondrial Dysfunction. Frontiers in cell and developmental biology 2021;9:616888.

86. Park H, Choi B, Hu J, Lee M. Injectable chitosan hyaluronic acid hydrogels for cartilage tissue engineering. Acta Biomaterialia 2013;9:4779-4786.

87. Yamada S, Sugahara K. Potential Therapeutic Application of Chondroitin Sulfate/Dermatan Sulfate. Current drug discovery technologies 2008;5:289-301.

88. Ghitman J, Biru EI, Cojocaru E, Pircalabioru GG, Vasile E, Iovu H. Design of new bioinspired GO-COOH decorated alginate/gelatin hybrid scaffolds with nanofibrous architecture: structural, mechanical and biological investigations. RSC advances 2021;11:13653-13665.

89. Lasocka I, Szulc-Dąbrowska L, Skibniewski M, Skibniewska E, Strupinski W, Pasternak I, et al. Biocompatibility of pristine graphene monolayer: Scaffold for fibroblasts. Toxicology in vitro 2018;48:276-285.

90. Boularaoui S, Al Hussein G, Khan KA, Christoforou N, Stefanini C. An overview of extrusion-based bioprinting with a focus on induced shear stress and its effect on cell viability. Bioprinting 2020;20:e00093.

91. Fakhruddin K, Hamzah MSA, Razak SIA. Effects of extrusion pressure and printing speed of 3D bioprinted construct on the fibroblast cells viability. IOP Conf Ser: Mater Sci Eng 2018;440:012042.

92. Semba JA, Aron Mieloch A, Tomaszewska E, Cywoniuk P, Dalibor Rybka J. Formulation and evaluation of a bioink composed of alginate, gelatin, and nanocellulose for meniscal tissue engineering. Int J Bioprint 2022;9:621.

93. Echave MC, Erezuma I, Golafshan N, Castilho M, Kadumudi FB, Pimenta-Lopes C, et al. Bioinspired gelatin/bioceramic composites loaded with bone morphogenetic protein-2 (BMP-2) promote osteoporotic bone repair. Materials Science & Engineering C 2021:112539.

94. Espona-Noguera A, Ciriza J, Cañibano-Hernández A, Fernandez L, Ochoa I, Saenz del Burgo L, et al. Tunable injectable alginate-based hydrogel for cell therapy in Type 1 Diabetes Mellitus. International Journal of Biological Macromolecules 2018;107:1261-1269.

95. Olmos-Juste R, Alonso-Lerma B, Pérez-Jiménez R, Gabilondo N, Eceiza A. 3D printed alginate-cellulose nanofibers based patches for local curcumin administration. Carbohydrate polymers 2021;264:118026.

96. Sun J, Li L, Xing F, Yang Y, Gong M, Liu G, et al. Graphene oxide-modified silk fibroin/nanohydroxyapatite scaffold loaded with urine-derived stem cells for immunomodulation and bone regeneration. Stem cell research & therapy 2021;12:591.

97. Cun X, Hosta-Rigau L. Topography: A Biophysical Approach to Direct the Fate of Mesenchymal Stem Cells in Tissue Engineering Applications. Nanomaterials 2020;10:2070.

98. Dank A, Aartman IHA, Wismeijer D, Tahmaseb A. Effect of dental implant surface roughness in patients with a history of periodontal disease: a systematic review and meta-analysis. International journal of implant dentistry 2019;5:12-11.

99. Yu Z, Xiao C, Huang Y, Chen M, Wei W, Yang X, et al. Enhanced bioactivity and osteoinductivity of carboxymethyl chitosan/nanohydroxyapatite/graphene oxide nanocomposites. RSC advances 2018;8:17860-17877.

100. Juhl 4, Otto J, Merife A, Zhang Y, Lemmon CA, Donahue HJ. Hydroxyapatite Particle Density Regulates Osteoblastic Differentiation Through β-Catenin Translocation. Frontiers in bioengineering and biotechnology 2020;8:591084.

101. Park H, Guo X, Temenoff JS, Tabata Y, Caplan AI, Kasper FK, et al. Effect of Swelling Ratio of Injectable Hydrogel Composites on Chondrogenic Differentiation of Encapsulated Rabbit Marrow Mesenchymal Stem Cells In Vitro. Biomacromolecules 2009;10:541-546.

102. Mahinroosta M, Jomeh Farsangi Z, Allahverdi A, Shakoori Z. Hydrogels as intelligent materials: A brief review of synthesis, properties and applications. Materials today chemistry 2018;8:42-55.

103. Guo Y, Yuan T, Xiao Z, Tang P, Xiao Y, Fan Y, et al. Hydrogels of collagen/chondroitin sulfate/hyaluronan interpenetrating polymer network for cartilage tissue engineering. J Mater Sci: Mater Med 2012;23:2267-2279.

104. Suvarnapathaki S, Wu X, Lantigua D, Nguyen MA, Camci-unal G. Hydroxyapatite-Incorporated Composite Gels Improve Mechanical Properties and Bioactivity of Bone Scaffolds. Macromol Biosci 2020;20:e2000176.

105. Lian B, De Luca S, You Y, Alwarappan S, Yoshimura M, Sahajwalla V, et al. Extraordinary water adsorption characteristics of graphene oxide. Chem Sci 2018;9:5106.

106. Wu Z, Su X, Xu Y, Kong B, Sun W, Mi S. Bioprinting three-dimensional cell-laden tissue constructs with controllable degradation. Scientific reports 2016;6:24474.

107. Eglin D, Mortisen D, Alini M. Degradation of synthetic polymeric scaffolds for bone and cartilage tissue repairs. Soft Matter 2009;5:938-947.

108. Guarino V, Caputo T, Altobelli R, Ambrosio L. Degradation properties and metabolic activity of alginate and chitosan polyelectrolytes for drug delivery and tissue engineering applications. AIMS materials science 2015;2:497-502.

109. Nesic D, Whiteside R, Brittberg M, Wendt D, Martin I, Mainil-Varlet P. Cartilage tissue engineering for degenerative joint disease. Advanced drug delivery reviews 2006;58:300-322.

110. Kim HD, Amirthalingam S, Kim SL, Lee SS, Rangasamy J, Hwang NS. Biomimetic Materials and Fabrication Approaches for Bone Tissue Engineering. Adv Healthcare Mater 2017;6:23.

111. Farrugia BL, Lord MS, Whitelock JM, Melrose J. Harnessing chondroitin sulphate in composite scaffolds to direct progenitor and stem cell function for tissue repair. Biomaterials science 2018;6:947-957.

112. Criado M, Rey JM, Mijangos C, Hernández R. Double-membrane thermoresponsive hydrogels from gelatin and chondroitin sulphate with enhanced mechanical properties. RSC advances 2016;6:105821-105826.

113. Hall ML, Krawczak DA, Simha NK, Lewis JL. Effect of dermatan sulfate on the indentation and tensile properties of articular cartilage. Osteoarthritis and cartilage 2008;17:655-661.

114. Raslan A, Saenz del Burgo L, Ciriza J, Pedraz JL. Graphene oxide and reduced graphene oxide-based scaffolds in regenerative medicine. International journal of pharmaceutics 2020;580:119226.

115. Singh YP, Bandyopadhyay A, Mandal BB. 3D Bioprinting Using Cross-Linker-Free Silk–Gelatin Bioink for Cartilage Tissue Engineering. ACS applied materials & interfaces 2019;11:33684-33696.

116. Guimarães, C.F., Gasperini, L., Marques, A.P. et al. The stiffness of living tissues and its implications for tissue engineering. Nat Rev Mater 2020; 5: 351–370.

117. Levett PA, Hutmacher DW, Malda J, Klein TJ. Hyaluronic Acid Enhances the Mechanical Properties of Tissue-Engineered Cartilage Constructs. PLoS ONE 2014;9: e113216.

118. Cao Y, Cheng P, Sang S, Xiang C, An Y, Wei X, et al. Mesenchymal stem cells loaded on 3D-printed gradient poly(ε-caprolactone)/methacrylated alginate composite scaffolds for cartilage tissue engineering. Regenerative biomaterials 2021;8:rbab019.

119. Zhang R, Ma J, Han J, Zhang W, Ma J. Mesenchymal stem cell related therapies for cartilage lesions and osteoarthritis. Am J Transl Res. 2019; 15;11(10):6275-6289.

120. Solorio LD, Fu AS, Hernández-Irizarry R, Alsberg E. Chondrogenic differentiation of human mesenchymal stem cell aggregates via controlled release of TGF-β1 from incorporated polymer microspheres. Journal of Biomedical Materials Research Part A 2010;92A:1139-1144.

121. Chatterjea A, LaPointe VLS, Barradas A, Garritsen H, Yuan H, Renard A, et al. Cell agreggation enhances bone formation by human mesenchymal stromal cells. Cells & Materials 2017;33:121-129.

122. Zhao H, Zhang Y, Liu Y, Zheng P, Gao T, Cao Y, et al. In Situ Forming Cellulose Nanofibril-Reinforced Hyaluronic Acid Hydrogel for Cartilage Regeneration. Biomacromolecules 2021;22:5097.

123. Motokawa K, Hahn SK, Nakamura T, Miyamoto H, Shimoboji T. Selectively crosslinked hyaluronic acid hydrogels for sustained release formulation of erythropoietin. Journal of Biomedical Materials Research Part A 2006;78A:459-465.

124. Ishikawa S, Iijima K, Sasaki K, Hashizume M, Kawabe M, Otsuka H. Cartilage Differentiation of Bone Marrow-Derived Mesenchymal Stem Cells in Three-Dimensional Silica Nonwoven Fabrics. Applied sciences 2018;8:1398.

125. Toh WS, Guo X, Choo AB, Lu K, Lee EH, Cao T. Differentiation and enrichment of expandable chondrogenic cells from human embryonic stem cells in vitro. Journal of cellular and molecular medicine 2009;13:3570-3590.

126. Di Crescenzo A, Zara S, Di Nisio C, Ettorre V, Ventrella A, Zavan BD, et al. Graphene Oxide Foils as an Osteoinductive Stem Cell Substrate. ACS Appl Bio Mater 2019;2:1643.

127. Zhang Y, Wu C, Guo S, Zhang J. Interactions of graphene and graphene oxide with proteins and peptides. Nanotechnology reviews 2013;2:27-45.

128. Ciriza J, Saenz del Burgo L, Virumbrales-Muñoz M, Ochoa I, Fernandez LJ, Orive G, et al. Graphene oxide increases the viability of C2C12 myoblasts microencapsulated in alginate. International journal of pharmaceutics 2015;493:260-270.

129. Saenz Del Burgo L, Ciriza J, Acarregui A, Gurruchaga H, Blanco FJ, Orive G, et al. Hybrid Alginate–Protein-Coated Graphene Oxide Microcapsules Enhance the Functionality of Erythropoietin Secreting C2C12 Myoblasts. Mol Pharmaceutics 2017;14:885.

128. You F, Chen X, Cooper DML, Chang T, Eames BF. Homogeneous hydroxyapatite/alginate composite hydrogel promotes calcified cartilage matrix deposition with potential for three-dimensional bioprinting. Biofabrication 2018;11:015015.

129. Zhang J, Eyisoylu H, Qin X, Rubert M, Müller R. 3D bioprinting of graphene oxide-incorporated cell-laden bone mimicking scaffolds for promoting scaffold fidelity, osteogenic differentiation and mineralization. Acta biomaterialia 2021;121:637-652.

130. Komori T. Signaling networks in RUNX2-dependent bone development. Journal of cellular biochemistry 2011;112:750-755.

131. Zhang J, Zhang F, Yang H, Huang X, Liu H, Zhang J, et al. Graphene Oxide as a Matrix for Enzyme Immobilization. Langmuir 2010;26:6083-6085.

132. Huang CK, Weibiao H, Zuk P, Jarrahy R, Rudkin GH, Ishida K, et al. Genetic Markers of Osteogenesis and Angiogenesis Are Altered in Processed Lipoaspirate Cells when Cultured on Three-Dimensional Scaffolds. Plastic and reconstructive surgery 2008;121:411-423.

Chapter 2

CONCLUSIONS

Taking into account the results obtained in the experimental works, the conclusions of this thesis are the following:

1. The NC-Alg bioink shows proper rheological properties to be extruded through extrusion-based bioprinting demonstrating good printability as well as scaffold formation. Moreover, the NC-Alg scaffolds possess good biological properties since cells are alive and metabolically active after bioprinting.

2. The HA inclusion into the NC-Alg bioink enhances the bioink mechanical properties regarding viscosity. Thus, HA improves printability and scaffold formation. Likewise, the HA promotes the viability, proliferation and metabolic activity of embedded D1-MSCs after bioprinting.

3. The autoclave sterilisation is the best option to sterilise NC-Alg-based bioinks compared to ionic radiation sterilisation such as β-radiation and γ-radiation. Additionally, between autoclave cycles, short-cycle autoclave shows to be the one that least alters the bioinks rheological properties. However, it was discarded for sterilising GO-containing bioinks due to GO chemical reduction.

4. The addition of CS and DS increases the NC-Alg bioink rheological properties, but CS further enhances the viscoelastic properties resulting in better printability and scaffold shape fidelity. Moreover, CS increases the scaffolds' biomechanics. Both, CS and DS, promote embedded cells' viability, proliferation and functionality. A chondrogenic differentiation pathway is observed by D1-MSCs inside CS and DS-containing scaffolds. Nevertheless, the DS addition further promotes cartilage formation.

5. The addition of HAP and GO reduces the rheological properties loss due to short-cycle autoclave sterilisation on NC-Alg bioink. Both, HAP and GO, increase scaffold mechanical properties, being GO the best compound to elevate the mechanics. The HAP and GO addition improve the bioink biological properties since embedded cells' viability, proliferation and metabolic activity are increased after bioprinting. The GO addition promotes a clear osteogenic

differentiation of embedded D1-MSCs.

6. The use of NC-Alg-based bioinks may be an excellent therapeutic approach for tissue regeneration since these bioinks are manageable through 3D bioprinting allowing the simulation of patient-specific demands. More specifically, these scaffolds may repair osteochondral defects as cells are viable, functional and able to differentiate into osteochondral cells.

Chapter 3

APPENDICES

Appendix 1

Progress in 3D Bioprinting Technology for Osteochondral Regeneration

Markel Lafuente-Merchan[1,2,3], Sandra Ruiz-Alonso[1,2,3], Fátima García-Villén[1,2,3] , Idoia Gallego[1,2,3], Patricia Gálvez-Martín[4], Laura Saenz-del-Burgo[1,2,3*] and José Luis Pedraz [1,2,3*]

[1] NanoBioCel Group, Laboratory of Pharmaceutics, School of Pharmacy, University of the Basque Country (UPV/EHU), Paseo de la Universidad 7, 01006 Vitoria-Gasteiz, Spain.
[2] Biomedical Research Networking Center in Bioengineering, Biomaterials and Nanomedicine (CIBER-BBN), Health Institute Carlos III, Paseo de la Universidad 7, 01006 Vitoria-Gasteiz, Spain.
[3] Bioaraba, NanoBioCel Research Group, 01009 Vitoria-Gasteiz, Spain.
[4] R&D Animal and Human Health, Bioibérica S.A.U., 08029 Barcelona, Spain.
[*] Correspondence: laura.saenzdelburgo@ehu.eus (L.S.-d.-B.); joseluis.pedraz@ehu.eus (J.L.P.)

Pharmaceutics 2022, 14:1578.
IF: 6.525 (2021) (Q1)
Cat: Pharmacology & Pharmacy
https://doi.org/10.3390/pharmaceutics14081578

Abstract

Osteochondral injuries can lead to osteoarthritis (OA). OA is characterized by the progressive degradation of the cartilage tissue together with bone tissue turnover. Consequently, joint pain, inflammation, and stiffness are common, with joint immobility and dysfunction being the most severe symptoms. The increase in the age of the population, along with the increase in risk factors such as obesity, has led OA to the forefront of disabling diseases. In addition, it not only has an increasing prevalence, but is also an economic burden for health systems. Current treatments are focused on relieving pain and inflammation, but they become ineffective as the disease progresses. Therefore, new therapeutic approaches, such as tissue engineering and 3D bioprinting, have emerged. In this review, the advantages of using 3D bioprinting techniques for osteochondral regeneration are described. Furthermore, the biomaterials, cell types, and active molecules that are commonly used for these purposes are indicated. Finally, the most recent promising results for the regeneration of cartilage, bone, and/or the osteochondral unit through 3D bioprinting technologies are considered, as this could be a feasible therapeutic approach to the treatment of OA.

Keywords: 3D bioprinting; osteoarthritis; tissue engineering; regenerative medicine; cartilage; bone.

1. Introduction

The aging of the population, together with the increase in the prevalence of risk factors such as obesity, physical inactivity, and extreme exercise, has placed osteoarticular diseases in the focus of medicine. Osteochondral defects are characterized by cartilage disruption together with bone damage. Joint traumas and injuries are the most common causes of osteochondral defects [1]. Nevertheless, joint tumors and infections can also be the triggers of osteochondral damage [2,3]. Furthermore, the rare disease osteochondritis dissecans should be also taken into consideration [4]. However, among them, osteoarthritis (OA) has gained notoriety by becoming the third most common condition associated with disability, after dementia and diabetes [5]. In fact, it is estimated that 250 million people are affected worldwide, and that the proportion of the population with an OA diagnosis will increase by 3% by the year 2032 [6]. This increase in prevalence will not only worsen the quality of life of the affected population, but will also entail an economic cost to healthcare systems.

1.1. Prevalence and Economic Burden

OA is a disease of the joints such as the knee, hip, and hand that affects 7% of the world population [7]. For example, in the US alone, 37% of people over the age of 65 suffer from this disease [8]. Age is the most important risk factor for the onset of the disease. Likewise, obesity is considered to be another important factor that contributes to the appearance of OA. In fact, due to the aging of the population and the rise in obesity rates, the prevalence of OA has risen by 48% in the last 30 years [9]. Furthermore, it is estimated that the prevalence of OA in the population aged over 45 will increase in the coming years. In addition, it has been shown that hard work activities, high-impact sports, and genetics can also influence the appearance of OA in younger individuals [6].

Given the increase in the disease's incidence, the economic costs associated with OA must be considered as another problem. In the US, it is estimated that the economic burden ranges between USD 3.4 and 13.2 billion per year

[8]. Globally, it is estimated that the medical costs associated with OA in rich countries are between 1 and 2.5% of the gross domestic product [6,10]. However, indirect costs due to work loss, medical leave, and premature retirements could increase the economic burden [11]. In fact, according to the World Health Organization (WHO), OA is in the top 10 diseases that cause work loss due to disability [12]. When it comes to indicating each cost separately, there is considerable disagreement in the literature due to the lack of uniform criteria across the studies, the country where the study was carried out, and the anatomical location and stage of OA [13]. For instance, in Spain, the annual cost is estimated at around EUR 1500 per patient. In addition, Loza et al. [13] conducted a breakdown of the economic expenses associated with knee and hip OA in Spain (Figure 1). According to them, direct costs were around 86%, which could be separated into medical costs (47%) and nonmedical costs (39%). Medical costs included expenses in terms of sanitary professional time (22%), hospital admissions (13%), medical tests and probes (7%), and drug costs (5%). Nonmedical costs were mainly related to house, work, and self-care assistance (29%), aid services (9%), and patient transport costs (1%). On the other hand, indirect costs were estimated to account for 14%; 8% went on assistance for housework, and 6% was due to loss of work, workplace absences, and a decrease in productivity [14]. Nevertheless, the total cost of OA drastically increased when the disease was in the severe stages and when the patients required hospitalization [13].

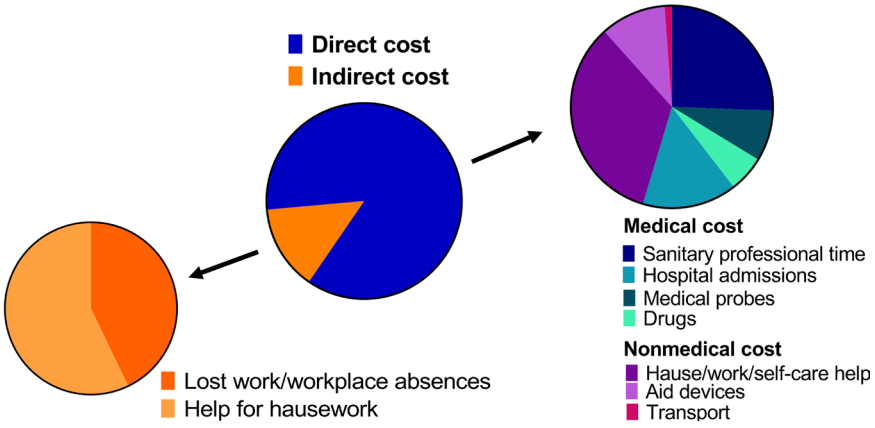

Figure 1. The economic cost of knee and hip OA in Spain. Data from [14].

Due to the increase in cases that not only worsen the quality of life of those affected patients, but also have a great economic cost, improvement of the treatment of this disease is a necessity.

Current treatments are mainly based on palliative drugs, with surgery being the last resort, and only in the most severe cases. However, as these treatments have been shown to be ineffective in the majority of cases, there is a necessity in the scientific community to develop new therapeutic approaches. In this regard, tissue engineering has drawn attention, since it combines different biomedical fields such as cell therapy, nanotechnology, and biomaterial science [15]. Furthermore, additive manufacturing technologies such as 3D bioprinting have emerged to facilitate tissue engineering purposes in a rapid and automatic manner [16]. Thus, the biofabrication of functional scaffolds that could regenerate damaged tissues is currently at its peak. However, prior to the fabrication of artificial tissues, it is necessary to achieve in-depth knowledge of the osteochondral tissue and OA.

1.2. Joint Anatomy and Physiology

Injuries to the osteochondral tissue may lead to OA. Thus, OA is a disorder that affects the whole joint [6]. Joints are areas of articulation between adjacent bones and cartilage for the purpose of providing stability and mobility [17]. Figure 2 shows the schematic organization of the joint tissue separated into two areas: cartilage and bone. At the same time, both cartilage and bone have different layers with their own composition and characteristics.

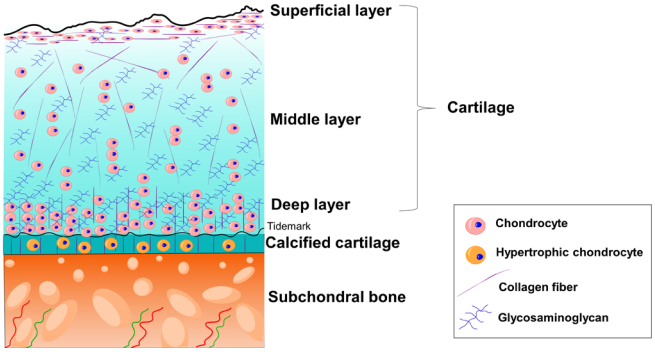

Figure 2. Schematic organization of osteochondral tissue.

Cartilage is an avascular, aneural, and alymphatic tissue that is found at the end of long bones [6]. It is composed of highly specialized cells known as chondrocytes and an extracellular matrix (ECM). This ECM is constituted of glycosaminoglycans (GAGs) and collagens that allow the retention of large amounts of water. Considering the avascular nature of the cartilage, this fluid not only allows the chondrocytes to be supplied with nutrients, but is also responsible for providing resistance to mechanical compression [18]. Consequently, cartilage is a tissue with significant biomechanics. For instance, the Young's modulus of cartilage is between 0.2 and 2 MPa [19]. At the same time, the articular cartilage is morphologically classified into three zones depending on chondrocyte organization, collagen fibril orientation, and GAG content.

The superficial layer is the thinner layer, and protects deeper layers from shear stresses. It is characterized by flattered chondrocytes, collagen fibrils oriented parallel to the articular surface, and low GAG content. The middle layer is the thickest layer, and functions as an anatomical and functional zone between the superficial layer and the deep layer. Chondrocytes are at low density and spherical, collagen fibrils are obliquely oriented, and the GAG content is increased. This layer is the first line of resistance to compressive forces. Finally, there is the deep layer. In this zone, chondrocyte density is increased, and they are arranged in columnar orientation. Collagen fibrils are orientated perpendicular to the surface, and the GAG content is the highest. The deep layer provides the greatest resistance to compressive forces [20–22].

Between the bone and the cartilage, there is a zone called calcified cartilage. This layer is separated from the deep cartilage layer by a boundary called the tidemark that represents the mineralization front [20,23]. Calcified cartilage is composed of hypertrophic chondrocytes, and its main function is to maintain the adhesion of the cartilage to the bone by anchoring the collagen fibrils of the deep zone to the subchondral bone [20,22–24].

Bone tissue, known as subchondral bone, is a fundamental tissue for the joint's proper functionality, since it absorbs the impacts and provides support. In addition, it distributes the mechanical loads throughout the joint with a gradual transition in stress and strain. In fact, bone is considered to be a hard

tissue, and its average Young's modulus ranges from 10 to 20 GPa [25]. This tissue is separated into two zones: subchondral bone plate and subchondral bone trabeculae. The first layer is a thin cortical lamella lying immediately under the calcified cartilage. It is composed of channels to circulate blood and lymphatic fluid from the bone trabeculae to the cartilage. In contrast, the subchondral bone trabeculae are more porous and metabolically active. They contain blood vessels, nerves, and bone marrow that supply the cartilage with nutrients and help in its metabolism [20,23,24].

Apart from osteochondral tissue, the joint unit is also composed of the synovial membrane and synovial fluid, which are involved in the pathogenesis of OA. The synovial membrane is a thin, non-articular layer composed of two cell types: (i) macrophages as a part of the immune system in the joint, and (ii) fibroblasts that secrete synovial fluid. Synovial fluid acts as a lubricant for the articular surface, and transports nutrients to the cartilage [17,20,24].

1.3. OA: Pathogenesis and Symptomatology

In OA, structural alterations in the articular cartilage and subchondral bone are found. As Figure 3 shows, cartilage loses its integrity and, thus, is more exposed to disruption from physical forces. To counteract cartilage erosion, chondrocytes increase the secretion of molecules that cause matrix degradation and pro-inflammatory mediators. On the other hand, bone turnover is increased, developing bone marrow lesions. In addition, there is a vascular invasion throughout the area, and the synovial membrane hypertrophies and macrophages are activated, releasing pro-inflammatory cytokines. Moreover, surrounding tissues, such as ligaments and periarticular muscles, are often affected as well [6]. OA is classified into four different stages, depending on the severity grade and the appearance of the symptoms.

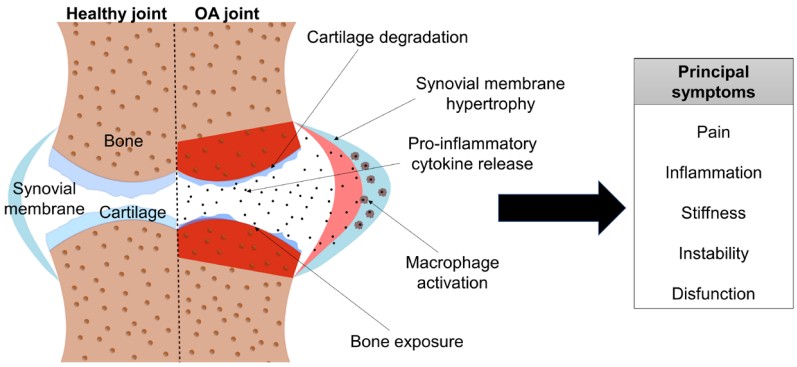

Figure 3. Schematic image of OA's pathology and symptoms.

In stage 0, also known as the pre-osteoarthritis stage, the joint seems normal and healthy. Nevertheless, cellular damage starts to occur without any symptoms. Stage 1, or the early stage, is characterized by the appearance of bone spurs, and cartilage begins to lose its integrity. In this stage the patient usually has no symptoms or only mild pain. Then, in the next stage-stage 2, or the mild stage-the cartilage starts to degrade due to enzyme release. Consequently, bone spurs grow and become painful. Joint pain and stiffness commonly appear during activities at this stage. As the disease progresses, stage 3 or the moderate stage appears. Here, cartilage shows obvious damage, and the space between the joints becomes narrower. Therefore, pain while moving is frequent, and joint stiffness worsens. Finally, stage 4, or severe OA, occurs. This stage is characterized by the presence of little cartilage or the absence of cartilage in severe cases. Synovial fluid is reduced, and bone may erode, provoking bone narrow damage. At this stage, significant pain and discomfort appear, stiffness and inflammation are severe, and joint dysfunction may occur [26–28].

In summary, affected people experience pain and inflammation, which are the most common and disabling symptoms. Moreover, muscle weakness and joint instability are frequent symptoms. Apart from physical symptomatology, psychological disorders due to pain together with insomnia and fatigue should be taken into account [6,9].

2. Current Treatments

OA is a progressive and degenerative joint disease with no cure. Treatments in the early stages of OA are focused on giving educational information to patients, weight loss, and moderate physical exercise, whereas when the disorder progresses, current treatment is based on alleviating the main disabling symptom, the chronic pain [29]. Therapeutic guidelines recommend starting with topical treatment and moving on to oral treatment when topical drugs do not relieve the pain. In more advanced stages of OA, intra-articular injections are the recommended treatment. Finally, when OA is in the severe stages and the aforementioned treatment becomes ineffective, surgery may be recommended. All of these treatments are summarized in Table 1.

Table 1. Summary of the benefits and side effects of the current treatments for OA.
Acronyms. OA: osteoarthritis; NSAIDs: nonsteroidal anti-inflammatory drugs; SYSADOA: Symptomatic slow-acting drugs in osteoarthritis; HA: hyaluronic acid; PRP: platelet rich plasma.

Treatment	Positive effects	Side effects
Acetaminophen or paracetamol	- First choice treatment - Good relieving pain	- Controversy about the effectiveness at long-term - Not anti-inflammatory effects - Hepatotoxic in abuse
Oral NSAIDs	- First choice treatment - Good relieving pain and improving joint function	- Gastrointestinal and cardiac issues at long-term and in abuse
SYSADOA	- Safe and well-tolerated - Pain relief and improvement in joint physical function	- Unclear therapeutic mechanisms - Discrepancies among therapeutic guides
Intra-articular injectable HA	- Safe and well-tolerated -Anti-inflammatory effects and pain reduction	- Benefits only at a short-term period - Repetitive intra-articular injections - Only in mild and moderate stages of OA
Intra-articular injectable corticosteroids	- Good reducing joint inflammation and dysfunction	- Benefits only at a short-term period - Repetitive intra-articular injections - Controversial benefits in no knee joints and at long-term period

Treatment	Positive effects	Side effects
Opiates	- Excellent pain killers when other treatments failed	- Tolerance and dependence - Negative benefit/risk ratio - Highly discouraged
Surgery	- Lasts therapeutic option - Relevant improvement specially in young patients	- More likely to have complications associated with surgery in the elderly population - Rejection probability - Pain is still recurrent
PRP	- OA symptoms relief	- Limited to knee - Variability among patients - Unclear dosage and plasma extraction protocols - Efficacy decreases with NSAIDs
Spherox™	- Osteochondral regeneration - General improvement	- Not available in all the hospitals - Highly costs and long regulatory procedures - Contraindicated in advanced OA - Only applicable for knee defects

2.1. Pharmacological Treatments

Topical treatment is based on topical nonsteroidal anti-inflammatory drugs (NSAIDs). These demonstrate good effectiveness for pain reduction, and the side effects that they may produce are rare. As they are usually well-tolerated and have an easy mode of administration, they are highly recommended in the first stages of the disease. Nevertheless, they become ineffective as the disease progresses and the pain increases [6,30,31].

When pain increases, oral drug intake is recommended. Among the used drugs, acetaminophen or paracetamol is a well-known drug to reduce mild-to-moderate pain [6,30]. It is usually prescribed because several guidelines recommend it for OA. However, there is an increasing controversy about its efficacy in this illness. Meta-analyses have revealed little in the way of satisfactory effects in comparison with placebo [6,30]. Furthermore, the hepatotoxic side effects after long-term usage with high doses are a drawback

to take into account [30]. Therefore, the use of this drug may be restricted to short-term periods [31].

NSAIDs are the treatment of choice, since it has been shown that they decrease pain and improve joint function [30]. However, long-term treatments at high doses have considerable side effects, such as gastrointestinal issues and nephrotoxicity [30,31]. COX2-selective inhibitors are a form of NSAIDs that may avoid these problems, but are contraindicated in patients with cardiovascular problems [31]. As a consequence, their use should be restricted to short treatment periods, making a good therapeutic approach for chronic diseases such as OA impossible.

Symptomatic slow-acting drugs in OA (SYSADOA), such as glucosamine and chondroitin sulfate (CS), are widely prescribed. CS is a GAG naturally found in the ECM, whereas glucosamine is a metabolic precursor of GAGs. There is much controversy in the literature regarding the use of these substances. They have the advantage of being safe and showing almost no side effects, but their therapeutic mechanism is unclear, and while some meta-analyses indicate their potential benefits in pain relief and improvement in physical joint function, others strongly discourage their use [30,31].

For patients who do not respond well to oral treatments, intra-articular injections of hyaluronic acid (HA) are recommended. HA is a molecule from the group of GAGs that are naturally found in the joints' synovial fluid. Its main function is the lubrication of the joints. It has also been reported to be chondroprotective against mechanical damage. It has been found that intra-articular injections of HA reduce pain, have anti-inflammatory effects, and promote GAG synthesis. It is generally safe and effective in mild-to-moderate stages of knee OA. As a drawback, its long-term effects are limited, and repetitive injections of HA are usually uncomfortable for patients [30,31].

In addition, intra-articular corticosteroids are very common drugs used to treat inflammatory-related diseases; therefore, they are expected to be beneficial to treat OA as well, by reducing joint inflammation, pain, and dys-

function. All of the clinical evidence has demonstrated pain reduction after corticosteroid injections. Nevertheless, this benefit has only been observed in short-term periods, and repetitive injections have not been associated with long-term pain reduction. In addition, as the studies have focused on knee joint treatment, whether these drugs are beneficial for other joints is unclear. Furthermore, a recent meta-analysis showed little improvement in joint function, and reported greater cartilage damage than in the placebo group after 2 years of corticosteroid administration. Thus, the use of this kind of drug for OA treatment has become controversial [6,30].

As an alternative, some guidelines recommend the use of opiates. Although they are quite effective in relieving pain, the side effects that they produce are extensive and serious, such as tolerance and dependence. In fact, opioid abuse has been recognized as an epidemic in the US, where great efforts are being made in order to reduce their use [32]. Apart from this serious problem, opioids have shown only a small improvement in the OA symptomatology, with an increase in side effects after opiate administration. Thus, the use of opiates is highly discouraged, and they should only be prescribed for short-term treatments and when other therapeutic options are not possible [6,30,31].

2.2. Surgery

Different surgical interventions have been carried out in the clinics. A bone marrow stimulation technique known as microfracture is recommended to treat small chondral defects (less than 2 cm^2). When the disease reaches the subchondral bone, osteochondral autograft transplantation is the suggested option. This surgical procedure is divided into mosaicplasty, which is based on transplanting multiple small, circular osteochondral grafts, and the single-plug technique, which consists of implanting a single, larger graft. Excellent results have been reported after the implementation of both techniques, but there are still disadvantages in terms of donor site morbidity and patient age limitation, as the procedure is restricted to patients over 50 years old [33]. In order to treat greater osteochondral defects, allograft implantation has been suggested, but there may be limitations in acquiring the graft due to donor unavailability [34].

Total joint replacement surgery or arthroplasty is the last therapeutic option. During this surgery, the damaged joint is replaced with an artificial implant that is made of metal, ceramic, or plastic [33]. This is recommended for patients with severe OA whose quality of life is considerably reduced. Clinically relevant improvements have been observed, but complications associated with surgery in the elderly population are common. Infections, neurovascular injury, and peri-implant fractures are the main complications. Additionally, implant rejections are around 12%, and pain is still a recurrent symptom [6,30].

2.3. Biological Therapies

Recently, apart from traditional drugs and surgery, treatments based on intra-articular injection of platelet-rich plasma (PRP) have attracted significant clinical interest. This therapy consists of inoculating autologous plasma on the joint, because it has been shown that the PRP releases bioactive molecules (e.g., growth factors, cytokines, or anti-inflammatory mediators). This has been reported to relieve OA symptoms and to demonstrate no side effects. Nevertheless, PRP is limited to the knee joint, and variability has been observed among patients. This can be explained by the absence of a clear dosage guide and the lack of a standardized plasma extraction protocol. Moreover, simultaneous treatment with PRP and NSAIDs reduces the PRP's efficacy [35,36].

Autologous chondrocyte implantation (ACI) has also been used for the treatment of osteochondral defects for years. This treatment, authorized by the European Medicines Agency (EMA) as an advanced therapy medicinal product, is based on the implantation of autologous chondrocytes in the joint to promote its regeneration and, therefore, alleviate the symptoms. In fact, Spherox™ is the only ACI product that has been commercialized. This therapy is based on the implantation of spherical aggregates that are composed of autologous human chondrocytes expanded *ex vivo* and an auto-synthetized extracellular matrix. However, this treatment has also shown some drawbacks, such as the necessity of expert surgeons for its application, as well as the

authorization of the hospital in which the therapy is applied. Moreover, *ex vivo* cell expansion requires strong regulatory procedures. Consequently, this treatment is not available in all hospitals, and it has high costs. In addition, it is contraindicated in advanced OA stages (i.e., stages 3 and 4), and it is only prescribed for knee joint defects [37].

In conclusion, current treatments can alleviate the symptoms produced by OA in the short-term. In the long-term, as the disease progresses and the pain becomes intense, current treatments fail to improve the patient's quality of life. In addition, given that the target population that suffers from OA is the elderly, the appearance of other diseases that could hinder the general use of these drugs should be highlighted. Therefore, new therapeutic approaches should be proposed.

3. New Therapeutic Approaches: Tissue Engineering and 3D Bioprinting

As mentioned above, one of the most interesting therapeutic approaches for OA is the use of ACI. This kind of cell therapy has been widely researched and improved, since it can protect cartilage from degradation and, consequently, cause remission of the disease's symptomatology. In fact, there are several studies, including clinical trials, in which this therapy has shown promising results [37]. Another approach that is gaining attention in cell therapy treatments is the use of mesenchymal stromal cells (MSCs), as it has been reported that the articular administration of MSCs in the knee relieves pain and improves its function [38]. Likewise, adipose-derived stromal cells (ASCs) have also been applied for chondral regeneration, since they can be harvested with reduced mobility at the donor site in comparison with other MSC sources [39]. Furthermore, both ASCs and MSCs have the potential to secrete anti-inflammatory and immunomodulatory molecules, which complement their administration as an OA treatment [40,41]. However, the long-term benefits are controversial. In addition, it has been proven that injection of MSCs through a needle compromises their viability due to shear forces and that, after administration, cells tend to migrate, making it difficult to secrete therapeutically

active molecules [40]. The implementation of a cellular support would not only avoid these drawbacks, but also take into account the mechanical properties that are of great importance in the regeneration of the joint. In fact, hydrogel-based cellular supports have been already studied with successful results in terms of mimicking native mechanical properties and improving cell viability [42,43].

In this context, tissue engineering, which brings together cell therapy, biomaterial engineering, and the delivery of drugs or therapeutic molecules, has become the most promising therapeutic approach (Figure 4) [16,44,45]. It is based on the manufacture of three-dimensional (3D) structures or scaffolds that support cells, allowing them to adhere, proliferate, and differentiate. These structures can also contain different elements, such as drugs, growth factors, and therapeutic molecules [16].

Among scaffold manufacturing techniques, 3D bioprinting has gained significance in recent years. This additive manufacturing technique is characterized by the fabrication of layer-by-layer structures via computer-aided design (CAD). CAD generates a G-code that can be read by the bioprinter [48]. The creation of the design in CAD as well as the modification of the G-code allows the total control of the shape and structure of the scaffold, granting bioprinting an advantage over traditional manufacturing techniques. Furthermore, bioprinting techniques permit the addition of high cell densities, while other techniques are unable to do so, or the cells have to be added after making the scaffold [49]. In fact, anatomically specific implants could be designed for each patient using this technology. Another challenge in the tissue engineering field for joint regeneration is the fact that the joint is made up of two tissues—cartilage and bone—which, in turn, have separate zones with different cell densities, compositions, and biomechanics. Three-dimensional bioprinting, as an additive technique, allows the manufacturing of scaffolds with different layers; therefore, the native tissue can be imitated. In addition, it is fast and automatic, and accepts a wide variety of materials, wmaking it a promising technique in this field [48,50]. The deposited material is known as bio-ink. These bio-inks are composed of cells and biomaterials to which other

molecules such as drugs, proteins, genetic material, or growth factors may be added [51]. However, the biomaterial, whether of natural or synthetic origin, has to meet certain requirements to be considered a bio-ink [50]. In the first place, it has to be biocompatible with the cells, since it has to support cell attachment, migration, proliferation, and differentiation. Second, it has to be biodegradable and, finally, it has to be printable, which necessitates taking into account its rheological properties and gelation kinetics. Moreover, the biomaterial must have proper mechanical properties and be bioactive [52].

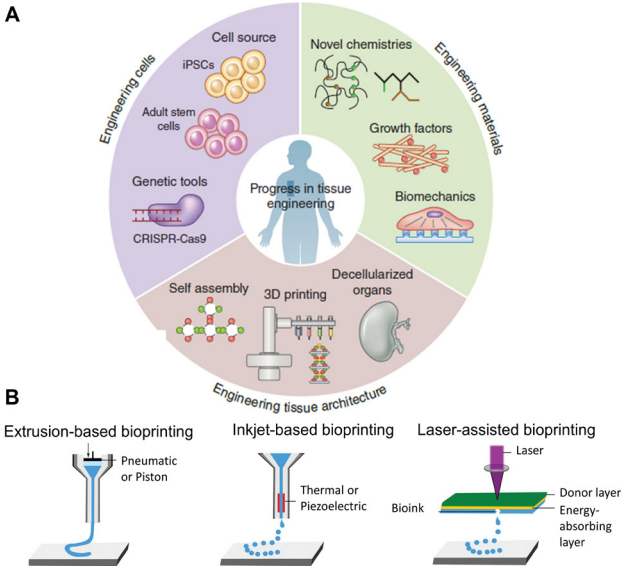

Figure 4. (A) Diagram of the elements used in tissue engineering. Adapted from [46]. (B) Scheme of different bioprinting methods. Adapted from [47].

There are different 3D bioprinting techniques, including extrusion-based, inkjet-based, and laser-assisted bioprinting (Figure 4B). Each of these techniques is based on different principles. Extrusion-based bioprinting is the most common technique, since it is easy to use, economical, and flexible in the use of a wide range of materials [53]. It is based on the continuous deposition of the bio-ink in a filament form through a needle via the application of mechanical pressure or air pressure (pneumatic). Inkjet-based bioprinting is characterized by the deposition of the bio-ink in a droplet form after the application of a piezoelectric or electrostatic drop-on-demand source. Laser-as-

sisted bioprinting uses a laser energy beam for the deposition of the bio-ink [53,54]. Several studies have implemented bioprinting techniques for joint regeneration. The majority of those studies focus on one of the two tissues involved—cartilage or bone—whereas fewer studies are based on the development of the whole osteochondral unit by 3D bioprinting.

3.1. 3D Bioprinting in Cartilage

Cartilage tissue lacks blood vessels, nerves, and a lymphatic system, making this tissue an ideal target for 3D bioprinting in comparison with other, more complex tissues [24,44]. Nevertheless, cartilage is subjected to high shear forces. Thus, the challenge, when it comes to bioprinting cartilage, is to meet the requirements in terms of mechanical properties, as well as to mimic the layered structure of the native tissue as closely as possible.

To obtain 3D structures resistant to mechanical pressures, some studies have focused on seeding cells on previously 3D-printed scaffolds, using thermoplastic polymers such as polycaprolactone (PCL) or polylactic acid (PLA) [55]. Electrospinning, which enables the fabrication of polymeric fibers, is another innovative technology that has been used for this purpose, since nanofibers reinforce the scaffold [56]. However, 3D bioprinting technology requires the inclusion of the biological part (living cells) in the bio-ink, so the use of these materials is unsuitable for cells, as these polymers need high temperatures to be extruded. For this reason, hydrogels are the most used option, as they have the ability to absorb water, are biocompatible with the cells, and are biodegradable.

Different biomaterials have been studied to develop bio-inks. Among them, biomaterials that are naturally found in osteochondral tissue such, as collagens or GAGs, have been proposed, as along with others that have greater printability characteristics or mechanical resistance, such as alginate, gelatin, or silk fibroin. All of these studies are represented in Table 2.

Table 2. Summary of the 3D bioprinting studies for cartilage.

Acronyms. COL: collagen; GAGs: glycosaminoglycans; ALG: alginate; NFC: nanofibrillated cellulose; HDiPSCs: Human-derived induced pluripotent stem cell; HA: hyaluronic acid; dECM: decellularized extracellular matrix; BMSCs: bone marrow stem cells; SF: silk fibroin; PEG: polyethylene glycol; PRP: platelet-rich plasma; Gel: gelatin; CH: chitosan; CS: chondroitin sulphate; AD-MSCs: adipose derived mesenchymal stem cells; GelMA: gelatin methacrylate; HAMA: Hyaluronic methacrylate; PCL: poly-caprolactone; PEGDA: polyethylene glycol diacrylate; GG: gellam gum; PLGA: poly-lactic-co-glycolic acid; ACPCs: articular cartilage progenitor cells.

Bioink	Cells	Technique	*In vivo*	Results	Ref
Type I COL	Rat chondrocytes	Extrusion-based bioprinting	Wistar Rats	· Good printability · Type II COL and GAGs accumulation *in vivo*	[58]
ALG/ COL ALG/ agarose	Rat primary chondrocytes	Extrusion-based bioprinting	No	· COL improves scaffold mechanical properties · COL enhances cell viability after bioprinting · Cells inside collagen scaffold increase chondrogenic gene expression and GAGs production	[59]
NFC/ALG	HDiPSCs co-cultured with irradiated human chondrocytes	Extrusion-based bioprinting	No	· NFC/ALG scaffolds better results in terms of cells proliferation, pluripotency maintenance, chondrogenic phenotype expression	[60]
ALG/ pig dECM/ TGF-β3	Human BMSCs	Extrusion-based bioprinting	No	· High cell viability after bioprinting · TGF-β3 sustained release from the scaffold · Higher concentrations of ECM enhance cells chondrogenic differentiation, but also osteochondral differentiation in a long-term · Native mechanical properties after the reinforcement with PCL fibers through 3D printing	[61]
Pig cartilage derived dECM/ Gel/ HA/ glycerol/ DMEM	Rabbit chondrocytes	Extrusion-based bioprinting	No	· Scaffold mechanical properties increase by dECM addition · Cell viability and proliferation is proportional to dECM concentration in the scaffold · dECM promotes cells to produce GAGs and COL.	[62]

SF/ goat cartilage derived dECM/ TGF-β3/ PEG 400	Rabbit BMSCs	Extrusion-based bioprinting	Nude mice	· Good printability · dECM enhances cell proliferation, viability, and chondrogenic differentiation after bioprinting · Sustained release of TGF-β3 which promotes GAGs and COL production · Cartilage ECM production as well as the increase of mechanical properties after *in vivo* implantation	[63]
SF/ rabbit PRP/ PEG 400	Rabbit chondrocytes	Extrusion-based bioprinting	No	· PRP increases scaffold mechanical properties · Sustained release of growth factors that are found in the PRP from the scaffold · PRP enhances cell viability and proliferation and promotes cell chondrogenic differentiation after bioprinting	[64]
SF/ Gel	Porcine primary chondrocytes	Extrusion-based bioprinting	Swiss inbred mice	· Porous and printable scaffolds · Low mechanical properties similar to soft tissues · High cell viability and proliferation after bioprinting · Cell chondrogenic differentiation inside scaffolds after bioprinting · Implanted scaffolds do not provoke long immune response	[65]
Hydroxybutil CH/oxidized CS	Human ADMSCs	Extrusion based bioprinting	C57BL/6 mice	· Good biocompatibility *in vivo* · Low immunotoxicity. Decrease in cytokines that degrade cartilage	[66]
Norbornene modified HA	Bovine BMSC	In situ crosslinkable extrusion-based bioprinting	No	· In situ crosslinking technique with visible light exposure · High cell viability after bioprinting with this technique · Cells chondrogenic differentiation and scaffold mechanical properties increase after bioprinting	[67]

Bioink	Cells	Technique	*In vivo*	Results	Ref
HAMA/ GelMA	Sheep AD-MSCs	In situ handheld extrusion-based bioprinting "Biopen"	Chondral defect sheep	· Good handling and applicability of Biopen · Cartilage regeneration and mechanical properties *in vivo* are good with Biopen, but not differences compared to conventionally bioprinted scaffold · Lack of adhesion to host tissue	[68]
GelMA/ PCL	Sheep chondrocytes	Extrusion-based bioprinting + PCL 3D printing	No	· High cell viability and proliferation after bioprinting · Good chondrogenic functionality of cell after bioprinting · High mechanical properties after the addition of PCL	[69]
GelMA/ PCL	Equine MSCs	Extrusion-based bioprinting + PCL melt electrowriting	No	· High cell viability and proliferation after bioprinting using both techniques · Cells produce GAGs and COL after bioprinting using both techniques	[70]
GelMa/PEGDA/ TGF-β1 -PLGA nanospheres	Human BMSCs	Stereolithography based 3D bioprinting	No	· PEGDA improves mechanics and printability · High cell viability and proliferation after bioprinting · TGF-β1 sustained release from the scaffold which promotes cell chondrogenic differentiation after bioprinting	[71]

ALG	Human AD-MSCS	Extrusion-based bioprinting + Aspiration-assisted bioprinting	No	· Layered scaffold simulating the deep and superficial layers of native cartilage · High cell viability after bioprinting · Mechanical properties similar to the native cartilage ones · Cells deposit COL fibers aligned with designed orientation	[72]
GelMA/GG GelMA/ GG/ (HAMA)	Equine chondrocytes/ MSCs/ ACPCs	Extrusion-based bioprinting	No	· HAMA improves printability · No differentiated cells show better results in terms of cartilage ECM production and differentiation · Layered scaffold with HAMA bioink simulating cartilage superficial layer with ACPCs and middle/deep layer with MSCs · Cells in layered scaffold show good chondrogenic differentiation, but no differences between layers	[73]

Collagen has been used for the production of bio-inks because it is an element that is widely distributed among mammalian tissues. Several types of collagen are known, from type I to XXI. However, most studies have focused on type II collagen, which is the main component of the cartilage ECM, and type I collagen, which is abundant in bone tissue.

Thus, in one of the studies in which collagen is used, Beketov et al. [57] argued that one of the drawbacks of using collagen is that scaffolds are often quite fragile. Hence, they proposed the use of high concentrations (4%) of type I collagen to develop a bio-ink with embedded rat chondrocytes. Using extrusion-based bioprinting (Figure 5A), they managed to obtain scaffolds with better printability and mechanics than other studies based on scaffolds with lower concentrations of collagen. Interestingly, after an *in vivo* study in rats, they showed the ability of these scaffolds to form cartilage ECM, rich in type II collagen and GAGs, as shown in Figure 5B [57].

Another proposal to increase the scaffolds' mechanics is the combination of collagen with another polymer, such as alginate or agarose. Thus, Yang et al. [58] developed alginate-based scaffolds with added collagen and agarose using extrusion-based bioprinting (Figure 5C(I)). They showed that by adding collagen to the scaffold, its mechanical properties, along with the viability of rat primary chondrocytes, increased compared to scaffolds with agarose (Figure 5C(II)). Furthermore, cells inside collagen-containing scaffolds had increased chondrogenic-phenotype gene expression as well as GAG production [58].

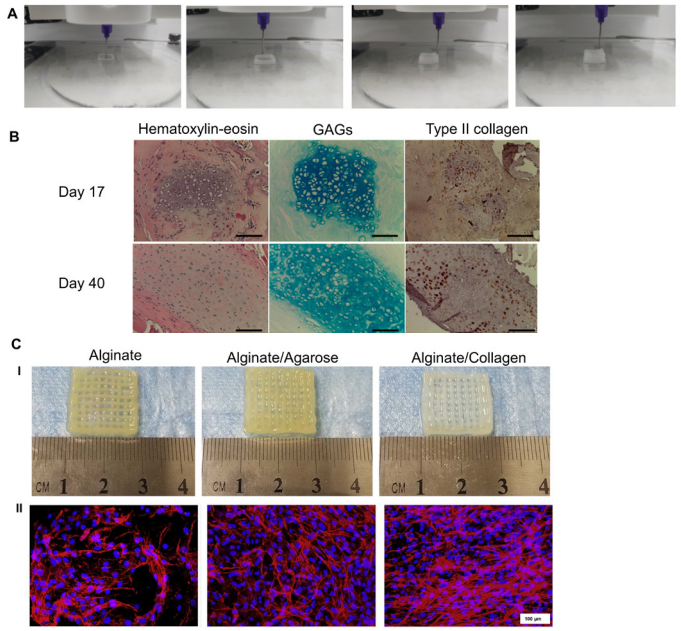

Figure 5. Collagen-based scaffolds: (A). Extrusion-based bioprinting of a 4% collagen scaffold. (B). Cartilage ECM evaluation after *in vivo* implantation. At day 40, GAG accumulation and type II collagen production were increased. Scale bar = 100 µm. Adapted from [57]. (C(I)). Macroscopic images of alginate, alginate–agarose, and alginate–collagen scaffolds. (C(II)). Rhodamine–phalloidin/Hoechst 33,258 staining after 14 days of bioprinting. Scale bar = 100 µm. Adapted from [58].

Alginate (Alg) is a natural polymer that has been widely used for cartilage bioprinting due to its biocompatibility and easy post-bioprinting crosslinking procedure. Nguyen et al. [59] used it as a component of their bio-ink in combination with nanofibrillated cellulose (NFC). On the other hand, they developed bio-inks based on NFC/HA. They embedded bio-inkhuman-derived induced pluripotent stem cells (iPSCs) co-cultured with irradiated human chondrocytes in these two bio-inks, and they bioprinted scaffolds using extrusion-based bioprinting. The scaffolds containing alginate showed better results, as cells maintained their pluripotency and chondrogenic phenotype in comparison with HA scaffolds, in which cells showed low proliferation capacity [59]. Mechanical properties that are of key importance for cartilage were not measured in this research. In another study, Rathan et al. [60] mixed alginate

with different concentrations of decellularized pig cartilage ECM (dECM) to obtain ECM-functionalized alginate bio-inks, in which human bone marrow MSCs and the chondrogenic growth factor TFG-β3 were included. They achieved bioprinted scaffolds through extrusion, and a sustained release of the growth factor. Moreover, they demonstrated that by increasing the concentration in the bio-ink from 0.2% to 0.4%bio-ink, cell proliferation and the chondrogenic differentiation were enhanced (Figure 6A). However, the authors suggested that, in a long-term, the osteogenic differentiation could also occur. Finally, they combined 3D bioprinting with 3D printing techniques to include PCL fibers that reinforced the scaffold, thus achieving mechanical properties similar to those of the native cartilage (Figure 6B) [60].

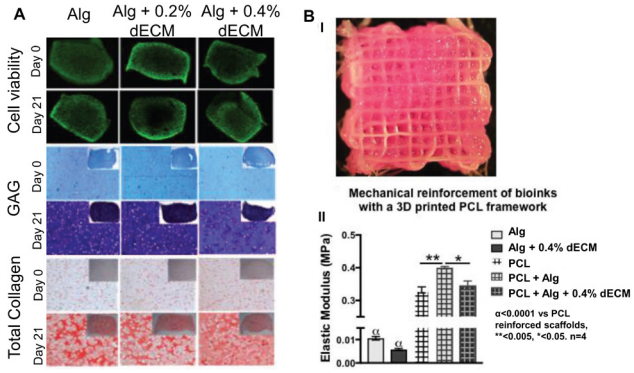

Figure 6. Alginate/dECM-based scaffolds: (A). Cell viability, histology, and immunostaining on days 0 and 21 showed good cell viability and high GAG and collagen production within 21 days. (B) Alginate/dECM 3D bioprinting and PCL 3D printing combination. (I) Representative image of the hybrid scaffold. (II) Mechanical properties are enhanced with PCL reinforcement. Adapted from [60].

As mentioned above, dECMs have been used as components in the tissue engineering field, as they are biologically and functionally closer to native tissues than polymers [62]. However, the drawback of these components is that they fail to meet the necessary rheological properties to be considered as bio-inks by themselves. Thus, Visscher et al. [61] used gelatin, HA, glycerol, and Dulbecco's modified Eagle's medium (DMEM) to fabricate a bio- ink containing pig-cartilage-derived dECM that had been methacrylated. They embedded rabbit chondrocytes into the bio-ink and manufactured scaffolds through extrusion-based bioprinting. Cell viability and proliferation were in-

creased proportionally to the dECM concentration. dECM also promoted cells to produce GAGs and collagen. In addition, the scaffold mechanical properties were also positively improved by the inclusion of dECM [61]. These promising results after including dECM have also been reported by other researchers.

Zhang et al. [62] proposed mixing decellularized goat cartilage ECM with silk fibroins. They included rabbit bone marrow MSCs, TGF-β3 as a chondrogenic growth factor, and polyethylene glycol (PEG) 400 as a crosslinker. After a rheological study to determine the optimal concentrations for the bio-ink, they managed to manufacture porous scaffolds via extrusion. The cell viability, proliferation, and chondrogenic differentiation were good, and were proportional to the amount of dECM. Furthermore, they obtained a sustained release of TGF-β3 from the scaffold, promoting the production of collagen and GAGs. Finally, bioprinted scaffolds were implanted subcutaneously in mice. *In vivo* results showed an increase in the production of GAGs and collagen, as well as in the scaffolds' mechanical properties, making these scaffolds a promising therapeutic approach for cartilage regeneration [62].

In a previous work by the same research group, Li et al. [63] developed a bio-ink by combining silk fibroin, rabbit platelet-rich plasma (PRP), rabbit chondrocytes, and PEG 400. After extrusion bioprinting, they showed that the addition of plasma increased the scaffolds' mechanical properties as well as cell viability and proliferation. Interestingly, the plasma contained various growth factors that were delivered from the scaffold to promote cell functionality and chondrogenic differentiation [63]. In fact, silk fibroin has gained popularity as a bio-ink component because it is biocompatible, biodegradable, and has remarkable mechanical strength [62]. Another work using silk fibroin as a bio-ink component was the one proposed by Singh et al [64]., who developed a bio-ink based on two types of silk fibroin, gelatin, and porcine primary chondrocytes. They obtained porous and printable scaffolds via extrusion-based bioprinting (Figure 7). Cells showed high viability and proliferation ability inside the scaffolds, as well as chondrogenic gene expression and cartilage ECM production. Moreover, the authors injected the bio-ink subcutaneously in mice to study their immune response. As a result, a long immune response

was not found, so they suggested the use of these scaffolds for cartilage regeneration. Nevertheless, the scaffold mechanical properties were lower (143 kPa) than those of native cartilage; therefore, the scaffolds would only be beneficial for soft tissue regeneration [64].

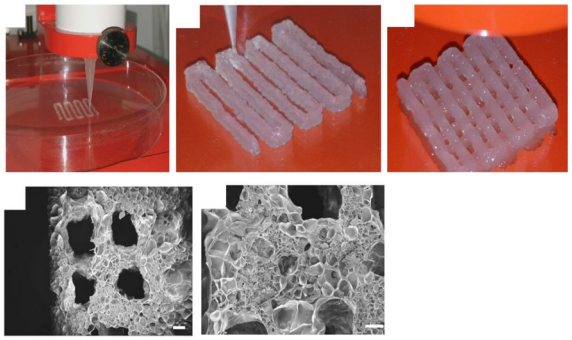

Figure 7. Silk fibroin (SF)-based scaffolds. Extrusion bioprinting process of SF + gelatin bio-ink, obtaining porous scaffolds. Scale bar = 200 μm. Adapted from [64].

Achieving mechanical properties in the scaffolds that are similar to those of human cartilage is challenging when using hydrogels such as alginate, silk fibroin, or collagen by themselves. Consequently, other bio-ink components have been proposed. For example, Li et al. [65] developed a bio-ink containing chemically modified chitosan to make it soluble, along with chondroitin sulfate, since it has been reported to be involved in the mechanical response of native cartilage as well as in cartilage regeneration [73]. They included human adipose-derived MSCs and used pluronic as sacrificial ink to give support to the scaffold. Once they manufactured the scaffolds by extrusion, they studied their biocompatibility in mice by subcutaneous implantation. Immune response decreased within the following days after implantation. Interestingly, cartilage-degradative cytokines were reduced as a consequence of the chondroitin's anti-inflammatory effects, suggesting the use of chondroitin for cartilage regeneration purposes [65]. However, the scaffolds' mechanical properties and how the chondroitin was involved in them were not shown.

Similar to chondroitin sulfate, HA has been reported to have promising properties for regenerating cartilage. However, it has poor rheological properties

for use as a bio-ink without any other supportive component(s). Galarraga et al. [66] modified hyaluronic acid to create norbornene-modified HA, which was crosslinkable with visible light. In addition, they developed an in situ crosslinking technique that consisted of exposing the bio-ink to visible light just after being extruded (Figure 8A). Thus, they developed HA scaffolds without the addition of any rheological component to the bio-ink. Bovine bone marrow MSCs were viable after bioprinting, indicating that the technique was biocompatible. Moreover, cells' chondrogenic differentiation and scaffold mechanical properties increased after bioprinting [66].

Other research groups have also developed *in situ* bioprinting techniques. In the case of Di Bella et al [67]., they used an extrusion-based handled bioprinting technique based on a coaxial system called "Biopen" (Figure 8A). The bio-ink was made of ovine adipose-derived MSCs, hyaluronic methacrylate, and gelatin methacrylate. The authors demonstrated high cell viability after using this technique in a previous work [74], and this study was focused on *in vivo* research using a chondral defect sheep model. They compared the use of the Biopen with scaffolds bioprinted using a conventional bioprinter. As a result, no differences were observed in terms of cartilage regeneration and mechanical properties between the scaffolds created by the Biopen and the conventional bioprinter; in fact, they were good in both cases. Nevertheless, Biopen-fabricated scaffolds showed better overall macroscopic and microscopic characteristics, together with excellent applicability and handling of the technique by the surgeons. As a point for improvement, both implants failed to adhere to the host tissue. Therefore, chemical modifications of the bio-ink could be needed [67].

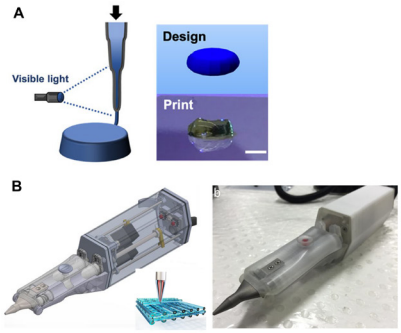

Figure 8. *In situ* bioprinting techniques: (A) In situ crosslinking technique consisting of exposing the bio-ink to visible light just after being extruded. Adapted from [66]. (B) "Biopen"extrusion-based handled bioprinting technique based on a coaxial system. Adapted from [67].

Gelatin methacrylate (GelMA) has also been widely applied in cartilage regeneration via 3D bioprinting due to its desirable fast crosslinking using UV light, together with its biodegradability, biocompatibility, and limited antigenicity. Ruiz-Cantu et al. [68] used extrusion-based bioprinting to manufacture porous scaffolds using a GelMA bio-ink with ovine chondrocytes. GelMA, as a cell carrier, proved to be good in terms of high cell viability and proliferation after bioprinting. In addition, cells also managed to produce GAGs and collagen. Despite the fact that mechanical properties increased after bioprinting, they did not achieve native cartilage values. Consequently, the authors proposed the addition of PCL through 3D printing as a mechanical support. The hybrid GelMA–PCL scaffold showed the same ability to maintain good cell viability (Figure 9A) and chondrogenic functionality after bioprinting. Interestingly, the mechanical properties strongly increased, suggesting the use of hybrid scaffolds as a cartilage regeneration strategy [68].

A similar approach was performed by de Ruijter et al. [69] In this case, the scaffold bioprinted by extrusion, and composed of GelMA and equine MSCs, was reinforced with PCL fibers using a melt electrowriting technique. This electrospinning technology uses a high-voltage electrical field to form sub-micrometer fibers from polymer melts. The authors showed that the inclusion of this technique had no negative effects on cell viability and proliferation. In fact, cells maintained the ability to produce GAGs and collagen after bioprin-

ting. Therefore, as Figure 9B shows, the inclusion of PCL with this technique may be a good option to increase the mechanical properties of scaffolds for cartilage regeneration [69].

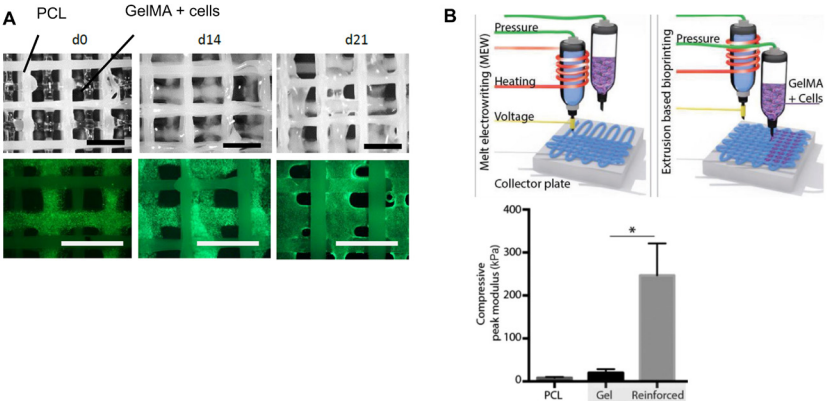

Figure 9. GelMA-based scaffold: (A) Representative bright-field and fluorescence images of hybrid scaffolds composed of PCL and GelMA. Scale bar = 2 mm. Adapted from [68]. (B) Schematic image of extrusion-based bioprinting and electrowriting techniques that improved scaffold mechanical properties * = $p < 0.05$. Adapted from [69].

Zhu et al. [70] proposed another bioprinting approach using GelMA/human bone marrow MSCs bio-ink. First, they included polyethylene glycol diacrylate (PEGDA) in order to increase the mechanical properties. Then, they added the growth factor TFG-β1 encapsulated in poly-lactic-co-glycolic acid (PLGA) to promote chondrogenic differentiation. Finally, they used stereolithography-based 3D bioprinting, which is a laser-assisted bioprinting method to manufacture scaffolds. As a result, they showed that PEGDA improved mechanical properties and printability. Importantly, cell viability and proliferation were high despite the crosslinking procedure with UV light. Moreover, a sustained release of TFG-β1 from the scaffold was found, which enhanced cells' chondrogenic phenotype expression after bioprinting [70]. Consequently, similar to extrusion-based bioprinting, with this technique, it is possible to obtain adequate scaffolds for cartilage regeneration purposes.

Apart from mechanics, the other challenge when it comes to bioprinting structures in order to substitute damaged cartilage is the creation of scaffolds

that simulate the internal layered structure of the native cartilage. To do so, Wu et al. [71] combined extrusion bioprinting with aspiration-assisted bioprinting (AAB), which allows precise positioning of spheroids by employing aspiration to lift individual spheroids and bioprint them onto a hydrogel. By using sodium alginate and human adipose-derived stem cells (ADSCs) they manufactured a two-layered scaffold simulating the deep and superficial layers of the cartilage. As Figure 10A shows, first, they developed the deeper layer through AAB by depositing spheroids vertically with the support of a pin ray. Then, the superficial layer was extruded horizontally on the other layer. The resulting scaffold showed high cell viability after both bioprinting techniques, as well as mechanical properties similar to those of the native cartilage (2.1 MPa). Interestingly, cells deposited collagen fibers aligned similarly to native cartilage [71].

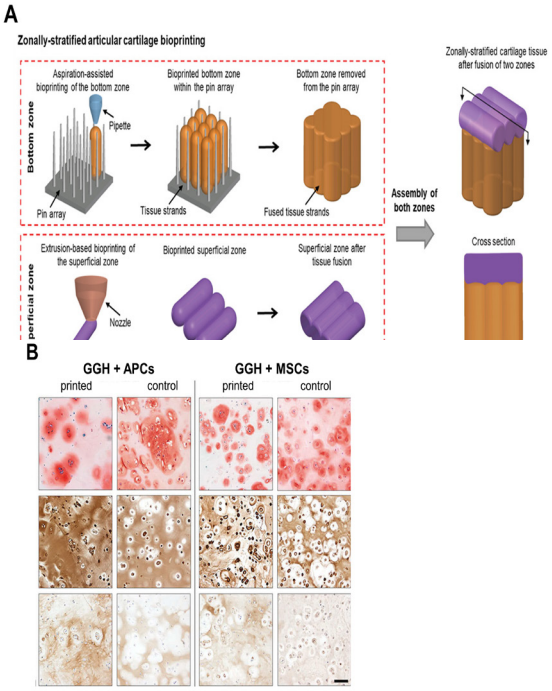

Figure 10. Layered scaffolds: (A) Schematic image of the manufacture of zonally stratified articular cartilage. Adapted from [71]. (B). Histological images of GAGs (safranin-O, top), collagen type II (middle), and collagen type I (bottom) matrix of APCs and MSCs in GelMA/gellan gum/HAMA (GGH) bioprinted scaffolds at day 42. Scale bar = 100 μm. Adapted from [72].

In another recent work, Mouser et al. [72] aimed to develop heterocellular cartilage constructs by using three different cell types: equine chondrocytes, MSCs, and articular cartilage progenitor cells (ACPC) which were reported to be in the superficial layer of the cartilage. To achieve this, cells were embedded into two inks composed of GelMA/gellan gum and GelMA/gellan gun/hyaluronic methacrylate (HAMA). Then, the authors created scaffolds using extrusion-based bioprinting. First, after evaluating which bio-ink had better results, they concluded that the addition of HAMA considerably improved the printability. Among the cells, the non-differentiated ones showed higher cartilage ECM production, but there were no significant differences in terms of including them in one ink or the other. Taking into account these data, they used GelMA/gellan gum/HAMA (GGH) bio-ink to fabricate scaffolds with a middle/deep layer containing MSCs and a superficial layer with ACPCs. As a result, the layered scaffold demonstrated positive staining of GAGs and collagen as well as chondrogenic gene expression (Figure 10B). However, the mechanical properties were not specified, and there were no differences between the two different layers; therefore, further studies need to be conducted [72].

3.2. 3D Bioprinting in Bone

OA is characterized by osteochondral damage that affects cartilage and bone tissues. For this reason, studies focused on the development of scaffolds using 3D bioprinting technology for bone regeneration have also been carried out. The ideal scaffold should take into account the structure and composition of human bone, and should not only have excellent mechanical properties, but also contain a porous structure, and be both osteoinductive and osteoconductive. In addition, bone tissue contains a vascular system; therefore, scaffolds should provide vascularization to nourish bone cells as well as cartilage tissue.

As a hard tissue, the mechanics and stiffness of the substitute scaffold are of key importance. Consequently, many of the studies use 3D printing technology with synthetic materials in which cells are seeded later on top of the fabricated scaffold [75]. Among them, PCL has gained notoriety due to its good mechanical properties, and because it favors cell adhesion and prolife-

ration [76]. In the field of 3D bioprinting, the use of hydrogels based on polymers such as alginate and GelMA is widespread, since they are good carriers for the cells. However, they have shown low bioactivity, and the bioprinted structures are usually soft and very different from native bone's mechanics. In order to overcome these inconveniences, researchers have been forced to include other elements, such as ceramics, glasses, or inorganic components (Table 3).

Table 3. Summary of the 3D bioprinting studies for bone regeneration.
Acronyms. ALG: alginate; PVA: polyvinyl alcohol; COL: collagen; HAP: hydroxyapatite; BMSCs: bone marrow stem cells; PCL: polycaprolactone; ECM: extracellular matrix; MC: methylcellulose; LAP: laponite; TCP: β-tricalcium phosphate; ADMSCs: adi-pose derived mesenchymal stem cells; GelMA: gelatin methacrylate; GO: graphene oxide; Gel: gelatin.

Bioink	Cells	Technique	*In vivo*	Results	Ref
ALG/ PVA/ HAP	Mouse calvaria 3T 3-E1 cells	Extrusion-based bioprinting	No	· PVA/HAP increase bioink rheological properties · Good cell viability after printing · Low mechanical properties	[78]
NanoHAP/ type I COL	Mouse D1-MSCs	Laser-based bioprinting	Calvaria defect rats	· Manufacture of scaffolds with two geometries; ring and disk · High viability and proliferation after bioprinting · Bone regeneration *in vivo* using disk scaffolds	[79]
RGD-γ-irradiated ALG/ nanoHAP pDNA complexes encoding TGF-β3 and BMP-2 growth factors	Porcine BMSCs	Extrusion-based bioprinting + PCL 3D printing	Nude mice	· High cell viability using PCL co-printing technique · High transfection rates · Bone ECM production and mineralization · Bone formation, immature osteoid detection, and vascularization *in vivo*	[80]
Vascular bioink: RGD-γ-irradiated ALG/MC/ nanoHAP nanoparticles loaded with VEGF Osteoinductive bioink: RGD-γ-irradiated ALG/ MC/ LAP/ BMP-2	Porcine BMSCs	Extrusion-based bioprinting + PCL 3D printing	Nude mice Femoral defect rats	- Increased vascularization in nude mice with VEGF gradient scaffolds · Bone formation and BMP-2 sustained release with osteoinductive scaffolds in nude mice · Increase in vessel volume and new bone formation using both bioinks based scaffolds in femoral defect rats	[81]

Bioink	Cells	Technique	*In vivo*	Results	Ref
Type I COL/ TCP	Preosteo-blasts cells (MC3T3-E1)	Extrusion-based bioprinting	No	· Highly porous scaffolds · Good cell viability and proliferation after bioprinting · TCP enhances scaffold mineralization after bioprinting with preosteoblasts cells · TCP promotes osteogenic markers and gene expression in hADMSCs after bioprinting	[82]
ALG/ GelMA/ highly angiogenic borate bioactive glass (13-93B3)	Human ADMSCs	Extrusion-based bioprinting + PCL 3D printing	No	· Glass enhanced scaffold stability after bioprinting by promoting alginate-GelMA crosslinking · Glass solutes induce a pH increase in the media that is toxic for cells	[83]
ALG/ GO	Human MSCs	Extrusion-based bioprinting	No	· GO enhances bioink rheological properties · Printability and scaffold mechanics are improved with GO · GO prevents cells from oxidative stress and promotes their differentiation to bone	[84]
ALG/ Gel/ GO	Human BMSCs	Extrusion-based bioprinting	No	· GO increases printability and scaffold fidelity ·Good cell viability, proliferation, and osteogenic differentiation after bioprinting · Higher GO concentrations increase DNA content and mineralization	[85]

Hydroxyapatite (HAP), as a major inorganic component of bone, has been found to be bioactive and osteoinductive [85]. For this reason, it was included in the work published by Bendtsen et al. [77], who developed alginate/polyvinyl alcohol (PVA)/HAP inks to obtain scaffolds through extrusion-based bioprinting. The addition of PVA/HAP enhanced the rheological properties as well as the viability of murine calvaria 3T3-E1 cells. Importantly, although mechanical properties increased with PVA/HAP, they did not resemble those of bone [77]. Similarly, Keriquel et al. [78] evaluated bioprinted scaffolds for bone regeneration in rat calvaria defects. To do so, a nanohydroxyapatite/collagen type 1 bio-ink with murine D1-MSCs was developed, and scaffolds with two geometries (ring and disk) were manufactured using laser-based bioprinting. Results showed high cell viability and proliferation as well as bone regeneration and formation *in vivo*, especially when using disk geometry scaffolds [78]. Despite these interesting results, biomechanics were not mentioned.

For osteochondral regeneration, HAP has been also used. For example, Cunniffe et al. [79] fabricated an RGD-γ-irradiated alginate and porcine bone marrow MSC bio-ink. Interestingly, they included nanohydroxyapatite complexed with plasmid DNA encoding TGF-β3 and BMP-2 growth factors. Extrusion-based bioprinting was used accompanied by PCL co-printing as a supporting mesh to provide mechanical stability to the construct (Figure 11). They achieved good cell viability with this co-printing technique, as well as high transfection rates. Moreover, higher ECM production and mineralization were observed with the plasmid-encoding growth factors. Finally, they performed an *in vivo* study by implanting the scaffold subcutaneously in nude mice. As a result, bone formation, immature osteoid, and vascularization were detected, suggesting a feasible approach for bone regeneration [79].

In a recent work by the same research group, Freeman et al. [80] applied this co-printing procedure with bio-ink extrusion and PCL to manufacture scaffolds. In this case, two different bio-inks were proposed: vascular and osteoinductive bio-inks. The vascular bio-ink was composed of RGD-γ-irradiated alginate/methylcellulose and hydroxyapatite nanoparticles loaded with the growth factor VEGF. On the other hand, the osteoinductive bio-ink was based

on RGD-γ-irradiated alginate/methylcellulose/Laponite/BMP-2 and porcine bone marrow MSCs. The obtained scaffolds were implanted subcutaneously in nude mice. VEFG gradient scaffolds were bioprinted with the vascular bio-ink, showing vascularization *in vivo*. In contrast, after the implantation of the osteoinductive scaffolds, bone formation and sustained release of BMP-2 due to Laponite clay were observed. Interestingly, the scaffolds containing both bio-inks were fabricated and evaluated in rat femoral defects. Results showed an increase in vessel volume as well as in new bone formation, indicating a promising therapeutic approach for bone regeneration [80]. As a point for improvement, further studies on mechanical properties should be performed.

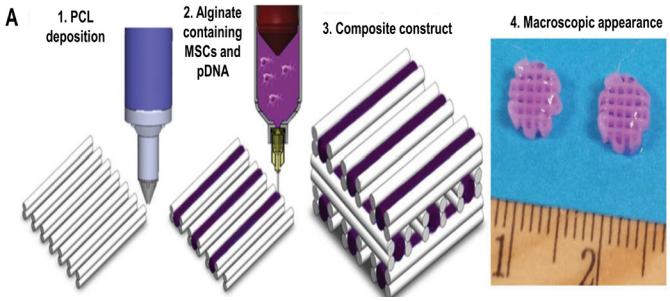

Figure 11. Schematic representation of the bioprinting process with co-printing of PCL and the bioprinting of the bio-ink composed of alginate, MSCs, and nHAP-pDNA complexes. Adapted from [79].

Another bioceramic that has been used for 3D bioprinting purposes is β-tricalcium phosphate (TCP). Like HAP, TCP has been reported to promote osteogenic differentiation of MSCs; therefore, Kim et al. [81] included this bioceramic in their collagen-type-I-based bio-ink. Highly porous scaffolds were obtained through extrusion-based bioprinting. However, the mechanical properties should have been improved, since the native bone values were not achieved. Biological evaluation was first carried out with preosteoblast cells (MC3T3-E1), showing good cell viability and proliferation as well as enhancement of mineralization after bioprinting. Then, human adipose-derived MSCs were used to evaluate their osteogenic differentiation capacity. As a result, TCP-containing scaffolds demonstrated matrix mineralization based on the increase in calcium and phosphorus. Furthermore, osteogenic markers and osteogenic gene expression increased with TCP. Interestingly, osteogenic

differentiation was also shown in alginate/TCP/hMSCs scaffolds without the need for adding an osteogenic culture medium [81]. Consequently, the use of TCP could be a promising approach for the manufacture of scaffolds for bone regeneration. Nevertheless, low mechanical properties (5.94 MPa) make these scaffolds best considered as temporary substitutes for damaged bone.

Glass can also be incorporated in the fabrication of scaffolds for bone regeneration. In the work proposed by Kolan et al. [82], the authors included the highly angiogenic borate bioactive glass (13-93B3), which was approved by the FDA for the treatment of skin burns and chronic wounds. They developed a bio-ink composed of alginate/GelMA and human adipose-derived MSCs using extrusion-based bioprinting to biofabricate the scaffolds. Like in the previous works, they carried out a PCL co-printing procedure to improve the stability and mechanical properties (from 0.3 MPa to 50.6 MPa). Then, two approaches were proposed: one consisting of the addition of the glass to the PCL, and another consisting of the inclusion of the glass directly in the bio-ink. Results showed a decrease in cell viability within the days after bioprinting when the glass was included within the PCL. The authors argued that the solubility of the glass may have produced solutes that increased the pH, which was harmful to the cells. Furthermore, alginate/GelMA layers lost their stability over time, which accentuated the decrease in cell viability. On the other hand, when the glass was added directly to the bio-ink, an initial cell viability decrease was observed due to pH shock toxicity, but cell recovery was shown during the days after bioprinting, since the glass promoted crosslinking between the alginate and GelMA, making the scaffolds more stable. The authors concluded that the glass could be interesting to manufacture more stable scaffolds, but that dynamic culture systems should be implemented or glass concentration should be optimized in order to avoid toxicity [82].

Another interesting approach for bone regeneration is the incorporation of inorganic components into the bio-ink. Among them, graphene oxide (GO) has gained notoriety because its functional groups enable the creation of strong interactions with various molecules [83,86]. Consequently, hydrogels with high mechanical properties have been obtained.

Choe et al. [83] added GO into a sodium alginate and human MSC bio-ink. They showed that by increasing the GO concentration from 0.05 mg/mL to 1 mg/mL, the bio-ink's rheological properties, printability (Figure 12A), scaffold stability, and me- chanics increased. Interestingly, GO protects cells from oxidative stress, and promotes osteogenic differentiation in terms of alkaline phosphatase enzyme (ALP) production and mineralization, along with osteogenic gene expression [83]. Likewise, Zhang et al. [84] included different concentrations of GO in their bio-ink composed of sodium alginate, gelatin, and human bone marrow MSCs. The GO improved extrusion-based printability and scaffold fidelity. Furthermore, as Figure 12B shows, cell viability and proliferation were good despite increasing GO concentrations from 0.5 mg/mL to 2 mg/mL. Furthermore, osteogenic differentiation was shown in scaffolds containing GO. Importantly, higher GO concentrations improved DNA content as well as mineral volume after bioreactor culture [84]. These two studies showed that the use of GO could be an interesting option for bone bioprinting, because it would not only improve the physical properties of the scaffold, but also promote osteogenesis.

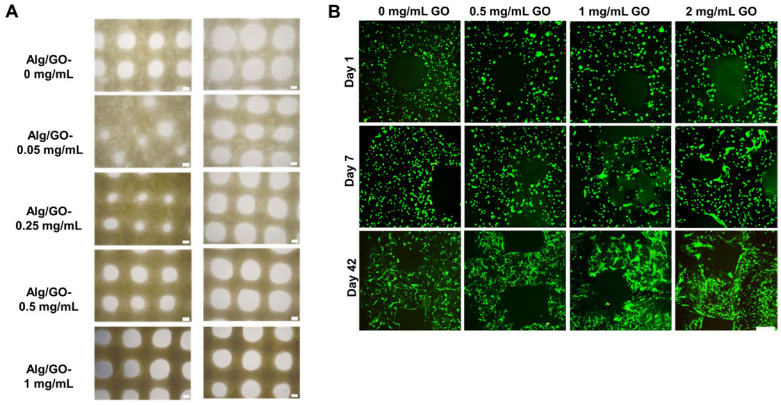

Figure 12. Graphene oxide scaffolds: (A) Optical images of the top view of the printed scaffolds, indicating better printability when GO increases from 0.05 mg/mL to 1 mg/mL. Scale bars = 300 µm. Adapted from [83]. (B) Cell viability in the 3D-bioprinted GO scaffolds at days 1, 7, and 42. Living cells are depicted in green, and dead cells are in red. Scale bar = 50 µm. Adapted from [84].

3.3. 3D Bioprinting in Osteochondral Units

The latest and most innovative approach to regenerate osteochondral injuries is the manufacture of 3D structures that contain both cartilage and bone tissues. Despite the fact that this is a complicated challenge due to all of the intrinsic characteristics that each tissue must meet, interesting and promising advances have been achieved (Table 4).

Table 4. Summary of the 3D bioprinting studies for cartilage and bone together.

Acronyms. Gel: gelatin; FGN: fibrinogen; HA: hyaluronic acid; PLGA: poly-lactic-co-glycolic acid; PCL: polycaprolactone; BMSCs: bone marrow stem cells; ECM: extracellular matrix; GAGs: glycosaminoglycans; COL: collagen; GelMA: gelatin methac-rylate SFMA: silk fibroin methacrylate; PTH: parathyroid hormone ALG: alginate; MC: methylcellulose; CPC: calcium phosphate cement.

Bioink	Cells	Technique	*In vivo*	Results	Ref
Gel/ FGN/ HA/glycerol and PLGA microspheres loaded with TGF-β3 for superficial layers and BMP-4 for deeper layers.	Rabbit BMSC	Extrusion-based bioprinting + PCL 3D printing	Nude mice Rabbit knee defect	· PCL gradient scaffolds to give structure · Excellent mechanical properties · Good cell viability and proliferation after bioprinting · Growth factors sustained release · Cartilaginous ECM production in mice after subcutaneous implantation · Chromogenic gene expression in the superficial layer and osteogenic markers detection in the deeper layers after *in vivo* in rabbits	[88]
GelMA/pluronic	Porcine BMSCs co cultured with chondrocytes	Inkjet-based bioprinting + extrusion-based bioprinting + PCL 3D printing	No	· Good integration of three techniques · Observation of osteochondral and chondral pathways · GAGs contents and mechanical properties as in native tissue	[89]
Bioink free	Porcine BMSCs	Inkjet-based bioprinting + PCL 3D printing	No	· Excellent cell viability after bioprinting · Cartilage like ECM production · COL alignment similar to native tissue after dynamic culture.	[90]
Cartilage bioink: GelMA/ SFMA/ PTH Bone bioink: GelMA/ SFMA	Rabbit chondrocytes Rabbit BMSCs	Extrusion-based bioprinting	Articular osteochondral defect rabbit	· Mechanical gradient scaffold · PTH inhibits chondrocyte hypertrophy, maintaining the hyaline phenotype · Osteochondral regeneration *in vivo*	[91]
ALG/ MC/ CPC	Human chondrocytes	Extrusion-based bioprinting	No	· Creation of three zone scaffolds · Cell viability decrease with CPC · Chondrogenic presence	[92]

For example, in a recent study, Sun et al. [87] combined extrusion-based bioprinting with PCL printing. By depositing thicker layers on the bottom and thinner layers on the superficial part, a PCL gradient scaffold was fabricated in which a bio-ink composed of gelatin, fibrinogen, HA, glycerol, and rabbit bone marrow MSCs was deposited between the PCL layers. Importantly, PLGA microspheres loaded with growth factors (i.e., TGF-β3 for the superficial part, and BMP-4 for the deeper part) were added. Thus, the authors aimed to generate cartilage in the superficial part and bone in the deep part. The obtained scaffold showed excellent mechanical properties that were similar to those of native tissue. Good cell viability and proliferation were also achieved, together with a sustained growth factor release. Importantly, chondrogenic ECM production was observed in the superficial layers after the implantation in nude mice. Finally, the scaffold was implanted in the rabbits' knees, and chondrogenic gene expression was quantified in the superficial layers, whereas osteogenic markers were found in the deeper layers [87]. These results seem to be promising for the regeneration of joint injuries; however, a further evaluation of joint functionality should be carried out.

In another study, Daly et al. [88] developed a multi-tool bioprinting procedure to manufacture tibial-like curvature structures (Figure 13). First, by using the printing technique, PCL structures containing microchambers were fabricated. Then, a bio-ink containing GelMA and porcine bone marrow MSCs was deposited inside the microchambers by extrusion-based bioprinting to manufacture the bone part (Figure 13A). Likewise, bio-ink- free microchannels were created with the sacrificial ink pluronic as a nutrient diffusion system. Finally, inkjet bioprinting was performed using only the culture media with MSCs co-cultured with chondrocytes as a bio-ink (Figure 13C). Afterwards, the obtained scaffold was cultured in a bioreactor. The results showed high cell viability (Figure 13B) together with an osteochondral pathway in the bone part and cartilaginous ECM production in the cartilage part. Importantly, the GAG content and the mechanical properties were in the range of native tissue [88]. Recently, the same research group focused on how to bring these structures to an *in vivo* study. To do so, first, they had to devise a system for fixation to the articular bone. Thus, Burdis et al. [89] developed a biodegrada-

ble microwell array pin of PCL via printing technology in order to insert it in a hole that was created in the subchondral bone. Then, a porcine bone marrow MSC suspension was deposited on this device through inkjet bioprinting. The results showed excellent cell viability and quantification of cartilage ECM components. Importantly, after the culture of the scaffold in a bioreactor, cartilage-like assembly in terms of collagen alignment was observed [89]. Although this study managed to devise an interesting method for scaffold implantation in the joint, mechanical testing remains pending.

Another approach was the one proposed by Deng et al. [90] They developed two bio-inks: cartilage and bone bio-inks. Their cartilage bio-ink was composed of gelatin methacrylate, silk fibroin methacrylate, and rabbit chondrocytes. Moreover, parathyroid hormone (PTH), which was reported to inhibit chondrocyte hypertrophy, was added. On the other hand, the bone bio-ink was based on gelatin methacrylate, silk fibroin methacrylate, and rabbit bone marrow MSCs. Extrusion-based bioprinting was used to create the silk fibroin gradient scaffolds. As a result, good printability and cell viability after bioprinting were obtained. In addition, the hyaline cartilage phenotype was maintained due to PTH. Interestingly, the scaffolds were implanted in rabbit articular osteochondral defects, showing good regeneration *in vivo*. In contrast, although the mechanical properties increased in the bone zone (211.10 kPa), they did not resemble those of native bone [90].

In another work, Kilian et al. [91] used alginate methylcellulose (Alg-MC) with human chondrocytes (hC) to fabricate the cartilage part, followed by an Alg-MC-hC mixed with calcium phosphate cement (CPC) to create calcified cartilage, and CMC alone to fabricate the bone part. They performed the bioprinting via extrusion. The results showed a decrease in viability with the CPC layer, even though chondrogenic markers such as GAGs and collagen type II were present [91].

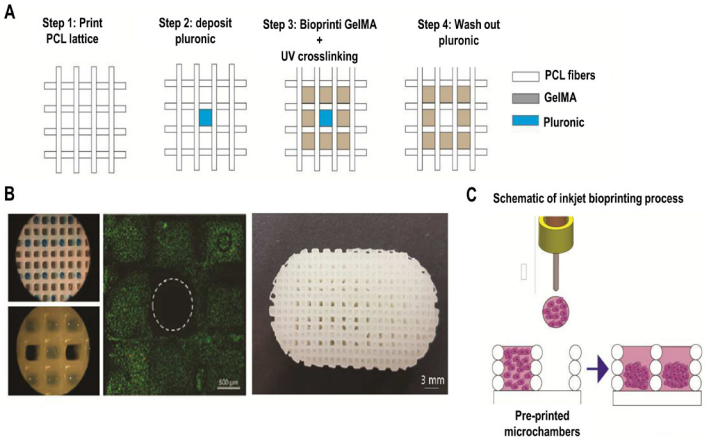

Figure 13. Multi-tool bioprinting procedure: (A) Schematic images of PCL printing and GelMA and pluronic bioprinting to create the bone region. (B) Macroscopic images of bioprinted scaffold. Live/dead analysis of MSC-laden GelMA bio-ink including microchannels after washing out pluronic. Scale bars = 0.5 mm and 3 mm. (C) Inkjet bioprinting procedure to obtain the cartilage part. Adapted from [88].

4. Current Limitations of 3D Bioprinting

Despite these advances, one of the greatest difficulties is the fabrication of scaffolds that possess similar mechanical properties to those of native tissues. Therefore, the inclusion of other novel polymers such as silk fibroin has been studied, resulting in an interesting component for these purposes. As an alternative, chemical modification, such as polymer methacrylation, has also been applied. However, this is a goal that has not been fully achieved yet, especially in the case of bone bioprinting, which requires superior mechanical properties to cartilage tissue. Additionally, printing technology has been combined with bioprinting in order to produce synthetic polymers with good mechanical properties, such as PCL, with more acceptable biomechanical values. On the other hand, in the case of bone, bioceramics such as HAP or inorganic components such as GO have been included in scaffolds to achieve desirable biomechanics. Furthermore, osteoconductivity and osteoinduction have also been enhanced by adding these components.

Another challenge is the fabrication of the entire osteochondral unit. Lately, thanks to the advantages provided by 3D bioprinting techniques, some interesting results have been obtained. Among these, the manufacture of biomaterial gradient scaffolds together with the addition of specific growth factors to the bio-inks has been shown to be successful.

From a more general point of view, while 3D printing has been acquiring clinical importance, 3D bioprinting technology is in its beginnings, and there has been no translation to clinical practice yet. This lack of translation could be due to safety, ethical, and regulatory issues. Safety problems are related to the materials used to fabricate the bio-inks. For instance, the use of mesenchymal and pluripotent stem cells has been widely expanded when it comes to manufacturing bio-inks, but they are not exempt from problems such as tumor formation [92]. Moreover, cell behavior may change after exposing the cells to high bioprinting pressures or to crosslinkers such as UV light [93]. Likewise, biomaterials of non- human origin, such as alginate or gelatin, are widely utilized in the bioprinting field, but few studies have focused on the immunological response *in vivo* or on possible pathogen transmission. In addition, treatments of animal origin could be ethically controversial to apply to certain populations with religious and cultural beliefs. On the other hand, the high cost of the bioprinting process could lead such therapy to be accessible only to people with high purchasing power, which would be ethically questionable [92]. Finally, there is a discussion among regulatory agencies about the category in which the bioprinted scaffolds should be classified. In fact, a bioprinting scaffold can be a medical device, an advanced therapy medicinal product, and a medicinal product at the same time, with different regulatory requirements and protocols [93].

5. Conclusions

The rise of 3D bioprinting technology has brought a wide range of opportunities to the tissue engineering field. Currently, 3D bioprinting technology allows the fabrication of structures that can regenerate tissues such as cartilage and bone. Thus, it opens the door to achieving the treatment of certain

osteoarticular diseases, such as OA, which not only has a high prevalence, but also entails an economic burden on healthcare systems. Until the appearance of this technology, current scaffolding techniques have failed in producing osteochondral tissue substitutes with adequate mechanical properties and a multilayered internal structure. However, 3D bioprinting allows the layer-by-layer manufacturing of structures that can resemble native tissues. Moreover, this technique can use a wide range of biomaterials, among which natural polymers stand out. Gelatin and alginate, together with the ECM components, such as collagen, HA, and chondroitin sulfate, have shown to be promising for osteochondral regeneration, since they demonstrate good biocompatibility, biodegradability, and non-cytotoxic properties. On the other hand, synthetic components such as methacrylate polymers and PCL, along with ceramics and graphene oxide, have also been applied for scaffold fabrication, especially in bone regeneration, since it requires high mechanical properties, osteoconduction, and osteoinduction. In addition, 3D bioprinting allows the use of high cell densities. Among them, chondrocytes have mostly been used to evaluate the biocompatibility of the ink and the bioprinting process. Meanwhile, the use of MSCs that have the ability to differentiate into specific cell types has attracted attention for scaffolds that regenerate cartilage and bone.

Other advantages of 3D bioprinting are that it is fast, automatic, and reproducible. Furthermore, this technique may bring personalized medicine closer to clinical practice since, on the one hand, biomaterials may be improved for specific organs and patients, and on the other hand, the doses of molecules, drugs, or biological components may be adjusted for each patient. For all of these reasons, 3D bioprinting may be a feasible technology to manufacture 3D structures that regenerate cartilage, bone, and both tissues at the same time. However, the improvement of biomechanical properties and the biofabrication of multilayered scaffolds to simulate native tissues are still drawbacks that need to be addressed. Additionally, safety, ethical, and regulatory concerns should also be taken into consideration in the future.

Funding: This research was funded by the BASQUE COUNTRY GOVERNMENT/ EUSKO JAURLARITZA (Department of Education, University and Research, Consolidated Groups IT907- 16). Author S.R.A. thank the BASQUE COUNTRY GOVERNMENT for the granted fellowship (PRE_2021_2_0153).

Informed Consent Statement: Not applicable.

Acknowledgments: This study was financially supported by the Basque Country Government (IT907- 16) and the University of the Basque Country UPV/EHU. The authors thank the Basque Government for the fellowship granted to Sandra Ruiz-Alonso (PRE_2021_2_0153). Likewise, the authors thank ICTS "NANBIOSIS", in particular the Drug Formulation Unit (U10) of the CIBER in Bioengineering, Biomaterials, and Nanomedicine (CIBER-BBN), at the University of the Basque Country (UPV/EHU) in Vitoria-Gasteiz.

Conflicts of Interest: The authors declare no conflict of interest. The company had no role in the design of the study; in the collection, analyses, or interpretation of data; in the writing of the manuscript, and in the decision to publish the results.

References

1. Xu, J.; Ji, J.; Jiao, J.; Zheng, L.; Hong, Q.; Tang, H.; Zhang, S.; Qu, X.; Yue, B. 3D Printing for Bone-Cartilage Interface Regeneration. Front. Bioeng. Biotechnol. 2022, 10, 828921. [CrossRef] [PubMed]

2. Poveda-Roda, R.; Bagán, J.V.; Sanchis, J.; Margaix, M. Pseudotumors and Tumors of the Temporomandibular Joint. A Review. Med. Oral Patol. Oral Cirugía Bucal 2013, 18, e392–e402. [CrossRef] [PubMed]

3. García-Arias, M.; Balsa, A.; Mola, E.M. Septic Arthritis. Best practice & research. Clin. Rheumatol. 2011, 25, 407–421.

4. Chau, M.M.; Klimstra, M.A.; Wise, K.L.; Ellermann, J.M.; Tóth, F.; Carlson, C.S.; Nelson, B.J.; Tompkins, M.A. Osteochondritis Dissecans. J. Bone Jt. Surg. 2021, 103, 1132. [CrossRef] [PubMed]

5. Hawker, G.A. OA Serious Disease. Clin. Exp. Rheumatol. 2019, 37, 3.

6. David, O.; Hunter, J.; Bierma-Zeinstra, S. Osteroarthritis. Lancet Semin. 2019, 393, 1745.

7. Jorgensen, C.; Simon, M. In Vitro Human Joint Models Combining Advanced 3D Cell Culture and Cutting-Edge 3D Bioprinting Technologies. Cells 2021, 10, 596. [CrossRef]

8. Daly, A.C.; Freeman, F.E.; Gonzalez-Fernandez, T.; Critchley, S.E.; Nulty, J.; Kelly, D.J. 3D Bioprinting for Cartilage and Osteochondral Tissue Engineering. Adv. Healthc. Mater. 2017, 6, 1700298. [CrossRef]

9. Hunter, D.J.; March, L.; Chew, M. OA in 2020 and beyond. Lancet Comm. 2020, 396, 1711. [CrossRef]

10. Hunter, D.J.; Schofield, D.; Callander, E. The Individual and Socioeconomic Impact of Osteoarthritis. Nat. Rev. Rheumatol. 2014,10, 437–441. [CrossRef]

11. Laires, P.A.; Canhão, H.; Rodrigues, A.M.; Eusébio, M.; Gouveia, M.; Branco, J.C. The Impact of Osteoarthritis on Early Exit from Work: Results from a Population-Based Study. BMC Public Health 2018, 18, 472. [CrossRef]

12. Critchley, S.E.; Kelly, D.J. Bioinks for Bioprinting Functional Meniscus and Articular Cartilage. J. 3D Print. Med. 2017, 1, 269.[CrossRef]

13. Puig-Junoy, J.; Ruiz Zamora, A. Socio-Economic Costs of Osteoarthritis: A Systematic Review of Cost-of-Illness Studies. Semin. Arthritis Rheum. 2014, 44, 531–541. [CrossRef]

14. Loza, E.; Lopez-Gomez, J.M.; Abasolo, L.; Maese, J.; Carmona, L.; Batlle-Gualda, E. Economic Burden of Knee and Hip Osteoarthritis in Spain. Arthritis Rheum. 2009, 61, 158–165. [CrossRef]

15. Ramos, T.; Moroni, L. Tissue Engineering and Regenerative Medicine 2019: The Role of Biofabrication—A Year in Review. Tissue Eng. Part C Methods 2020, 26, 91–106. [CrossRef]

16. Derakhshanfar, S.; Mbeleck, R.; Xu, K.; Zhang, X.; Zhong, W.; Xing, M. 3D Bioprinting for Biomedical Devices and Tissue Engineering: A Review of Recent Trends and Advances. Bioact. Mater. 2018, 3, 144–156. [CrossRef]

17. Bhat, A.; Janarthanan, M. Human Joint Anatomy and Physiology. In Pediatric Rheumatology; Springer: Berlin/Heidelberg,Germany, 2016; pp. 29–35.

18. Nesic, D.; Whiteside, R.; Brittberg, M.; Wendt, D.; Martin, I.; Mainil-Varlet, P. Cartilage Tissue Engineering for Degenerative Joint Disease. Adv. Drug Deliv. Rev. 2006, 58, 300–322. [CrossRef]

19. Daly, A.C.; Critchley, S.E.; Rencsok, E.M.; Kelly, D.J. A Comparison of Different Bioinks for 3D Bioprinting of Fibrocartilage and Hyaline Cartilage. Biofabrication 2016, 8, 045002. [CrossRef]

20. Johnston, T.P. Anatomy and Physiology of the Oral Mucosa. In Oral Mucosal Drug Delivery and Therapy; Springer: Boston, MA,USA, 2015; pp. 1–15.

21. Gadjanski, I.; Vunjak-Novakovic, G. Challenges in Engineering Osteochondral Tissue Grafts with Hierarchical Structures. Expert Opin. Biol. Ther. 2015, 15, 1583–1599. [CrossRef]

22. Denoix, J.; Jeffcott, L.B.; McIlwraith, C.W.; van Weeren, P.R. A Review of Terminology for Equine Juvenile Osteochondral Conditions (JOCC) Based on Anatomical and Functional Considerations. Vet. J. 2013, 197, 29–35. [CrossRef]

23. Li, G.; Yin, J.; Gao, J.; Cheng, T.S.; Pavlos, N.J.; Zhang, C.; Zheng, M.H. Subchondral Bone in Osteoarthritis: Insight into Risk Factors and Microstructural Changes. Arthritis Res. Ther. 2013, 15, 223. [CrossRef] [PubMed]

24. Sophia Fox, A.J.; Bedi, A.; Rodeo, S.A. The Basic Science of Articular Cartilage: Structure, Composition, and Function. Sports Health 2009, 1, 461–468. [CrossRef] [PubMed]

25. Guimarães, C.F.; Gasperini, L.; Marques, A.P.; Reis, R.L. The stiffness of living tissues and its implications for tissue engineering.Nat. Rev. Mater. 2020, 5, 351. [CrossRef]

26. Schiphof, D.; Boers, M.; Bierma-Zeinstra, S.M.A. Differences in Descriptions of Kellgren and Lawrence Grades of Knee Os- teoarthritis. Ann. Rheum. Dis. 2008, 67, 1034–1036. [CrossRef]

27. Kohn, M.D.; Sassoon, A.A.; Fernando, N.D. Classifications in Brief: Kellgren-Lawrence Classification of Osteoarthritis. Clin. Orthop. Relat. Res. 2016, 474, 1886–1893. [CrossRef]

28. Kolasinski, S.L.; Neogi, T.; Hochberg, M.C.; Oatis, C.; Guyatt, G.; Block, J.; Callahan, L.; Copenhaver, C.; Dodge, C.; Felson, D.; et al. 2019 American College of Rheumatology/Arthritis Foundation Guideline for the Management of Osteoarthritis of the Hand, Hip, and Knee. Arthritis Rheumatol. 2020, 72, 220–233. [CrossRef]

29. Grässel, S.; Muschter, D. Recent Advances in the Treatment of Osteoarthritis. F1000 Res. 2020, 9, 325. [CrossRef]

30. Primorac, D.; Molnar, V.; Matišic´, V.; Hudetz, D.; Jelecˇ, Ž.; Rod, E.; Cˇ ukelj, F.; Vidovic´, D.; Vrdoljak, T.; Dobricˇic´, B.; et al. Comprehensive Review of Knee Osteoarthritis Pharmacological Treatment and the Latest Professional Societies' Guidelines. Pharmaceuticals 2021, 14, 205. [CrossRef]

31. Anandacoomarasamy, A.; March, L. Current Evidence for Osteoarthritis Treatments. Ther. Adv. Musculoskelet. Dis. 2010, 2, 17–28. [CrossRef]

32. Trasolini, N.A.; McKnight, B.M.; Dorr, L.D. The Opioid Crisis and the Orthopedic Surgeon. J. Arthroplast. 2018, 33, 3379–3382.e1. [CrossRef]

33. Bartha, L.; Vajda, A.; Duska, Z.; Rahmeh, H.; Hangody, L. Autologous Osteochondral Mosaicplasty Grafting. J. Orthop. Sports Phys. Ther. 2006, 36, 739–750. [CrossRef]

34. Robinson, A.; Lindsay, A.; Vidal, A.; Frank, R.M. Osteochondral Autograft Transfer (OATS). Oper. Tech. Sports Med. 2020, 28, 150781. [CrossRef]

35. Belk, J.W.; Kraeutler, M.J.; Houck, D.A.; Goodrich, J.A.; Dragoo, J.L.; McCarty, E.C. Platelet-Rich Plasma Versus Hyaluronic Acid for Knee Osteoarthritis: A Systematic Review and Meta-Analysis of Randomized Controlled Trials. Am. J. Sports Med. 2021, 49, 249–260. [CrossRef]

36. Everts, P.; Onishi, K.; Jayaram, P.; Lana, J.F.; Mautner, K. Platelet-Rich Plasma: New Performance Understandings and Therapeutic Considerations in 2020. Int. J. Mol. Sci. 2020, 21, 7794. [CrossRef]

37. Hulme, C.H.; Perry, J.; McCarthy, H.S.; Wright, K.T.; Snow, M.; Mennan, C.; Roberts, S. Cell Therapy for Cartilage Repair. Emerg. Top. Life Sci. 2021, 5, 575–589. [CrossRef]

38. Jevotovsky, D.S.; Alfonso, A.R.; Einhorn, T.A.; Chiu, E.S. Osteoarthritis and Stem Cell Therapy in Humans: A Systematic Review.Osteoarthr. Cartil. 2018, 26, 711–729. [CrossRef]

39. Vilela, C.A.; Correia, C.; Da, A.; Morais, S.; Santos, C.; Gertrudes, A.C.; Moreira, E.S.; Frias, A.M.; Learmonth, D.A.; Oliveira, P.; et al. In Vitro and in Vivo Performance of Methacrylated Gellan Gum Hydrogel Formulations for Cartilage Repair. J. Biomed. Mater. Res. Part A 2018, 106, 1987–1996. [CrossRef]

40. Delplace, V.; Boutet, M.; Le Visage, C.; Maugars, Y.; Guicheux, J.; Vinatier, C. Osteoarthritis: From Upcoming Treatments to Treatments Yet to Come. Joint, bone, spine. Rev. Rhum. 2021, 88, 105206.

41. Manferdini, C.; Trucco, D.; Saleh, Y.; Gabusi, E.; Dolzani, P.; Lenzi, E.; Vannozzi, L.; Ricotti, L.; Lisignoli, G. RGD-Functionalized Hydrogel Supports the Chondrogenic Commitment of Adipose Mesenchymal Stromal Cells. Gels 2022, 8, 382. [CrossRef]

42. Trucco, D.; Vannozzi, L.; Teblum, E.; Telkhozhayeva, M.; Gilbert, D.; Nessim, S.; Affatato, H.; Al-Haddad, G.; Lisignoli; Ricotti, L. Graphene Oxide-Doped Gellan Gum-PEGDA Bilayered Hydrogel Mimicking the Mechanical and Lubrication Properties of Articular Cartilage. Adv. Healthc. Mater. 2021, 10, 2001434. [CrossRef]

43. Yao, H.; Kang, J.; Li, W.; Liu, J.; Xie, R.; Wang, Y.; Liu, S.; Wang, D.; Ren, L. Novel B -TCP/PVA Bilayered Hydrogels with Considerable Physical and Bio-Functional Properties for Osteochondral Repair. Biomed. Mater. 2018, 13, 015012. [CrossRef] [PubMed]

44. Roseti, L.; Desando, G.; Cavallo, C.; Petretta, M.; Grigolo, B. Articular Cartilage Regeneration in Osteoarthritis. Cells 2019, 8, 1305. [CrossRef] [PubMed]

45. Zhu, W.; Ma, X.; Gou, M.; Mei, D.; Zhang, K.; Chen, S. 3D Printing of Functional Biomaterials for Tissue Engineering. Curr. Opin. Biotechnol. 2016, 40, 103–112. [CrossRef]

46. Khademhosseini, A.; Langer, R. A Decade of Progress in Tissue Engineering. Nat. Protoc. 2016, 11, 1775. [CrossRef] [PubMed]

47. Foyt, D.A.; Norman, M.D.A.; Yu, T.T.L.; Gentleman, E. Exploiting Advanced Hydrogel Technologies to Address Key Challenges in Regenerative Medicine. Adv. Healthc. Mater. 2018, 7, 1700939. [CrossRef] [PubMed]

48. Hölzl, K.; Lin, S.; Tytgat, L.; Van Vlierberghe, S.; Gu, L.; Ovsianikov, A. Bioink Properties before, during and After 3D Bioprinting. Biofabrication 2016, 8, 032002. [CrossRef]

49. Turnbull, G.; Clarke, J.; Picard, F.; Riches, P.; Jia, L.; Han, F.; Li, B.; Shu, W. 3D Bioactive Composite Scaffolds for Bone Tissue Engineering. Bioact. Mater. 2018, 3, 278–314. [CrossRef]

50. Gungor-Ozkerim, P.S.; Inci, I.; Zhang, Y.S.; Khademhosseini, A.; Dokmeci, M.R. Bioinks for 3D Bioprinting: An Overview. Biomater. Sci. 2018, 6, 915–946. [CrossRef]

51. Ruiz-Alonso, S.; Lafuente-Merchan, M.; Ciriza, J.; Saenz-del-Burgo, L.; Pedraz, J.L. Tendon Tissue Engineering: Cells, Growth Factors, Scaffolds and Production Techniques. JCR 2021, 333, 448–486. [CrossRef]

52. Abdollahiyan, P.; Oroojalian, F.; Mokhtarzadeh, A.; Guardia, M. Hydrogel-Based 3D Bioprinting for Bone and Cartilage Tissue Engineering. Biotechnol. J. 2020, 15, 2000095. [CrossRef]

53. Wu, Y.; Kennedy, P.; Bonazza, N.; Yu, Y.; Dhawan, A.; Ozbolat, I. Three-Dimensional Biopritning of Articular Cartilage: A systematic review. Cartilage 2021, 12, 76. [CrossRef]

54. Ruiz-Alonso, S.; Villate-Beitia, I.; Gallego, I.; Lafuente-Merchan, M.; Puras, G.; Saenz-Del-Burgo, L.; Pedraz, J.L. Current Insights into 3D Bioprinting: An Advanced Approach for Eye Tissue Regeneration. Pharmaceutics 2021, 13, 308. [CrossRef]

55. Cao, Y.; Cheng, P.; Sang, S.; Xiang, C.; An, Y.; Wei, X.; Shen, Z.; Zhang, Y.; Li, P. Mesenchymal Stem Cells Loaded on 3D-Printed Gradient Poly(E-Caprolactone)/Methacrylated Alginate Composite Scaffolds for Cartilage Tissue Engineering. Regen. Biomater. 2021, 8, rbab019.

56. Chen, W.; Xu, Y.; Liu, Y.; Wang, Z.; Li, Y.; Jiang, G.; Mo, X.; Zhou, G. Three-Dimensional Printed Electrospun Fiber-Based Scaffold for Cartilage Regeneration. Mater. Des. 2019, 179, 107886. [CrossRef]

57. Beketov, E.E.; Isaeva, E.V.; Yakovleva, N.D.; Demyashkin, G.A.; Arguchinskaya, N.V.; Kisel, A.A.; Lagoda, T.S.; Malakhov, E.P.; Kharlov, V.I.; Osidak, E.O.; et al. Bioprinting of Cartilage with Bioink Based on High-Concentration Collagen and Chondrocytes. Int. J. Mol. Sci. 2021, 22, 11351. [CrossRef]

58. Yang, X.; Lu, Z.; Wu, H.; Li, W.; Zheng, L.; Zhao, J. Collagen-Alginate as Bioink for Three-Dimensional (3D) Cell Printing Based Cartilage Tissue Engineering. Mater. Sci. Eng. C 2018, 83, 195–201. [CrossRef]

59. Nguyen, D.; Hägg, D.A.; Forsman, A.; Ekholm, J.; Nimkingratana, P.; Brantsing, C.; Kalogeropoulos, T.; Zaunz, S.; Concaro, S.; Brittberg, M.; et al. Cartilage Tissue Engineering by the 3D Bioprinting of iPS Cells in a Nanocellulose/Alginate Bioink. Sci. Rep. 2017, 7, 658. [CrossRef]

60. Rathan, S.; Dejob, L.; Schipani, R.; Haffner, B.; Möbius, M.E.; Kelly, D.J. Fiber Reinforced Cartilage ECM Functionalized Bioinks for Functional Cartilage Tissue Engineering. Adv. Healthc. Mater. 2019, 8, 1801501. [CrossRef]

61. Visscher, D.O.; Lee, H.; van Zuijlen, P.P.M.; Helder, M.N.; Atala, A.; Yoo, J.J.; Lee, S.J. A Photo-Crosslinkable Cartilage-Derived Extracellular Matrix Bioink for Auricular Cartilage Tissue Engineering. Acta Biomater. 2021, 121, 193–203. [CrossRef]

62. Zhang, X.; Liu, Y.; Luo, C.; Zhai, C.; Li, Z.; Zhang, Y.; Yuan, T.; Dong, S.; Zhang, J.; Fan, W. Crosslinker-Free Silk/Decellularized Extracellular Matrix Porous Bioink for 3D Bioprinting-Based Cartilage Tissue Engineering. Mater. Sci. Eng. C. 2021, 118, 111388. [CrossRef]

63. Li, Z.; Zhang, X.; Yuan, T.; Zhang, Y.; Luo, C.; Zhang, J.; Liu, Y.; Fan, W. Addition of Platelet-Rich Plasma to Silk Fibroin Hydrogel Bioprinting for Cartilage Regeneration. Tissue Eng. Part A 2020, 26, 886–895. [CrossRef]

64. Singh, Y.P.; Bandyopadhyay, A.; Mandal, B.B. 3D Bioprinting using Cross-Linker-Free Silk–Gelatin Bioink for Cartilage Tissue Engineering. ACS Appl. Mater. Interfaces 2019, 11, 33684–33696. [CrossRef]

65. Li, C.; Wang, K.; Zhou, X.; Li, T.; Xu, Y.; Qiang, L.; Peng, M.; Xu, Y.; Xie, L.; He, C.; et al. Controllable Fabrication of Hydroxybutyl Chitosan/Oxidized Chondroitin Sulfate Hydrogels by 3D Bioprinting Technique for Cartilage Tissue Engineering. Biomed. Mater. 2019, 14, 025006. [CrossRef]

66. Galarraga, J.H.; Kwon, M.Y.; Burdick, J.A. 3D Bioprinting Via an in Situ Crosslinking Technique Towards Engineering Cartilage Tissue. Sci. Rep. 2019, 9, 19987. [CrossRef] [PubMed]

67. Di Bella, C.; Duchi, S.; O'connell, C.D.; Blanchard, R.; Augustine, C.; Yue, Z.; Thompson, F.; Richards, C.; Beirne, S.; Onofrillo, C.; et al. In Situ Handheld Three-dimensional Bioprinting for Cartilage Regeneration. J. Tissue Eng. Regen. Med. 2017, 12, 611. [CrossRef] [PubMed]

68. Ruiz-Cantu, L.; Gleadall, A.; Faris, C.; Segal, J.; Shakesheff, K.; Yang, J. Multi-Material 3D Bioprinting of Porous Constructs for Cartilage Regeneration. Mater. Sci. Eng. C. 2020, 109, 110578. [CrossRef] [PubMed]

69. de Ruijter, M.; Ribeiro, A.; Dokter, I.; Castilho, M.; Malda, J. Simultaneous Micropatterning of Fibrous Meshes and Bioinks for the Fabrication of Living Tissue Constructs. Adv. Healthc. Mater. 2019, 8, 1800418. [CrossRef] [PubMed]

70. Zhu, W.; Cui, H.; Boualam, B.; Masood, F.; Flynn, E.; Rao, R.D.; Zhang, Z.; Zhang, L.G. 3D Bioprinting Mesenchymal Stem Cell-Laden Construct with Core–shell Nanospheres for Cartilage Tissue Engineering. Nanotechnology 2018, 29, 158101. [CrossRef]

71. Wu, Y.; Ayan, B.; Moncal, K.K.; Kang, Y.; Dhawan, A.; Koduru, S.V.; Ravnic, D.J.; Kamal, F.; Ozbolat, I.T. Hybrid Bioprinting of Zonally Stratified Human Articular Cartilage using Scaffold-Free Tissue Strands as Building Blocks. Adv. Healthc. Mater. 2020, 9, 2001657. [CrossRef]

72. Mouser, V.H.M.; Levato, R.; Mensinga, A.; Dhert, W.J.A.; Gawlitta, D.; Malda, J. Bio-Ink Development for Three-Dimensional Bioprinting of Hetero-Cellular Cartilage Constructs. J. Connect. Tissue Res. 2018, 61, 137. [CrossRef]

73. Lafuente-merchan, M.; Ruiz-alonso, S.; Zabala, A.; Gálvez-martín, P.; Marchal, J.A.; Vázquez-lasa, B.; Gallego, I.; Saenz-del-burgo, L.; Pedraz, J.L. Chondroitin and Dermatan Sulfate Bioinks for 3D Bioprinting and Cartilage Regeneration. Macromol. Biosci. 2022, 22, e2100435. [CrossRef]

74. O'connell, C.D.; Di Bella, C.; Thompson, F.; Augustine, C.; Beirne, S.; Cornock, R.; Richards, C.J.; Chung, J.; Gambhir, S.; Yue, Z.; et al. Development of the Biopen: A Handheld Device for Surgical Printing of Adipose Stem Cells at a Chondral Wound Site. Biofabrication 2016, 8, 015019. [CrossRef]

75. Bhattacharjee, A.; Bose, S. 3D Printed Hydroxyapatite—Zn2+ Functionalized Starch Composite Bone Grafts for Orthopedic and Dental Applications. Mater. Des. 2022, 221, 110903. [CrossRef]

76. Genova, T.; Roato, I.; Carossa, M.; Motta, C.; Cavagnetto, D.; Mussano, F. Advances on Bone Substitutes through 3D Bioprinting. Int. J. Mol. Sci. 2020, 21, 7012. [CrossRef]

77. Bendtsen, S.T.; Quinnell, S.P.; Wei, M. Development of a Novel Alginate-polyvinyl Alcohol-hydroxyapatite Hydrogel for 3D Bioprinting Bone Tissue Engineered Scaffolds. J. Biomed. Mater. Res. 2017, 105, 1457. [CrossRef]

78. Keriquel, V.; Oliveira, H.; Rémy, M.; Ziane, S.; Delmond, S.; Rousseau, B.; Rey, S.; Catros, S.; Amédée, J.; Guillemot, F.; et al. In Situ Printing of Mesenchymal Stromal Cells, by Laser-Assisted Bioprinting, for in Vivo Bone Regeneration Applications. Sci. Rep. 2017, 7, 1178. [CrossRef]

79. Cunniffe, G.M.; Gonzalez-Fernandez, T.; Daly, A.; Sathy, B.N.; Jeon, O.; Alsberg, E.; Kelly, D.J. Three-Dimensional Bioprinting of Polycaprolactone Reinforced Gene Activated Bioinks for Bone Tissue Engineering. Tissue Eng. Part A 2017, 23, 891. [CrossRef]

80. Freeman, F.E.; Pitacco, P.; van Dommelen, L.H.A.; Nulty, J.; Browe, D.C.; Shin, J.Y.; Alsberg, E.; Kelly, D.J. 3D Bioprinting Spatiotemporally Defined Patterns of Growth Factors to Tightly Control Tissue Regeneration. Sci. Adv. 2020, 6, eabb5093. [CrossRef]

81. Kim, W.; Kim, G. Collagen/Bioceramic-Based Composite Bioink to Fabricate a Porous 3D hASCs-Laden Structure for Bone Tissue Regeneration. Biofabrication 2019, 12, 015007. [CrossRef]

82. Kolan, K.C.R.; Semon, J.A.; Bromet, B.; Day, D.E.; Leu, M.C. Bioprinting with Human Stem Cells-Laden Alginate-Gelatin Bioink and Bioactive Glass for Tissue Engineering. Int. J. Bioprint. 2019, 5, 3. [CrossRef]

83. Choe, G.; Oh, S.; Seok, J.M.; Park, S.A.; Lee, J.Y. Graphene Oxide/Alginate Composites as Novel Bioinks for Three-Dimensional Mesenchymal Stem Cell Printing and Bone Regeneration Applications. Nanoscale 2019, 11, 23275–23285. [CrossRef] [PubMed]

84. Zhang, J.; Eyisoylu, H.; Qin, X.; Rubert, M.; Müller, R. 3D Bioprinting of Graphene Oxide-Incorporated Cell-Laden Bone Mimicking Scaffolds for Promoting Scaffold Fidelity, Osteogenic Differentiation and Mineralization. Acta Biomater. 2021, 121, 637–652. [CrossRef] [PubMed]

85. Kumar, A.; Kargozar, S.; Baino, F.; Han, S.S. Additive Manufacturing Methods for Producing Hydroxyapatite and Hydroxyapatite- Based Composite Scaffolds: A Review. Front. Mater. 2019, 6, 313. [CrossRef]

86. Raslan, A.; Saenz del Burgo, L.; Ciriza, J.; Pedraz, J.L. Graphene Oxide and Reduced Graphene Oxide-Based Scaffolds in Regenerative Medicine. Int. J. Pharm. 2020, 580, 119226. [CrossRef]

87. Sun, Y.; You, Y.; Jiang, W.; Wang, B.; Wu, Q.; Dai, K. 3D Bioprinting Dual-Factor Releasing and Gradient-Structured Constructs Ready to Implant for Anisotropic Cartilage Regeneration. Sci. Adv. 2020, 6, 37. [CrossRef]

88. Daly, A.C.; Kelly, D.J. Biofabrication of Spatially Organised Tissues by Directing the Growth of Cellular Spheroids within 3D Printed Polymeric Microchambers. Biomaterials 2019, 197, 194–206. [CrossRef]

89. Burdis, R.; Chariyev-Prinz, F.; Kelly, D.J. Bioprinting of Biomimetic Self-Organised Cartilage with a Supporting Joint Fixation Device. Biofabrication 2021, 14, 015008. [CrossRef]

90. Deng, C.; Yang, J.; He, H.; Ma, Z.; Wang, W.; Zhang, Y.; Li, T.; He, C.; Wang, J. 3D Bio-Printed Biphasic Scaffolds with Dual Modification of Silk Fibroin for the Integrated Repair of Osteochondral Defects. Biomater. Sci. 2021, 9, 4891–4903. [CrossRef]

91. Kilian, D.; Ahlfeld, T.; Akkineni, A.R.; Bernhardt, A.; Gelinsky, M.; Lode, A. 3D Bioprinting of Osteochondral Tissue Substitutes— In Vitro-Chondrogenesis in Multi-Layered Mineralized Constructs. Sci. Rep. 2020, 10, 8277. [CrossRef]

92. Kirillova, A.; Bushev, S.; Abubakirov, A.; Sukikh, G. Bioethical and Legal Issues in 3D Bioprinting. Int. J. Bioprint. 2020, 6, 272. [CrossRef]

93. Gilbert, F.; O'Connell, C.D.; Mladenovska, T.; Dodds, S. Print Me an Organ? Ethical and Regulatory Issues Emerging from 3D Bioprinting in Medicine. Sci. Eng. Ethics 2017, 24, 73–91. [CrossRef]

Appendix 2

Development, characterization and sterilisation of Nanocellulose-alginate-(hyaluronic acid)-bioinks and 3D bioprinted scaffolds for tissue engineering

Markel Lafuente-Merchan[1,2,3], Sandra Ruiz-Alonso[1,2,3], Albert Espona-Noguera[1,2] , Patricia Gálvez-Martín[4,5], Elena López-Ruiz[6,7,8], Juan Antonio Marchal[6,7,9], Maria Luisa López-Donaire[2,10], Alaitz Zabala[11], Jesús Ciriza[1,2], Laura Saenz-del-Burgo[1,2,3*] and José Luis Pedraz [1,2,3*]

[1] NanoBioCel Group, Laboratory of Pharmaceutics, School of Pharmacy, University of the Basque Country (UPV/EHU), Paseo de la Universidad 7, 01006 Vitoria-Gasteiz, Spain.
[2] Biomedical Research Networking Center in Bioengineering, Biomaterials and Nanomedicine (CIBER-BBN), Health Institute Carlos III, Paseo de la Universidad 7, 01006 Vitoria-Gasteiz, Spain.
[3] Bioaraba, NanoBioCel Research Group, 01009 Vitoria-Gasteiz, Spain.
[4] R&D Animal and Human Health, Bioibérica S.A.U., 08029 Barcelona, Spain.
[5] Department of Pharmacy and Pharmaceutical Technology, Faculty of Pharmacy, University of Granada, Granada, Spain.
[6] Biopathology and Regenerative Medicine Institute (IBIMER), Centre for Biomedical Research, University of Granada, 18100 Granada, Spain.
[7] Instituto de Investigación Biosanitaria de Granada (ibs.GRANADA), Andalusian Health Service (SAS), University of Granada, Granada, Spain.
[8] Department of Health Sciences, University of Jaén, 23071 Jaén, Spain.
[9] Department of Human Anatomy and Embryology, Faculty of Medicine, University of Granada, 18016 Granada, Spain.
[10] Institute of Polymer Science and Technology, ICTP-CSIC, Juan de la Cierva 3, 28006 Madrid, Spain.
[11] Surface Technologies, Mondragon University-Faculty of Engineering, Loramendi 4, 20500 Arrasate-Mondragon, Spain.
[*] Correspondence: laura.saenzdelburgo@ehu.eus; joseluis.pedraz@ehu.eus

Materials Science & Engineering C, 2021, 126:112160.
IF: 8.547 (2021) (Q1)
Cat: Biomaterials & Bioengineering
https://doi.org/10.1016/j.msec.2021.112160

Abstract

3D-bioprinting is an emerging technology of high potential in tissue engineering (TE), since it shows effective control over scaffold fabrication and cell distribution. Biopolymers such as alginate (Alg), nanofibrillated cellulose (NC) and hyaluronic acid (HA) offer excellent characteristics for use as bioinks due to their excellent biocompatibility and rheological properties. Cell incorporation into the bioink requires sterilisation assurance, and autoclave, β-radiation and γ-radiation are widely used sterilisation techniques in biomedicine; however, their use in 3D-bioprinting for bioinks sterilisation is still in their early stages. In this study, different sterilisation procedures were applied on NC-Alg and NC-Alg-HA bioinks and their effect on several parameters was evaluated. Results demonstrated that NC-Alg and NC-Alg-HA bioinks suffered relevant rheological and physicochemical modifications after sterilisation; yet, it can be concluded that the short cycle autoclave is the best option to sterilise both NC-Alg based cell-free bioinks, and that the incorporation of HA to the NC-Alg bioink improves its characteristics. Additionally, 3D scaffolds were bioprinted and specifically characterized as well as the D1 mesenchymal stromal cells (D1-MSCs) embedded for cell viability analysis. Notably, the addition of HA demonstrates better scaffold properties, together with higher biocompatibility and cell viability in comparison with the NC-Alg scaffolds. Thus, the use of MSCs containing NC-Alg based scaffolds may become a feasible tissue engineering approach for regenerative medicine.

Keywords: 3D bioprinting; Sterilisation; Bioinks; Tissue engineering.

1. Introduction

Three-dimensional (3D) bioprinting is an emerging additive manufacturing technology with great potential for use in the field of tissue engineering (TE) and regenerative medicine. [1] 3D-bioprinting is also applied in the development of drug screening models, as well as tumor models and cell-based sensors. [2] Among tissue fabrication techniques, 3D-bioprinting has the advantage of being precise in simulating native tissues and mechanical properties. As a result, a great deal of progress has been achieved in the fabrication of tissues such as bone in which mechanical characteristics are highly important. [3,4] Additionally, scaffolds to cartilage regeneration have been widely studied too. In fact, scaffolds to regenerate articular cartilage have been achieved *in vitro*. [2,5] One of the tissues in which this technology has focused most is the skin. It has been reported many available literature with *in vivo* results, which printed skin substitutes for wounds and burns has been successfully obtained. [3,6,7] On the other hand, it has been applied in more complex structures such as cornea, [8] heart [9] and tendon. [10] However, despite the emerging increase in their usage, there is little information about its step forward to clinical practice. Thus, more research is still needed.

This technology is based on the deposition of a biomaterial embedded with cells in a previously arranged form, in order to create complex structures that mimic native biological tissues. [1,2] This mixture of one or more biomaterials, together with the cells of interest depending on the application, is known as bioink, and requires specific rheological and mechanical properties, so it can be used as bioprinting material. In addition, bioinks must be non-toxic and biocompatible, [2,11] given that bioprinted scaffolds final purpose is their use in clinical practise.

These biological and medical applications require a compulsory sterilisation step so that the scaffolds do not cause infections in the clinics. [12] Furthermore, unlike other medical devices that are sterilised in a final step before their biological applications, [13] bioinks must be sterilised prior to the incorporation of the cellular component, which is usually carried out just

before the bioprinting procedure itself. However, despite the importance of this sterilisation step, the alternatives for sterilising different biomaterials have been poorly studied.

Common sterilisation techniques have focused on achieving the highest degree of elimination of pathogens. Nevertheless, for 3D-bioprinting, not only must sterility be ensured, but also the procedure should not be too aggressive for the biomaterials that constitute the bioinks. Among the sterilisation techniques filtration, high temperatures, gases and radiation have been applied for the sterilisation of hydrogels used for regenerative medicine. [12] However, the high viscosity values that bioinks need to meet in order to be processed by the 3D printer, render filtration technique difficult to implement. On the other side, bioinks containing biomaterials sensitive to temperature can be damaged after being exposed to high temperatures by using autoclave. [11,14] As an alternative, the use of gases, such as ethylene oxide, have safety issues in terms of flammability, highly toxic residues and cancerous nature that must be taken into account. [12,15,16] In this context, Ultra-Violet light (UV), gamma (γ) radiation and beta (β) radiation have been applied for this purpose. [16–20] Ionising radiations have shown good assurance of sterility, [11,16] no chemical residues [15] and immediate results. [16] Yet, γ-radiation and β-radiation require complex application procedures and have an elevated cost,[16] whereas UV sterility assurance is dubious in value due to the low penetration capacity in highly viscous bioinks. [17]

After this review of the commonest methods of sterilisation, and given the little information available in the literature regarding the application of different sterilisation procedures to obtain safe bioinks, we planned to carry out an in-depth study of the effects of the application of the most promising sterilisation techniques, such as heat and radiation, onto bioinks composed of nanofibrillated cellulose (NC), sodium alginate (Alg) and hyaluronic acid (HA).

These biomaterials have been widely applied in biomedicine with promising results in different areas. NC is characterized by its high water content capacity, good biocompatibility and excellent physical and chemical properties.

[18,19] Furthermore, it has stood out in different applications as drug and protein delivery, [20] gene therapy [21] and wound healing. [22] On the other hand, Alg has become one of the most studied biopolymers in 3D-bioprinting. [23,24] It offers fast gelling capacity when it is mixed with divalent cations, such as calcium, which enables the manufacturing of manageable scaffolds after bioprinting.[23] Furthermore, its high biocompatibility makes it the ideal material for 3D-bioprinting. [2,11,23,25] The NC and Alg mixture as a bioink has been applied for the fabrication of 3D bioprinted scaffolds for cartilage regeneration as NC mimics the bulk collagen matrix of the cartilage tissue and Alg hydrogels have been reported to regenerate cartilage *in vivo*. [2,26,27]

Additionally, HA has been often used both to modify the bioinks rheological properties in order to favour the bioprinting process and in the fabrication of hydrogels for regenerative medicine. It has shown excellent biodegradability as well as biocompatibility properties, [18,28–30] and is involved in many biological processes such as cell adhesion, [18,29] migration and growth, [31,32] as well as in inflammatory processes and wound healing. [29,33,34] In addition, HA is a major component of native cartilage and it has been reported that controls chondrocyte metabolism and cartilage regeneration. [29] In fact, HA together with NC and Alg, has been applied for the fabrication of hydrogels and 3D printed structures for cartilage regeneration. [2,35] Furthermore, NC-Alg based hydrogels have resulted in gradual extracellular matrix formation and cartilage regeneration *in vivo* in nude mice models. [36]

Acknowledging the importance of selecting the best biomaterials to develop specific bioinks for 3D-bioprinting, as well as the relevance of choosing the correct sterilisation technique, this study is focused on evaluating the effect of three different sterilisation methods on these highly often employed materials. Two modalities of autoclaving (short and long cycle), as well as the sterilisation by β- and γ-radiation were used. Then, the effect of these procedures on the main properties of the biomaterials were analysed, as they are crucial for a correct printing. Next, an evaluation of whether the sterilised NC-Alg based bioinks (NC-Alg and NC-Alg-HA bioinks) in the manufacturing of 3D printed scaffolds that may be useful for regenerative medicine purposes was conduc-

ted. Finally, NC-Alg and NC-Alg-HA bioinks were loaded with murine D1 mesenchymal stem cells (D1-MSCs) before printing and the biological response of these cells included in 3D printed scaffolds was evaluated.

2. Materials and methods

2.1. Materials

Ultra-pure low-viscosity high guluronic acid sodium alginate (UPLVG) (Mw > 200 kDa) was purchased from FMC Biopolymer (Sandvika, Norway). Hyaluronic acid (Mw 600–800 kDa) was obtained from Bioiberica (Barcelona, Spain). Nanofibrillated cellulose was purchased from Sappi Europe (Brussels, Belgium). D-mannitol, calcium chloride and 3-(4,5-dimethylthiazol-2-yl)-2,5-diphenyltetrazoliumbromid (MTT) *in vitro* toxicology assay were purchased from Sigma-Aldrich (Madrid, Spain). Fetal bovine serum (FBS), fetal calf serum (FCS) and penicillin/streptomycin (P/S) were purchased from Fisher Scientific (Madrid, Spain). DPBS code BE17-513F was purchased from Lonza (Porriño, Spain). Alamar blue® was purchased from Bio-Rad científica (Madrid, Spain). LIVE/DEAD™ Viability/Cytotoxicity kit was purchased from Life Technologies (Madrid, Spain).

2.2. Bioinks preparation

Two different bioinks were prepared. Nanocellulose-alginate (NC- Alg) and nanocellulose-alginate-hyaluronic acid (NC-Alg-HA) bioinks.

For the NC-Alg bioink, first, a 10% (w/v) Alg solution was prepared in D-mannitol (1%). Then, NC was added and mixed until complete homogenization. The final bioink proportion of NC:Alg was 80:20 (v/v), and the final concentration of Alg in the NC-Alg bioink was 2% (w/v).

In order to prepare the NC-Alg-HA bioink, Alg and HA were dissolved in a D-mannitol solution to make an initial 10% (w/v) and 5% (w/v) solution, respectively. Then, NC was added and mixed until complete homogenization. The final bioink proportion of NC:Alg-HA was 80:20 (v/v), and in the NC-Alg-HA bioink the final concentration of Alg was 2% (w/v) and the concentration

of HA was 1% (w/v). Afterwards, bioinks were stored at 4 ◦C.

2.3. Sterilisation

Three sterilisation techniques were studied for each cell-free bioink: autoclave which includes short cycle and long cycle procedures, β-radiation and γ-radiation. For each technique 5–10 mL were sterilised by depositing the bioinks into closed sterile syringes

2.3.1. Sterilisation by short cycle autoclaving

This process was performed by AJL Ophthalmic (Miñano, Spain) in an industrial autoclave F0A2/B model. This autoclaving process was carried out for 54 min. The cycle started at 0.96 bar pressure and 15–18 ◦C temperature. Next, for 22 min the pressure and temperature increased until being set at 3.70–3.60 bar and 123–124 ◦C, respectively. The sterilisation occurred with these parameters set for 3.04 min. Afterwards, refrigeration process occurred and pressure and temperature decreased to 1.60 bar and 50–55 ◦C for 26 min. Finally, the cycle finished after 54 min with 1.05 bar pressure and around 50 ◦C temperature.

2.3.2. Sterilisation by long cycle autoclaving

The long cycle autoclaving process was performed in a clean autoclave ST DRY PV-II 75 L from Biotech (Barcelona, Spain). The sterilisation step occurred at 2 bar pressure and 121 ◦C for 30 min followed by an atmospheric purge in which pressure decreased around 0 bar and temperature was maintained at 121 ◦C. The whole process was carried out in 80 min. Fig. 1 shows the differences between short and long cycle autoclaving processes.

2.3.3. Sterilisation by β-radiation

β-radiation was performed according to ISO 11137 by Ionisos Iberica (Cuenca, Spain). [37] The samples were irradiated by a Rhodotron TT200, capable of generating a beam with energy of 10 MeV and a maximum power of 80 kW. The speed of the samples going under the beam was adjusted to guarantee the minimum dose of 25 kGy and homogeneity of dose was ensu-

red by passing the samples twice.

2.3.4. Sterilisation by γ-radiation

The sterilisation of the samples by γ-radiation was performed in a Mark I–30137Cs irradiator from J.L. Shepherd and Associates (San Fernando, United States). The system was calibrated by relative film dosimetry using Gafchromic EBT3 film as a dosimetry system. The average dose rate was 3.2 Gy. min^{-1} for radiation position. A dose rate is used for calculating radiation exposure times until achieving the required total dose, 25 kGy.

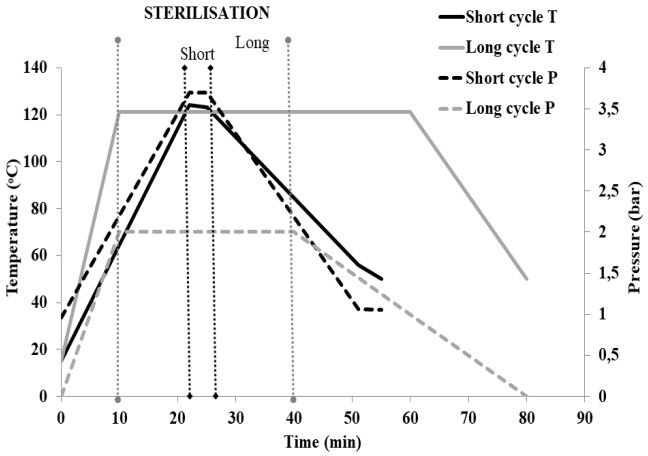

Fig. 1. Comparison between short cycle and long cycle autoclaving procedures.

2.4. Sterility testing

Sterility testing was conducted for NC-Alg and NC-Alg-HA cell-free bioinks after being sterilised by short and long cycle autoclaving procedures, β-radiation and γ-radiation.

The test was carried out by direct inoculation of 1 mL of sample (bioink) in the microbiology medium to test for the growth of yeast, fungi, aerobic, and anaerobic bacteria according to the European Pharmacopeia. [38] Two microbiological media were used: Thioglycollate Penase Broth (9 mL) (TPB) to detect anaerobic and aerobic bacteria, and Tryptic Soy Penase Broth (9 mL)

(TSPB) which is a soybean casein digest medium, to detect fungi and aerobic bacteria, both were purchased from VWR International (Radnor, United States). For each media (TPB and TSPB), sterility test and growth promotion test of aerobes, anaerobes and fungi were previously verified. The inoculated media with each bioink were incubated for 14 days at 35 ◦C and 22 ◦C for TPB and TSPB respectively. All samples were visually inspected every day to observe if media showed turbidity. After 14 days, if there had been microbial growth, the medium would have shown turbidity. This assay was performed under aseptic conditions inside a safety cabinet in a clean room.

2.5. Bioinks characterization

2.5.1. Rheological study

Rheological properties were measured at room temperature using the rheometer AR1000 from TA Instruments (New Castle, United States) with a flat stainless steel plate of 40 mm geometry. Two different rheological measurements were performed: viscosity and viscoelasticity.

In the steady flow measurement, viscosity was evaluated through a shear rate sweep from 0.1 to 100 s^{-1} followed by a second sweep from 100 to 0.1 s^{-1}. In addition, to study the bioinks viscoelasticity (storage modulus (G') and loss modulus (G")), 2% strain was set and the oscillation frequency sweeps were established from 0.1 to 100 Hz.

2.5.2. Macroscopic characteristics, osmolality and pH determination

The physical appearance of the bioinks was inspected visually before and after sterilisation. Macroscopic aspect and colour were evaluated.

Osmolality was determined by the cryoscopic osmometer Osmomat 030-D Gonotec (Berlin, Germany). In this assay, 50 µL of each bioink was analysed by determining the freezing depression point.

The pH was determined by pH-meter GLP 21 from Crison (Barcelona, Spain). Each sample was studied in triplicate.

2.6. 3D printing

The bioinks were printed using an extrusion-based 3D bioprinter Bio X from Cellink (Gothenburg, Sweden). Circular grid-like scaffolds of 15 mm diameter and 4 layers were printed through a 27 G conical nozzle. Printing parameters were set depending on the bioink. For NC-Alg bioink 4 mm/s printing speed and 20–22 kPa extrusion pressure was required. On the other hand, 4 mm/s printing speed and 24–26 kPa extrusion pressure were set for the NC-Alg-HA bioink. Finally, printed scaffolds were submerged in a 100 mM calcium solution in order to perform the crosslinking procedure.

2.7. Scaffolds characterization

2.7.1. Scanning electron microscopy (SEM)

Samples were coated with a thin layer of gold (~ 15 nm) using an Emitech K550X ion-sputter after critical point drying. Then, samples were observed in a S-3400 Scanning Electron Microscope from Hitachi (Elk Grove Village, United States). The voltage used was 15 kV and the working distance was around 20 mm.

2.7.2. Surface and architectural structure study

The surface topography and architecture of the scaffolds were characterized using an optical profilometer from Sensofar S-NEOX (Barcelona, Spain) through focus variation method. The measurements were post-processed using the metrological software SensoMAP Premium 7.4 from Digital Surf (Besançon, France). The scaffolds were characterized in hydrated state after wiping with a dry lint free wipe.

For architectural study, a measurement of 6484 x 4880 μm^2 area at 3 locations on 3 independently printed samples for each condition were acquired using a 10x objective (lateral sampling: 1.29 µm, vertical resolution: 25 nm). The deposited strut height and thickness were characterized and the deposited material volume was computed through the 3D parameter Vm. [39] Finally, measurements were binarized, and the aspect ratio (Dmax/Dmin) was computed in order to characterize the grid morphology. Surface topography

was characterized based on measurements of 873 × 656 μm^2 acquired at 3 different locations with a 20x objective (lateral sampling: 0.65 µm, vertical resolution: 8 nm). 3D topographical parameters belonging to height (Sq), spatial (Sal) and hybrid (Sdr) from ISO 25178-2 [40] were computed on cropped areas of 150 × 150 μm^2.

2.7.3. Swelling

To evaluate the swelling behaviour, 0.6 x 15 mm^2 NC-Alg and NC-Alg-HA scaffolds were printed. Then, the scaffolds were lyophilized in Telstar cryodos Freeze Dryer (Terrassa, Spain) and weighted in order to obtain the dried weight. Dried scaffolds were immersed in Dulbecco's phosphate-buffered saline (DPBS) with calcium and magnesium at 37 ◦C to estimate their swelling capacity. At selected time points, scaffolds were removed from DPBS, water excess was removed using filter paper and then scaffolds were reweighed. The swelling in % was calculated in every time point by using the following equation:

$$\text{Swelling (\%)} = \frac{W_{wet} - W_{dried}}{W_{dried}} \times 100$$

Where W_{wet} and W_{dried} correspond to wet and dried weight, respectively.

2.7.4. Degradation study

To evaluate the degradation process, the 3D printed NC-Alg and NC-Alg-HA scaffolds area were measured. Scaffolds were placed in DMEM at 37 ◦C and, at selected time points, they were measured again. After performing the measurements, scaffolds were returned to the culture medium. The area loss in % was calculated by using the following equation:

$$\text{Area loss (\%)} = \frac{A_{before} - A_{after}}{A_{before}} \times 100$$

Where A_{before} and A_{after} correspond to the scaffold area before introducing it in DMEM and after passing selected time inside the media.

2.8. Biological studies of bioprinted scaffolds

2.8.1. Cytotoxicity assay

In vitro cytotoxicity test was determined according to ISO 10993-5-2009. [41] Adhesion, indirect and direct methods were performed to evaluate potential cytotoxicity of bioinks in mouse L929 fibroblasts. Disks were bioprinted following the aforementioned procedure (see section 2.6). Cells were cultured in complete media and seeded at a cell density of 3.123×10^4 cells/cm^2.

In the adhesion assay, NC-Alg and NC-Alg-HA bioprinted disks were set on 24 well plates and cells were seeded on top of them. Then, after 4 h of incubation, cell viability was measured using the MTT *in vitro* toxicity assay following manufacture's recommendations. Cells directly seeded onto the plate were used as controls.

In the indirect method assay, bioprinted disks were incubated with DMEM for 24 h to obtain a conditioned media and cells were seeded at the same density as before onto independent wells. Then, disks were removed and the conditioned media was added to the cells. In direct method assay, cells were also seeded and cultivated for 24 h onto culture plates and exposed directly to the printed disk by placing them onto seeded cells. After 24 h of incubation, cell viability was measured in both assays using the same MTT procedure. Cells not exposed to conditioned media or cells with no bioprinted disk exposure were used as controls. In all assays, the absorbance was recorded using an Infinitive M200 microplate reader from TECAN Trading AG (Männedorf, Switzerland) at 570 nm with reference wavelength set at 650 nm.

Cell viability was calculated using the following equation:

$$\text{Cell viability (\%)} = \frac{\text{Testing sample OD570}}{\text{Untreated blank OD570}} \times 100$$

SiX independent experiments were conducted with three replicates per experiment. Cell viability above 70% was considered as non-toxic according to ISO 10993-5-2009.

2.8.2. D1-MSCs culture conditions and 3D-bioprinting

Murine D1-MSCs from ATCC (Virginia, United States) were cultured in T-flasks with DMEM supplemented with 10% (v/v) FBS and 1% (v/v) P/S. They were maintained at 37 ◦C in a humidified atmosphere containing 5% CO_2. Medium was regularly changed. At 80% of confluence, cells were sub-cultured.

For the 3D-bioprinting process, cells were incorporated and resuspended in the bioinks at 2.5 x 10^6 and 5 x 10^6 cell/mL density. Then they were bioprinted following the previously explained procedure (see section 2.6). Immediately after this, bioprinted scaffolds were crosslinked by adding a 100 mM $CaCl_2$ solution. These constructs were kept in the calcium solution for 5 min after which they were cultured in a complete medium. This whole process was performed at room temperature, under aseptic conditions.

2.8.3. Metabolic activity determination

The metabolic activity of the embedded D1-MSCs was determined weekly using the AlamarBlue® assay (AB). 15 mm circular grid-like bioprinted scaffolds were placed in 24 well plates with the solution containing 10% of AB in complete medium and then, they were incubated for 24 h at 37 ◦C. The fluorescence was read on an Infinite M200 microplate reader from TECAN Trading AG (Männedorf, Switzerland) at excitation 560 nm and 590 nm emission wavelength. Wells containing culture media were used as negative controls. At least five wells were placed for each condition.

2.8.4. Cell viability qualitative determination by fluorescence microscopy

Cell viability determination was carried out weekly using the LIVE/DEAD™ Viability/Cytotoxicity Kit. Constructs were washed four times with DPBS before performing the staining with 100 mM calcein AM in DPBS on 24 well plates for 40 min at room temperature in the dark. Then, the calcein solution was removed and a 0.8 μM ethidium homodimer-1 solution was added. The constructs were incubated for another 10 min at 37 ◦C and then, they were washed again with DPBS. Next, samples were observed under a Nikon TMS microscope (Hampton, United States) with the excitation/emission settings for calcein AM (495/515 nm) and ethidium homodimer (495/635 nm). At least

three independent experiments were analysed for each condition.

2.9. Statistics

Statistical analysis was performed with IBM SPSS software. Data were expressed as mean standard deviation and differences were considered significant when $p < 0.05$. Student's t-test to detect significant differences between two groups and ANOVA to multiple comparisons was used. Depending on the results of the Levene test of homogeneity of variances, Bonferroni or Tamhane post-hoc test was applied. For non-normally distributed data, Mann-Whitney nonparametric analysis was applied.

3. Results and discussion

3D-bioprinting is generally considered to be a powerful manufacture technique in TE since it allows the fabrication of scaffolds and artificial tissues in a controlled way. [2,11] Nonetheless, when introducing cells on supportive inks, the sterilisation assurance must be taken into account. Thus, three different sterilisation techniques, short and long cycle autoclaving, β-radiation and γ-radiation, on the NC-Alg and NC-Alg-HA cell-free bioinks were evaluated.

First, the sterility of all cell-free bioinks was studied according to the European Pharmacopeia to ensure no contamination. After carrying out the sterilisation methods, bioinks were incubated in the corresponding media for 14 days. Bioinks observation resulted in no turbidity detection (data not shown), which proved that NC-Alg and NC-Alg-HA bioinks were completely free of contaminating microorganisms after sterilisation by autoclaving with short and long procedures, β-radiation and γ-radiation. All negative control tubes were negative after the required incubation period.

The lack of contamination indicated that any of these methods are useful for NC-Alg based bioinks sterilisation. However, these processes may imply important physicochemical changes on bioinks characteristics resulting in bioprinting failure. [11] For this reason, the first objective was to study

whatever these sterilisation methods provoke relevant modifications on the characteristics that are of key importance for the printing process, such as the rheological and the physicochemical features.

3.1. Effect of different sterilisation methods on NC-Alg-based bioinks

3.1.1. Rheological properties

Bioprinting through the extrusion procedure requires the study of some fundamental properties of the bioinks such as their rheological characteristics. The rheological characterization of the NC-Alg based bioinks was studied by steady flow and oscillatory shear measurements before and after sterilisation.

Before sterilisation, NC-Alg and NC-Alg-HA bioinks showed shear thinning behaviour with a decrease in viscosity under shear strain. In addition, when shear rate values decreased, viscosity values return to the initial levels showing a thixotropic behaviour (Fig. 2). These properties are extremely useful for extrusion-based bioprinting because the deposition of the bioink is facilitated when it is extruded through a nozzle since the applied pressure decreases the bioink viscosity. Just after exiting the nozzle, the shear stress is removed and bioink viscosity increases sharply due to thixotropy. [42] Interestingly, the addition of HA to the NC-Alg bioink showed an enhancement on the viscosityvalues, achieving around 500 Pa.s at 0.1 s^{-1} shear rate (Fig. 2B), whereas without HA only a value of 400 Pa.s was achieved (Fig. 2A). This suggests that the addition of HA improves the NC-Alg bioink rheological properties and, therefore, its printability by extrusion.

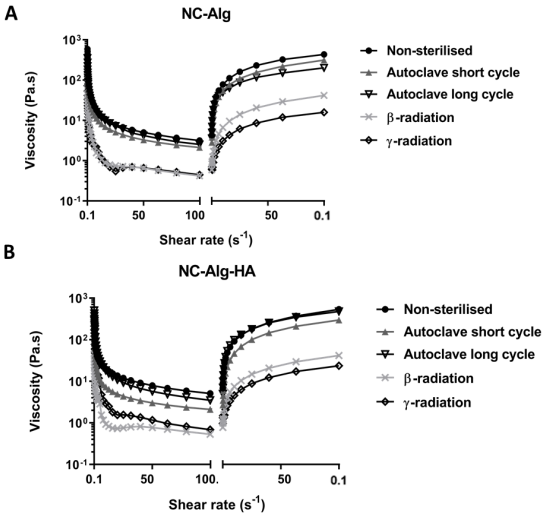

Fig. 2. Effect of sterilisation methods on NC-Alg (A) and NC-Alg-HA (B) bioinks rheological properties. Viscosity values were measured before and after sterilisation by short and long cycle autoclaving, β-radiation and γ-radiation.

The viscosity increase due to the incorporation of HA has been previously reported in the literature. One study indicated an improvement of the shear thinning property by increasing the HA content up to 50% on a gelatin-based bioink. [43] Moreover, higher viscosity values improve the printing fidelity, as the formation of filaments is better in comparison with low viscosity bioinks, which spread out on the bioprinting plate when extruded. [42] Therefore, our bioinks were expected to be easily bioprinted by the extrusion 3D bioprinter.

In Fig. 2 it can also be observed the effect of the proposed sterilisation methods. Although all samples maintained the thixotropic property, there were remarkable differences among the effects of the sterilisation procedures.

Short and long cycle autoclaved bioinks showed similar viscosity values compared to the non-sterilised bioinks, which suggests that these sterilised bioinks would show good printable properties. Nonetheless, an important modification in this parameter was observed on both bioinks after the ionising radiation treatments. Sterilisation by γ-radiation consists of the disruption of the DNA double helix of microorganisms due to the high doses of free radicals that are formed after electron excitation. Similar to γ-radiation, β-radiation

damages the DNA of microorganisms but, it does have lower penetration capacity than γ-radiation and requires higher dose rates. [15,44]. In this study, the same dose of 25 kGy was applied for both radiation procedures. The rheological study showed a sharp decrease in viscosity for both bioinks. In fact, although ionising radiations have been widely used as sterilisation methods in several biomedical fields, their destructive effects are known. [11,45] When comparing both radiation types, studies in the literature are inconclusive; one study showed that after applying β and γ-radiations on PLGA spheres, radicals were formed due to polymer destruction, independently of the radiation type. [46,47] However, another study on scaffolds fabricated with L-lactide (LLA), ε-caprolactone (CL) and 1.5-dioxepane-2-one (DXO) polymers, indicated that γ-radiation caused more important damages on the polymers. [16] Therefore, the effects of radiation-based sterilisation techniques on different materials depends not only on the type of radiation but also on the bioinks composition. Regarding this fact, it has been published that when these two radiation types were applied on hydroxypropyl-methyl cellulose (HPMC) and gelatin hydrogels, the viscosity reduction was more evident on HPMC-based gels, probably because its polymer chains are longer compared to gelatin. [43] In our case, γ-radiation provoked a considerable viscosity decrease in our two bioinks, which is in accordance with other studies reporting that γ-radiation causes chain scission on cellulose derived polymers [48] and Alg-based bioinks. [11]

Comparing NC-Alg and NC-Alg-HA bioinks, it was observed that the addition of HA on the NC-Alg mixture appeared to protect this bioink from the harmful effects of γ-radiation (Fig. 2B). However, the NC-Alg-HA bioink still showed a lower viscosity in comparison with its non-sterilised control bioink. In fact, modifications in the physical and chemical nature of the polymeric HA have also been reported after radiation. [49] Moreover, degradation of polysaccharides by the cleavage of the glycosidic bonds can occur after ionising radiations. [11,48] The chain scission results in molecular weight reduction, which is reflected on viscosity. [42]

Afterwards, in order to study bioinks viscoelastic properties, frequency

sweep measurements were performed. Fig. 3A shows that in both non-sterilised bioinks the storage modulus G' and loss modulus G" increased under frequency. As G' was higher than G", both bioinks showed an elastic solid-like behaviour. The loss modulus G" was higher when HA was added (at 100 Hz, NC-Alg G" was 808 Pa and with HA 1506 Pa), whereas the storage modulus G' was similar for both bioinks (NC-Alg was 2200 Pa and NC-Alg-HA was 2295 Pa). Therefore, the incorporation of HA in the NC-Alg bioink was able to enhance the viscous modulus.

Next the sterilisation effect on viscoelasticity was evaluated. Independently of the applied sterilisation technique, both bioinks maintained the elastic solid-like behaviour. However, changes on G' and G" values were observed. As Fig. 3B shows, after short cycle autoclaving procedure, both bioinks showed similar G' and G" values, but a slight increase in viscoelasticity was observed when compared to non- sterilised bioinks (at 100 Hz, sterile NC-Alg G" was 1497 Pa and NC- Alg- HA was 1655 Pa). In contrast, after long cycle autoclaving, the NC-Alg bioink showed higher G' and G" values compared to the HA bioink (at 100 Hz, sterile NC-Alg G' and G" were 2592 Pa and 1416 Pa respectively, and with HA were 853 Pa and 826 Pa respectively) (Fig. 3C). In addition, viscoelasticity values of the NC-Alg bioink were slightly higher in comparison with the non-sterilised sample. In contrast, the HA containing bioink showed a reduction on G' and G" values after sterilisation. This suggests that after the application of a long cycle autoclaving process, HA was probably damaged resulting in a lower viscous modulus value (G"). Importantly, it has been described that the viscosity of 0.5–2% HA aqueous solutions decreases when the temperature increases due to hydrogen bond breakage, resulting in weakening of the entanglement couplings. [50,51]

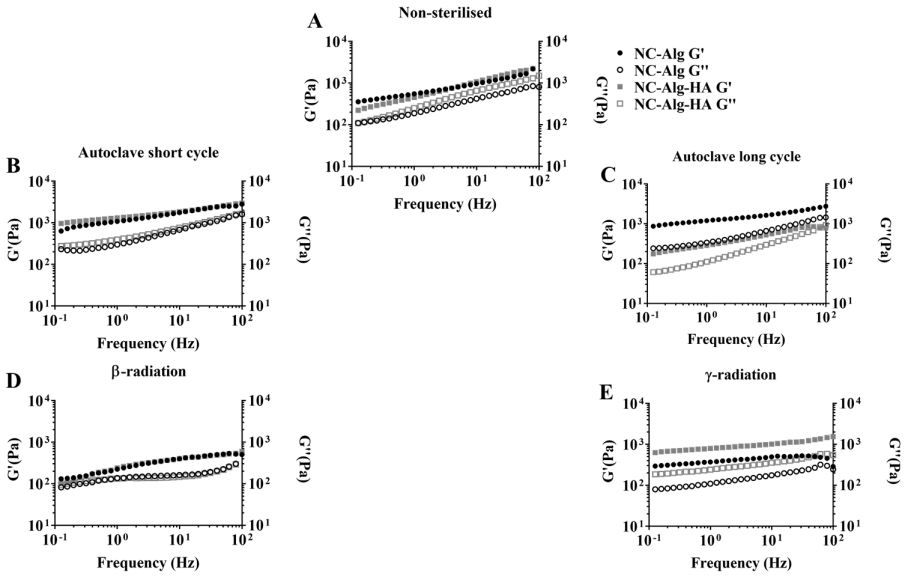

Fig. 3. Effect of sterilisation methods on NC-Alg and NC-Alg-HA bioinks frequency sweep measurements and viscoelasticity modules (G' and G"). A) Non-sterilised B) Short cycle autoclave; C) Long cycle autoclave; D) β-radiation; E) γ-radiation.

After the application of β-radiation (Fig. 3D), viscoelasticity properties of both bioinks decreased comparing to the non-sterilised samples (at 100 Hz, NC-Alg sterile bioink G' and G" were 504 Pa and 224 Pa, respectively and NC-Alg-HA were 598 Pa and 210 Pa, respectively). This sharp reduction on viscoelasticity properties of both bioinks might be related with the molecular weight loss of cellulose, which has been already reported after β-radiation. [52] After γ-radiation (Fig. 3E) differences between the two bioinks were detected; While the NC-Alg bioink showed a reduction on viscoelasticity in comparison to the non-sterilised sample, the NC-Alg-HA bioink demonstrated higher G' and G" values. This suggests that the NC-Alg bioink G' and G" values were modified after the application of both radiation types, but the NC-Alg-HA bioink only was damaged by β-rays. This may be explained by the overheating that β-rays may cause. [44]

3.1.2. Physicochemical properties

Next, macroscopic characteristics, osmolality and pH of NC-Alg and NC-

Alg-HA bioinks were studied before and after sterilisation. Between the NC-Alg and the NC-Alg-HA bioinks there were not significant differences regarding their physical appearance. Both were white and homogenous. After applying any of the sterilisation techniques evaluated, bioinks maintained their physio-chemical characteristics (supplementary material).

The osmolality study indicated no significant differences between both non-sterilised bioinks (0.0653 ± 0.0005 Osmol/kg for NC-Alg and 0.0883 ± 0.0006 Osmol/kg for NC-Alg-HA) (Fig. 4A). NC-Alg-HA bioink demonstrated higher osmolality values which suggests more physiological behaviour. Hyaluronic is a component of extracellular matrix in many tissues and, as much as the other glycosaminoglycans, may increase the osmolality of solutions [53]. Nonetheless, since physiological osmolality values are around 0.28 Osmol/kg, both bioinks showed to be hypoosmotic. However, no negative effects have been detected on cell behaviour due to cell embedded scaffolds culture is carried out inside abundant culture media. Subsequently osmolality was measured again in order to know if the sterilisation methods had any effect on this parameter. After both autoclaving procedures, NC-Alg bioink showed an increase in osmolality ($p < 0.001$). Similarly, these procedures enhanced the osmolality values of the HA-containing bioink (short cycle ($p < 0.001$) and long cycle ($p < 0.01$)). In contrast, after β-radiation only the NC-Alg bioink osmolality increased significantly ($p < 0.001$). Importantly, the effect was more accentuated after γ-radiation. In this case, osmolality values increased significantly on both bioinks ($p < 0.001$). It is known that degradation of biopolymers and polysaccharides could occur after heating or radiation treatments inducing molecular weight reductions. The occurred chain scission might increase the presence of radicals and osmotically active solutes in the media. [44,46] Therefore, it can be hypothesized that biopolymer structural changes occurring because of the sterilisation processes would increase bioinks osmolality. On the other hand, both non-sterilised bioinks showed pH values close to the physiological ones (7.29 ± 0.04 for NC-Alg and 6.28 ± 0.03 for NC-Alg-HA), and after sterilisation, the pH values were maintained without significant variations, as it is shown in Fig. 4B

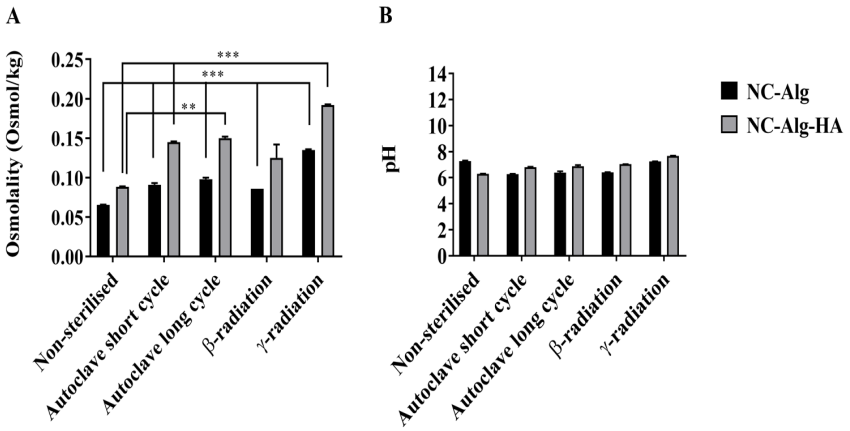

Fig. 4. Effect of sterilisation methods on NC-Alg and NC-Alg-HA bioinks A) Osmolality and B) pH. Values represent mean ± SD. ***: $p < 0.001$; **: $p < 0.01$.

3.2. Printability determination of bioinks

Once the NC-Alg and NC-Alg-HA bioinks had been characterized and the effects of the different methods of sterilisation had been evaluated, printability evaluation was required. Scaffolds were fabricated by the extrusion bioprinter following the parameters described before (section 2.6). The rheological studies in which the NC-Alg-HA bioink showed higher viscosity than the NC-Alg bioink resulted in the need of applying a higher pressure on bioprinting in order to be able to extrude the bioink through the nozzle (from 20 kPa of NC-Alg to 26 kPa of NC-Alg-HA). In addition, printability was evaluated after sterilisation.

After autoclaving (short and long cycle), similar bioprinting parameters were maintained. As an example, it can be observed in Figure 5A1 that the macroscopic appearance complied accurately with the computer design of the scaffold. Figure 5A2 shows the scaffold obtained after sterilising the NC-Alg-HA bioink by short cycle autoclaving. The printing results, together with rheological properties, indicated that bioinks sterilised through autoclave were adequate for extrusion printing. In contrast, when radiated bioinks were used, extrusion led to wide viscous strands which required lower extrusion pressu-

res and printing speed. The obtained scaffolds revealed lack of shape fidelity (supplementary material). These findings are supported by the accentuated decrease in viscosity showed in the rheological study. As discussed before, main-chain scission and crosslinking damages caused by ionising radiations avoided the bioprinting of properly defined scaffolds and, therefore, the scaffolds were unable to maintain their shape.

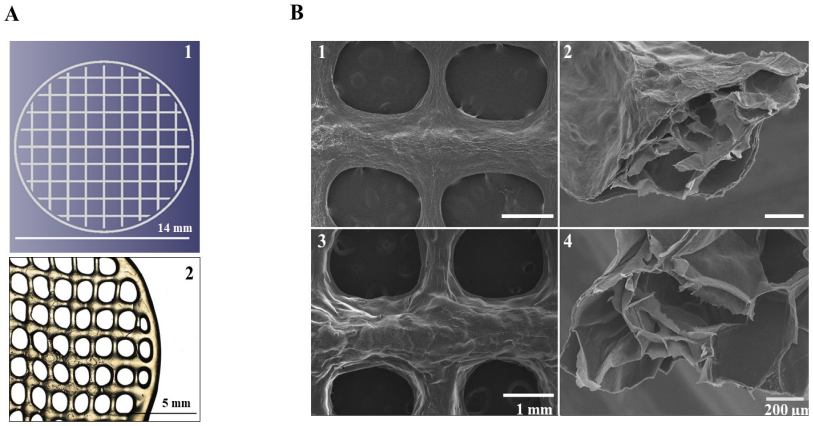

Fig. 5. Morphological characterization. A) Computer assisted design of the scaffold (1) vs bioprinted scaffold after autoclaving the NC-Alg-HA bioink by short cycle. Scale bar in 1: 14 mm and in 2: 5 mm (2). B) Representative scanning electron microscopy images of NC-Alg (1–2) and NC-Alg-HA (3–4) scaffolds. Scale bar in 1 and 3: 1 mm; in 2 and 4: 200 µm.

According to the rheological studies and the analysis of the physicochemical properties of the two cell-free bioinks as well as the printability study, it could be concluded that the sterilisation by using the short cycle autoclaving technique had the lowest effect on the original characteristics of the bioinks. Therefore, it was elected as the best option for sterilising both the NC-Alg and the NC-Alg-HA bioinks. However, prior to the introduction of cells in order to analyse the application of these scaffolds for TE, other aspects such as the 3D printed scaffolds characterization were evaluated.

3.3. Morphological characterization of printed scaffolds

3.3.1. Scanning electron microscopy (SEM)

NC-Alg and NC-Alg-HA scaffolds were analysed by SEM in order to observe

their external and internal structure that has been recognised as important factors for defining cellular behaviour. [39] The superficial structure showed that scaffolds with HA presented more fibrous structures (Fig. 5B, 3). In addition, the inner part of the scaffolds were observed by making crosscuts. A porous internal structure with channel-like arrangement was found in both scaffolds, which suggests that proper oxygen and nutrients transport can be ensured for achieving high cell viability and proliferation.

3.3.2. Surface and architectural structure study

In order to attain a more in-depth study of the architectural structures of both scaffolds, an optical profilometer technique was used. No reference has been found to this technique being used for studying printed scaffolds. Fig. 6A shows representative axonometric 3D images of the measurements carried out in the bioprinted scaffolds. Architectural differences can be observed between NC-Alg and NC-Alg-HA scaffolds. In fact, the NC-Alg-HA grid morphology is less rounded compared to the NC-Alg bioink, which generated more oblong shaped grids. In addition, the NC-Alg-HA scaffolds presented a significantly higher amount of deposited material compared to the NC-Alg scaffolds (3.51 ± 0.55 mm^3 NC-Alg scaffolds *versus* 7.53 ± 2.10 mm^3 NC-Alg-HA scaffolds) (Fig. 6B). However, both printed scaffolds presented a similar grid area and aspect ratio as Fig. 6C shows. The higher amount of deposited material in NC-Alg-HA scaffolds could be explained by the rheological and printability studies in which the NC-Alg-HA bioink showed higher viscosity than the NC-Alg bioink. This enhancement in viscosity resulted in the need for the application of a higher pressure on the bioprinting technique in order to be able to extrude the bioink through the nozzle. This increment in pressure may involve a higher amount of HA-containing bioink being extruded and, therefore, the amount of material deposited in the scaffolds.

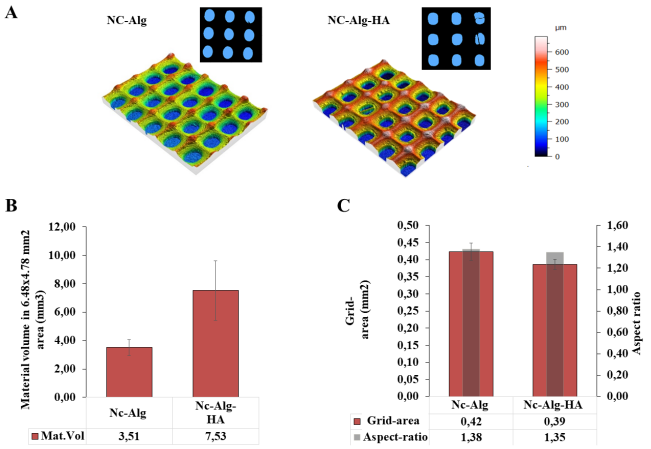

Fig. 6. Surface and architectural structure study of NC-Alg and NC-Alg-HA 3D printed scaffolds. A) Representative images of the topology measurements and binarized areas of the printed scaffolds. B) Deposited material volume analysis. C) Grid area and aspect ratio computed from binarized data analysis. Values represent mean ± SD.

This phenomenon was also shown in Fig. 7A-B in which NC-Alg-HA printed structures resulted in significantly thicker scaffolds on Y axis ($p < 0.01$) compared to the NC-Alg scaffolds (NC-Alg scaffolds, in Y direction 432 ± 30 µm; NC-Alg-HA scaffolds, 552 ± 24 µm). NC-Alg-HA scaffolds also resulted in a significantly greater height on two axis ($p < 0.01$) (NC-Alg scaffold, in X direction 345 ± 30 µm and in Y direction 215 ± 28 µm; NC-Alg-HA scaffolds, in X direction 549 ± 63 µm and in Y direction 476 ± 29 µm) (Fig. 7A-B). The strut shape also varied according to the direction for both bioinks, presenting a smaller height and thickness of the struts in the Y direction. However, despite the fact that NC-Alg-HA bioink was extruded in a higher quantity, the obtained scaffolds did not show loss of structure fidelity. In fact, both scaffolds grid areas were similar.

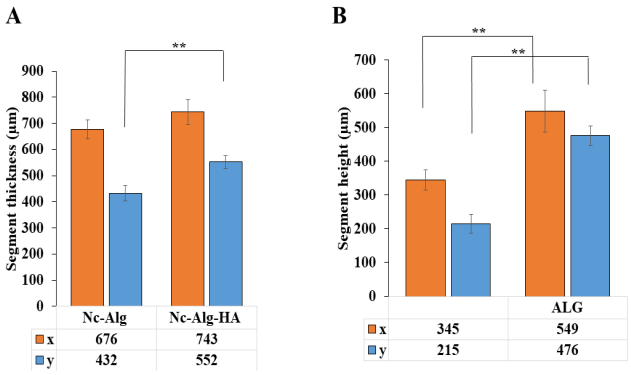

Fig. 7. Surface and architectural structure study on NC-Alg and NC-Alg-HA scaffolds. Analysis of the strut architecture of the bioprinted scaffolds in terms of thickness (A) and height (B). Values represent mean ± SD. **: $p < 0.01$.

Regarding the surface topography, it has been reported that it affects cells differentiation and tissue formation, such as bone. [54] NC-Alg printed scaffolds presented greater height characteristics (Sq, Fig. 8A). However, the NC-Alg-HA bioprinted scaffolds reported a superior developed surface area (Sdr Fig. 8B). The biggest topographical difference was observed in terms of lateral characteristics (Sal Fig. 8C). The bigger Sal parameter value on NC-Alg scaffolds indicates in Fig. 8D that the NC-Alg surface was dominated by larger wavelength components (texture presents bigger spacing) while NC-Alg-HA printed scaffolds presented a less spaced texture. However, there were no significant differences between both scaffolds, and the implication of these parameters on cells differentiation should be analysed in future studies.

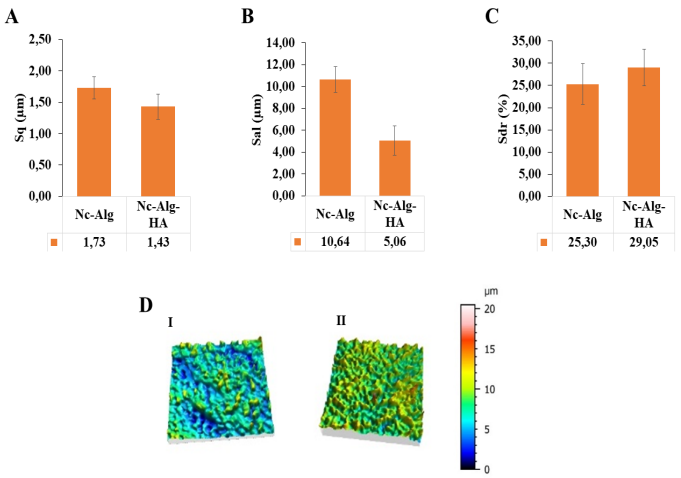

Fig. 8. Surface and architectural structure study on NC-Alg and NC-Alg-HA scaffolds. A-C) 3D topographical parameters describing height (Sq), lateral (Ssal) and hybrid (Sdr) characteristics of the scaffolds. Values represent mean ± SD. D) Representative axonometric projections of the topographical measurements of the NC-Alg (I) and NC-Alg-HA (II) scaffolds.

3.4. Swelling determination and scaffolds degradation analysis

Before introducing cells into the NC-Alg and NC-Alg-HA bioinks for printing the 3D scaffolds, swelling and degradation analysis of cell-free structures was performed.

The evaluation of swelling is important since it relates to substance exchange when used for biomedical applications as well as many other properties such as flexibility and mechanical properties. [55,56] In our study, water uptake by both printed scaffolds increased over the time until they reached the equilibrium with NC-Alg scaffolds reached it within 6 to 8 h, whereas the NC-Alg-HA scaffolds reached this steadiness earlier, within 3 to 4 h (Fig. 9A). Our results indicated fast swelling properties, which may be caused by the hydrophilicity of NC, Alg and HA. Some studies have reported that high elasticity values resulted in faster water uptake. [57] This may explain why the NC-Alg-HA scaffolds reached the equilibrium faster than the NC-Alg scaffolds.

On the other hand, although no statistically significant differences were

detected, the NC-Alg scaffolds water uptake was slightly higher (NC-Alg scaffolds swelling 95.61 ± 0.84% *versus* 94.34 ± 0.01% in NC-Alg-HA scaffolds). As it has been reported, dense bioinks swelling values decrease due to their dense inner structure. [55] Thus, this may explain why the HA-containing scaffolds absorbed less water, as this bioink had higher viscosity than the NC-Alg.

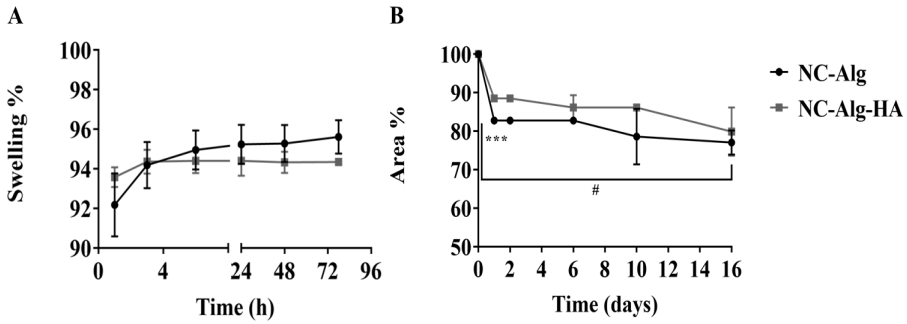

Fig. 9. NC-Alg and NC-Alg-HA printed scaffolds swelling determination (A) and degradation rate (B). Values represent mean ± SD. ***: $p < 0.001$, comparison between both scaffolds. #: $p < 0.05$, comparison between days in the same scaffold.

Degradation studies are essential in the evaluation of scaffolds behaviour and its implications on cells studies, such as differentiation and *in vivo* tissue formation. [58,59] Furthermore, a desirable feature in regenerative medicine would be the synchronization of scaffold degradation with the replacement by natural tissue produced from cells. [60] As Fig. 9B shows, NC-Alg and NC-Alg-HA scaffolds decreased their area during the first 24 h this reduction being more accentuated for the scaffolds without HA ($p < 0.001$) (NC-Alg 17.21 ± 0.15% area reduction *versus* 11.50 ± 0.36% in NC-Alg-HA scaffolds). The degradation rate was more progressive during the remainder of the assay. At the final point (day 16th), the total area reduction in the NC-Alg scaffolds was 22.94 ± 3.12% *versus* 20.10 ± 6.25% in the NC-Alg-HA scaffolds. It is noteworthy that the water content uptake ability of hydrophilic scaffolds causes major degradation rates because of the decreasing the density of cross-linking and crystallization, as has been reported in Alg based scaffolds. [61]

As the swelling assay demonstrated, both scaffolds had high water uptake capacity; nevertheless, the addition of HA prevented from a faster degradation of scaffolds during the first hours after printing. Importantly, degradation rate is related with the material characteristics and crosslinking procedure. Thus, highly crosslinked scaffolds showed slow degradation rates *in vitro* which made cell proliferation and protein release difficult to achieve. [62] On the other hand, fast degradative scaffolds have been demonstrated to be inefficient in tissue regeneration. [60] Our both scaffolds showed a controlled degradation values over the time, however, modelling of degradation processes *in vivo* may be needed in order to understand how it repercuss in tissue regeneration.

3.5. Biological analysis

3.5.1. Cytotoxicity analysis of the bioinks

Once bioinks and scaffolds were characterized, cytotoxicity evaluation was needed prior to the introduction of cells into inks. To analyse any potential harmful effects of NC-Alg based inks on cell viability, the adhesion, direct contact and indirect contact cytotoxicity tests were performed according to ISO 10993-5-2009 [41] (Fig. 10).

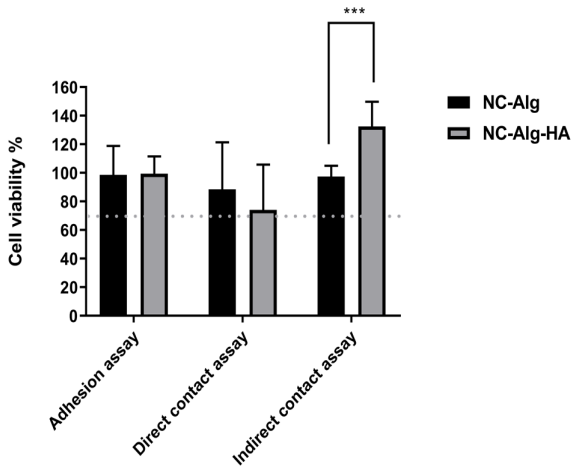

Fig. 10. Cytotoxicity analysis of NC-Alg and NC-Alg-HA bioinks in adhesion, direct contact and indirect contact assays. Values represent mean ± SD. ***: $p < 0.001$.

In the adhesion assay, both bioinks showed similar cell viability (NC-Alg bioink 98.55 ± 20.30% and NC-Alg-HA bioink 99.34 ± 12.20%). Similarly, the direct contact assay showed that cell viability was above 70%, which indicates that both bioinks have no potential harmful effects on L929 cells (NC-Alg 88.53 ± 32.91% and NC-Alg-HA 74.12 ± 31.62%). Importantly, the addition of HA on the NC-Alg base bioink resulted in a significantly higher cell viability ($p < 0.001$). HA constitutes the basic component of extracellular matriX in some tissues and it has been described for being involved in a wide variety of biological procedures, such as cell signalling mediation, regulation of cell adhesion and proliferation. [63] This assay was performed by adding conditioned DMEM that previously had been in contact with the bioink, onto seeded L929 cells. It may be that the presence of HA on the media enhanced cell viability and proliferation. Another study reports that cell viability increases by adding HA supplemented media as it decreases mitochondrial DNA damage while enhancing DNA repair capacity, cell viability, preservation of ATP levels, and amelioration of apoptosis. [63]

3.5.2. Viability and metabolic activity of D1-MSCs in the bioprinted scaffolds

Once the non-toxicity had been ensured different densities of previously sterilised (by short cycle autoclave) murine D1-MSCs were mixed. MSCs are widely applied in tissue regenerative fields since they characterize by their potential to differentiate into a variety of cell types, including osteoblasts, chondrocytes, adipocytes and myocytes. [64] D1 cell line was previously reported to have the capacity to differentiate spontaneously into osteoblasts, and in adipocytes when using pro-adipogenic agents. [32,64] After an analysis of the available literature no unique adequate cell density to seed was found; in fact, in other studies a wide range of densities have been used. Thus, in this study, cell densities between 1×10^6 and 5×10^6 cell/mL were selected. However, the lowest density of 1×10^6 cell/mL showed very low viability values and proliferation rates (supplementary material) and therefore, the assays were continued with 2.5×10^6 and 5×10^6 cell/mL. Then, circular grid-like constructs of 15 mm diameter and 4 layers in height were bioprinted through a 27 G nozzle by the extruder bioprinter. In order to evaluate the feasibility

of NC-Alg and NC-Alg-HA constructs as adequate 3D structures to maintain cell survival, the metabolic activity as well as viability of embedded cells were determined at several time points.

As Fig. 11 shows, cells were alive in the NC-Alg scaffolds as well as in those containing HA at both cell densities after the bioprinting process. Several studies have previously indicated that cell viability may decrease after extrusion-based bioprinting procedures due to the huge stress that cells might suffer during the process. [56] In this study, however, biological assays demonstrated high cell survival in both 3D constructs after the bioprinting process, which suggests that the shear thinning behaviour of bioinks may be acting as a protection factor for the cells. [30]

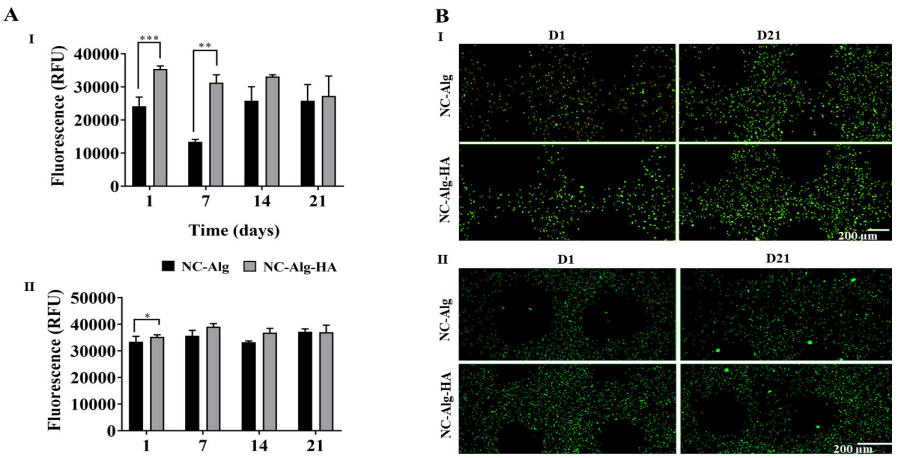

Fig. 11. Cell viability studies. A) Metabolic activity assay at two different cell densities: I) 2.5 × 10^6 cell/mL and II) 5 × 10^6 cell/mL. Values represent mean ± SD. ***: $p < 0.001$; **: $p < 0.01$; *: $p < 0.05$. B) Representative fluorescence micrographs of live/dead stained scaffolds I) 2.5 × 10^6 cell/mL and II) 5 × 10^6 cell/mL, showing live (green) and dead (red) cells at day 1 and 21 after bioprinting. Scale bar 200 µm.

The metabolic activity of these cells was assayed over 3 weeks (Fig. 11A). As expected, the metabolic activity was higher when a higher cell density was added to the bioink before 3D-bioprinting. Over time, apart from a reduction on the arbitrary fluorescence units (RFU) on day 7 for the 2.5 x 10^6 cell/mL density in the NC-Alg scaffolds, the measured metabolic activity was stable in

both scaffolds at both cell densities. Now, when a comparison is made, the HA seems to protect the cells during the first days or the first week. This effect was more prominent for the lower cell density condition (day 1, $p < 0.001$ and day 7, $p < 0.01$). The significantly higher cell metabolism in the HA containing scaffolds may be related to the improvement of the rheological properties of the bioink when HA was added. Besides, the positive effects of HA on cells have been widely described. It has been reported that the addition of HA on Alg hydrogels promotes MSCs viability and functionality. [31] Other studies have shown that HA containing bioinks improve cell differentiation of hMSCs. [65] In fact, stem cells receive signals from the environment; therefore, HA, as an extracellular matrix component, significantly influences all these biological responses.

The live/dead staining was carried out for 21 days. Fig. 11B corroborated cell survival and shows that embedded cells were homogeneously distributed in bioprinted scaffolds. Then, L/D pictures were analysed using Image J software in order to show the percentage between cells alive (in green) and dead (in read). At D1 after bioprinting, results showed that cell viability was higher on scaffolds containing HA at 2.5 x 10^6 cell/mL density (NC-Alg scaffolds 80 ± 23% and the HA containing scaffolds 90 ± 12%). This tendency was repeated at 5 x 10^6 cell/mL density, being on NC-Alg scaffolds 72 ± 6% and on NC-Alg-HA scaffolds 95 ± 7%. Furthermore, at D21 after bioprinting NC-Alg-HA scaffolds showed higher cells alive than NC-Alg scaffolds too. This corroborates the protective function of HA that has been previously dis- cussed. In addition, when comparing the two cell densities, cells aggregates were found at 5 x 10^6 cell/mL density on both constructs at the end of the assay. As one study reported, cell aggregates may be necessary to induce the differentiation of MSCs into chondrocytes in 3D cultures, [66] which suggests that NC-Alg based scaffolds may become a feasible tissue engineering approach for cartilage regeneration at high cell densities.

4. Conclusions

First, this study was focused on sterilisation of bioinks for 3D-bioprinting.

Since UV has been found to be ineffective [17] and ethylene oxide resulted in cancerous chemical residue, [15] a study was carried out the most commonly used sterilisation techniques in the biomedical field: autoclave by short and long procedures, β-radiation and γ-radiation. All techniques were effective ensuring the sterility of NC-Alg and NC-Alg-HA cell-free bioinks. Nevertheless, based on fundamental properties for bioinks such as rheology, physicochemical and printability, short cycle autoclaving was found to be the best sterilisation technique for NC-Alg based bioinks. Moreover, the addition of HA to the bioink resulted in the improvement of rheological properties which had repercussions on the printing procedure, as well as in bioink physiological behaviour.

Further, an evaluation of the bioprinted scaffolds to be used for tissue engineering was also conducted. The structure, swelling and degradation of both scaffolds were also evaluated. In addition, the biological studies with D1-MSCs-loaded constructs showed better results in HA-containing matrices, which indicates that NC-Alg-HA mixtures are an excellent bioink for the development of 3D bioprinted scaffolds for TE and regenerative medicine of cartilage tissue.

Author statement

Markel Lafuente-Merchan: Conceptualization, Methodology, Investigation, Formal analysis, Writing - Original Draft. Sandra Ruiz-Alonso: Investigation, Methodology. Albert Espona-Noguera: Investigation, Methodology. Patricia Galvez-Martin: Conceptualization, Methodology, Writing - Review & Editiing. Elena López-Ruiz: Writing - Review & Editing. Juan Antonio Marchal: Writing - Review & Editing. Maria Luisa López- Donaire: Writing - Review & Editing. Alaitz Zabala: Methodology, Investigation, Writing - Review & Editing. Jesús Ciriza: Writing - Review & Editing. Laura Saenz del Burgo: Conceptualization, Methodology, Writing - Review & Editing, Supervision, Project administration. José Luis Pedraz: Conceptualization, Methodology, Writing - Review & Editing, Supervision, Project administration, Funding acquisition.

Declaration of competing interest

The authors declare that they have no known competing financial interests or personal relationships that could have appeared to influence the work reported in this paper.

Acknowledgements

Author thanks the Basque Government for granted fellowship to S. Ruiz-Alonso (PRE_2020_2_0143). This study was financially supported by the Basque Country Government (IT907-16), the Ministerio de Economía, Industria y Competitividad (FEDER funds, project RTC-2016- 5451-1), Fundación Mutua Madrileña (project FMM-

AP17196-2019), the Instituto de Salud Carlos III, ERDF funds (DTS19/00145) and by the Consejería de Economía, Conocimiento, Empresas y Universidad, Junta de Andalucía (project no. PY18-2470 and SOMM17/6109/UGR, FEDER Funds). Authors also wish to thank the intellectual and technical assistance from the ICTS "NANBIOSIS", more specifically by the Drug Formulation Unit (U10) of the CIBER in Bioengineering, Biomaterials & Nanomedicine (CIBER-BBN) at the University of Basque Country (UPV/EHU).

References

[1] S. Derakhshanfar, R. Mbeleck, K. Xu, X. Zhang, W. Zhong, M. Xing, 3D bioprinting for biomedical devices and tissue engineering: a review of recent trends and advances, Bioactive Materials. 3 (2018) 144–156.

[2] D Nguyen, DA Hagg, A Forsman, J Ekholm, P Nimkingratana, C Brantsing, et al. Cartilage tissue engineering by the 3D bioprinting of iPS cells in a Nanocellulose/ alginate bioink, Sci. Rep. 7 (2017) 658–10.

[3] Z Xie, M Gao, AO Lobo, TJ Webster. 3D bioprinting in tissue engineering for medical applications: the classic and the hybrid, Polymers. 12 (2020) 1717.

[4] J. Li, L. He, C. Zhou, Y. Zhou, Y. Bai, F.Y. Lee, et al., 3D printing for regenerative medicine: from bench to bedside, MRS Bull. 40 (2015) 145–154.

[5] Y.P. Singh, A. Bandyopadhyay, B.B. Mandal, 3D bioprinting using cross-linker-free silk–gelatin bioink for cartilage tissue engineering, ACS Appl. Mater. Interfaces 11 (2019) 33684–33696.

[6] M Varkey, DO Visscher, van Zuijlen, Paul P. M, A Atala, JJ Yoo. Skin bioprinting: the future of burn wound reconstruction? Burns and trauma. 7 (2019) 4.

[7] P. He, J. Zhao, J. Zhang, B. Li, Z. Gou, M. Gou, et al., Bioprinting of skin constructs for wound healing, Trauma. 6 (2018).

[8] M Fuest, GH Yam, JS Mehta, DF Duarte Campos. Prospects and challenges of translational corneal bioprinting, Bioengineering (Basel). 7 (2020) 71.

[9] S. Yoo, O. Thabit, E.K. Kim, H. Ide, D. Yim, A. Dragulescu, et al., 3D printing in medicine of congenital heart diseases, 3D print med 2 (2016).

[10] T.K. Merceron, M. Burt, Y. Seol, H. Kang, S.J. Lee, J.J. Yoo, et al., A 3D bioprinted complex structure for engineering the muscle–tendon unit, Biofabrication. 7 (2015).

[11] E. Hodder, S. Duin, D. Kilian, T. Ahlfeld, J. Seidel, C. Nachtigall, et al., Investigating the effect of sterilisation methods on the physical properties and cytocompatibility of methyl cellulose used in combination with alginate for 3D- bioplotting of chondrocytes, J. Mater. Sci. Mater. Med. 30 (2019) 1–16.

[12] R. Galante, T.J.A. Pinto, R. Colaço, A.P. Serro, Sterilization of hydrogels for biomedical applications: a review, J. Biomed. Mater. Res. 106 (2017) 2472.

[13] M. Di Foggia, U. Corda, E. Plescia, P. Taddei, A. Torreggiani, Effects of sterilisation by high-energy radiation on biomedical poly-(e-caprolactone)/hydroXyapatite composites, J. Mater. Sci. Mater. Med. 21 (2010) 1789–1797.

[14] C.D. O'Connell, C. Onofrillo, S. Duchi, X. Li, Y. Zhang, P. Tian, et al., Evaluation of sterilisation methods for bio-ink components: gelatin, gelatin methacryloyl, hyaluronic acid and hyaluronic acid methacryloyl, Biofabrication. 11 (2019), 035003.

[15] K.A. Faraj, K.M. Brouwer, P.J. Geutjes, E.M. Versteeg, P.G.P. Wismans, J. A. Deprest, et al., The effect of ethylene oXide sterilisation, Beta irradiation and gamma irradiation on collagen fibril-based scaffolds, J. Tissue Eng. Regen. Med. 8 (2011) 460–470.

[16] Z. Dai, J. Ronholm, Y. Tian, B. Sethi, X. Cao, Sterilization techniques for biodegradable scaffolds in tissue engineering applications, Journal of Tissue Engineering. 7 (2016), 2041731416648810.

[17] T. Lorson, M. Ruopp, A. Nadernezhad, J. Eiber, U. Vogel, T. Jungst, et al., Sterilization methods and their influence on physicochemical properties and bioprinting of alginate as a bioink component, ACS omega. 5 (2020) 6481–6486.

[18] L. Valot, J. Martinez, A. Mehdi, G. Subra, Chemical insights into bioinks for 3D printing, Chem. Soc. Rev. 48 (2019) 4049–4086.

[19] A. Sheikhi, J. Hayashi, J. Eichenbaum, M. Gutin, N. Kuntjoro, D. Khorsandi, et al., Recent advances in nanoengineering cellulose for cargo delivery, J. Control. Release 294 (2019) 53–76.

[20] S. Salimi, R. Sotudeh-Gharebagh, R. Zarghami, S.Y. Chan, K.H. Yuen, Production of Nanocellulose and its applications in drug delivery: a critical review, ACS Sustain. Chem. Eng. 7 (2019) 15800–15827.

[21] A. Sharma, M. Thakur, M. Bhattacharya, T. Mandal, S. Goswami, Commercial application of cellulose nano-composites – a review, Biotechnology Reports. 21 (2019), e00316.

[22] A. Basu, J. Lindh, E. Ålander, M. Strømme, N. Ferraz, On the use of ion-crosslinked nanocellulose hydrogels for wound healing solutions: physicochemical properties and application-oriented biocompatibility studies, Carbohydr. Polym. 174 (2017) 299–308.

[23] E AXpe, ML Oyen. Applications of alginate-based bioinks in 3D bioprinting, Int. J. Mol. Sci. 17 (2016) 1976.

[24] F. Yu, X. Han, K. Zhang, B. Dai, S. Shen, X. Gao, et al., Evaluation of a polyvinyl alcohol-alginate based hydrogel for precise 3D bioprinting, J. Biomed. Mater. Res. A 106 (2018) 2944–2954.

[25] A Murua, M de Castro, G Orive, RM Hernández, JL Pedraz. In Vitro Characterization and In Vivo Functionality of Erythropoietin-Secreting Cells Immobilized in Alginate Poly-l-Lysine Alginate Microcapsules, Biomacromolecules. 8 (2007) 3302–3307.

[26] K. Markstedt, A. Mantas, I. Tournier, H. Martínez Ávila, D. Hägg, P. Gatenholm, 3D bioprinting human chondrocytes with Nanocellulose–alginate bioink for cartilage tissue engineering applications, Biomacromolecules. 16 (1900) 1489–1496.

[27] E Ruvinov, T Tavor Re'em, F Witte, S Cohen. Articular cartilage regeneration using acellular bioactive affinity-binding alginate hydrogel: a 6-month study in a mini-pig model of osteochondral defects, Journal of orthopaedic translation. 16 (2019) 40–52.

[28] M. Rubert, M. Alonso-Sande, M. Monjo, J. Ramis, Evaluation of alginate and hyaluronic acid for their use in bone tissue engineering, Biointerphases. 7 (2012) 1–11.

[29] S. Ansari, I. Diniz, C. Chen, T. Aghaloo, B. Wu, S. Shi, et al., Alginate/hyaluronic acid hydrogel delivery system characteristics regulate the differentiation of periodontal ligament stem cells toward chondrogenic lineage, J. Mater. Sci. Mater. Med. 28 (2017) 1–12.

[30] C Antich, J de Vicente, G Jiménez, C Chocarro, E Carrillo, E Montanñez, et al. Bio-inspired hydrogel composed of hyaluronic acid and alginate as a potential bioink for 3D bioprinting of articular cartilage engineering constructs, Acta Biomater. 106 (2020) 114–123.

[31] A Cañibano-Hernández, L Saenz del Burgo, A Espona-Noguera, G Orive, RM Hernández, J Ciriza, et al. Alginate microcapsules incorporating hyaluronic acid recreate closer in vivo environment for Mesenchymal stem cells, Mol. Pharm. 14 (2017) 2390–2399.

[32] A Cañibano-Hernández, L Saenz del Burgo, A Espona-Noguera, G Orive, RM Hernández, J Ciriza, et al. Hyaluronic acid promotes differentiation of Mesenchymal stem cells from different sources toward pancreatic progenitors within three-dimensional alginate matriXes, Mol. Pharm. 16 (2019) 834–845.

[33] E López-Ruiz, G Jiménez, L Álvarez de Cienfuegos, C Antic, R Sabata, JA Marchal, et al. Advances of hyaluronic acid in stem cell therapy and tissue engineering, including current clinical trials, European cells & materials. 37 (2019) 186–213.

[34] J. Leppiniemi, P. Lahtinen, A. Paajanen, R. Mahlberg, S. Metsä-Kortelainen, T. Pinomaa, et al., 3D-printable bioactivated Nanocellulose–alginate hydrogels, ACS Appl. Mater. Interfaces 9 (2017) 21959.

[35] M. Müller, M. Müller, E. Öztürk, E. Öztürk, Ø. Arlov, Ø. Arlov, et al., Alginate sulfate–Nanocellulose bioinks for cartilage bioprinting applications, Ann. Biomed. Eng. 45 (2017) 210–223.

[36] T. Möller, M. Amoroso, D. Hagg, C. Brantsing, N. Rotter, P. Apelgren, et al., In vivo Chondrogenesis in 3D bioprinted human cell-laden hydrogel constructs, plastic and reconstructive surgery, Global open. 5 (2017), e1227.

[37] ISO 1137-3-2018 sterilization of health care products- radiation-part 1: requirements for development, validation and routine control of a sterilization process for medical devices — amendment 2: revision to 4.3.4 and 11.2.

[38] Council of Europe. Chapter 2.6.1. Sterility. The European Pharmacopoeia, 9.0. ed.; EDQM: Strasbourg, France, 2017.

[39] A. Zabala, L. Blunt, R. Tejero, I. Llavori, A. Aginagalde, W. Tato, Quantification of dental implant surface wear and topographical modification generated during insertion, Surface Topography: Metrology and Properties. 8 (2020) 15002.

[40] ISO 25178-2 2012 Geometrical Product Specifications (GPS)—Surface Texture: Areal: II.Terms, definitions and surface texture parameters, 2012.

[41] ISO 10993-5:2009 Biological Evaluation of Medical Devices. Part 5: Tests for in Vitro CytotoXicity, International Organization for Standardization, Geneva, Switzerland, 2009.

[42] K. Hólzl, S. Lin, L. Tytgat, S. Van Vlierberghe, L. Gu, A. Ovsianikov, Bioink properties before, during and after 3D bioprinting, Biofabrication. 8 (2016), 032002.

[43] S. Sakai, H. Ohi, M. Taya, Gelatin/hyaluronic acid content in hydrogels obtained through blue light-induced gelation affects hydrogel properties and adipose stem cell behaviors, Biomolecules. 9 (2019) 342.

[44] F. Cilurzo, F. Selmin, P. Minghetti, L. Montanari, C. Lenardi, F. Orsini, et al., Comparison between gamma and beta irradiation effects on hydroXypropylmethylcellulose and gelatin hard capsules, AAPS PharmSciTech 6 (2005) E586–E593.

[45] W.B. Hugo, A brief history of heat, chemical and radiation preservation and disinfection, Int. Biodeterior. Biodegradation 36 (1995) 197–217.

[46] J.A. Bushell, M. Claybourn, H.E. Williams, D.M. Murphy, An EPR and ENDOR study of γ- and β-radiation sterilization in poly (lactide-co-glycolide) polymers and microspheres, J. Control. Release 110 (2005) 49–57.

[47] L. Montanari, F. Cilurzo, F. Selmin, B. Conti, I. Genta, G. Poletti, et al., Poly(lactide-co-glycolide) microspheres containing bupivacaine: comparison between gamma and beta irradiation effects, J. Control. Release 90 (2003) 281–290.

[48] F. EL-Ashhab, L. Sheha, M. Abdalkhalek, H.A. Khalaf, The influence of gamma irradiation on the intrinsic properties of cellulose acetate polymers, Journal of the Association of Arab Universities for Basic and Applied Sciences. 14 (2013) 46–50.

[49] E. Daar, L. King, A. Nisbet, R.B. Thorpe, D.A. Bradley, Viscosity changes in hyaluronic acid: irradiation and rheological studies, Appl. Radiat. Isot. 68 (2010) 746–750.

[50] J.G. Prieto, M.M. Pulido, J. Zapico, A.J. Molina, M. Gimeno, P. Coronel, et al., Comparative study of hyaluronic derivatives: rheological behaviour, mechanical and chemical degradation, Int. J. Biol. Macromol. 35 (2005) 63–69.

[51] A Maleki, A Kjøniksen, B Nyström. Anomalous viscosity behavior in aqueous solutions of hyaluronic acid, Polym. Bull. 59 (2007) 217–226.

[52] M Driscoll, A Stipanovic, W Winter, K Cheng, M Manning, J Spiese, et al. Electron beam irradiation of cellulose. Radiation physics and chemistry. 78 (2009) 539–542.

[53] P Snetkov, K Zakharova, S Morozkina, R Olekhnovich, M Uspenskaya. Hyaluronic acid: the influence of molecular weight on structural, physical, Physico-chemical, and degradable properties of biopolymer, Polymers. 12 (2020) 1800.

[54] K. YongBok, K. GeunHyung, Collagen/alginate scaffolds comprising core (PCL)– shell (collagen/alginate) struts for hard tissue regeneration: fabrication, characterisation, and cellular activities, J. Mater. Chem. B 1 (2013) 3185.

[55] F. Yu, X. Cao, Y. Li, L. Zeng, J. Zhu, G. Wang, et al., Diels–Alder crosslinked HA/PEG hydrogels with high elasticity and fatigue resistance for cell encapsulation and articular cartilage tissue repair, Polym. Chem. 5 (2014) 5116–5123.

[56] W. Li, J. Kang, Y. Yuan, F. Xiao, H. Yao, S. Liu, et al., Preparation and characterization of PVA-PEEK/PVA-β-TCP bilayered hydrogels for articular cartilage tissue repair, Compos. Sci. Technol. 128 (2016) 58–64.

[57] A. Espona-Noguera, J. Ciriza, A. Cañibano-Hernández, L. Fernandez, I. Ochoa, L. Saenz del Burgo, et al., Tunable injectable alginate-based hydrogel for cell therapy in type 1 diabetes mellitus, Int. J. Biol. Macromol. 107 (2018) 1261–1269.

[58] J. Patterson, R. Siew, S.W. Herring, A.S.P. Lin, R. Guldberg, P.S. Stayton, Hyaluronic acid hydrogels with controlled degradation properties for oriented bone regeneration, Biomaterials. 31 (2010) 6772–6781.

[59] S. Tang, S.M. Vickers, H. Hsu, M. Spector, Fabrication and characterization of porous hyaluronic acid–collagen composite scaffolds, J. Biomed. Mater. Res. A 82A (2007) 323–335.

[60] H. Sung, C. Meredith, C. Johnson, Z.S. Galis, The effect of scaffold degradation rate on three-dimensional cell growth and angiogenesis, Biomaterials. 25 (2004) 5735–5742.

[61] M. Farokhi, F. Jonidi Shariatzadeh, A. Solouk, H. Mirzadeh, Alginate based scaffolds for cartilage tissue engineering, A Review, International Journal of Polymeric Materials and Polymeric Biomaterials. 69 (2020) 230–247.

[62] Z. Wu, X. Su, Y. Xu, B. Kong, W. Sun, S. Mi, Bioprinting three-dimensional cell- laden tissue constructs with controllable degradation, Sci. Rep. 6 (2016) 24474.

[63] H. Park, B. Choi, J. Hu, M. Lee, Injectable chitosan hyaluronic acid hydrogels for cartilage tissue engineering, Acta Biomater. 9 (2013) 4779–4786.

[64] O. Juffroy, D. Noël, A. Delanoye, O. Viltart, I. Wolowczuk, C. Verwaerde, Subcutaneous graft of D1 mouse mesenchymal stem cells leads to the formation of a bone-like structure, Differentiation. 78 (2009) 223–231.

[65] J. Kim, I.S. Kim, T.H. Cho, K.B. Lee, S.J. Hwang, G. Tae, et al., Bone regeneration using hyaluronic acid-based hydrogel with bone morphogenic protein-2 and human mesenchymal stem cells, Biomaterials. 28 (2006) 1830–1837.

[66] B. Sayyar, M. Dodd, L. Marquez-Curtis, A. Janowska-Wieczorek, G. Hortelano, Fibronectin-alginate microcapsules improve cell viability and protein secretion of encapsulated factor IX-engineered human mesenchymal stromal cells, Artificial Cells, Nanomedicine, and Biotechnology. 43 (2015) 318–327.

Supplementary material

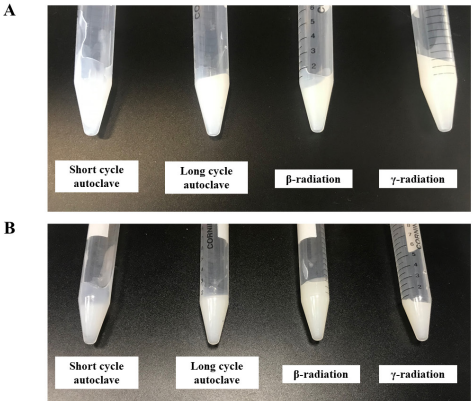

Fig. S1. Macroscopic characteristics of NC-Alg based bioinks after sterilisation by different methods. A) NC-Alg bioink and B) NC-Alg-HA bioink. Both bioinks showed white and homogeneous characteristic after sterilisation.

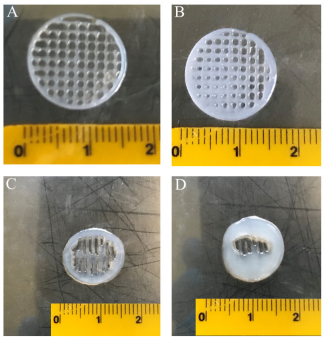

Fig. S2. Printability study of sterilised NC-Alg bioink. A) Short cycle autoclave; B) Long cycle autoclave; C) β-radiation and D) γ-radiation. Scaffolds shape fidelity loss was observed after sterilisation by ionising radiations.

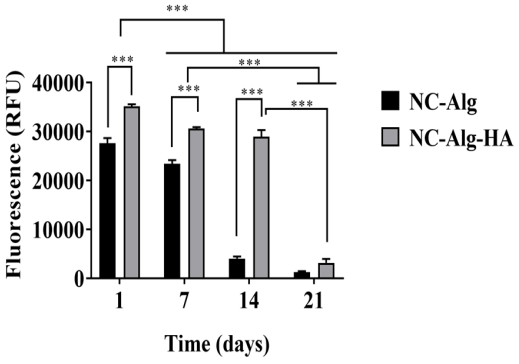

Fig. S3. Cell metabolic activity assay at $1x10^6$ cell/mL density. Values represent mean ± SD. ***: $p<0.001$; **: $p<0.01$.

Appendix 3

Chondroitin and Dermatan Sulfate Bioinks for 3D Bioprinting and Cartilage Regeneration

Markel Lafuente-Merchan[1,2,3], Sandra Ruiz-Alonso[1,2,3], Alaitz Zabala[4], Patricia Gálvez-Martín[5], Juan Antonio Marchal[6,7,8,9], Blanca Vázquez-Lasa[2,10], Idoia Gallego[1,2,3], Laura Saenz-del-Burgo[1,2,3*] and José Luis Pedraz [1,2,3*]

[1] NanoBioCel Group, Laboratory of Pharmaceutics, School of Pharmacy, University of the Basque Country (UPV/EHU), Paseo de la Universidad 7, 01006 Vitoria-Gasteiz, Spain.
[2] Biomedical Research Networking Center in Bioengineering, Biomaterials and Nanomedicine (CIBER-BBN), Health Institute Carlos III, Paseo de la Universidad 7, 01006 Vitoria-Gasteiz, Spain.
[3] Bioaraba, NanoBioCel Research Group, 01009 Vitoria-Gasteiz, Spain.
[4] Mechanical and Industrial Manufacturing Department, Mondragon Unibertsitatea, Loramendi 4, Mondragón 20500, Spain.
[5] R&D Animal and Human Health, Bioibérica S.A.U., 08029 Barcelona, Spain.
[6] Biopathology and Regenerative Medicine Institute (IBIMER), Centre for Biomedical Research, University of Granada, 18100 Granada, Spain.
[7] Instituto de Investigación Biosanitaria de Granada (ibs.GRANADA), Andalusian Health Service (SAS), University of Granada, Granada, Spain.
[8] Department of Human Anatomy and Embryology, Faculty of Medicine, University of Granada, 18016 Granada, Spain.
[9] BioFab i3D Lab - Biofabrication and 3D (bio)printing singular Laboratory, University of Granada, 18100 Granada, Spain
[10] Institute of Polymer Science and Technology, ICTP-CSIC, Juan de la Cierva 3, 28006 Madrid, Spain.
[*] Correspondence: laura.saenzdelburgo@ehu.eus; joseluis.pedraz@ehu.eus

Macromolecular Bioscience, 2022, 22:2100435
IF: 4.979 (2022) (Q1)
Cat: Biomaterials & Bioengineering
https://doi.org/10.1002/mabi.202100435

Abstract

Cartilage is a connective tissue which a limited capacity for healing and repairing. In this context, osteoarthritis (OA) disease may be developed with high prevalence in which the use of scaffolds may be a promising treatment. In addition, three-dimensional (3D) bioprinting has become an emerging additive manufacturing technology because of its rapid prototyping capacity and the possibility of creating complex structures. This study is focused on the development of nanocellulose-alginate (NC-Alg) based bioinks for 3D bioprinting for cartilage regeneration to which it is added chondroitin sulfate (CS) and dermatan sulfate (DS). First, rheological properties are evaluated. Then, sterilization effect, biocompatibility, and printability on developed

NC-Alg-CS and NC-Alg-DS inks are evaluated. Subsequently, printed scaffolds are characterized. Finally, NC-Alg-CS and NC-Alg-DS inks are loaded with murine D1-MSCs-EPO and cell viability and functionality, as well as the chondrogenic differentiation ability are assessed. Results show that the addition of both CS and DS to the NC-Alg ink improves its characteristics in terms of rheology and cell viability and functionality. Moreover, differentiation to cartilage is promoted on NC-Alg-CS and NC-Alg-DS scaffolds. Therefore, the utilization of MSCs containing NC-Alg-CS and NC-Alg-DS scaffolds may become a feasible tissue engineering approach for cartilage regeneration.

Keywords: 3D bioprinting; Bioinks; Cartilage; Chondroitin sulfate; Dermatan sulfate; Tissue engineering.

1. Introduction

Osteoarthritis (OA) is the common form of arthritis and it has become the third incapacitating disease after diabetes and dementia. [1] OA is characterized by structural changes at joint level due to cartilage degradation. Moreover, the increase of extracellular matrix (ECM)-degrading enzymes and inflammatory cytokines [2] acelerate tissue degradation which result in joints pain, deformity, instability, and reduction of motion and function. [1,2]

Cartilage is a connective tissue of diarthrodial joints. [3] It is composed of low metabolic activity cells, chondrocytes, which are surrounded of a highly structured ECM. [2] ECM is predominately based on water, collagens and glycosaminoglycans (GAGs), and together with chondrocytes, its principal function is to give support to articulations. Cartilage provides a smooth, lubricated surface to articulations and facilitates the transmission of loads with a low frictional coefficient. [3] However, as it is devoid of blood vessels, lymphatic system and nerves, itpacity for healing and repairing is limited. [2–4] In addition, injuries in this tissue degenerate progressively to very grave diseases such as OA. [4] Despite the fact that OA has a rising prevalence, [1] the current pharmacological and surgical treatments are ineffective. [1,2,5] For this reason, recent therapeutic advances such as gene therapy, [6] cell therapy, [7] and tissue engineering [8] have become promising treatments. [2]

Tissue engineering is attracting increasing interest, since it allows combining different technologies. It is based on the use of scaffolds, which act not only as supportive cell structures but also as structures that are designed to imitate as closely as possible native tissues. [2,9,10] Three-dimensional (3D) bioprinting has become an emerging additive manufacturing technology in tissue engineering because of its rapid prototyping capacities and creating complex formulations. [4,11] It is based on the deposition of biomaterials, either embedded with cells or depositing them later on, in micrometer scale to form structures comparable to biological tissues. [10,12] However, the deposited biomaterial, termed as bioink when it contains a biological component or as ink when it is cell-free composite, requires specific characteristics in order to

imitate the physiological structure of tissues and support living cells. [12,13]

Chondroitin sulfate (CS) has high potential in bioinks for cartilage regeneration since it is a GAG found in cartilage ECM. It is composed of repeating D-glucuronic acid-N-acetylgalactosamine sulfated (disaccharide unit) [14] and it has numerous biological properties. CS promotes cell differentiation, [15] the attainment of pluripotency, provides mechanical protection and cell-ECM interactive capability equipping the cell with mechanoresponsive properties. [16] In addition, it has also anti-inflammatory activity [14,17] and regulates the metabolism of cartilage tissue. [14] Apart from its biological activity, physical properties such as water [16] and nutrient absorption, [17] cytocompatibility and mechanical strength have been reported. [16] Thus, CS may help to restore cartilage function and has become a treatment for OA disease. [15,17]

Similarly to CS, dermatan sulfate (DS) is one of the GAGs in articular cartilage and it is a major component of connective tissue matrix, cell surface and basement membranes. [18] The chemical composition of DS is the same as that of CS, but it differs in some of the glucuronate residues that undergo epimerization to form iduronate. [18,19] It has been shown that DS, as other GAGs, could manipulate mesenchymal stromal cells (MSC) behavior regarding adhesion and proliferation. [20] Moreover, DS plays an important role in modulating chondrogenesis and may promote MSC differentiation [20] and maturation. [18,21]

Despite the fact that GAGs offer advantages as scaffold components, since they intrinsically have greater stability and lower immunogenicity compared to most ECM proteins, [20] the addition of other components is often required in order to improve the bioink structural stability. [22] Alginate (Alg) is a widely used polysaccharide in tissue regenerative fields because of its high water content, biocompatibility and non-toxic properties. [23–25] Moreover, it offers fast gelling capacity when is mixed with divalent cations, such as calcium, which enables the manufacture of manipulable scaffolds after bioprinting. [24] In addition, to maintain the structure of the bioprinted scaffolds and improve

bioprinting properties, more viscous polymers such as nanofibrillated cellulose (NC) may be added. [23,26] NC is characterized by high water content, adequate biocompatibility and exceptional physical and chemical properties. [27] Interestingly, the NC imitates the bulk collagen matrix of the cartilage [23] so the use of NC-Alg based bioinks in cartilage regeneration has been recently reported in literature. [23,26]

This study is focused on the development of NC-Alg based bioinks for 3D bioprinting for cartilage regeneration. For this purpose, CS and DS were separately added to NC-Alg inks in order to develop NC-Alg-CS and NC-Alg-DS inks. First, both inks were characterized in terms of rheology, cytotoxicity and printability. Then, scaffolds were printed and their external and inner structure, as well as swelling and degradation kinetics was evaluated. Finally, previously sterilized NC-Alg-CS and NC-Alg-DS inks were loaded with murine D1 MSCs engineered to secrete erythropoietin (D1-MSCs-EPO) [28] and cell viability, functionality and differentiation to cartilage were assessed.

2. Results and Discussion

One of the main objectives in the field of 3D bioprinting is to develop inks with proper rheological behavior, printability and biocompatibility. Hydrogels based on natural polymers have taken advantage of their high water content and excellent compatibility with cells as well as with native tissues to be selected as ink components among other materials. Thus, we have developed in a previous study, [29] NC-Alg based bioinks with good results in terms of printability and viability of embedded cells. In the present study, we want to go one step further and demonstrate the ability of these bioinks to form cartilage tissue. Therefore, CS and DS were added, which are naturally found in ECM cartilage and provide different properties such as water [16] and nutrient absorption, [17] the enhancement of mechanical properties, [16] and the promotion of cell proliferation, differentiation and maturation. [15,20] Then, its effects on inks and scaffolds were evaluated, as well as its benefits on cell viability and cartilage differentiation.

2.1. Ink Fabrication and Rheological Characterization

Different concentrations of CS and DS (1%, 3%, 5%, and 10%) were respectively added to the NC-Alg ink and their rheological behavior was evaluated. In steady flow measurement (Figure 1), both, the addition of CS and DS, resulted in a slightly increase on viscosity values of NC-Alg ink. Moreover, the viscosity increase was proportional to the CS and DS concentrations, being the more viscous inks, the ones composed of NC-Alg-CS 10% and NC-Alg-DS 10%. The relationship between polymer concentration and viscosity explains the increase of viscosity when higher proportion of CS or DS was added. [13]

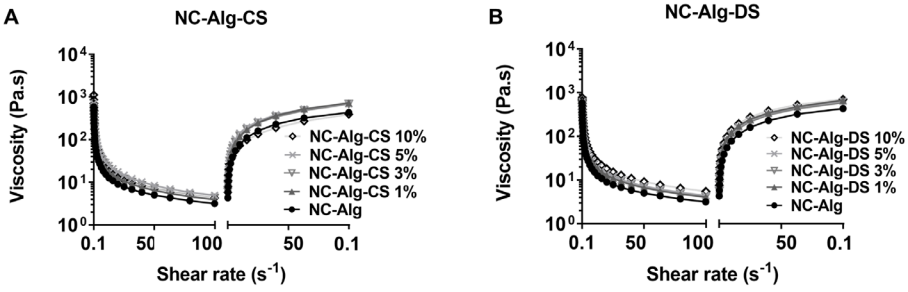

Figure 1. Rheological steady flow measurement of A) NC-Alg-CS inks and B) NC-Alg-DS inks at different concentrations.

Interestingly, all formulations showed shear thinning behavior as viscosity values decrease under shear rate, with a recovery on viscosity when the shear rate was returned to initial values. Shear thinning behavior is essential to print through extrusion as viscosity of the ink must decrease to pass through the printer needle. Besides, when the ink is deposited on the printer bed, the viscosity must return to initial so as to maintain scaffold shape.

Despite the fact that all formulations met these properties, inks containing CS showed higher viscosity values in comparison with NC-Alg-DS inks. However, the NC-Alg-CS 10% ink in Figure 1A, showed a lower viscosity recovery, which would indicate less capacity to maintain the shape fidelity of the

scaffolds after printing compared to its equivalent NC-Alg-DS 10% in which this effect was not seen (Figure 1B).

On the other hand, frequency sweep rheological measurement was performed in order to evaluate viscoelastic properties of the inks with different concentrations of CS and DS. The results in Figure 2 show the elastic modulus (G') and viscous modulus (G'') of the inks at different frequencies. The addition of both, CS (Figure 2A) and DS (Figure 2B), resulted in an increase in viscoelastic values in comparison with the NC-Alg ink, being this increase proportional to the CS and DS concentrations. Although both, CS and DS, increased the values of G' and G'', differences were observed between them. In fact, the inks containing CS showed higher viscoelasticity values (Figure 2A). It has been reported that GAGs have naturally good viscoelastic properties due to their chemical composition, since a high viscosity allows a good lubrication of the joint and a good rigidity provides protection against mechanical damage. [30,31]

In addition, the relation between G''/G' was evaluated by the value of tan δ in Figure 2C. According to the literature, values of tan δ close to 1 indicate that the inks extrude uniformly and require low extrusion pressures, nevertheless, exhibit poor shape fidelity. On the other hand, inks with tan δ closer to 0 are robust, but require higher printing pressures and a uniform extrusion is difficult. [32] Among fabricated inks, no significant differences were observed. Results showed tan δ values between 0 and 1, which indicated that all NC-Alg-CS and NC-Alg-DS inks were feasible to be printed by extrusion. In fact, all the values were between 0.35–0.47 which has been demonstrated to be optimal for balancing smooth extrusion, shape fidelity, and cell viability in alginate-gelatin bioinks. [33]

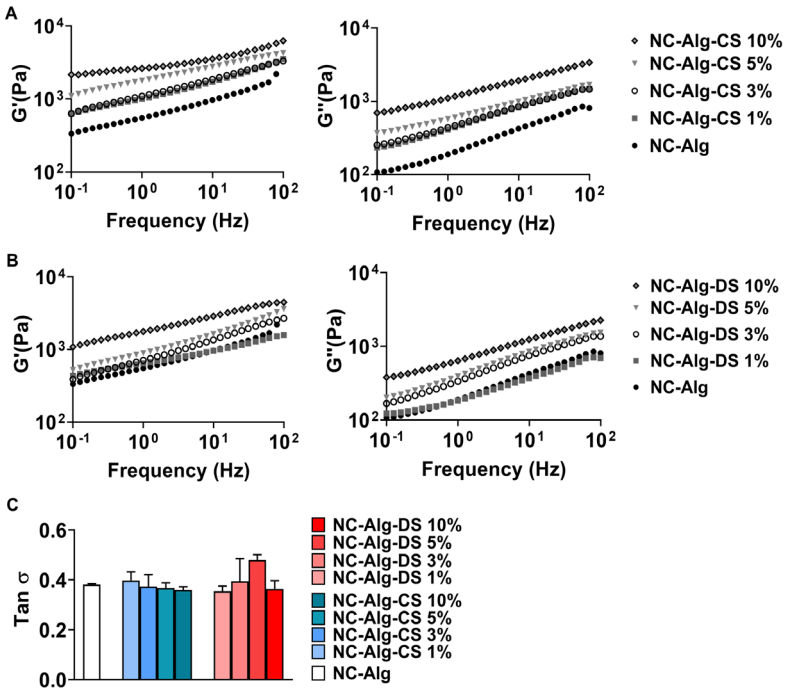

Figure 2. Rheological frequency sweep measurements. Viscoelasticity modules G′ and G″ of A) NC-Alg-CS inks and B) NC-Alg-DS inks at different concentrations. C)Tan δ values of all developed inks. Values represent mean ± SD.

According to the rheological studies, the addition of different concentrations of CS and DS improves proportionally viscosity and viscoelastic properties of the base NC-Alg ink. Despite the fact that all the formulations were feasible to be printed by extrusion, the concentration of 10% of CS and DS seemed to be the However, bioinks with values of G′ below 5000 Pa require less extrusion pressures when are printed, and, therefore, are better for cell viability. [32] The ink containing 10% CS reached values of G′ of 6000 Pa. Thus, it was discarded. In contrast the formulation containing 10% of DS did not exceed this value, but it was also discarded in order to observe the differences after adding CS and DS with an equivalent concentration. As a consequence, the following formulations of NC-Alg-CS 5% and NC-Alg-DS 5% were elected to perform the following experimental studies.

2.2. Rheological and physicochemical evaluation after sterilisation

Before incorporating cells into the NC-Alg-DS and NC-Alg-CS inks, complete sterility must be ensured. Therefore, inks were sterilised by short cycle autoclave, which was already demonstrated to be the less harmful method for NC-Alg inks. [29] Sterility tests indicated that NC-Alg based inks were free of containing microorganisms since no turbidity was detected after sterilisation (data not shown). Then, it was verified if the process had changed fundamental properties for 3D bioprinting such as rheology and physicochemical properties.

As it can be seen in Fig. 3A. a slight decrease in viscosity was observed. However, the two inks maintained the shear thinning behaviour and the ability to recover the viscosity after finishing the pressure, which suggests that no problems when being printed can be expected. In addition, the viscoelastic properties were not modified (Fig. 3B). In fact, the G' and G'' values were very similar between non-sterile and sterile inks for both, NC-Alg-CS and NC-Alg-DS inks.

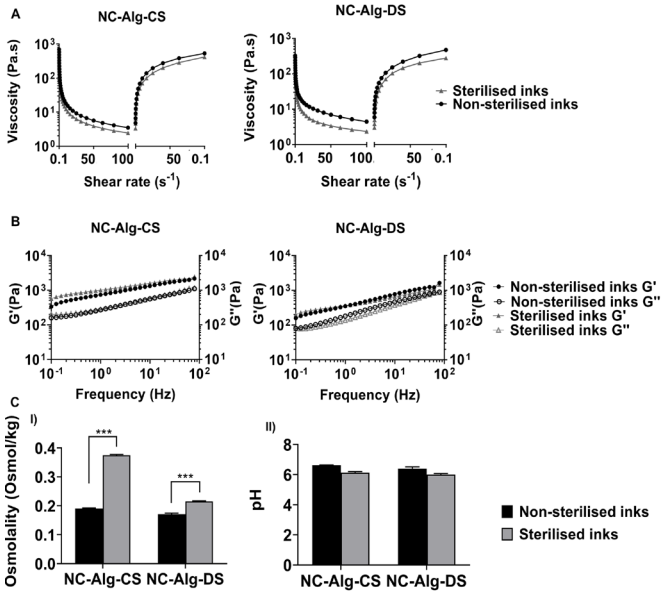

Figure 3. Evaluation of the sterilisation procedure on NC-Alg-CS and NC-Alg-DS inks properties. A) Rheological steady flow measurement. B) Frequency sweep rheological measurement. C) Physicochemical study I) Osmolality and II) pH values represent mean ± SD. ***: $p < 0.001$.

On the other hand, the pH and osmolality of the inks were evaluated after sterilisation (Fig. 3C). No significant variations were observed after sterilisation for all formulations in pH measurements in comparison with non-sterile inks (Fig. CII). Conversely, osmolality was affected by sterilisation. All the inks showed (Fig. 3CI) an increase in osmolality values after autoclaving ($p < 0.001$). A degradation has been reported, in terms of molecular weight loss, in biopolymers after heating, which would cause the release of osmotically active solutes to the media, [34] and, therefore, the increase of osmolality values in the inks. Nevertheless, these changes in osmolality were not detrimental to cells that were subsequently embedded, since high viability values were observed in biological studies.

According to rheological and physicochemical properties, inks maintained the properties to be feasible to be printed through extrusion bioprinter.

2.3. Cytotoxicity evaluation

For 3D bioprinting, a successful ink must meet not only with good rheological properties, but also with good biocompatibility. To evaluate biocompatibility of NC-Alg-CS and NC-Alg-DS inks, the adhesion, direct contact and indirect contact cytotoxicity tests were performed in concordance with the ISO 10993-5-2009. [35]

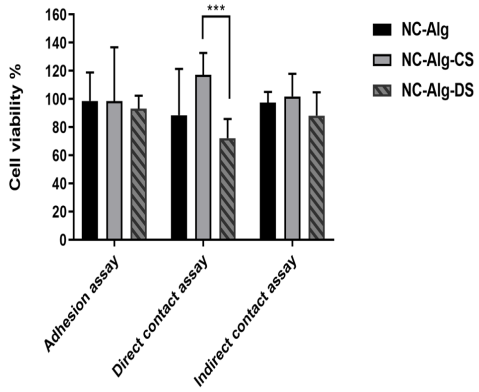

Figure 4. Cytotoxicity evaluation of NC-Alg-CS and NC-Alg-DS inks in adhesion, direct contact and indirect contact assays. Values represent mean ± SD. ***: $p < 0.001$.

As it is shown in Fig. 4, in the adhesion assay, the addition of CS and DS to the NC-Alg ink demonstrated high cell viability which was similar to NC-Alg ink. Similarly, indirect contact assay showed high cell viability of L929 fibroblasts and no significant differences among the inks (NC-Alg-CS ink 101.85 ± 16.10%, NC-Alg-DS ink 92.31 ± 16.50% and NC-Alg ink 97.35 ± 7.65%). On the other hand, the percentage of live cells after direct contact test was high in all the cases, although statistically significant differences were observed between NC-Alg-CS and NC-Alg-DS inks, being cell viability higher on NC-Alg-CS inks ($p < 0.001$). The contribution of GAGs such as chondroitin and dermatan in cellular behaviour has been previously reported in many studies. [20,36] In fact, in the consulted literature it has not been seen that dermatan was more toxic than chondroitin. Therefore, this difference was due to the ability of the cells to adhere to NC-Alg-DS ink, which implied that fewer cells remained in the well plate and cell viability was lower than in the other inks. Anyway, in accordance with ISO standards, a reduction on cell viability by more than 30% is considered as a potentially cytotoxic effect. Consequently, the evaluated inks did not present cytotoxicity.

2.4. 3D printing and printability evaluation

Once the inks were characterized, printing studies were carried out. At the time of printing 15 mm grid-like scaffolds, differences were observed between the parameters to be applied in the bioprinter. The NC-Alg ink required printing pressures of 25 kPa, while the inks containing CS and DS needed pressures close to 30 kPa. These differences were due to the increase in viscosity and viscoelasticity that CS and DS produced in the inks. In addition, these rheological improvements resulted in differences in the obtained scaffolds, being CS (Fig. 5C) and DS (Fig. 5D) printed scaffolds the ones that resembled the best the computer assisted design (Fig. 5A). In fact, diameter measurements of the printed scaffolds resulted in higher shape fidelity on NC-Alg-CS scaffolds (NC-Alg-CS scaffolds 15.34 ± 0.05 mm, NC-Alg-DS scaffolds 15.86 ± 0.32 mm and NC-Alg scaffolds 16.26 ± 0.24 mm *versus* the 15 mm of the computerised design). Moreover, closer images of the scaffolds demonstrated that in the scaffolds containing CS the grid structure was squarer, which im-

plies more similarity to the design. In contrast, in the scaffold with DS a more oval grid structures were observed, being the NC-Alg scaffolds the one that differed the most from the original design. Alginate based inks have been found to have difficulties in obtaining printed scaffolds with high resolution. [37] For this reason, the addition of viscous materials such as gelatin or nanocellulose has proven to be effective in obtaining scaffolds with good printability that maintain shape fidelity when compared to computerised design. [38,39] In a recent study it has been seen that inks composed of nanocellulose and 2.5-5% alginate have good results in terms of printability. [38] In this study, 2% alginate was used, so a lower resolution in NC-Alg scaffolds could be expected. The addition of both CS and DS improved the rheological properties and, therefore, the resolution and shape fidelity of the printed scaffolds were enhanced.

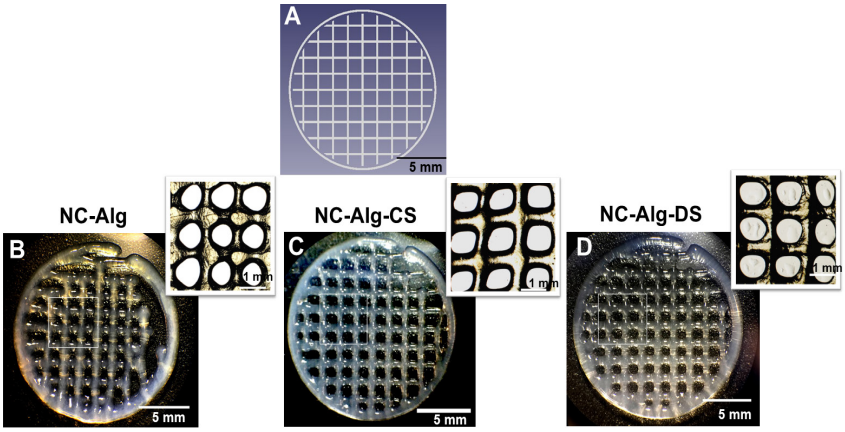

Figure 5. Printability study. Computer assisted design of the scaffolds (A). Macroscopic images of printed scaffolds being NC-Alg (B), NC-Alg-CS (C) and NC-Alg-DS (D). Scale bar 5 mm and 1 mm.

2.5. Scaffold characterization

2.5.1. Surface and architectural study

NC-Alg, NC-Alg-CS and NC-Alg-DS scaffolds were characterized using optical profilometry in order to obtain an in-depth evaluation of scaffolds surface and architecture. As Fig.6A shows, differences were observed among scaffolds. The CS scaffolds showed less height compared to the DS and NC-Alg

scaffolds, suggesting a greater resemblance to the computerized scaffold that was designed with a height of 200 µm for each layer and, therefore, 400 µm at the intersections. In fact, when the area of the grid was analysed (Fig. 6B), the scaffolds containing CS were the ones that most closely resembled the theoretical grid area value of the design of 0.6 mm^2 (NC-Alg-CS scaffolds grid area 0.55 ± 0.09 mm^2, NC-Alg-DS grid area 0.52 ± 0.04 mm^2 and NC-Alg scaffolds grid are 0.42 ± 0.03 mm^2).

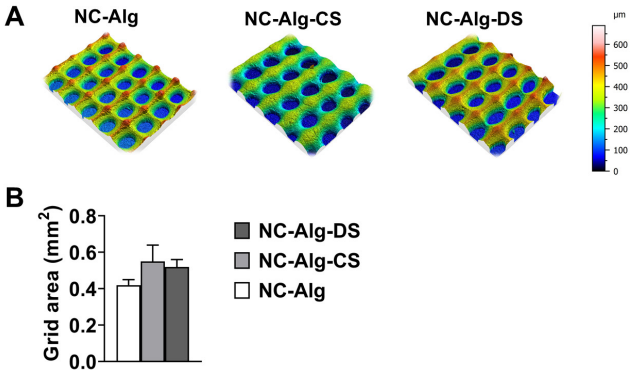

Figure 6. Surface and architectural characterization on NC-Alg, NC-Alg-CS and NC-Alg-DS scaffolds. A) Images of topology measurements and binarized areas of the printed scaffolds. B) Grid area measurements from binarized data analysis. Values represent mean ± SD.

In addition, the layer thickness and height of scaffolds were analysed in Fig. 7. The printing process was carried out with a 0.2 mm needle diameter according to the thickness of each layer pre-established by the design. As Fig.7A shows, the layer thickness was slightly higher in all scaffolds than in the original design. Furthermore, differences between the thickness in the X direction and in the Y direction were observed, being thicker in the Y direction. Although no statistically significant differences were shown among scaffolds, the ones containing DS and NC-Alg demonstrated higher thickness in the X direction compared to scaffolds with CS. On the other hand, the height of the scaffolds layers was slightly higher in the Y direction than in the X direction. (Fig. 7B). When a comparison is made, scaffolds containing DS were statistically higher in the X direction ($p < 0.001$) and in the Y direction ($p < 0.01$) in comparison with NC-Alg-CS scaffolds. Moreover, NC-Alg scaffolds heigh in X direction was also higher than scaffolds containing CS ($p < 0.01$). The

good rheological properties that exhibited CS inks support these results, which show a height and thickness in both X and Y directions, more similar to those established by the computer design and the printing needle. On the contrary, a lower viscoelasticity in NC-Alg-DS and NC-Alg inks caused them to flow more in the printing process, obtaining thicker structures.

These results reinforce the conclusion drawn from the printability study, in which the addition of CS to the ink improved the resemblance of printed scaffolds to the original design in comparison with inks containing DS. As a consequence, and taking into account the rheological studies, it can be concluded that in terms of printability and the formation of scaffolds, the addition of CS to the NC-Alg ink is better than the addition of DS.

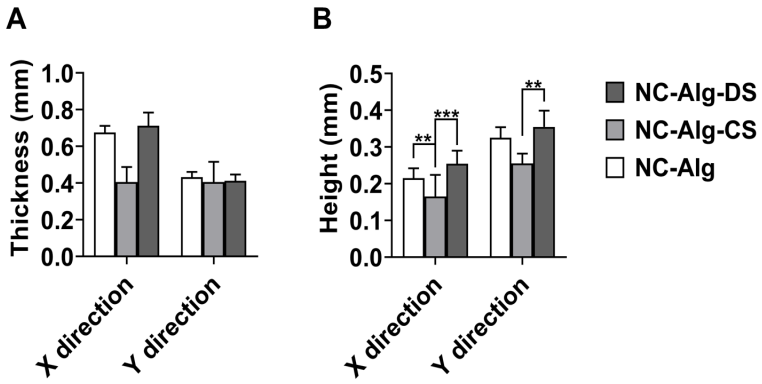

Figure 7. Surface and architectural characterization on NC-Alg, NC-Alg-CS and NC-Alg-DS scaffolds. Evaluation of the strut architecture of the printed scaffolds in terms of thickness (A) and height (B). Values represent mean ± SD. ***: $p < 0.001$, **: $p < 0.01$.

Finally, the roughness of the scaffolds was evaluated (see Fig. 8). Scaffolds containing DS showed an increase in roughness that was visualized in the Sdr parameter, this rise being significant in comparison with scaffolds containing CS ($p < 0.05$). In addition, the Sdr % was lower in CS scaffolds than in NC-Alg scaffolds. These differences were also observed in topographical images in Fig. 8B, in which a higher rough surface was observed in NC-Alg-DS scaffolds whereas a smoother surface was observed in scaffolds containing CS. It has been reported that roughness is related to the success of the implant, thus,

in clinical trials, it has been seen that the roughest implants have higher survival rates than the smoothest ones, when implanted in tissues such as bone. [40] Furthermore, a rough topography has shown to improve MSCs adhesion. [41,42] Taking into account the importance of the roughness on cell behaviour, a greater cellular adhesion may be expected in the NC-Alg-DS scaffolds. However, it would be necessary to deepen with *in vivo* studies to evaluate these differences among scaffolds after implantation.

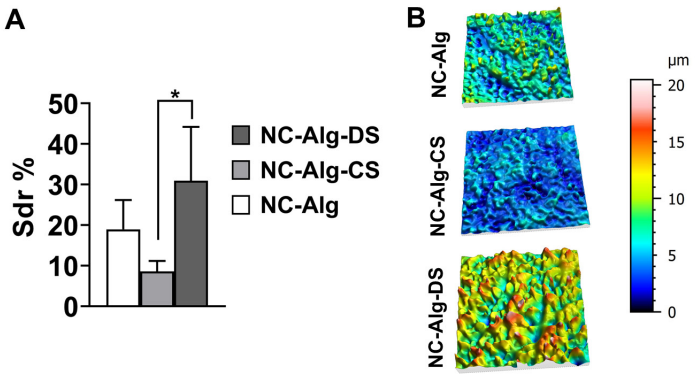

Figure 8. Surface and architectural structure characterization on scaffolds. A) 3D topographical parameters describing hybrid (Sdr) characteristics of the NC-Alg, NC-Alg-CS and NC-Alg-DS scaffolds. Values represent mean ± SD. *: $p < 0.05$. B) Representative axonometric projections of the topographical measurements of scaffolds.

2.5.2. Scanning electron microscopy (SEM)

NC-Alg-CS and NC-Alg-DS printed scaffolds were evaluated by SEM in order to evaluate the external and internal structures. As Fig. 9 shows, scaffolds containing CS showed similar external structure to the DS scaffolds. In addition, a higher quantity of fibres was observed in both, CS and DS scaffolds, in comparison with NC-Alg scaffolds. Then, crosscut were made to observe the internal structure of all the scaffolds so as to ascertain their porosity. A porous scaffold implies an exchange of fluids and nutrients that would be necessary for embedded cells viability. [43] All scaffolds showed a porous internal structure and, therefore, the assurance of the cells to be maintained alive inside them.

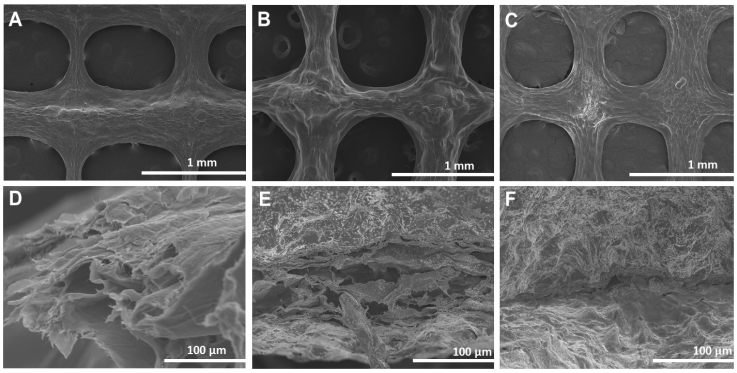

Figure 9. Representative scanning electron images of NC-Alg (A-D), NC-Alg-CS scaffolds (B-E) and NC-Alg-DS scaffolds (C-F). Scale bar in A and B: 1 mm and in C and D: 100 µm.

2.5.3. Swelling and degradation

The swelling behaviour is an important property of printed scaffolds and tissue engineering as it is related to the diffusion of nutrients and signalling molecules. [44] Fig. 10A shows the swelling behaviour of NC-Alg-CS and NC-Alg-DS scaffolds. NC-Alg scaffolds were used as controls. Results demonstrated good swelling properties for both scaffolds, which was to be expected due to the high water absorption capacity of the biopolymers that were used for printing the scaffolds. [45] Interestingly, scaffolds containing CS and DS showed a statistically significant lower water uptake ability in comparison with NC-Alg scaffolds in the majority of studied times. Swelling degree is usually related to the crosslinking density, consequently, inks with high dense inner structures show a decrease in swelling degree. [46] The addition of CS and DS to the base ink formed by NC-Alg showed an increase in viscosity and viscoelastic properties indicating a denser structure, which would explain the lower swelling

On the other hand, Fig. 10B shows the degradation study of NC-Alg-CS and NC-Alg-DS scaffolds. Degradation studies are of great importance for regenerative medicine because it may affect the medical application. An ideal degradation performs with the regeneration or replacement of native tissue while the scaffold is being degraded. [47] Both scaffolds, showed the same

degradation behaviour, being the first 24 h when the reduction of the scaffold area was more important ($p < 0.05$). Furthermore, there were no differences in comparison with the scaffold without CS and DS. In fact, after 10 days of study the area reduction of NC-Alg-CS scaffolds were 73 ± 3.40%, NC-Alg-DS scaffolds 79.85 ± 0.05% and NC-Alg scaffolds 78.62 ± 7.21%. Thus, the NC-Alg based scaffolds showed a controlled degradation behaviour over the time, which would imply good medical applicability. Cartilage is a complex and specific tissue in which is difficult to estimate the optimal biodegradation time of tissue engineered scaffolds. Therefore, the time required for tissue regeneration depends on the cartilage defect identification, function and the location. [48] In addition, the degradation rate could be modified by making chemical modifications to the alginate. Thus, phosphorylated alginate has been applied to fabricate hydrogels that were more resistant to degradation. [49] Alternatively, degradation kinetics have been also controlled by varying the molecular weight of the alginate. [50] However, *in vivo* studies need to be carried out to study in depth the degradation processes.

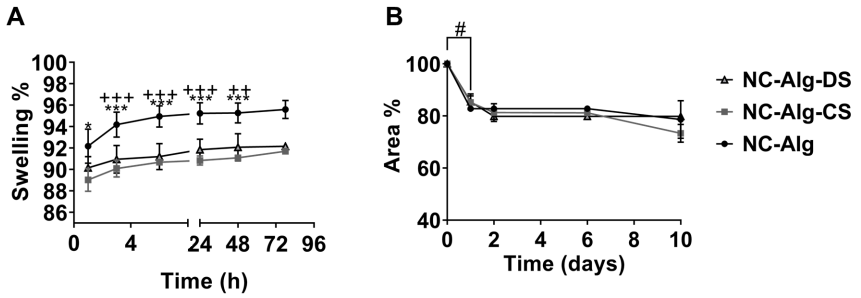

Figure 10. NC-Alg-CS and NC-Alg-DS printed scaffolds swelling determination (A) and degradation rate (B). NC-Alg scaffolds were used as controls. Values represent mean ± SD. ***: $p < 0.001$; *: $p < 0.05$ comparison between NC-Alg-CS and NC-Alg scaffolds. +++: $p < 0.001$; ++: $p < 0.01$ comparison between NC-Alg-DS and NC-Alg scaffolds. #: $p < 0.05$, comparison between days in the same scaffolds.

2.5.4. Mechanical properties

Mechanical properties of scaffolds were analysed because cartilage is a tissue that is subjected to great forces of tension and compression. Thus, compression Young's modulus was obtained as is an intrinsic material property that describes the material's stiffness or resistance to elastic deformation under load.

Results showed in Fig. 11 a significant increase in the Young`s modulus in the scaffolds containing CS ($p < 0.001$). On the other hand, NC-Alg-DS scaffolds showed similar values to the control scaffold composed of NC-Alg. It has been previously described in the literature that CS is responsible for the mechanical resistance of tissues such as cartilage through the electrostatic repulsions of its sulphate groups. [16,51,52] Furthermore, contrary to CS, it has been suggested that DS has no effect on mechanical properties, which would explain the results obtained in this study. [53] Despite the increase in terms of mechanical properties after the addition of CS, all the printed scaffolds did not approach the values of native cartilage (0.2-2 MPa). [54] The mechanical properties of cartilage derive from its complex composition and well-organised internal structure. [53] The scaffolds used in this study were immature as they did not contain chondrocytes to secrete matrix components that enhance mechanical properties such as collagen. In addition, compression modulus is strongly subjected to the solid content. In this study, printed scaffolds showed around 90-95% of water content, whereas cartilage is composed of 70-80% fluid. [55] For this reason, hydrogel-based materials are usually employed to perform in local injuries in conjunction with cartilage tissue instead of substitutes of the total tissue.

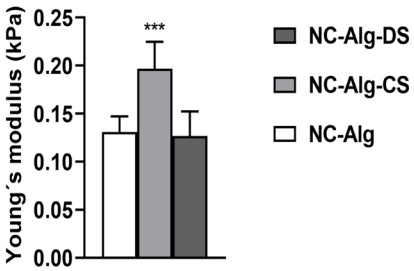

Figure 11. Young`s modulus analysis of printed NC-Alg-CS, NC-Alg-DS and NC-Alg scaffolds. Values represent mean ± SD. ***: $p < 0.001$.

2.6. Biological analysis

2.6.1. Cell viability, metabolism and functionality evaluation

For tissue engineering applications, the survival of the cells within the ink is essential. In this study, D1-MSCs-EPO were introduced into the bioink and their viability and functionality were analysed after 21 days of bioprinting. MSCs have the potential to differentiate into chondrocytes among other cell types, thus, their use in the field of tissue engineering to regenerate cartilage is quite wide. [56,57] Furthermore, cells genetically modified to release EPO were use due to the fact that its functionality inside the ink can be easily measured. A cell density of 5 x 10^6 cells/mL was elected since high cell densities as well as the pneumatic pressure applied during bioprinting may be stressful for embedded cells and *in vitro* quantification at low cell densities may result problematic. This was verified in a previous study in which cell densities of 1 x 10^6 cells/mL showed low cell viability and metabolic activity inside NC-Alg scaffolds. [29] In this study, we tested if the addition of CS and DS to the NC-Alg scaffolds can enhance cell viability and metabolism, as well as, functionality. As it is shown in Fig. 12A, metabolic activity of D1-MSCs-EPO increased over the time after bioprinting, which suggests cell proliferation inside the scaffolds. Interestingly, the addition of CS and DS improved cells metabolism at 1, 7 and 14 days after bioprinting in comparison with the control scaffold

composed only of NC-Alg. Furthermore, the improvement in cell metabolism was significantly greater ($p < 0.001$) in the NC-Alg-DS scaffolds during the first three studied times after bioprinting. Similarly, cells inside NC-Alg-CS scaffolds showed higher metabolic activity at days 1 and 7 after bioprinting ($p < 0.001$) and at day 14 ($p < 0.05$) in comparison with control scaffolds. At day 21, all the scaffolds showed similar cell metabolic activity. The increase in cell metabolism during the first days after bioprinting may be due to the fact that bioinks with higher viscoelastic properties protect encapsulated cells from the stress caused by the bioprinting process itself. [58] As shown in the rheological results, the addition of CS and DS increased these properties of the ink and, consequently, the cell viability after bioprinting is expected to be higher than in the NC-Alg scaffolds.

D1-MSCs-EPO viability was analysed by the Live/Dead™ staining at day 1 and 21 after bioprinting. The results in Fig. 12B show that the cells inside all the scaffolds were homogeneously distributed. When a comparison was made, no visual differences were observed at day 1 after bioprinting among all the scaffolds in which live cells were predominant (in green). On the contrary, at day 21 after bioprinting, higher fluorescent intensity was observed in the live cells of the scaffolds containing CS and DS, which may suggest higher cell viability in these scaffolds than in the NC-Alg scaffolds. In fact, after analysing the images using Image J software to show the percentage between cells alive (in green) and dead (in red), it was seen that NC-Alg-DS scaffolds showed 88.14 ± 2.62% cell viability, NC-Alg-CS scaffolds showed 80.11 ± 1.85% cell viability and NC-Alg scaffolds showed 77.77 ± 6.80% cell viability. Furthermore, cell aggregates were observed in the CS and DS scaffolds, which has been demonstrated to favour the differentiation of MSCs into chondrocytes. [59] Surprisingly, this visual appreciation does not agree with the studies of cell metabolism, since it would be expected that the higher the cell viability, the higher the metabolism. Possibly, more quantitative techniques might give us more accurate cell viability data. However, what is certain is the involvement of CS and DS in cellular biological processes, which has been reported in another studies. [15,60] In fact, cell viability as well as cell metabolic activity have been reported to increase in scaffolds containing both CS and DS. [16,21]

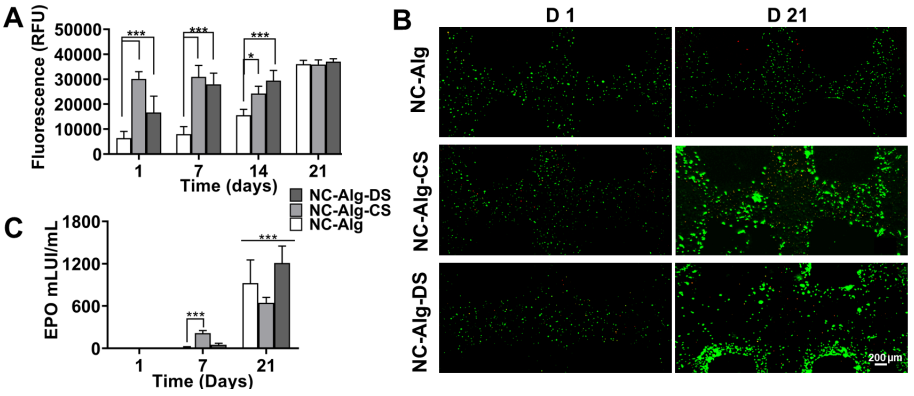

Figure 12. Cell viability and functionality studies inside NC-Alg-CS, NC-Alg-DS and NC-Alg scaffolds. A) Metabolic activity assay. B) Representative fluorescence micrographs of live/dead stained scaffolds, showing live (green) and dead (red) cells at day 1 and 21 after bioprinting. Scale bar 200 µm. C) EPO release quantification. Values represent mean ± SD. ***: $p < 0.001$; *: $p < 0.05$.

Finally, in order to evaluate the functionality of the cells embedded in the NC-Alg-CS and NC-Alg-DS scaffolds,the release of EPO hormone was evaluated after bioprinting. As Fig. 12C shows, there was no EPO release on day 1 after bioprinting in any of the scaffolds, which could be explained by the stress suffered by the cells during the bioprinting process. However, at day 7, a slight increase in the EPO release was observed in all the scaffolds. Moreover, this increase was more significant ($p < 0.001$) in the scaffolds containing CS compared to the controls, NC-Alg scaffolds. At the end of the assay, the release of the hormone increased significantly compared to day 1 and 7, with the scaffolds containing DS being the ones with the highest EPO release (NC-Alg-DS 1209.34 ± 240.88 mLUI/mL, NC-Alg-CS 643.98 ± 78.74 mLUI/mL and NC-Alg 925.21 ± 327.99 mLUI/mL). Results suggest that cells maintained their functionality inside all scaffolds after bioprinting. The increase in the production of EPO by the cells may be related to the boost of metabolic activity and viability at day 21. The release of EPO hormone by MSCs has already been described in cells embedded in alginate hydrogels. [61] Furthermore, it has been possible to obtain a controlled release of EPO *in vivo* in hyaluronic hydrogels as drug carrier systems. [62] In this study, the obtained scaffolds show a good release of the hormone and, therefore, may be used for the re-

lease of therapeutic agents.

2.6.2. Differentiation evaluation to cartilage

Once it has been studied that the NC-Alg-CS and NC-Alg-DS scaffolds enhance the viability of embedded D1-MSC-EPO, their capacity to differentiate to cartilage was evaluated. In this case, unmodified D1-MSC were used as they have already shown to be able to differentiate into chondrocytes, osteocytes and adipocytes when they are encapsulated in alginate and hyaluronic hydrogels. [61]

After 21 days in culture with differentiating medium, the bioprinted NC-Alg-CS and NC-Alg-DS scaffolds were stained with Alcian blue, which stains GAGs, and Safranin-O (red), which detects cartilage. NC-Alg scaffolds were used as controls. As it can be seen in Fig. 13, differences were observed among the stained scaffolds. In the scaffolds containing DS (Fig. 13C), darker areas were observed with the alcian blue staining, which indicates the production of GAGs by the embedded cells. Moreover, darker areas were also observed in the CS scaffolds (Fig. 13B) with this staining. Additionally, NC-Alg-CS and NC-Alg-DS scaffolds stained with safranin-O showed darker areas as well as the cells that had been released from the scaffolds were stainned (Fig. 13E-F). Conversely, in the scaffolds without CS or DS (Fig. 13A-D) these dark areas were not appreciated, which indicates a greater degree of differentiation in the scaffolds containing CS and DS.

Then, the hydroxyproline assay was carried out to quantify the production of collagen, which, being one of the components of the cartilage ECM, would indicate the capacity of bioprinted scaffolds to produce a niche similar to the biological one. Results in Fig. 13G show that hydroxyproline was detected in all the scaffolds. Nevertheless, no statistically significant differences were observed among them. However, the scaffolds containing DS and CS seem to have higher amounts of hydroxyproline compared to the NC-Alg scaffolds. This may indicate that there is an ECM production similar to native cartilage, which would indicate differentiation of D1-MSCs within the scaffolds to chondrocytes. It was observed in a study using chitosan scaffolds that the joint

addition of dermatan and chondroitin increased collagen deposition, however, it was also suggested that the deposition of other components of the ECM such as GAGs is more accentuated. [63] In another study based on hyaluronic scaffolds, a higher deposition of GAGs was also observed than of collagen accumulation. [64] In this study, a GAG quantification was not performed, which could have given us a closer approximation of cartilage ECM production than that of collagen accumulation in which no significant differences between scaffolds were observed.

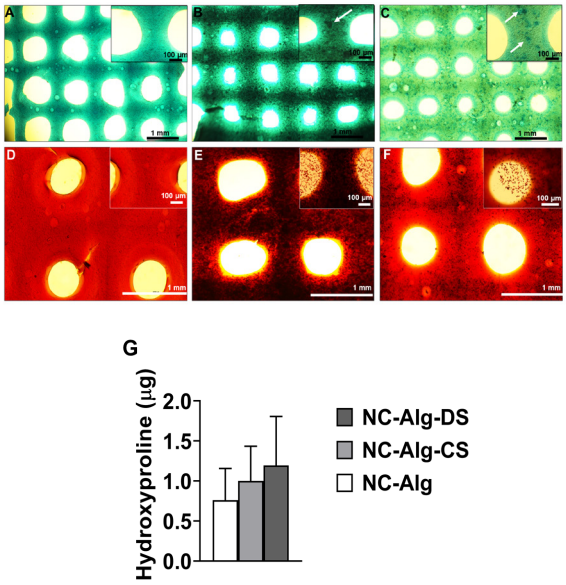

Figure 13. Chondrogenic differentiation evaluation of bioprinted scaffolds. Alcian blue staining of NC-Alg scaffolds (A), NC-Alg-CS scaffolds (B) and NC-Alg-DS scaffolds (C). Safranin-O staining of NC-Alg scaffolds (D), NC-Alg-CS scaffolds (E) and NC-Alg-DS scaffolds (F). Hydroxyproline quantification of bioprinted scaffolds (G). Values represent mean ± SD. Scale bar 1 mm and 100 µm.

The stainings, together with the quantification of collagen by the hydroxyproline assay, indicate that in the presence of CS and DS, the D1-MSCs have higher ability to differentiate to cartilage. In fact, it has already been reported previously that both, CS and DS, regulate chondrogenesis and promote maturation and differentiation of mesenchymal stem cells. [20]

Next, in order to obtain a more in-depth evaluation of the differentiation

degree to cartilage, RT-PCR studies were carried out. In this study, the expression of chondrogenic marker genes such as aggrecan (*ACAN*), collagen type 1 and 2 (*COL1*, *COL2*) and *SOX9* was analysed.

As it is shown in Fig.14, the relative expression of all the genes was measured after 1 and 21 days of bioprinting. As Fig. 14A shows, the NC-Alg-CS and NC-Alg-DS scaffolds obtained an increase in expression of the *SOX9* gene at day 21 after bioprinting compared to the NC-Alg scaffolds, which decreased compared to day 1. *SOX9* is a chondrogenic transcription factor that regulates chondrocyte differentiation and cartilage ECM production. [65] Furthermore, greater differences were observed when it comes to the *ACAN* gene expression (Fig. 14B). Scaffolds containing DS increased significantly ($p < 0.001$) the *ACAN* expression on day 21 compared to day 1 and NC-Alg scaffolds. In addition, interestingly enough, the NC-Alg-CS scaffolds showed a significantly higher amplified *ACAN* expression ($p < 0.001$) at day 21 in comparison with other kind of scaffolds. The *ACAN* gene is a chondrogenic differentiation marker as well as the major structural component of the cartilage tissue. [4] It has been proven that in the presence of CS, the hMSCs seeded onto the scaffolds accelerate chondrogenesis and maintain their chondrogenic phenotype. [14] Moreover, it has been shown that after the oral administration of CS in OA patients, the production of proteoglycans is increased, [66,67] which may explain the high expression of this gen in the scaffolds containing CS. In addition, *COL2* is also a chondrogenic marker as indicates suitable ECM production necessary for cartilage regeneration. [14] The highest increase of this gene at day 21 was only observed in the DS scaffolds ($p < 0.05$), while in both the CS and control scaffolds only a slight increase was seen (Fig. 14C). In a chondrogenesis differentiation, *COL2* increases while *COL1* decreases, since *COL1* is expressed in undifferentiated chondrocytes or other intermediate cells such as fibroblasts and osteoblasts. [68]

As Fig. 14D shows, in the NC-Alg-DS scaffolds, *COL1* decreases slightly on day 21, indicating, together with the increase in *COL2* and *ACAN*, differentiation to cartilage. On the other hand, the expression of *COL1* was increased in the CS scaffolds, which may indicate no chondrogenic differentiation. However, the high expression of *ACAN* indicates a cartilaginous tissue. Overall, cells

embedded in CS and DS scaffolds satisfactorily expressed cartilage phenotype compared to cells inside the NC-Alg scaffolds.

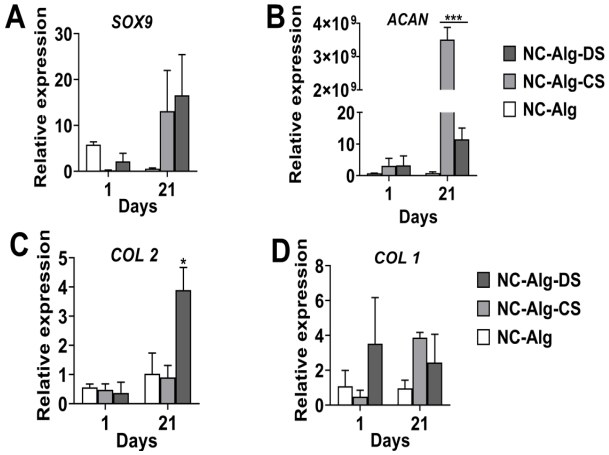

Figure 14. Chondrogenic gene expression of D1-MSCs embedded on NC-Alg, NC-Alg-CS and NC-Alg-DS bioprinted scaffolds. RT-PCR was carried out after 1 and 21 days of bioprinting. Values represent mean ± SD. ***: $p < 0.001$; *: $p < 0.05$.

3. Conclusions

The study focuses on whether the addition of CS and DS improves the characteristics of the ink based on NC-Alg as well as the observation of the biological effects on bioprinted scaffolds with these components. The CS showed better results than the DS in terms of rheological properties, which was reflected in the printability study. In addition, scaffolds surface and architectural studies reinforced these results, as the scaffolds with CS had a greater similarity to the computerized design than the DS scaffolds. The characterization in terms of SEM, swelling and degradation resulted in similarities between the contribution of CS and DS on the NC-Alg scaffolds. However, the addition of CS resulted in higher scaffold mechanical properties than DS scaffolds. On the other hand, in the *in vitro* results, a greater improvement was seen when adding DS than CS in the metabolic activity and functionality of embedded D1-MSCs-EPO. Furthermore, both DS and CS induced cells to express genes that indicated differentiation to cartilage, being the DS scaffolds the ones that followed a more typical cartilaginous gene expression profile.

Overall, both, the addition of CS and DS, improved the characteristics of the NC-Alg based bioink. While the CS provided an improvement in printability, the DS showed better biological properties of the embedded cells. Although the combination of the two elements in a single bioink may be the best option, this study showed that the NC-Alg-DS ink would be the preference choice to achieve scaffolds feasible for their application in cartilage tissue engineering.

4. Material and Methods

4.1. Materials

Ultra-pure low-viscosity high guluronic acid sodium alginate (UPLVG) was obtained from FMC Biopolymer (Sandvika, Norway). Chondroitin sulfate and dermatan sulfate were acquired from Bioiberica (Barcelona, Spain). Nanofibrillated cellulose was obtained from Sappi Europe (Brussels, Belgium). D-mannitol, calcium chloride and 3-(4,5-dimethylthiazol-2-yl)-2,5-diphenyltetrazoliumbromid (MTT) *in vitro* toxicology assay were acquired from Sigma-Aldrich, (Madrid, Spain). Fetal bovine serum (FBS), fetal calf serum (FCS) and penicillin/streptomycin (P/S) were obtained from Gibco (San Diego, USA). DPBS code BE17-513F was purchased from Lonza (Porriño, Spain). Alamar blue® was purchased from Bio-Rad científica (Madrid, Spain). LIVE/DEAD® Viability/Cytotoxicity kit was purchased from Life Technologies (Madrid, Spain).

4.2. Inks formulation

Different concentrations of CS and DS were proposed in order to fabricate the inks: 1%, 3%, 5% and 10% (w/v).

To prepare nanocellulose-alginate-chondroitin sulfate (NC-Alg-CS) ink, Alg and CS powders were dissolved in a D-mannitol solution to a final 2% (w/v) and 1%, 3%, 5% and 10% (w/v) concentrations, respectively. Afterward, NC was incorporated at 80% (v/v) proportion of the final solution and everything was mixed until complete homogenization.

The nanocellulose-alginate-dermatan sulfate (NC-Alg-DS) ink was fabricated similarly by dissolving Alg and DS powders in a D-mannitol solution to a final 2% (w/v) and 1%, 3%, 5% and 10% (w/v) concentrations, respectively. Subsequently, NC was added at 80% (v/v) proportion of the final solution and everything was mixed until complete homogenization.

4.3. Inks characterization

4.3.1. Rheological study

Rheological properties of all bioinks were measured on the AR100 rheometer from TA Instruments (New Castle, USA). In order to analyse viscosity, steady flow measurements were conducted through a shear rate sweep from 0.1 to 100 s^{-1}. Then, a second sweep from 100 to 0.1 s^{-1} was set. On the other hand, oscillatory shear measurements were carried out to evaluate the inks viscoelasticity properties (elastic modulus (G') and viscous modulus (G")), oscillation frequency sweeps were set from 0.1 to 100 Hz and strain was established in 2%. Tan δ values were obtained from the G"/G' relation. Studies were carried out at room temperature using a flat geometry. Three replicates per experiment were conducted.

4.3.2. Sterilisation process and evaluation of its effect on the inks

Fabricated inks were sterilised using short cycle autoclave that was previously reported to be the less harmful technique. [29] This procedure was conducted by AJL Ophthalmic (Miñano, Spain) in an industrial autoclave F0A2/B model. The short autoclave started at 15–18 ºC temperature and at 0.96 bar pressure. Then, for 22 min the temperature and pressure increased until being established at 123–124 ºC and 3.60–3.70 bar, respectively. With these parameters set, the sterilisation occurred for 3.04 min. Subsequently, cooling process occurred for 26 min with a decrease in the temperature and pressure to 50–55 ºC and 1.60 bar. Finally, after 54 min, the autoclave cycle ended with around 50 ºC temperature and 1.05 bar pressure.

Afterward, the sterilisation effect on inks properties was evaluated. First,

sterility test was conducted for NC-Alg based inks by carrying out a direct inoculation of 1 mL of sample in the microbiological medium to determine for the growth of anaerobic, and aerobic bacteria, fungi and yeast, in accordance with the European Pharmacopeia. [69] Then, previously aforementioned rheological studies were carried out. In addition, a cryoscopic osmometer Osmomat 030-D from Gonotec (Berlin, Germany) was used to determine the osmolality. For this study, 50 µL of each ink was evaluated by quantifying the freezing point depression. On the other hand, a pH-meter GLP 21 from Crison (Barcelona, Spain) was used to determine the pH. Each sample was assayed in triplicate.

4.3.3. Cytotoxicity study

Three different assays were carried out to determine *in vitro* cytotoxicity of the inks in concordance with the ISO 10993-5-2009 [35]: Direct and indirect cytotoxicity and adhesion assays. Mouse L929 fibroblasts were used to perform all the experiments and a cell density of 3.123×10^4 cells/cm^2 was established to seed the cells.

In the direct and indirect cytotoxicity assays cells were seeded and maintained in culture for 24 h. Afterward, they were exposed directly to the NC-Alg, NC-Alg-CS and NC-Alg-DS circular scaffolds placing them onto the seeded cells in the direct assay, or by adding conditioned media (media that has been in contact with the scaffolds for 24 h) in the indirect cytotoxicity test. After 24 h, cell viability was estimated in both assays using MTT *in vitro* toxicity assay kit following manufacture´s recommendations. Cells with no scaffold exposure or cells not exposed to conditioned media were used as controls. On the other hand, in the adhesion assay, cells were seeded directly onto the scaffolds. After 4 h cell viability was quantified using the same MTT procedure. Cells directly seeded onto the plate were used as controls.

In all assays, an Infinitive M200 microplate reader from TECAN Trading AG (Männedorf, Switzerland) was used to determine the absorbance at 570 nm with reference wavelength set at 650 nm. Cell viability was calculated using the following equation (1):

$$\text{Cell viability (\%)} = \frac{\text{Testing sample OD570}}{\text{Untreated blank OD570}} \times 100 \qquad (1)$$

Six independent assays were carried out with three replicates per assay. In concordance with the ISO 10993-5-2009, a cell viability above 70% was contemplated as non-toxic.

4.4. 3D printing

An extrusion-based 3D bioprinter Bio X from Cellink (Gothenburg, Sweden) was used to print the inks. Circular grid-like scaffolds of 15 mm diameter and 2 layers were printed using a 27 G conical needle. Printing parameters were established at 4-5 mm/s printing speed and 25-30 kPa extrusion pressure for all inks. After printing, crosslinking process was carried out by submerging the scaffolds in a 100 mM calcium solution for 5 min.

Afterward, scaffolds were observed under a Nikon AZ100 microscope from Izasa Scientific (Barcelona, Spain) in order to take macroscopic images.

4.5. Scaffolds characterization

4.5.1. Surface and architectural structure study

An optical profilometer from Sensofar S-NEOX (Barcelona, Spain) through focus variation method was used to characterize the surface topography and architecture of the scaffolds. A metrological software SensoMAP Premium 7.4 from Digital Surf (Besançon, France) was applied to post-process all the measurements. The scaffolds were analysed in hydrated state after wiping with a dry lint free wipe.

To perform the architectural analysis, a 6484 x 4880 μm^2 area measurement was acquired at 3 locations on 3 independently printed samples for each condition using a 10x objective (side sampling: 1.29 µm, vertical resolution: 25 nm). The thickness and height of the deposited strut were measured and a quantification of the deposited material volume was carried out through the

3D parameter Vm. [70] Then, measurements were binarized, and in order to analyse the pore morphology, the aspect ratio (Dmax/Dmin) was determined. To evaluate the surface topography, a measurement of 873 x 656 μm^2 at 3 independent areas were acquired using a 20x objective (lateral sampling: 0.65 µm, vertical resolution: 8 nm). 3D topographical parameter belonging hybrid (Sdr) from ISO 25178-2 [71] was determined on cropped areas of 150 x 150 μm^2.

4.5.2. Scanning electron microscopy (SEM)

After critical point drying, an Emitech K550X ion-sputter was used to coat the scaffolds with a thin layer of gold (15 nm). Afterward, a Hitachi S-3400 Scanning Electron Microscope from Hitachi (Illinois, USA) was used to observe the samples using a 15 kV voltage and around 20 mm of working distance.

4.5.3. Swelling study

NC-Alg-CS and NC-Alg-DS printed scaffolds of 0.4 x 15 mm^2 were used in order to analyse the swelling behaviour. First, a Telstar cryodos Freeze Dryer (Terrassa, Spain) was used to lyophilize all the scaffolds. Then, they were weighted to determine the dried weight. Finally, to evaluate their swelling capacity, dried scaffolds were submerged in Dulbecco's phosphate-buffered saline (DPBS) with calcium and magnesium at 37 ^oC. At chosen time points, scaffolds were removed from DPBS, water excess was removed using filter paper and scaffolds were reweighed. NC-Alg scaffolds were used as controls. The % of swelling was computed in every time point by using the following equation (2):

$$\text{Swelling (\%)} = \frac{W_{wet} - W_{dried}}{W_{dried}} \times 100 \qquad (2)$$

Where W_{wet} and W_{dried} are wet weight and dried weight, respectively.

4.5.4. Degradation study

NC-Alg-CS and NC-Alg-DS scaffolds area was calculated to analyse the degradation process. Afterward, scaffolds were placed in DMEM at 37 ^oC and, at selected time points, the area was measured again. Then, samples were

returned to the culture medium after conducting the measurements, NC-Alg scaffolds were used as controls. The area loss in % was computed by using the following equation (3):

$$\text{Area loss (\%)} = \frac{A_{before} - A_{after}}{A_{before}} \times 100 \qquad (3)$$

Where A_{before} and A_{after} correspond to the scaffold area before introducing in DMEM and after passing selected time in DMEM.

4.5.5. Mechanical properties

NC-Alg-CS and NC-Alg-DS scaffolds of 15 mm diameter and 0.4 mm heigh were analysed in a TA.XT.plusC Texture Analyser from Aname Instrumentación Cientifica (Madrid, Spain) to determine mechanical properties. A compression test was performed with a load cell of 5 kg and 20 mm cylinder probe. Test speed was set at 0.5 mm/s and at maximum of 80% strain. Compression Young's modulus was determined as the slope of stress-strain curve in the linear elastic range. Six replicates per sample were conducted and NC-Alg scaffolds were used as control.

4.6. D1-MSCs-EPO culture conditions, bioinks preparation and 3D Bioprinting

Murine D1-MSCs purchased from ATCC (Virginia, USA) were engineered to secrete erythropoietin (D1-MSCs-EPO) [28]. T-flasks with DMEM supplemented with 10% (v/v) FBS and 1% (v/v) P/S were used to perform the cell culture. Cells were sustained at 37 ^{o}C in a humidified atmosphere containing 5% CO_2. They were subcultured at 80% confluence and culture medium was regularly replaced.

To carry out 3D bioprinting process, the inks were developed as previously mentioned (see section 2.2). Then, a 5 x 10^6 cells/mL density was incorporated into the inks using a cell mixer device in order to obtain the bioinks. Afterward, they were bioprinted following the aforementioned process (see section 2.4). Crosslinking procedure was carried out after bioprinting by sub-

merging the scaffolds for 5 min in a 100 mM $CaCl_2$. Finally, they were deposited in complete medium for their culture. The whole process was conducted under aseptic conditions and at room temperature.

4.7. Biological studies of bioprinted scaffolds

4.7.1. Metabolic activity determination

The AlamarBlue® assay (AB) was used to determine the metabolic activity of embedded D1-MSCs-EPO. The process was performed by placing bioprinted circular grid-like scaffolds of 15 mm diameter in 24 well plates with a solution containing 10% of AB in complete medium. Next, a 4 h of incubation at 37 ºC was carried out. Finally, an Infinite M200 microplate reader from TECAN Trading AG (Männedorf, Switzerland) was used to read the fluorescence at excitation 560 nm and 590 nm emission wavelength. Wells containing culture media were used as negative controls. At least twelve samples were conducted for each condition.

4.7.2. Qualitative cell viability determination by fluorescence microscopy

The LIVE/DEAD® Viability/Cytotoxicity Kit was used to evaluate weekly cell viability. Scaffolds were rinsed in DPBS and placed in the staining solution with 100 mM calcein AM. After an incubation of 40 min at room temperature and protected from de light, the calcein solution was removed to add a solution containing 0.8 µM ethidium homodimer-1. Then, scaffolds were incubated for 10 min at 37 ºC. Finally, samples were washed again with DPBS and a Nikon TMS microscope (Virginia, USA) was used to observe them. It was set a wavelength of excitation 495 nm/emission 515 nm (for calcein AM staining) and excitation 495 nm/emission 635 nm (for ethidium homodimer staining). At least three independent tests were conducted for each condition. Afterwards, the obtained images were analysed with the image J software to quantify the percentage of live and dead cells.

4.7.3. EPO secretion

EPO secretion was determined using Quantikine IVD Human EPO ELISA Kit from R&D Systems (Madrid, Spain). The secretion for 24 h from supernatants

at days 1, 7 and 21 after bioprinting was quantified. Cell embedded scaffolds were incubated with 500 µL of DMEM for 24 h at 37 ^{o}C. Then supernatants were collected. Supernatants without scaffolds were used as controls. Three independent samples for each condition were assayed.

4.8. Differentiation

4.8.1. Chondrogenic differentiation

NC-Alg, NC-Alg-CS and NC-Alg-DS scaffolds containing 5 x 10^6 D1-MSCs /mL were differentiated into chondrocytes. Chondrogenic differentiation medium was composed of DMEN-High glucose from ATCC (Virginia, USA) supplemented with 10% fetal bovine serum, 1% P/S, 10 ng/mL TGF-β1, 50 nM L-ascorbic acid and 6.25 µg/mL bovine insulin, all purchased from Merck (Madrid, Spain). Scaffolds were cultured in differentiation medium which was changed every 3 days for 21 days. Complete medium without supplements was used for the culture of controls.

4.8.2. Histological staining and collagen production

After 21 days of culture with differentiation medium, scaffolds were washed with DPBS and fixed with 4% formaldehyde. To evaluate chondrogenic differentiation of embedded D1-MSCs scaffolds were stained with Alcian Blue and Safranin-O, both purchased from Merck (Madrid, Spain). Afterward, scaffolds were observed under a Nikon AZ100 microscope from Izasa Scientific (Barcelona, Spain).

The total collagen secreted by chondrocytes in the scaffolds was estimated by hydroxyproline assay kit from Merck (Madrid, Spain). Scaffolds were digested in acid solution after 1 and 21 days of culture and hydroxyproline was quantified following the manufacturer instructions. L-hydroxyproline was used as a standard and scaffolds without differentiation medium were used as negative controls. The absorbance was read at 550 nm on an Infinite M200 microplate reader from TECAN Trading AG (Männedorf, Switzerland). Results were expressed as D21/D1, where D21 (final value) is the amount of hydroxyproline at day 21 and D1 (initial value) at day 1.

4.8.3. Gene expression by RT-PCR

The chondrogenic effect of NC-Alg-CS and NC-Alg-DS scaffolds was evaluated using a quantitative real-time PCR assay. NC-Alg scaffolds were used as controls. Scaffolds were disaggregated incubating them for 15 min at 37 ºC in 1 mg/mL alginate lyase and 1.5% (w/v) sodium citrate, both purchased from Merck (Madrid, Spain). Total mRNA was extracted using TRIzol Reagent and was quantified with a SimpliNano nanodrop from GE Healthcare Life Sciences (Madrid, Spain). The conversion of RNA to cDNA was performed using Fast Gene Scriptase II, cDNA Synthesis Kit from Genetics Nippon Europe (Düren, Germany). Real-time PCRs were performed using StepOnePlus Real-Time PCR Systems from Fisher Scientific (Madrid, Spain). Fluorogenic qRT-PCR-based (TaqMan) assay and specific primers for *ACAN*, *COL1*, *COL2* and *SOX9* were used to quantify the target genes. The expression of all genes was normalized to the housekeeping gene glyceraldehyde-3-phosphate dehydrogenase (*GAPDH*) and to gene expression of untreated samples. Relative expression was calculated with the $2^{-\Delta\Delta CT}$ method.

4.9. Statistical analysis

IBM SPSS software was applied to conduct the statistical analysis. Data were expressed as mean ± standard deviation and differences were considered significant when $p < 0.05$. Student's t-test to identify significant differences between two groups and ANOVA to multiple comparisons were used. Depending on the results of the Levene test of homogeneity of variances, Bonferroni or Tamhane post-hoc test was applied. For non-normally distributed data, Mann-Whitney nonparametric analysis was applied.

Acknowledgements

The authors thank the Basque Government for granted fellowship to S. Ruiz-Alonso (PRE_2020_2_0143). This study was financially supported by the Basque Country Government (IT907-16), the Ministerio de Economía, Industria y Competitividad (FEDER funds, project RTC-2016-5451-1). They also wish to thank the intellectual and technical assistance from the ICTS "NANBIOSIS," more specifically by the Drug Formulation Unit (U10) of the CIBER in Bioengineering, Biomaterials & Nanomedicine (CIBER-BBN) at the University of Basque Country (UPV/EHU). This research was also supported by Fundación Mutua Madrileña (project FMM-AP17196-2019), Consejería de Economía,

Conocimiento, Empresas y Universidad de la Junta de Andalucía (ERDF funds, projects B-CTS-230-UGR18, SOMM17-6109, and P18-FR-2465), and the Instituto de Salud Carlos III, ERDF funds (DTS19/00145 and DTS21/00098). The authors also thank to Spanish Ministry of Science and Innovation (MICINN) (project PID2020- 114086RB-100).

Conflict of Interest
The authors declare no conflict of interest.

Data Availability Statement
Research data are not shared.

References

[1] G. A. Hawker, Clin. Exp. Rheumatol. 2019, 120, 3.

[2] L. Roseti, G. Desando, C. Cavallo, M. Petretta, B. Grigolo, Cell 2019, 8, 1305.

[3] A. J. Sophia Fox, A. Bedi, S. A. Rodeo, Sports Health 2009, 1, 461.

[4] Y. P. Singh, A. Bandyopadhyay, B. B. Mandal, ACS Appl. Mater. Inter- faces 2019, 11, 33684.

[5] A. Ghouri, P. G. Conaghan, Clin. Exp. Rheumatol. 2019, 37, S124.

[6] E. C. Rodriguez-Merchan, L. A. Valentino, Arch. Bone Jt. Surg. 2019, 7, 79.

[7] R. Zhang, J. Ma, J. Han, W. Zhang, J. Ma, Am. J. Transl. Res. 2019, 11, 6275.

[8] S. Vega, M. Kwon, J. Burdick, Eur. Cells Mater. 2017, 33, 59.

[9] W. Zhu, X. Ma, M. Gou, D. Mei, K. Zhang, S. Chen, Curr. Opin. Biotech- nol. 2016, 40, 103.

[10] S. Derakhshanfar, R. Mbeleck, K. Xu, X. Zhang, W. Zhong, M. Xing, Bioact. Mater. 2018, 3, 144.

[11] L. Valot, J. Martinez, A. Mehdi, G. Subra, Chem. Soc. Rev. 2019, 48, 4049.

[12] P. S. Gungor-Ozkerim, I. Inci, Y. S. Zhang, A. Khademhosseini, M. R. Dokmeci, Biomater. Sci. 2018, 6, 915.

[13] K. Hölzl, S. Lin, L. Tytgat, S. Van Vlierberghe, L. Gu, A. Ovsianikov, Biofabrication 2016, 8, 032002.

[14] P. Agrawal, K. Pramanik, V. Vishwanath, A. Biswas, A. Bissoyi, P. K. Patra, J. Biomed. Mater. Res., Part B 2018, 106, 2576.

[15] M. Bishnoi, A. Jain, P. Hurkat, S. Jain, Glycoconjugate J. 2016, 33, 693.

[16] B. L. Farrugia, M. S. Lord, J. M. Whitelock, J. Melrose, Biomater. Sci. 2018, 6, 947.

[17] J. H. Elisseeff, S. Fermanian, D. Wang, B. Sharma, S. Varghese, D. H. Fairbrother, I. Strehin, J. Gorham, B. Cascio, Nat. Mater. 2007, 6, 385.

[18] C. B. Foldager, C. Bünger, A. B. Nielsen, M. Ulrich-Vinther, S. Munir, H. Everland, M. Lind, Int. Orthop. 2012, 36, 1507.

[19] J. Valcarcel, R. Novoa-Carballal, R. I. Pérez-Martín, R. L. Reis, J. A. Vázquez, Biotechnol. Adv. 2017, 35, 711.

[20] B. E. Uygun, S. E. Stojsih, H. W. T. Matthew, Tissue Eng., Part A 2009, 15, 3499.

[21] Y.-L. Chen, H.-P. Lee, H.-Y. Chan, L.-Y. Sung, H.-C. Chen, Y.-C. Hu, Biomaterials 2007, 28, 2294.

[22] M. I. Neves, M. Araújo, L. Moroni, R. M. P. Da Silva, C. C. Barrias, Molecules 2020, 25, 978.

[23] D. Nguyen, D. A. Hägg, A. Forsman, J. Ekholm, P. Nimkingratana, C. Brantsing, T. Kalogeropoulos, S. Zaunz, S. Concaro, M. Brittberg, A. Lindahl, P. Gatenholm, A. Enejder, S. Simonsson, Sci. Rep. 2017, 7, 658.

[24] E. Axpe, M. Oyen, Int. J. Mol. Sci. 2016, 17, 1976.

[25] F. Yu, X. Han, K. Zhang, B. Dai, S. Shen, X. Gao, H. Teng, X. Wang, L. Li, H. Ju, W. Wang, J. Zhang, Q. Jiang, J. Biomed. Mater. Res., Part A 2018, 106, 2944.

[26] M. Müller, E. Öztürk, Ø. Arlov, P. Gatenholm, M. Zenobi-Wong, Ann. Biomed. Eng. 2017, 45, 210.

[27] A. Sheikhi, J. Hayashi, J. Eichenbaum, M. Gutin, N. Kuntjoro, D. Khor- sandi, A. Khademhosseini, J. Controlled Release 2019, 294, 53.

[28] H. Gurruchaga, J. Ciriza, L. Saenz Del Burgo, J. R. Rodriguez-Madoz, E. Santos, F. Prosper, R. M. Hernández, G. Orive, J. L. Pedraz, Int. J. Pharm. 2015, 485, 15.

[29] M. Lafuente-Merchan, S. Ruiz-Alonso, A. Espona-Noguera, P. Galvez- Martin, E. López-Ruiz, J. A. Marchal, M. L. López-Donaire, A. Zabala, J. Ciriza, L. Saenz-Del-Burgo, J. L. Pedraz, Mater. Sci. Eng., C 2021, 126, 112160.

[30] T. J. Lujan, C. J. Underwood, N. T. Jacobs, J. A. Weiss, J. Appl. Physiol. 2009, 106, 423.

[31] A. Silipo, Z. Zhang, F. J. Cañada, A. Molinaro, R. J. Linhardt, J. Jiménez- Barbero, ChemBioChem 2008, 9, 240.

[32] Y. J. Shin, R. T. Shafranek, J. H. Tsui, J. Walcott, A. Nelson, D.-H. Kim, Acta Biomater. 2021, 119, 75.

[33] T. Gao, G. J. Gillispie, J. S. Copus, A. K. Pr, Y.-J. Seol, A. Atala, J. J. Yoo, S. J. Lee, Biofabrication 2018, 10, 034106.

[34] Z. Dai, J. Ronholm, Y. Tian, B. Sethi, X. Cao, J. Tissue Eng. 2016, 7, 204173141664881.

[35] ISO 10993-5:2009 Biological Evaluation of Medical Devices. Part 5: Tests for In Vitro Cytotoxicity. International Organization for Standardization; Geneva, Switzerland 2009.

[36] S. Yamada, K. Sugahara, Curr. Drug Discovery Technol. 2008, 5, 289.

[37] K. Markstedt, A. Mantas, I. Tournier, H. Martínez Ávila, D. Hägg, P. Gatenholm, Biomacromolecules 2015, 16, 1489.

[38] L. Ouyang, R. Yao, Y. Zhao, W. Sun, Biofabrication 2016, 8, 035020.

[39] Z. M. Jessop, A. Al-Sabah, N. Gao, S. Kyle, B. Thomas, N. Badiei, K. Hawkins, I. S. Whitaker, Biofabrication 2019, 11, 045006.

[40] A. Dank, I. H. A. Aartman, D. Wismeijer, A. Tahmaseb, Int. J. Implant Dent. 2019, 5, 12.

[41] Z. Schwartz, J. Y. Martin, D. D. Dean, J. Simpson, D. L. Cochran, B. D. Boyan, J. Biomed. Mater. Res. 1996, 30,145.

[42] X. Cun, L. Hosta-Rigau, Nanomaterials 2020, 10, 2070.

[43] S.-M. Lien, L.-Y. Ko, T.-J. Huang, Acta Biomater. 2009, 5, 670.

[44] H. Park, X. Guo, J. S. Temenoff, Y. Tabata, A. I. Caplan, F. K. Kasper, A. G. Mikos, Biomacromolecules 2009, 10, 541.

[45] M. Mahinroosta, Z. Jomeh Farsangi, A. Allahverdi, Z. Shakoori, Mater. Today Chem. 2018, 8, 42.

[46] Y. Guo, T. Yuan, Z. Xiao, P. Tang, Y. Xiao, Y. Fan, X. Zhang, J. Mater. Sci.: Mater. Med. 2012, 23, 2267.

[47] Z. Wu, X. Su, Y. Xu, B. Kong, W. Sun, S. Mi, Sci. Rep. 2016, 6, 24474.

[48] D. Eglin, D. Mortisen, M. Alini, Soft Matter 2009, 5, 938.

[49] V. Guarino, T. Caputo, R. Altobelli, L. Ambrosio, AIMS Mater. Sci. 2015, 2, 497.

[50] E. Alsberg, H. J. Kong, Y. Hirano, M. K. Smith, A. Albeiruti, D. J. Mooney, J. Dent. Res. 2003, 82, 903.

[51] M. Criado, J. M. Rey, C. Mijangos, R. Hernández, RSC Adv. 2016, 6, 105821.

[52] J. Thiele, Y. Ma, S. M. C. Bruekers, S. Ma, W. T. S. Huck, Adv. Mater. 2014, 26, 125.

[53] M. L. Hall, D. A. Krawczak, N. K. Simha, J. L. Lewis, Osteoarthr. Cartil. 2009, 17, 655.

[54] Y. P. Singh, A. Bandyopadhyay, B. B. Mandal, ACS Appl. Mater. Inter- faces 2019, 11, 33684.

[55] F. Mirahmadi, M. Tafazzoli-Shadpour, M. A. Shokrgozar, S. Bonakdar, Mater. Sci. Eng., C 2013, 33, 4786.

[56] P. K. Gupta, A. K. Das, A. Chullikana, A. S. Majumdar, Stem Cell Res. Ther. 2012, 3, 25.

[57] K. Pelttari, E. Steck, W. Richter, Injury 2008, 39, 58.

[58] C. Antich, J. De Vicente, G. Jiménez, C. Chocarro, E. Carrillo, E. Mon- tañez, P. Gálvez-Martín, J. A. Marchal, Acta Biomater. 2020, 106, 114.

[59] L. D. Solorio, A. S. Fu, R. Hernández-Irizarry, E. Alsberg, J. Biomed. Mater. Res., Part A 2010, 92A, 1139.

[60] J. M. Trowbridge, R. L. Gallo, Glycobiology 2002, 12, 117R.

[61] A. Cañibano-Hernández, L. Saenz Del Burgo, A. Espona-Noguera, G. Orive, R. M. Hernández, J. Ciriza, J. L. Pedraz, Mol. Pharmaceutics 2017, 14, 2390.

[62] K. Motokawa, S. K. Hahn, T. Nakamura, H. Miyamoto, T. Shimoboji, J. Biomed. Mater. Res., Part A 2006, 78A, 459.

[63] Y.-L. Chen, H.-C. Chen, H.-Y. Chan, C.-K. Chuang, Y.-H. Chang, Y.-C. Hu, Biotechnol. Bioeng. 2008, 101, 821.

[64] J. Hauptstein, T. Böck, M. Bartolf-Kopp, L. Forster, P. Stahlhut, A. Nadernezhad, G. Blahetek, A. Zernecke-Madsen, R. Detsch, T. Jüngst, J. Groll, J. Teßmar, T. Blunk, Adv. Healthcare Mater. 2020, 9, 2000737.

[65] S. Ishikawa, K. Iijima, K. Sasaki, M. Hashizume, M. Kawabe, H. Ot- suka, Appl. Sci. 2018, 8, 1398.

[66] C. L. Deal, R. W. Moskowitz, Rheum. Dis. Clin. N. Am. 1999, 25, 379.

[67] R. A. A. Muzzarelli, F. Greco, A. Busilacchi, V. Sollazzo, A. Gigante, Carbohydr. Polym. 2012, 89, 723.

[68] W. S. Toh, X.-M. Guo, A. B. Choo, K. Lu, E. H. Lee, T. Cao, J. Cell. Mol. Med. 2009, 13, 3570.

[69] Council of Europe. Sterility. The European Pharmacopoeia, 9th ed., EDQM, Strasbourg, France 2017, Ch. 2.6.1.

[70] A. Zabala, L. Blunt, R. Tejero, I. Llavori, A. Aginagalde, W. Tato, Surf. Topogr.: Metrol. Prop. 2020, 8, 015002.

[71] ISO 25178-2 2012 Geometrical product specifications (GPS)— Surface texture: Areal: II. Terms, definitions and surface texture pa- rameters, 2012.

Appendix 4

3D Bioprinted Hydroxyapatite or Graphene Oxide Containing Nanocellulose-Based Scaffolds for Bone Regeneration

Markel Lafuente-Merchan[1,2,3], Sandra Ruiz-Alonso[1,2,3], Fátima García-Villén[1,2,3], Alaitz Zabala[4], Ana M. Ochoa de Retana[5], Idoia Gallego[1,2,3], Laura Saenz-del-Burgo[1,2,3*] and José Luis Pedraz [1,2,3*]

[1] NanoBioCel Group, Laboratory of Pharmaceutics, School of Pharmacy, University of the Basque Country (UPV/EHU), Paseo de la Universidad 7, 01006 Vitoria-Gasteiz, Spain.
[2] Biomedical Research Networking Center in Bioengineering, Biomaterials and Nanomedicine (CIBER-BBN), Health Institute Carlos III, Paseo de la Universidad 7, 01006 Vitoria-Gasteiz, Spain.
[3] Bioaraba, NanoBioCel Research Group, 01009 Vitoria-Gasteiz, Spain.
[4] Mechanical and Industrial Manufacturing Department, Mondragon Unibertsitatea, Loramendi 4, Mondragón 20500, Spain.
[5] Department of Organic Chemistry I, Faculty of Pharmacy and Lascaray Research Center, University of the Basque Country (UPV/EHU), Paseo de la Universidad 7, Vitoria 01006, Spain.
[*] Correspondence: laura.saenzdelburgo@ehu.eus; joseluis.pedraz@ehu.eus

Macromolecular Bioscience, 2022, 11:2200236
IF: 4.979 (2022) (Q1)
Cat: Biomaterials & Bioengineering
https://doi.org/10.1002/mabi.202200236

Abstract

Bone tissue is usually damaged after big traumas, tumors, and increasing aging-related diseases such as osteoporosis and osteoarthritis. Currenttreatments are based on implanting grafts, which are shown to have several inconveniences. In this regard, tissue engineering through the 3D bioprinting technique has arisen to manufacture structures that would be a feasible therapeutic option for bone regenerative medicine. In this study, nanocellulose–alginate (NC–Alg)-based bioink is improved by adding two different inorganic components such as hydroxyapatite (HAP) and graphene oxide (GO). First, ink rheological properties and biocompatibility are evaluated as well as the influence of the sterilization process on them. Then, scaffolds are characterized. Finally, biological studies of embedded murine D1 mesenchymal stem cells engineered to secrete erythropoietin are performed. Results show that the addition of both HAP and GO prevents NC–Alg ink from viscosity lost in the sterilization process. However, GO is reduced due to short cycle autoclave sterilization, making it incompatible with this ink. In addition, HAP and GO have different influences on scaffold architecture and surface as well as in swelling capacity. Scaffolds mechanics, as well as cell viability and functionality, are promoted by both elements addition. Additionally, GO demonstrates an enhanced bone differentiation capacity.

Keywords: 3D bioprinting; Bioinks; Bone; Graphene oxide; Hydroxiapatite; Tissue engineering.

1. Introduction

Bone is a connective tissue which is part of the skeletal system. Its main function is to provide mobility and protection to organs. In addition, it is involved in blood cell generation and homeostasis maintenance as well as in mineral storage and blood pH regulation [1]. It is characterized by having high porosity, vascularity and strong mechanical properties [2-4].

Due to its characteristics, bone tissue has the potential to regenerate by itself in case of minor injuries. However, this capacity is limited and becomes ineffective in case of excessive damage such as in big traumas, bone infections and tumours [1,5]. Furthermore, bone degenerative diseases that are closely related to the increase in population age are becoming more prevalent. Among them, osteoporosis and rheumatic diseases such as osteoarthritis have gained notoriety [1,5].

Current therapeutic treatment is based on prosthesis implantation. Among the implant materials, metals such as titanium, ceramics and polymers such as polyethylene have been commonly used. However, they still present some drawbacks in terms of high rigidity, lack of integration in native tissue and the absence of biodegradability and bioactivity properties [6,7]. On the other hand, bone transplantations have arisen as an alternative treatment to overcome the aforementioned problems. Nevertheless, autografts and allografts are related to the risk of donor site morbidity, chronic pain and graft supply limitations. Moreover, in xenografts transplantations, the risk of pathogen transmission should be added [8]. In addition, it is common for patients who have undergone bone surgery to present long recovery times, high rates of implant rejection and the necessity to have recurrent surgeries.

In this context, in order to avoid the aforementioned drawbacks, 3D bioprinting has gained notoriety when it comes to fabricating implantable structures for bone substitutes or regeneration. As an additive technique, 3D bioprinting has the advantage of creating scaffolds in a fast, automatic and reproducible manner [9]. The technique is based on the layer-by-layer depo-

sition of a bioink, which may be composed of a wide range of biomaterials and cell types [9,10]. In addition, bioactive molecules such as drugs, growth factors and genetic material can be included [10]. In this regard, to manufacture scaffolds for bone regeneration, the bioink and, therefore, the bioprinted scaffold must meet certain requirements such as being biodegradable, bioactive and biocompatible [11].

Hydroxyapatite (HAP) is an inorganic ceramic formed of calcium and phosphate $Ca_{10}(PO_4)_6(OH)_2$ [12]. As native bone is composed of 70% of HAP, it has been widely used as a biomaterial to create structures for bone regeneration [12,13]. In fact, it has been shown to be bioactive and osteoconductive as well as to provide excellent mechanical properties. [14] Moreover, due to its high porosity, HAP scaffolds have been reported to promote cell migration and osteogenic differentiation [14,15]. It has also been proven that HAP improves cell attachment and integration to native tissue in metallic implants that have been previously covered with this ceramic [12].

Lately, graphene has gained a presence in different fields such as optics, engineering and electronics due to its excellent electroconductivity, and thermochemical and mechanical properties. Graphene oxide (GO) is formed by a sheet of sp^2 hybridized carbon atom with oxygen containing functionalities [16]. This chemical derivative has been widely applied in biomedicine as a drug, protein, genes and peptide carrier for its controlled delivery. In the tissue engineering field, GO based hydrogels have been shown to be biodegradable, biocompatible and enhance the mechanical rigidity of manufactured structures [16,17]. Consequently, GO has been used for the regeneration of tissues that require high mechanical strength such as bone or vascular tissue [17]. In addition, it has been reported that GO promotes osteogenesis in metal implants as well as mineralization. Furthermore, proliferation and osteogenic differentiation of mesenchymal stem cells (MSC) have been observed after GO addition *in vitro* and *in vivo* [8,18].

In summary, both HAP and GO have been shown to have interesting properties to be used in the formulation of bioinks for bone regeneration. Howe-

ver, for bioprinting, not only must these bioactive properties be taken into account, but also other important bioink characteristics such as printability and crosslinking procedure [11]. For good printability, bioinks should have adequate rheological properties. Thus, it is necessary to add a rheological modifier such as nanofibrillated cellulose (NC). In addition, NC has shown to have good mechanical properties and cytocompatibility [19]. On the other hand, sodium alginate (Alg) has been proposed due to its instant gel formation with divalent cations such as calcium [20]. Alg is a well-known polysaccharide in the tissue engineering field as it is biocompatible, biodegradable and non-toxic [20,21]. In fact, Alg and NC have been already applied to manufacture scaffolds through 3D bioprinting for bone regeneration [19,22].

In this study, NC-Alg-HAP and NC-Alg-GO bioinks were developed for the manufacturing of scaffolds through 3D bioprinting for bone regeneration. First, ink rheological properties and biocompatibility were evaluated. Afterwards, the sterilisation process was analysed. Then, scaffolds were printed to analyse the printability, swelling and degradation kinetics. Finally, D1 MSCs modified to produce erythropoietin hormone (D1-MSCs-EPO) were included in the NC-Alg-HAP and NC-Alg-GO inks in order to observe cell proliferation, viability and functionality. Additionally, cell osteogenic differentiation was assayed to evaluate the application of NC-Alg-HAP and NC-Alg-GO scaffolds for bone regeneration purposes.

2. Material and Methods

2.1. Materials

Hydroxyapatite was purchased from Merck (Madrid, Spain). Graphene oxide was obtained from Graphenea (San Sebastian, Spain). Ultra-pure low-viscosity high guluronic acid sodium alginate (UPLVG) was acquired from FMC Biopolymer (Sandvika, Norway). Nanofibrillated cellulose was purchased from Sappi Europe (Brussels, Belgium). Fetal calf serum (FCS), fetal bovine serum (FBS) and penicillin/streptomycin (P/S) were acquired from Gibco (San Diego, USA). 3-(4,5-dimethylthiazol-2-yl)-2,5-diphenyltetrazoliumbromid (MTT) *in vi-*

tro toxicology assay, calcium chloride, D-mannitol, dexamethasone, β-glycerophosphate, L- ascorbic acid, alginate lyase, and sodium citrate were obtained from Merck, (Madrid, Spain). LIVE/DEAD® Viability/Cytotoxicity kit was obtained from Life Technologies (Madrid, Spain). Alamar blue® was acquired from Bio-Rad científica (Madrid, Spain). DPBS code BE17-513F was obtained from Lonza (Porriño, Spain). Murine D1-MSCs were obtained from ATCC (Virginia, USA).

2.2. Inks development

Two inks were proposed. In order to formulate nanocellulose-alginate-hydroxyapatite (NC-Alg-HAP) ink, HAP was dispersed at 1% (w/v) in a 2% (w/v) Alg solution. Then, NC was added at 80% (v/v) of the final solution and everything was mixed to obtain a homogeneous ink. Likewise, nanocellulose-alginate-graphene oxide (NC-Alg-GO) ink was prepared by dispersing a GO solution of 50 µg/mL in a 2% (w/v) Alg solution. Afterwards, NC was included at 80% (v/v) of the final solution and everything was homogenized to obtain the ink.

2.3. Inks characterization

2.3.1. Rheological study

Inks´ rheological properties were analysed by performing two different assays; steady flow measurement and oscillatory shear measurement. In the first study, viscosity was evaluated by conducting a shear rate sweep from 0.1 to 100 s^{-1} followed by a subsequent shear rate from 100 to 0.1 s^{-1}. Meanwhile, the viscoelasticity properties in terms of elastic modulus (G') and viscous modulus (G") were obtained in the oscillatory shear measurement establishing 2% of strain and an oscillation frequency sweep from 0.1 to 100 Hz. In addition, Tan δ values were acquired from the G"/G' relation. All the measurements were conducted on an AR100 rheometer from TA Instruments (New Castle, USA) with a flat 40 mm stainless steel plate and at room temperature.

2.3.2. Cytotoxicity analysis

In vitro cytotoxicity of NC-Alg-HAP and NC-Alg-GO inks was evaluated through three different assays; adhesion, direct and indirect assays. In order to perform all the studies, circular structures were printed and mouse L929 fibroblasts from ATCC (Virginia, USA) at 3.123 x 10^4 cells/cm^2 cell density were used. Cells were culture in EMEM supplemented with 10% (v/v) FCS and 1% (v/v) P/S at 37 ºC in humidified 5% CO_2 atmosphere. In the adhesion test, cells were seeded onto the printed disks and cell viability was measured after 4 h of incubation. As controls, cells directly seeded onto a culture plate were used. Conversely, in the direct and indirect tests, cells were seeded onto culture plates and were maintained in DMEM for 24 h. Then, printed disks were placed onto seeded cells in the direct assay and, DMEM which had been in touch with the NC-Alg-HAP or NC-Alg-GO printed disks, were added in the indirect contact assay. After 24 of incubation, cell viability was measured in both tests. Cells with no disk exposure were used as controls. To determine cell viability in all the assays, MTT *in vitro* toxicity assay kit was used following the manufacturer´s recommendations, and the absorbances were obtained at 570 nm with a reference wavelength of 650 nm using an Infinitive M200 microplate reader from TECAN Trading AG (Männedorf, Switzerland). Six independent samples were conducted.

Each experiment was carried out following the ISO 10993-5-2009 rule [23]. Cell viability was calculated applying the following equation (1) and a cell viability above 70% was considered as non-toxic.

$$\text{Cell viability (\%)} = \frac{\text{Testing sample OD570}}{\text{Untreated blank OD570}} \times 100 \qquad (1)$$

2.3.3. Inks sterilisation test

The sterilisation process of NC-Alg-HAP and NC-Alg-GO inks was carried out in a short cycle autoclave by AJL Ophthalmic (Miñano, Spain) in accordance with a previous study [24]. An industrial autoclave F0A2/B model was used with a maximum of 123-124 ºC temperature and 3.60-3.70 bar pressure. The

sterilisation was performed in 3.04 min.

Then, the repercussions of the sterilisation process on inks properties were analysed. First, inks physical appearance was observed. Then, rheological measurements were conducted as previously described (2.3.1 part)

2.3.4. FT-IR analysis of graphene ink

Fourier Transform Infrared (FT-IR) spectra were performed with a Nicolet is10 spectrometer from Thermo Scientific (Madrid, Spain) using an attenuated total reflectance (ATR) technique. The spectra were obtained in the range 4000–500 cm^{-1} at room temperature, with a resolution of 4 cm^{-1} and 32 scans.

2.4. 3D Printing

Scaffolds were printed by using an extrusion-based 3D bioprinter Bio X from Cellink (Gothenburg, Sweden). The scaffolds' shape consisted of a circular grid-like form of 15 mm diameter and 2 layers. Different printing parameters were set depending on the ink. To print NC-Alg-HAP ink, a 22 G conical needle was used and printing parameters were established at 15-18 kPa printing pressure and 4-5 mm/s printing speed. On the other hand, NC-Alg-GO ink was printed using a 27 G conical needle, 22-25 kPa printing pressure and 4-5 mm/s printing speed. NC-Alg ink was printed as control ink using the same parameters to NC-Alg-GO ink. Subsequently, all printed scaffolds were crosslinked by submerging them in a 100 mM calcium solution for 5 min.

Afterwards, macroscopic pictures were taken in a Nikon AZ100 microscope from Izasa Scientific (Barcelona, Spain) to evaluate the printability.

2.5 Scaffold characterization

2.5.1. Surface and architectural characterization

Cryo-SEM images were acquired in a TM-4000 Scanning Electron Microscope from Hitachi (Illinois, USA). Scaffolds were in a hydrated state and were

frozen a - 20ºC using a cryogenic module. Afterwards, samples were observed using a 5 kV voltage.

Hydrated NC-Alg-HAP and NC-Alg-GO scaffolds were characterized with an optical profilometer from Sensofar S-NEOX (Barcelona, Spain) in order to evaluate their surface and architecture. A focus variation method was utilized. Then, to process all the data a metrological software SensoMAP Premium 7.4 from Digital Surf (Besançon, France).

Architectural characterization was acquired by measuring an area of 6484 x 4880 μm^2 at 3 locations on 3 independently printed scaffolds. A 10x objective (side sampling: 1.29 µm, vertical resolution: 25 nm) was used for each condition.

Scaffold surface evaluation was carried out by measuring 3 independent areas of 873 x 656 μm^2 on the scaffolds with a 20x objective (lateral sampling: 0.65 µm, vertical resolution: 8 nm).

2.5.2. Swelling

NC-Alg-HAP and NC-Alg-GO scaffolds were lyophilized in a Telstar cryodos Freeze Dryer (Terrassa, Spain) in order to evaluate their swelling behaviour. Freeze-drying process was performed in 40 h. First, samples were progressively frozen at -50 ºC for 3 h. Then, primary drying process was carried out in which chamber pressure and temperature were set at 0.2 mBar and -50 ºC, respectively. After 5 h, the pressure was maintained but the temperature increased at 20 ºC for 7 h. Finally, chamber pressure was removed and secondary drying process was conducted at a 20 ºC during 24 h. After that, their dried weight was obtained. Then, samples were submerged in Dulbecco's phosphate-buffered saline (DPBS) with calcium and magnesium at 37 ºC to determine their swelling capacity. Finally, at selected time points, scaffolds were removed from DPBS, water excess was eliminated using filter paper and they were reweighted. NC-Alg constructs were utilized as control. The assay was carried out in triplicate and, at every time point, the swelling % was calculated applying the following equation (2):

$$\text{Swelling (\%)} = \frac{W_{wet} - W_{dried}}{W_{dried}} \times 100 \qquad (2)$$

Where W_{wet} corresponds to wet weight and W_{dried} is dried weight

2.5.3. Degradation study

Degradation study of NC-Alg-HAP and NC-Alg-GO scaffolds was performed by measuring their area. Then, printed constructs were submerged in DMEM at 37 ºC. Afterwards, at chosen time points, scaffolds were removed from DMEM to measure their area again. Subsequently, constructs were returned to the DMEM. The study was conducted in triplicate and NC-Alg constructs were used as control. The area loss in % was calculated by applying the following equation (3):

$$\text{Area loss (\%)} = \frac{A_{before} - A_{after}}{A_{before}} \times 100 \qquad (3)$$

Where A_{before} and A_{after} correspond to scaffold area before placing them in DMEM and after passing chosen time in the culture media, respectively.

2.5.4. Mechanical properties evaluation

Mechanical properties of printed scaffolds were carried out in a TA.XT.plusC Texture Analyser from Aname Instrumentación Cientifica (Madrid, Spain). A cylinder probe of 5 kg and 20 mm was used to perform all the experiments. Measurements were conducted in a compression test form by setting a 0.5 mm/s test speed and a maximum of 80% strain. Compression Young's modulus was calculated from the slope of the stress/strain curve. Six replicates per scaffold were performed and NC-Alg scaffolds were applied as controls.

2.6. Cell culture and 3D bioprinting

To perform the 3D bioprinting procedure, first, NC-Alg-HAP and NC-Alg-GO inks were prepared as aforementioned (see section 2.2). Then, bioinks were prepared by mixing the inks with murine D1-MSCs engineered to secrete erythropoietin hormone (D1-MSCs-EPO) at $5x10^6$ cell/mL [25].

Cell culture was carried out in T-flasks with DMEM supplemented with 10% (v/v) FBS and 1% (v/v) P/S. Cells were cultured in a humidified atmosphere containing 5% CO_2 and at 37 ºC. Culture medium was frequently substituted and at 80% of confluence, they were subcultured.

Finally, scaffolds were manufactured through the 3D bioprinting technique as previously mentioned (see section 2.4). Afterwards, they were placed in a complete medium for their culture. NC-Alg bioink was prepared and bioprinted as control. The whole procedure was carried out under aseptic conditions and at room temperature.

2.7. *In vitro* biological evaluation

2.7.1. Cell viability assay by fluorescence microscopy

Cell viability was qualitatively evaluated with the LIVE/DEAD™ Viability/ Cytotoxicity Kit. First, scaffolds were washed with DPBS and incubated in a staining solution containing 100 mM calcein AM for 40 min protected from the light and at room temperature. Then, the calcein solution was removed and a 0.8 µM ethidium homodimer-1 was added. After an incubation of 10 min at 37 ºC, constructs were rinsed in DPBS and observed in a Nikon TMS microscope (Virginia, USA) with an excitation/emission wavelength of 495/515 nm for the calcein AM staining and 495/635 nm for the ethidium homodimer staining. Three independent assays were evaluated for each condition and the Image J software was used to analyse the acquired pictures in order to quantify the percentage of live and dead cells.

2.7.2. Metabolic activity study

D1-MSCs-EPO metabolic activity was determined by using the Alamar Blue® assay (AB). The assay was carried out by depositing bioprinted scaffolds in a solution containing 10% AB in a complete medium. Then, samples were incubated at 37 ºC for 4 h. Finally, fluorescence was determined in an Infinitive M200 microplate reader from TECAN Trading AG (Männedorf, Switzerland). It was set at an excitation wavelength of 560 nm and an emission wavelength

of 590 nm. Scaffolds with no embedded cells were used as negative controls. At least, six samples were conducted for each condition.

2.7.3. EPO secretion quantification

EPO secretion was assayed using Quantikine IVD Human EPO ELISA Kit from R&D Systems (Madrid, Spain). At days 1, 7, 14 and 21 after bioprinting, scaffolds were placed with 500 µL of DMEM at 37 ºC for 24 h. Then, supernatants were examined to quantify EPO secretion. Supernatants from scaffolds without cells were used as negative controls. Three independent samples for each condition were conducted.

2.8. Osteogenic differentiation

D1-MSCs into NC-Alg, NC-Alg-HAP and NC-Alg-GO scaffolds were differentiated to osteoblasts. Bioprinted constructs were cultured in an osteogenic differentiation medium composed of complete culture media supplemented with 100 nM dexamethasone, 20 mM β-glycerophosphate and 50 µM L-ascorbic acid. They were cultured for 21 days and the differentiation medium was replaced every 3 days. A complete medium without supplements was utilized to culture the controls.

2.8.1. Mineralization assay

Mineralization evaluation of cells inside bioprinted scaffolds was carried out with Alizarin Red S staining, purchased from Merck (Madrid, Spain). At 21 days after bioprinting, scaffolds were removed from the differentiation culture medium and were washed with PBS. Next, they were fixed with 4% formaldehyde for 30 min. Afterwards, Alizarin Red S solution was added to stain calcium deposits. Finally, scaffolds were washed and were observed under a Nikon AZ100 microscope.

2.8.2. Alkaline phosphatase (ALP) activity quantification

ALP activity was determined after maintaining the bioprinted scaffolds in the osteoinductive medium for 1 and 21 days. First, scaffolds were disaggregated by incubating them in 1 mg/mL alginate lyase solution at 37 ºC for 15

min. Next, ALP activity was quantified by using Alkaline Phosphatase Assay Kit (fluorometric). The assay was performed following the manufacturer's recommendations and fluorescence was read at 360 nm and 440 nm excitation/emission wavelength, respectively. Three replicates were conducted per condition.

2.8.3. RT-PCR

The osteogenic effect of NC-Alg-HAP, NC-ALG-GO and NC-Alg scaffolds was determined using a quantitative real-time PCR study. First, a solution of 1.5% (w/v) sodium citrate and 1 mg/mL alginate lyase were applied to disaggregate the scaffolds. Then, TRIzol reagent, from Merck (Madrid, Spain), was added to extract the total mRNA. Afterwards, the total mRNA was measured with a SimpliNano nanodrop from GE Healthcare Life Sciences (Madrid, Spain) and was converted to cDNA applying the Fast Gene Scriptase II, cDNA Synthesis Kit from Genetics Nippon Europe (Düren, Germany). Finally, real-time PCRs were conducted with StepOnePlus Real-Time PCR Systems from Fisher Scientific (Madrid, Spain). The specific primers for *RUNX2*, *ALP*, osteocalcin (*OSTC*) and osteopontin (*SPP1*) were used to determine the target genes by using a fluorogenic qRT-PCR based (TaqMAN) assay. Glyceraldehyde-3-phosphate dehydrogenase (*GAPDH*) was used as the housekeeping gene. Gene expression was normalized to *GAPDH* and to gene expression of undifferentiated samples. The $2^{-\Delta\Delta CT}$ method was applied to calculate the relative expression of all the genes.

2.9. Statistics

Statistical analysis was conducted with IBM SPSS® software. Data were indicated as mean ± standard deviation. Significant differences were considered when $p < 0.05$. To determine significant differences between two groups student´s t-test was used, whereas ANOVA was applied to analyse multiple groups. Depending on the results of the Lavene test of homogeneity of variances, Tamhane post-hoc test or Bonferroni test was utilized. Mann-Whitney nonparametric test was used to analyse non-normally distributed data.

3. Results and discussion

Natural polymers have been shown to be excellent components to develop ink for 3D bioprinting since they are biocompatible and biodegradable. Thus, we previously fabricated a bioink composed of NC and Alg, which showed good printability and suitability with cells [24]. In this research work, we have focused on the improvement of NC-Alg bioink in order to regenerate bone tissue. For this purpose, two different inorganic components were added. HAP which apart from being the main element in the bone extracellular matrix, has been reported to be biocompatible, osteoinductive and reinforce the bone mechanics [12,26]. We have previously demonstrated that by reinforcing gelatin scaffolds with this type of HAP, good osteoinductive properties together with excellent biocompatibility *in vitro* and *in vivo* were obtained [27]. HAP concentrations above 3% resulted in printing needle obstruction in a previous screening process. Therefore, ceramic concentration in the NC-Alg ink was reduced to 1%, which has been probed to promote cell viability and bone differentiation ability on Alg scaffolds [28].

On the other hand, GO was added since it has been gained notoriety in biomedicine. As a consequence of its ability to bond with diverse biomolecules such as DNA, proteins and antibodies, it has been used as drug delivery system, protein carrier or biosensor component [29,30]. In tissue engineering fields, it has been reported to favour osteogenic differentiation of cells and to supply the hydrogels with excellent mechanical properties [17]. In a previous study, it was concluded that the 50 µg/mL of GO was the best concentration for cell viability and functionality in Alg microcapsules [31]. In fact, it was reported that GO concentrations above 50 µg/mL may induce cellular damage and toxicity [30]. In this regard, the effect of adding these two elements on inks properties as well as on scaffolds characteristics was evaluated. Additionally, their influence on cell viability, functionality and osteogenic differentiation was assayed.

3.1. Rheological study

NC-Alg ink was modified by adding separately HAP and GO. Then, rheological behaviour was evaluated in Fig 1. In steady flow measurement (Fig 1A), all the studied inks showed similar results, which consisted of shear-thinning flow behaviour followed by a thixotropic behaviour. Shear-thinning behaviour is a characteristic of pseudoplastic materials and suggested the suitability of the inks with extrusion-based bioprinting since ink viscosity must be decreased to go through the printing needle. In addition, thixotropy indicated a viscosity recovery after being the ink extruded, which ensured the shape of the printed structure. Although all inks types showed this behaviour and were suitable for extrusion bioprinting, no differences were observed when HAP or GO were included to the NC-Alg ink. It was reported in another research work that either HAP or GO may increase the viscosity values of the inks [18,32]. However, these inorganic materials are not considered rheological modifiers. Therefore, the viscosity of the inks increased with the concentration of HAP and GO inside the inks, which was higher than the concentrations used in our study.

On the other hand, in Fig. 1B viscoelasticity behaviour was analysed in terms of elastic modulus G' and viscous modulus G". All the inks demonstrated a more elastic behaviour than a viscous performance. Moreover, the addition of HAP or GO resulted in no changes in viscoelasticity values in comparison with the NC-Alg ink.

Then, the G"/G' relation was calculated with the Tan δ value in Fig 1C. Results showed no statistical differences among the inks, being all of them between 0.3-0.5. According to the literature, inks with Tan δ closer to 1 showed more fluidity and, therefore, scaffold shape fidelity is difficult to obtain. In contrast, with values closer to 0, inks showed more robust behaviour which compromised extrusion. In addition, viscoelasticity and Tan δ are related to cell viability within the inks. Thus, very fluid inks do not have the necessary viscosity to protect the cells from the forces exerted in the bioprinting process, while very robust inks require high printing pressures that damage the cell viability. In this study, all the inks showed a Tan δ value that is optimal

for maintaining high cell viability, good shape fidelity and uniform extrusion [33].

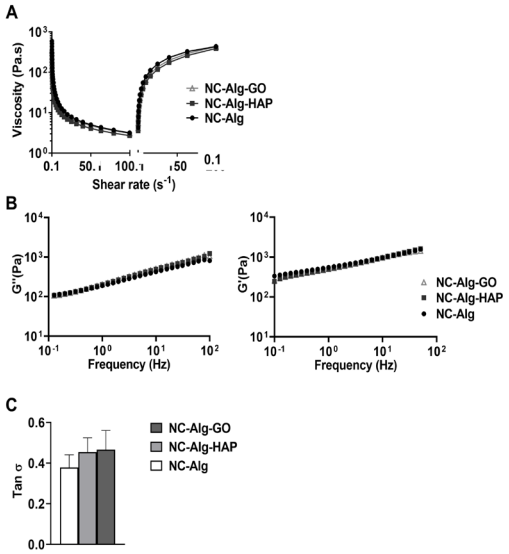

Figure 1. Rheological characterization of NC-Alg, NC-Alg-HAP and NC-Alg-GO inks. A) Steady flow measurement. B) Viscoelasticity measurement in terms of G′ and G″ modulis. C) Relationship between G″/G′ expressed in tan δ. Values represent mean ± SD.

3.2. Sterilisation effects evaluation

3D printing differs from 3D bioprinting in the inclusion into the ink of the biological component, which is usually composed of cells. However, this step requires an absence of pathogens or microorganisms that may damage the cells. Consequently, developed inks were sterilised in a short cycle autoclave and, after that, they were characterized again by rheology to verify whether the sterilisation process has any effect on their composition. In a previous study, the short cycle autoclave showed to be the best option to sterilise NC-Alg inks, despite the fact that it was demonstrated to cause a slight decrease in terms of viscosity and viscoelasticity values (Fig 2C) in comparison with non-sterilised NC-Alg inks [24]. In this study, however, as Fig 2AI and 2BI show, the addition of HAP or GO, resulted in no differences in viscosity values between non-sterilised and sterilised inks. Indeed, both inks maintained shear-thinning and thixotropic behaviour, which suggested excellent printabi-

lity and scaffold fabrication. Similarly, NC-Alg-HAP and NC-Alg-GO inks were not affected by short autoclave when viscoelasticity values of sterilised and non-sterilised inks were compared (Fig 2BI and 2BII).

The rheological properties of HAP composites depend on suspension concentration and pore size. It has been reported that HAP is stable at temperatures below 500 ºC [34], therefore, it was expected to maintain its chemical composition and, as a consequence, had no influence on ink rheological properties. Importantly, HAP addition prevented NC-Alg ink from a rheological properties' reduction. It was previously shown that HAP prevented Alg based hydrogel from temperature decomposition. According to this study, HAP may have displaced sodium ions of alginate avoiding its degradation. Consequently, Alg-HAP hydrogels showed higher mass after high temperature exposition which could be related to rheological properties maintenance after sterilisation [35].

On the other hand, the GO containing ink showed similar behaviour to NC-Alg-HAP in terms of no rheological alteration. GO has been reported to reinforce polymeric inks in terms of stiffness and strength [36]. Thus, NC-Alg-GO ink could have higher mechanical properties than NC-Alg ink and, therefore, demonstrates greater resistance to the sterilisation process.

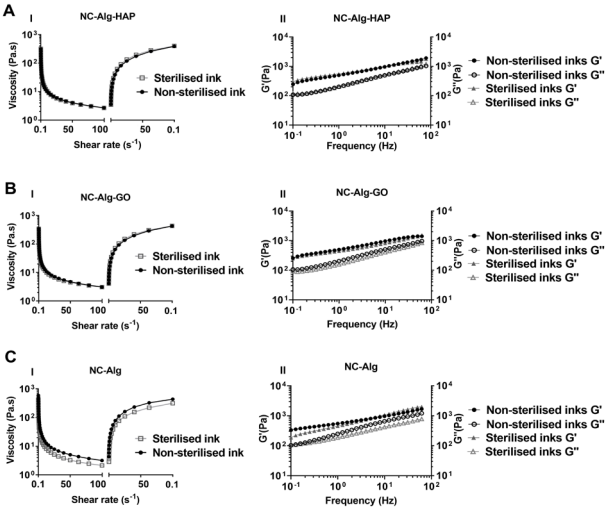

Figure 2. Rheological evaluation of inks after autoclave sterilisation. A) NC-Alg-HAP ink, B) NC-Alg-GO ink and C) NC-Alg ink. I) Steady flow measurement. II) Viscoelasticity measurement.

According to rheological measurements, both sterilised inks demonstrated good properties to be printable through extrusion bioprinting. However, sterilised NC-Alg-GO ink showed a colour change, becoming darker than non-sterilised ink (data not shown). Consequently, an additional study was carried out with this ink in order to verify any chemical modification as a consequence of the sterilisation process.

To do so, FT-IR analysis was conducted (Fig. 3). Results showed differences between short cycle autoclaved NC-Alg-GO ink and the non-sterilised one. These spectra differences were predominantly found between carbon and oxygen bonds. A peak was detected at 1763 cm^{-1} wave number in non-sterilised ink corresponding to C=O stretching vibration. Additionally, in non-sterilised ink peaks were detected at 1204 cm^{-1} and 1077 cm^{-1} wave numbers related to C-O and C-O-C stretching vibrations, respectively. Finally, a C-OH stitching vibration was measured on 1299 and 1131 cm^{-1} wave numbers in non-sterilised ink. In contrast, in the sterilised NC-Alg-GO ink all these peaks were not detected, indicating bonds loss between carbon and oxygen molecules.

Therefore, it can be concluded that GO was reduced due to the autoclave process. The lack of oxygen containing functional groups in reduced GO has been correlated with an increase in cell toxicity in comparison with GO [37]. Likewise, thermally reduced GO has been related to cell death and genotoxicity [38]. Consequently, the short cycle autoclave technique was discarded to sterilise NC-Alg-GO inks. As an alternative, the NC-Alg ink was sterilised by autoclave and GO was subsequently included after being sterilised with UV.

A

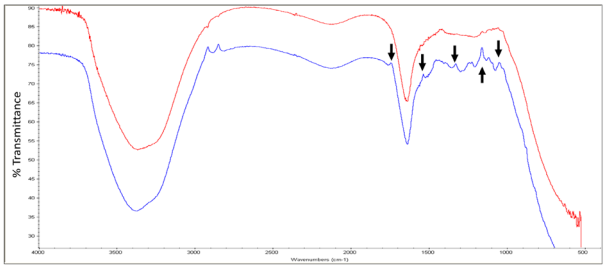

B

Sample	C=O cm^{-1}	C-O cm^{-1}	C-OH cm^{-1}	C-O-C cm^{-1}
Non-sterilised NC-Alg-GO	1763	1204	1299 1131	1077
Sterilised NC-Alg-GO	-	-	-	-

Figure 3. FT-IR assay of NC-Alg-GO ink before and after short cycle autoclave sterilisation. A) FT-IR spectra showing the % transmittance differences. In red: sterilised ink; in blue: non-sterilised ink. B) Table of the signalled results from FT-IR spectra.

3.3 Cytotoxicity study

Cytotoxicity study of sterilised NC-Alg-HAP and NC-Alg-GO inks was conducted to analyse their biocompatibility (Fig 4). In the direct contact assay, results showed high L929 fibroblasts viability when both, HAP and GO were added to NC-Alg ink. In addition, in the indirect contact assay, cell viability was also high for all the ink types. Taking into account that in both assays the cell viability was above 70%, it can be concluded that the inks have good biocompatibility. In contrast, in the adhesion assay, statistically ($p < 0.01$) lower cell viability was observed in GO containing inks in comparison with NC-Alg inks. It has been reported that GO has adhesive properties [39]. In fact, previous work showed good adherence of L929 fibroblasts to a GO monolayer [40]. However, they used a longer cell incubation time before cell viability measurement than in our study, which could explain the observed low cell viability. In any case, cell viability was higher than 70%, which would indicate good biocompatibility

The properties that GO has to cells be adhered, have been previously reported [39]. In fact, a research work demonstrated the good adherence

of L929 fibroblasts to a GO monolayer [40]. Therefore, the low cell viability showed on NC-Alg-GO inks could be because the incubation time was shorter than in the rest of the consulted research works. In any case, cell viability was higher than 70%, which would indicate good biocompatibility.

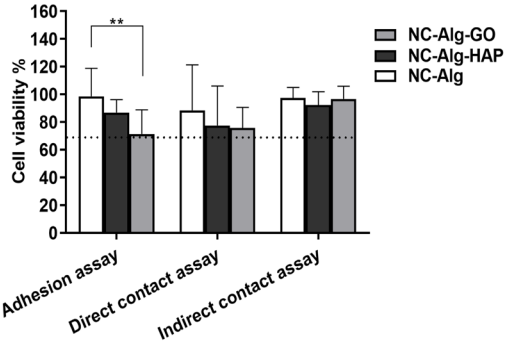

Figure 4. Cytotoxicity study of NC-Alg-HAP and NC-Alg-GO inks by adhesion, direct contact and indirect contact assays. NC-Alg ink was used as control. Values represent mean ± SD. ** $p < 0.01$.

3.4 Printability evaluation

15 mm diameter grid-like scaffolds were printed through extrusion 3D bioprinting technique. A 27 G conical needle was used and printing parameters of 22-25 kPa pressure and 4-5 mm/s speed were set since printable scaffolds with good shape fidelity were manufactured with NC-Alg inks in previous studies [24,41]. In addition, no differences among the inks were observed in rheological measurements, therefore, it was expected to have the same printability properties. However, printing difficulties in terms of needle obstruction were observed with NC-Alg-HAP inks. Consequently, HAP containing scaffolds were printed using a higher diameter needle of 22 G, and, to maintain a constant extrusion flow, printing pressure was reduced to 15-18 kPa. In contrast, NC-Alg-GO scaffolds were properly printed by setting the same printing parameters and needle diameter as NC-Alg scaffolds. These printing differences were due to the HAP particles that blocked the narrowest needle. In fact, HAP particle size was around 200-300 μm, while GO average flake size was from

nm up to 10 µm. After printing, scaffold general and in-depth images were acquired (Fig. 5). Results showed an acceptable printability with NC-Alg-HAP and NC-Alg-GO inks compared to the computerized design (Fig. 5A). Furthermore, a slight improvement could be observed in the scaffolds that contained inorganic components compared to the control, probably due to the enhancement in mechanical properties of these materials [17,42], thus, making them more stable than NC-Alg inks. Upon closer examination, no differences were observed among the scaffolds. All of them presented an oblong grid structure with a similar grid area measurement (NC-Alg-HAP 0.41 ± 0.05 mm^2, NC-Alg-GO 0.38 ± 0.10 mm^2 and NC-Alg 0.42 ± 0.03 mm^2).

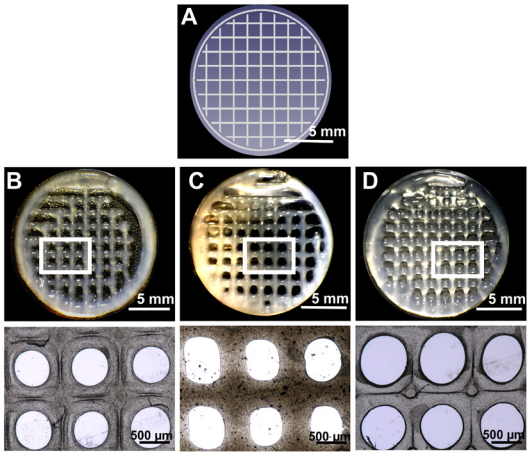

Figure 5. Printability assay. Macroscopic pictures of printed scaffolds A) Computerised design of the scaffolds. B) NC-Alg C) NC-Alg-HAP, and D) NC-Alg-GO. Scale bar 5 mm and 500 µm.

3.5 Scaffold structure characterization

The architecture and surface of printed NC-Alg-HAP and NC-Alg-GO scaffolds were characterized using SEM and optical profilometer techniques. As shown in Fig. 6 scaffolds structure was different depending on the addition of HAP and GO. In fact, the scaffolds containing HAP presented a flatter architecture in the SEM images compared to those containing GO, which sowed more concavity (Fig. 6A). These results were confirmed by optical profilometry pictures where the HAP scaffolds showed a height of around 200-300 µm at intersections, while those containing GO showed a greater height (400-500

μm). When a comparison was made with the NC-Alg scaffolds, it was shown that the differences in the scaffold architecture were due to the HAP, since the GO scaffolds showed a similar architecture to the controls. The characterization was carried out after the crosslinking procedure with $CaCl_2$ aqueous solution. Therefore, it could be theorized that the hydrophilicity of the polymers together with the properties of GO to capture water molecules [43], made both, NC-Alg-GO and NC-Alg scaffolds, more swollen than the NC-Alg-HAP scaffolds. On the contrary, HAP particles inside the scaffold matrix could cause hydrophilicity lost. Thus, achieving to flatten the scaffolds. These results were verified later in the swelling study.

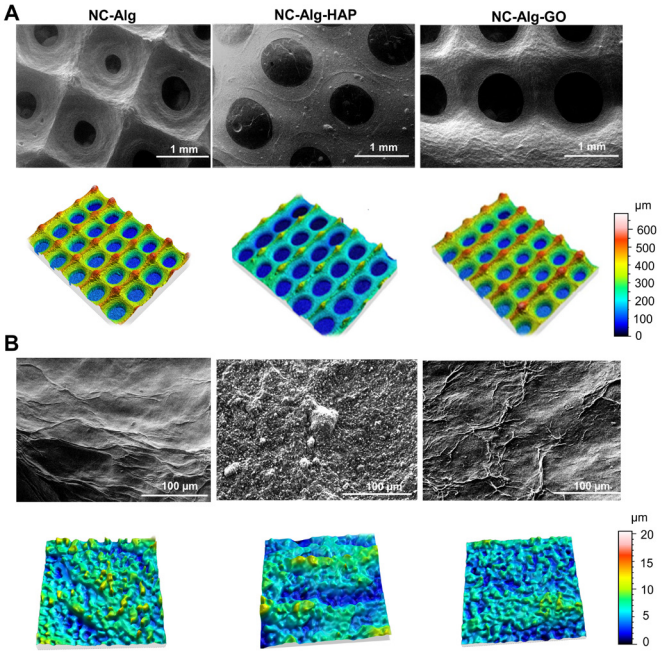

Figure 6. Printed scaffold characterization. Representative SEM images of NC-Alg, NC-Alg-HAP and NC-Alg-GO scaffolds. Optical profilometer images of the scaffolds 3D topographical measurements. A) Architecture characterization. B) Surface evaluation. Scale bat 1 mm and 100 μm.

On the other hand, the surface of the scaffolds was characterized in order to evaluate their roughness. Scaffolds roughness is an important parameter since it has been described that scaffolds with rougher surfaces tend to

enhance MSCs adhesion and osteogenic differentiation in comparison with smooth scaffolds [44]. Furthermore, rough implants have been demonstrated to be more successful than smoothest ones [45]. Consequently, several studies covered different implant types such as titanium ones to enhance successful implantation *in vivo* as well as in the clinics. According to optical profilometer images in Fig. 6B, all the scaffolds showed a similar surface roughness between 0 and 10 μm. However, when SEM pictures were observed, different surface roughness was shown. In fact, the HAP containing scaffolds demonstrated a granulose surface due to HAP particles.

In contrast, GO scaffolds had a fibrous surface appearance that was similar to NC-Alg scaffolds. This fibrous roughness could be due to NC fibers in the scaffold. These results were in concordance with other research works in which the addition of HAP to the scaffolds proved to increase their roughness and, therefore, cell viability and osteogenic differentiation [46]. Regarding the GO, another work reported similar results in terms of no roughness increase after GO addition in titanium scaffolds [47]. Nevertheless, all the scaffolds showed a rough surface, which would indicate good cell adhesion, the promotion of cell osteogenic differentiation and excellent implantability in bone tissue.

3.6 Swelling and degradation study

A swelling (S) study was carried out in order to analyse the water uptake capacity of all the printed constructs. Swelling capacity is related to scaffold permeability and, therefore, to the transport of nutrients and gases into the scaffold [48]. In this study, as Fig. 7A shows, in all the scaffolds the percentage of swelling increased until the equilibrium was reached within 24 h. In addition, all the scaffolds showed high water uptake capacity, which suggests good permeability and cell nourishment. It has been previously described that inks composed of Alg or NC have high water uptake capacity due to the hydrophilic characteristics of the polymers [49]. Importantly, differences among scaffolds were observed when inorganic components such as HAP and GO were added. S% was statistically lower in NC-Alg-HAP scaffolds in comparison with NC-Alg-GO and control scaffolds in the majority of time points. It was ex-

pected that by adding HAP the water uptake capacity would be reduced since HAP particles did not leave space for water particles. It has also been reported that the swelling capacity decreased while HAP concentrations increased in scaffolds [42].

In contrast, NC-Alg-GO scaffolds demonstrated the same swelling properties as NC-Alg scaffolds, which indicated that the inclusion of GO particles did not displace water molecules. In fact, it has been widely described the capacity of graphene molecules to create strong hydrogen bonds with water molecules [43] and, therefore, the GO-containing scaffolds swelling properties are high. These swelling properties have been also showed in another study in which increasing GO concentrations resulted in higher water absorption [50]. Despite the fact of swelling reduction due to HAP, all scaffolds showed high swelling properties (> 90%) which suggested excellent nutrient transport into the scaffold.

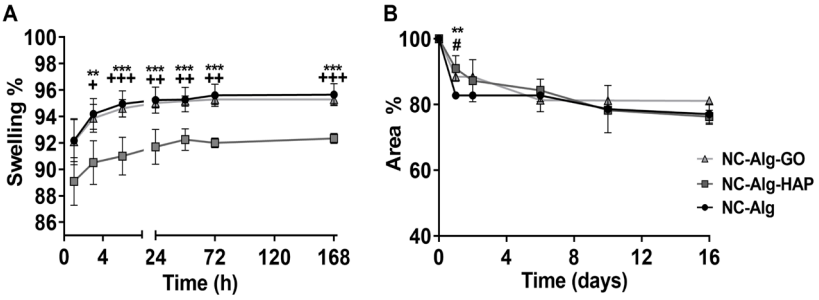

Figure 7. Characterization of NC-Alg-HAP, NC-Alg-GO and NC-Alg scaffolds A) Swelling assay B) Degradation study. Values represent mean ± SD. *** $p < 0.001$; **$p < 0.01$ comparison between NC-Alg-HAP and NC-Alg. +++ $p < 0.001$; ++ $p < 0.01$; + $p < 0.05$ comparison between NC-Alg-HAP and NC-Alg-GO. # $p < 0.05$ comparison between NC-Alg-GO and NC-Alg scaffolds.

For regenerative medicine applications, scaffold degradation kinetics should be taken into account to determine its applicability. When it comes to bone, the implanted scaffolds must be stable with a controlled degradation rate to enable bone regeneration. In this regard, a degradation assay of NC-Alg-HAP and NC-Alg-GO scaffolds was performed for 16 days (Fig. 7B). Both scaffolds showed similar degradation kinetics being the main area loss in the first days of the assay. Importantly, scaffolds containing HAP or GO demonstrated less

area loss in comparison with NC-Alg scaffolds at the beginning of the study. In fact, this resistance to the degradation process was statistically significant in HAP scaffolds ($p < 0.01$) and in GO scaffolds ($p < 0.05$) within 24 h of the assay. At the end of the assay, all the scaffolds showed a similar area loss that was around 20%. The degradation study indicated a controlled degradation behaviour of NC-Alg-HAP and NC-Alg-GO scaffolds, suggesting good stability of the scaffolds, which is essential for the early stages of bone regeneration [51]. Furthermore, the degradation kinetics may be modified depending on medical applications. It has been reported that varying molecular weight of the alginate as well as by chemical modifications such as phosphorylation could accelerate or reduce scaffold degradation kinetics [52]. Likewise, the degradation rate could be influenced by reducing the particles size and increasing the porosity of the HAP or by the chemical modification of the GO [17,53].

3.7 Mechanical properties evaluation

Mechanics in bone are fundamental for proper tissue functionality such as movement support and organ protection [3]. Consequently, scaffolds and grafts to be implanted require adequate mechanical properties. For this reason, compression Young´s modulus was acquired since it is a material parameter that represents the material´s resistance or stiffness to deformation under load. As it is shown in Fig 8, Young´s modulus parameter increased significantly ($p < 0.001$) when HAP and GO were added to the Nc-Alg ink. Interestingly, GO containing scaffolds demonstrated higher mechanical properties than HAP scaffolds ($p < 0.001$). It has been widely described that both inorganic elements enhanced scaffold mechanical properties [14,17]. HAP has been used to fabricate orthopedic implants since it has been demonstrated to be a mechanically competent material with similar physical properties to native bone tissue. In addition, by increasing HAP concentrations, scaffold mechanical properties may be improved as it has been proven in gelatin-based hydrogels [42]. Similarly, GO has been reported to have superior mechanical properties. As a result, it has been applied to reinforce materials for diverse purposes such as electronics and mechanics [16]. In the tissue engineering

field, GO has been utilized to improve scaffolds' mechanical properties because of the reinforcing effect of GO in the polymer matrix [54]. Despite the fact that both materials increased scaffold mechanical properties, were far from bone mechanical properties (10-20 GPa) [55]. Bone is a stiff tissue and it is difficult to obtain similar mechanics with scaffolds based on soft hydrogels.

According to the literature, similar mechanics to those of bone could be obtained by using metals such as titanium, bioglasses or synthetic polymers such as polycaprolactone (PCL) [56]. In this regard, either ceramic scaffold based only on HAP or high GO concentration composites have shown to be mechanically similar to bone, therefore, increasing HAP and GO concentrations on the ink would improve mechanical properties. However, biocompatibility and printability would be compromised.

Taking into account these results, NC-Alg-HAP and NC-Alg-GO scaffolds could be used in local injuries to support the regeneration of damaged bone or to partial bone ruptures.

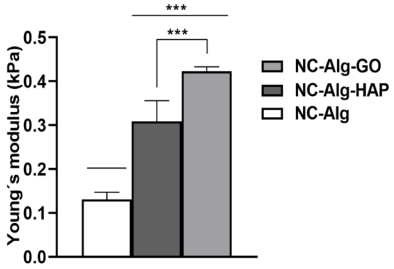

Figure 8. Young's modulus measurements of printed NC-Alg-HAP, NC-Alg-GO, and NC-Alg scaffolds. Values represent mean ± SD. ***p < 0.001.

3.8 Cell viability and functionality study

Good cell survival and functionality inside the scaffold will ensure clinical applicability for bone regeneration purposes. For this reason, D1-MSCs-EPO were added to the NC-Alg-HAP and NC-Alg-GO inks, and their biological response in terms of cell metabolism, viability and EPO release was evaluated within 21 days of bioprinting. Cell density was established at 5 x 10^6 cells/mL in order to avoid problems when evaluating cells *in vitro*, since cells death

due to extrusion pressures of the bioprinter together with low cell densities within the bioink proved to be unsatisfactory for obtaining clear results in a previous study [24]. Cell metabolic activity was measured weekly for 21 days (Fig. 9A). Results showed that the metabolism of cells embedded in all the scaffolds increased over time. Importantly, scaffolds containing HAP and GO demonstrated higher cell metabolic activity along the study compared to NC-Alg scaffolds. Furthermore, the improvement in cell metabolic activity was significant in NC-Alg-HAP scaffolds on days 1, 7 ($p < 0.001$) and 14 ($p < 0.05$) after bioprinting in comparison with control scaffolds. Likewise, cells embedded in GO containing scaffolds showed a significantly higher ($p < 0.001$) metabolic activity at the first time points of the assay when it was compared to NC-Alg scaffolds. These results suggested cell proliferation within the scaffolds after bioprinting. Furthermore, the addition of HAP and GO into the NC-Alg based bioink improved the metabolic activity of embedded cells, suggesting that cells were more viable and functional than those inside control bioinks.

These results were in concordance with other studies in which the HAP inside polymeric scaffolds enhanced cell migration and viability [12]. Similarly, it has been reported that the metabolic activity of stem cells was higher in the presence of GO [57]. On the other hand, HAP and GO containing sterile bioinks showed an improvement in the rheological properties that, together with the increase in the mechanical properties, suggested greater protection of the cells against the damage caused by the bioprinting process.

D1-MSCs-EPO viability was evaluated by Live/Dead™ assay in Fig. 9B. Obtained images showed no visual differences among the scaffolds at day 1 after bioprinting. Cells inside the scaffolds were mostly alive (in green) and were well distributed throughout the scaffolds. In contrast, at day 21 after bioprinting, differences were observed between cells inside NC-Alg-HAP and NC-Alg-GO scaffolds. In fact, cells in HAP containing scaffolds tended to form aggregates while in GO scaffolds cell aggregates were not found. Cell aggregates were also visualized in the NC-Alg scaffolds. It has been reported in the literature that cell aggregates promoted osteogenic differentiation of MSCs [58]. The absence of cell aggregation inside NC-Alg-GO scaffolds could be explained with the increase in scaffold mechanics, which make the GO

containing bioink stiffer than the others. Additionally, oxide derivatives of graphene have found to reduce aggregation due to its high hydrophilic nature [59]. Importantly, higher green fluorescent intensity was obtained in scaffolds containing HAP and GO in comparison with NC-Alg scaffolds, indicating higher cell viability inside scaffolds containing inorganic components. In addition, it was expected to be higher cell viability in HAP and GO scaffolds in accordance with cell metabolic activity results.

Finally, D1-MSCs-EPO were used to determine cell functionality inside bioprinted scaffolds. The quantification of this hormone was selected as it has been previously probed that it can be easily measured from cells encapsulated in Alg hydrogels [60]. As shown in Fig. 9C, EPO release increased over time in all the scaffolds indicating good cell functionality after bioprinting. When a comparison was made, NC-Alg-HAP scaffolds showed higher amounts of EPO release in comparison with NC-Alg-GO and control scaffolds. Furthermore, the hormone was quantified from the first day of the assay in HAP scaffolds while in GO scaffolds EPO release was not observed until day 14 after bioprinting. Importantly, this increase in EPO release on HAP containing scaffolds was statistically significant at day 14 ($p < 0.001$). Moreover, NC-Alg scaffolds showed also a significantly higher EPO release at day 14 than NC-Alg-GO scaffolds. At the end of the study, NC-Alg-HAP scaffolds demonstrated higher amounts of EPO release than GO and control scaffolds ($p < 0.001$) (NC-Alg-HAP 1483.90 ± 128. 46 mLUI/mL, NC-Alg-GO 337.93 ± 63.10 mLUI/mL and NC-Alg 925.21 ± 327. 99 mLUI/mL).

It can be suggested that the enhancement in EPO release in HAP scaffolds was due to the increase in its production as cell viability and cell metabolism were higher than in NC-Alg scaffolds. Furthermore, HAP has already been used as a carrier of EPO for drug delivery purposes [61]. Similar EPO production and release could be expected in cells inside GO containing scaffolds since better cell viability and metabolism were also seen than in the control scaffolds. However, GO has been described to interact with diverse molecules including proteins, therefore, it could be suspected that EPO hormone was adhered to GO, which prevented its release to the medium. This EPO adhesion has also been described in Alg-GO microcapsules [31]. In order to avoid hor-

mone attachment to GO, the same authors proposed to cover GO with FBS or bovine serum albumin (BSA) [62]. Thus, it can be assumed that EPO release may have been under quantified.

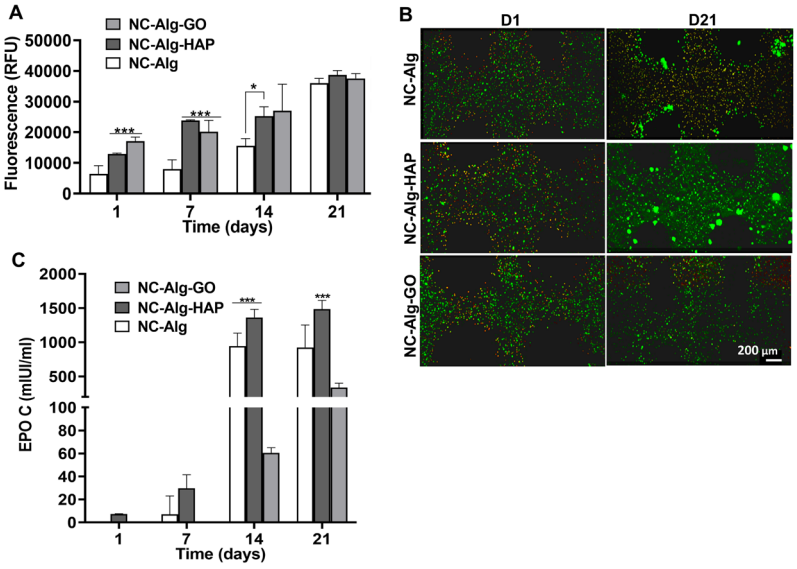

Figure 9. D1-MSCs-EPO viability and functionality assays inside NC-Alg-HAP, NC-Alg-GO, and NC-Alg scaffolds. A) Cell metabolic activity evaluation. B) Representative fluorescence pictures scaffolds at days 1 and 21 of bioprinting after live/dead staining, showing live (green) and dead (red) cells. Scale bar 200 µm. C) EPO release assay. Values represent mean ± SD. *** $p < 0.001$; ** $p < 0.01$; * $p < 0.05$.

In conclusion, biological results showed that D1-MSCs-EPO cells inside HAP and GO containing scaffolds were viable, active and functional, indicating excellent biocompatibility of inorganic elements with cells. However, to determine the feasibility of these scaffolds to regenerate bone tissue, osteogenic differentiation studies were also carried out.

3.9 Osteogenic differentiation

D1-MSCs were used to evaluate their osteogenic differentiation inside NC-Alg-HAP and NC-Alg-GO scaffolds. It has been previously described the ability of MSCs to differentiate in different cell lines such as chondrocytes, myocytes, adipocytes and osteoblasts [63]. Therefore, they have been widely applied for

tissue engineering and regenerative medicine purposes. Likewise, D1-MSCs have been used to differentiate to osteoblasts inside Alg based hydrogels in a previous research work [64].

First, bioprinted scaffolds were stained with Alizarin Red after being 21 days in the differentiation medium. Alizarin Red stains in red the calcium deposits which is a characteristic of the mineralized osteogenic matrix. As shown in Fig 10A, all the scaffolds were stained after 21 days of culture suggesting osteogenic differentiation. On the contrary, cells inside scaffolds that were in non-differentiated media did not produce mineralization, as the Alizarin Red staining was removed. Despite the fact that GO containing scaffolds that were treated with non-differentiated media showed higher rests of the staining, it was concluded that this was due to the ability of GO to adhere to diverse molecules. The staining results were inconclusive in terms of evaluating whether the addition of HAP and GO had a positive effect on promoting osteogenic differentiation since NC-Alg scaffolds were also stained.

Consequently, the activity of the alkaline phosphatase (ALP) enzyme was quantified. ALP enzyme is an osteogenic marker that is produced by osteoblasts. Therefore, the presence of ALP would indicate osteogenic differentiation. Results, showed in Fig. 10B, an increase in ALP activity along the days in all the scaffolds. In addition, the enzyme activity increase was significant in HAP scaffolds ($p < 0.001$) and in GO scaffolds ($p < 0.05$). Importantly, at day 21 of the assay, cells inside NC-Alg-HAP cells demonstrated a significantly ($p < 0.05$) higher ALP production than NC-Alg-GO and NC-Alg scaffolds (0.66 ± 0.08 nMol in NC-Alg-HAP, 0.32 ± 0.10 nMol in NC-Alg-GO and 0.31 ± 0.05 nMol in NC-Alg). These results suggested the promotion of the differentiation capacity of D1-MSCs to osteoblasts due to HAP, which was previously described in the literature. It has been proved that HAP as a porous and rough material can stimulate osteogenic differentiation and osteoblast maturation [65]. As a result, the same ALP increment was observed in Alg-HAP scaffolds [28] and in NC-HAP scaffolds [66]. Regarding GO, results indicated an ALP enzyme production over time suggesting osteogenic differentiation. However, the results were similar to NC-Alg scaffolds indicating no influence on the differentiation

capacity of D1-MSCs. This went against what the literature describes since osteoinductive properties have been attributed to the GO molecule. In fact, in other research works, ALP activity increased when GO was added into the bioink [18,67]. ALP upregulates early bone formation by promoting its mineralization. Low ALP levels on NC-Alg-GO ink may suggest the completion of the early calcification period and the beginning of the late maturation process of cells [67]. Furthermore, it is also known the ability of GO to adhere to diverse molecules including enzymes. Consequently, an exhaustive study on differentiation such as gene expression quantification was to perform.

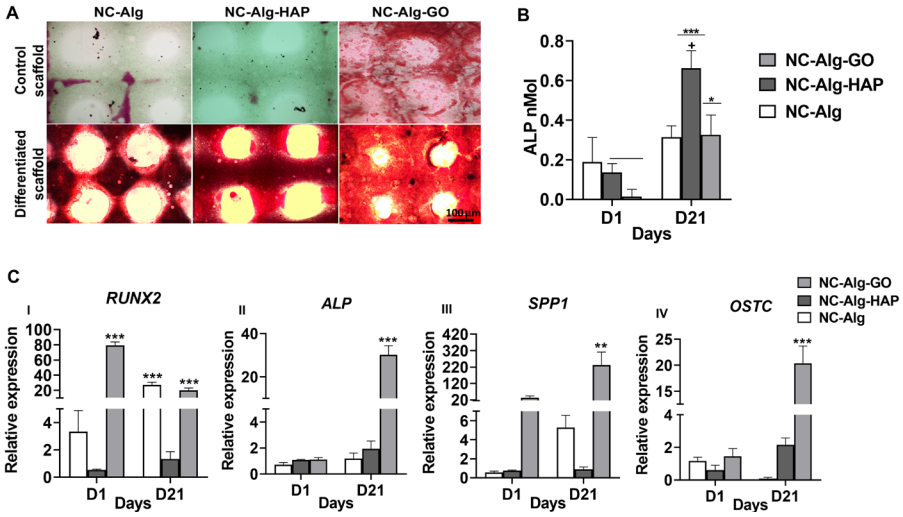

Figure 10. Osteogenic differentiation study of embedded D1-MSC. A) Alizarin red staining of NC-Alg, NC-Alg-HAP, and NC-Alg-GO scaffolds. Scale bar 100 µm B) Alkaline phosphatase (ALP) enzyme quantification assay at days 1 and 21 of bioprinting. C) Osteogenic gene expression of cells. RT-PCR was performed after 1 and 21 days. Values represent mean ± SD. *** $p < 0.001$; ** $p < 0.01$; * $p < 0.05$.

Finally, RT-PCR was conducted to evaluate the relative gene expression of cells inside NC-Alg-HAP and NC-Alg-GO scaffolds. Osteogenic gene markers such as *RUNX2*, *ALP*, *OSTC* and *SPP1* were analysed in Fig. 10C.

RUNX2 is an essential transcription factor that plays a key role in the formation of osteoblasts [68]. As shown in Fig. 10CI the expression of *RUNX2* was greater ($p < 0.001$) in scaffolds containing GO at day 1 in comparison

with HAP scaffolds and control. Likewise, gene expression in GO scaffolds was significantly elevated ($p < 0.001$) at day 21 when compared to HAP sample. However, it was significantly lower than in control scaffolds ($p < 0.001$).

ALP gene is associated with osteogenic differentiation and encodes the ALP enzyme (previously analysed in this study) [69]. Results in Fig. 10CII showed an increase in *ALP* expression over time in all the scaffolds. Importantly, gene expression was increased ($p < 0.001$) in GO scaffolds compared to the NC-Alg-HAP and NC-Alg scaffolds. Surprisingly, *ALP* gene expression did not agree with the results obtained from the quantification of the enzyme in which HAP scaffolds showed the greatest enzyme activity. Reviewing the literature, HAP containing hydrogels or scaffolds showed to obtain similar *ALP* gene expression and enzyme activity values to this study[18,51,65]. Likewise, other studies have demonstrated that GO promoted *ALP* gene expression which is in accordance with the results of this study [18,67]. Therefore, it can be suggested that the quantification of ALP enzymatic activity in GO scaffolds may have been lower than it had to be. The enzyme underquantification may be due to the capacity of GO to adhere to various molecules [70]. In fact, GO has been previously used to immobilise enzymes [71].

SPP1 gene regulates the production of osteopontin, which is a protein of the bone extracellular matrix [72]. Fig. 10CIII shows that GO enhanced cells expression of the *SPP1* gene at days 1 and 21, being the gene expression at day 21 significantly higher ($p < 0.01$) than the gene expression in NC-Alg-HAP and control scaffolds. Furthermore, HAP scaffolds demonstrated less gene expression than control at the end of the assay, even though this difference was not statistically relevant. *SPP1* gene is regulated by *RUNX2* gene [73], which could explain the low expression in HAP scaffolds.

Finally, *OSTC* gene expression was assayed since it is related to mature bone [72]. Results (Fig. 10CIV) showed an increase in gene expression in both, HAP and GO scaffolds over time, meanwhile gene expression was barely observed in NC-Alg scaffolds at day 21. Thus, it can be concluded bone differentiation within HAP and GO scaffolds. Interestingly, the addition of GO to the scaffold increased ($p < 0.001$) *OSTC* gene expression in comparison with HAP scaffolds.

Taking into account the differentiation study, it can be concluded that the D1-MSCs differentiated into bone cells within the NC-Alg and NC-Alg-HAP scaffolds. Furthermore, this differentiation was futher promoted by adding GO to the bioink, which has been already widely described in the literature. When a comparison was made, it should be noted that osteogenic expression was considerably increased by GO, indicating greater bone differentiation of D1-MSCs than those in HAP scaffolds. This difference between HAP and GO may be occurred because of the adhesion of GO to the osteoinductive molecules such as those used in the differentiation medium [73]. Thus, making GO scaffolds more osteoinductive than HAP ones.

4. Conclusions

Inorganic components have shown to be a good option to create scaffolds for bone tissue engineering. Thus, HAP and GO have been added to NC-Alg based inks in order to evaluate whether they affect ink properties, scaffold characteristics and embedded D1-MSCs biologic behaviour. No rheological differences were observed after the inclusion of HAP and GO in the ink. However, the sterilisation study revealed a rheological properties maintenance after short cycle autoclave sterilisation. Importantly, NC-Alg-GO ink demonstrated an incompatibility with autoclave sterilisation due to a GO reduction, therefore, another sterilisation method such as UV had to be carried out. Scaffold characterization study showed differences between HAP and GO scaffolds in terms of architecture and swelling properties. In fact, GO scaffolds presented higher swelling capacity and therefore, a greater height and concave structure. On the other hand, both, the addition of HAP and GO increased the scaffold stability and mechanical properties, being the GO the one that showed the greatest improvement in scaffold mechanics.

Finally, biological studies showed good biocompatibility of D1-MSC with HAP and GO since high cell metabolic activity values as well as high cell viability were observed in those scaffolds. NC-Alg-HAP scaffolds demonstrated cell differentiation to bone, but the addition of GO to the scaffolds promoted a higher expression of osteogenic markers in D1-MSC, suggesting that GO has

greater osteoinductive properties than HAP. According to this study, NC-Alg-HAP and NC-Alg-GO scaffolds would be a feasible therapeutic option for bone tissue engineering, being those that contain GO the best option.

Acknowledgements
This work was financially supported by the Basque Country Government (IT907-16) and the University of the Basque Country UPV/EHU. The authors thank the Basque Government for the granted fellowship to Sandra Ruiz-Alonso (PRE_2021_2_0153). Likewise, the authors thank ICTS "NANBIOSIS", in particular by the Drug Formulation Unit (U10) of the CIBER in Bioengineering, Biomaterials and Nanomedicine (CIBER-BBN) at the University of the Basque Country (UPV/EHU) in Vitoria-Gasteiz.

Conflict of Interest
The authors declare no conflict of interest.

Data Availability Statement
Research data are not shared.

References

[1] P. Bhattacharjee, B. Kundu, D. Naskar,H.-W. Kim, T. K. Maiti, D. Bhattacharya, S. C. Kundu, Acta Biomater. 2017, 63, 1.

[2] G. Tozzi, A. De Mori, A. Oliveira, M. Roldo, Materials 2016, 9, 267.

[3] H. D. Kim, S. Amirthalingam, S. L. Kim, S. S. Lee, J. Rangasamy, N. S. Hwang, Adv Healthcare Mater. 2017, 6, 23.

[4] C. Wang,W.Huang, Y. Zhou, L. He, Z.He, Z. Chen, X.He, S. Tian, J. Liao, B. Lu, Y. Wei, M. Wang, Bioact. Mater. 2020, 5, 82.

[5] J. Filipowska, K. A. Tomaszewski, L. Nied´zwiedzki, J. A. Walocha, T. Nied´zwiedzki, Angiogenesis 2017, 20, 291.

[6] L. Roseti, V. Parisi, M. Petretta, C. Cavallo, G. Desando, I. Bartolotti, B. Grigolo, Mater. Sci. Eng., C 2017, 78, 1246.

[7] X. Bai, M. Gao, S. Syed, J. Zhuang, X. Xu, X.-Q. Zhang, Bioact. Mater. 2018, 3, 401.

[8] J. C. Boga, S. P. Miguel, D. De Melo-Diogo, A. G. Mendonça, R. O. Louro, I.D. J. Correia, Colloids Surf., B 2018, 165, 207.

[9] W. Zhu, X. Ma, M. Gou,D.Mei, K. Zhang, S. Chen, Curr.Opin. Biotechnol. 2016, 40, 103.

[10] P. S. Gungor-Ozkerim, I. Inci, Y. S. Zhang, A. Khademhosseini, M. R. Dokmeci, Biomater. Sci. 2018, 6, 915.

[11] K. Hölzl, S. Lin, L. Tytgat, S. Van Vlierberghe, L. Gu, A. Ovsianikov, Biofabrication 2016, 8, 032002.

[12] N. Ramesh, S. C. Moratti, G. J. Dias, J. Biomed. Mater. Res., Part B 2018, 106, 2046.

[13] Q. Fu, M. N. Rahaman, F. Dogan, B. S. Bal, J. Biomed. Mater. Res., Part B 2008, 86B, 125.

[14] A. Das, D. Pamu, Mater. Sci. Eng., C 2019, 101, 539.

[15] S. T. Bendtsen, S. P. Quinnell, M. Wei, J. Biomed. Mater. Res. 2017, 105, 1457.

[16] A. Raslan, L. Saenz Del Burgo, J. Ciriza, J. L. Pedraz, Int. J. Pharm. 2020, 580, 119226.

[17] B. D. Holt, Z. M. Wright, A. M. Arnold, S. A. Sydlik, Wiley Interdiscip. Rev.: Nanomed. Nanobiotechnol. 2017, 9, 3.

[18] J. Zhang, H. Eyisoylu, X.-H. Qin, M. Rubert, R. Müller, Acta Biomater. 2021, 121, 637.

[19] M. Müller, E. Öztürk, Ø. Arlov, P. Gatenholm, M. Zenobi-Wong, Ann. Biomed. Eng. 2017, 45, 210.

[20] E. Axpe, M. L. Oyen, Int. J. Mol. Sci. 2016, 17, 1976.

[21] F. Yu, X. Han, K. Zhang, B. Dai, S. Shen, X. Gao, H. Teng, X. Wang, L. Li, H. Ju, W. Wang, J. Zhang, Q. Jiang, J. Biomed. Mater. Res., Part A 2018, 106, 2944.

[22] D. Nguyen, D. A. Hägg, A. Forsman, J. Ekholm, P. Nimkingratana, C. Brantsing, T. Kalogeropoulos, S. Zaunz, S. Concaro, M. Brittberg, A. Lindahl, P. Gatenholm, A. Enejder, S. Simonsson, Sci. Rep. 2017, 7, 658.

[23] ISO 10993-5:2009 Biological Evaluation of Medical Devices. Part 5: Tests for In Vitro Cytotoxicity. International Organization for Standardization, Geneva, Switzerland 2009.

[24] M. Lafuente-Merchan, S. Ruiz-Alonso, A. Espona-Noguera, P. Galvez-Martin, E. López-Ruiz, J. A. Marchal, M. L. López-Donaire, A. Zabala, J. Ciriza, L. Saenz-Del-Burgo, J. L. Pedraz, Mater. Sci. Eng., C 2021, 126, 112160.

[25] H. Gurruchaga, J. Ciriza, L. Saenz Del Burgo, J. R. Rodriguez-Madoz, E. Santos, F. Prosper, R. M. Hernández, G. Orive, J. L. Pedraz, Int. J. Pharm. 2015, 485, 15.

[26] Y. Li, L. Yang, Y. Hou, Z. Zhang, M. Chen, M. Wang, J. Liu, J. Wang, Z. Zhao, C. Xie, X. Lu, Bioact. Mater. 2022, 18, 213.

[27] M. C. Echave, I. Erezuma, N. Golafshan,M. Castilho, F. B. Kadumudi, C. Pimenta-Lopes, F. Ventura, A. Pujol, J. J. Jimenez, J. A. Camara, R. Hernáez-Moya, L. Iturriaga, L. Sáenz Del Burgo, I. Iloro, M. Azkargorta, F. Elortza, R. Lakshminarayanan, T. H. Al-Tel, P. García-García, R. Reyes, A. Delgado, C. Évora, J. L. Pedraz, A. Dolatshahi-Pirouz, G. Orive, Mater. Sci. Eng., C 2021, 134, 112539.

[28] F. You, X. Chen, D. M. L. Cooper, T. Chang, B. F. Eames, Biofabrication 2018, 11, 015015.

[29] A. Raslan, J. Ciriza, A. M. Ochoa de Retana, M. L. Sanjuán, M. S. Toprak, P. Galvez-Martin, L. Saenz-Del-Burgo, J. L. Pedraz, Pharmaceutics 2021, 13, 1473.

[30] A. Raslan, L. Saenz Del Burgo, A. Espona-Noguera, A. M. Ochoa de Retana, M. L. Sanjuán, A. Cañibano-Hernández, P. Galvez-Martin, J. Ciriza, J. L. Pedraz, Pharmaceutics 2020, 12, 543.

[31] J. Ciriza, L. Saenz Del Burgo, M. Virumbrales-Muñoz, I. Ochoa, L. J. Fernandez, G. Orive, R. M. Hernandez, J. L. Pedraz, Int. J. Pharm. 2015, 493, 260.

[32] M. Maas, U. Hess, K. Rezwan, Curr. Opin. Biotechnol. 2014, 19, 585.

[33] T. Gao, G. J. Gillispie, J. S. Copus, A. K. Pr, Y.-J. Seol, A. Atala, J. J. Yoo, S. J. Lee, Biofabrication 2018, 10, 034106.

[34] K. Tõnsuaadu, K. A. Gross, L. Plûduma, M. Veiderma, J. Therm. Anal. Calorim. 2011, 110, 647.

[35] J. A. Sánchez-Fernández, G. Presbítero-Espinosa, L. Peña-Parás, E. I. R. Pizaña, K. P. V. Galván, M. Vopálenský,M. Vopálenský, I. Kumpová, L. E. Elizalde-Herrera, Polymers 2021, 13, 2927.

[36] B. G. Compton, N. S. Hmeidat, R. C. Pack,M. F. Heres, J. R. Sangoro, JOM 2017, 70, 292.

[37] J. Zhang, H.-Y. Cao, J.-Q. Wang, G.-D. Wu, L. Wang, Front. Cell Dev. Biol. 2021, 9, 616888.

[38] S. Mittal, V. Kumar, N. Dhiman, L. K. S. Chauhan, R. Pasricha, A. K. Pandey, Sci. Rep. 2016, 6, 39548.

[39] J. Ghitman, E. I. Biru, E. Cojocaru, G. G. Pircalabioru, E. Vasile, H. Iovu, RSC Adv. 2021, 11, 13653.

[40] I. Lasocka, L. Szulc-Dabrowska, M. Skibniewski, E. Skibniewska, W. Strupinski, I. Pasternak, H. Kmie`c, P. Kowalczyk, Toxicol. In Vitro 2018, 48, 276.

[41] M. Lafuente-merchan, S. Ruiz-alonso, A. Zabala, P. Gálvez-martín, J. A. Marchal, B. Vázquez-lasa, I. Garrido, L. Saenz-del-Burgo, J. L. Pedraz, Macromol. Biosci. 2022, 22, 2100435.

[42] S. Suvarnapathaki, X.Wu, D. Lantigua, M. A. Nguyen, G. Camci-unal, Macromol. Biosci. 2020, 20, 2000176.

[43] B. Lian, S. De Luca, Y. You, S. Alwarappan, M. Yoshimura, V. Sahajwalla, S. C. Smith, G. Leslie, R. K. Joshi, Chem. Sci. 2018, 9, 5106.

[44] X. Cun, L. Hosta-Rigau, Nanomaterials 2020, 10, 2070.

[45] A.Dank, I. H. A. Aartman, D. Wismeijer, A. Tahmaseb, Int. J. Implant Dent. 2019, 5, 12.

[46] W. Yang, W. Han, W. He, J. Li, J. Wang, H. Feng, Y. Qian, Mater. Sci. Eng., C 2016, 60, 45.

[47] W. Dong, L. Hou, T. Li, Z. Gong, H. Huang, G. Wang, X. Chen, X. Li, Sci. Rep. 2015, 5, 18266.

[48] H. Park, X. Guo, J. S. Temenoff, Y. Tabata, A. I. Caplan, F. K. Kasper, A. G. Mikos, Biomacromolecules 2009, 10, 541.

[49] M. Mahinroosta, Z. Jomeh Farsangi, A. Allahverdi, Z. Shakoori, Mater. Today Chem. 2018, 8, 42.

[50] J. Zhang, H. Eyisoylu, X.-H. Qin, M. Rubert, R. Müller, Acta Biomater. 2021, 121, 637.

[51] F. Xing, Z. Chi, R. Yang, D. Xu, J. Cui, Y. Huang, C. Zhou, C. Liu, Int. J. Biol. Macromol. 2021, 184, 170.

[52] E. Alsberg, H. J. Kong, Y. Hirano, M. K. Smith, A. Albeiruti, D. J. Mooney, J. Dent. Res.. 2003, 82, 903.

[53] J. G. Dellinger, A. M. Wojtowicz, R. D. Jamison, J Biomed Mater Res A 2006, 77A, 563.

[54] S. D. Purohit, R. Bhaskar, H. Singh, I. Yadav, M. K. Gupta, N. C. Mishra, Int. J. Biol. Macromol. 2019, 133, 592.

[55] C. F. Guimarães, L. Gasperini, A. P. Marques, R. L. Reis, Nat. Rev. Mater. 2020, 5, 351.

[56] S. K. Nandi, A. Mahato, B. Kundu, P. Mukherjee, Mater. Biomed. Eng. 2019, 2, 21.

[57] A. Di Crescenzo, S. Zara, C. Di Nisio, V. Ettorre, A. Ventrella, B. Zavan, P. Di Profio, A. Cataldi, A. Fontana, ACS Appl. Bio Mater. 2019, 2, 1643.

[58] A. Chatterjea, V. Lapointe, A. Barradas, H. Garritsen, H. Yuan, A. Renard, C. A. Van Blitterswijk, J. De Boer, Eur. Cells Mater. 2017, 33, 121.

[59] P. Bellet, M. Gasparotto, S. Pressi, A. Fortunato, G. Scapin, M. Mba, E. Menna, F. Filippini, Nanomaterials 2021, 11, 404.

[60] A. Cañibano-Hernández, L. Saenz del Burgo, A. Espona-Noguera, G. Orive, R. M. Hernández, J. Ciriza, J. L. Pedraz, Mol. Pharmaceutics 2017, 14, 2390.

[61] K.-I. Nagasaki, T. Ikoma, S.-I. Katsuda, T. Tonegawa, J. Tanaka, T. Nakamura, H. Sato, S. Ito, N. Sasaki, T. Agui, Vet. Med. Sci. 2009, 71, 729.

[62] L. Saenz Del Burgo, J. Ciriza, A. Acarregui, H. Gurruchaga, F. J. Blanco, G. Orive, R. M. Hernández, J. L. Pedraz, Mol. Pharmaceutics 2017, 14, 885.

[63] O. Juffroy, D. Noël, A. Delanoye, O. Viltart, I. Wolowczuk, C. Verwaerde, Differentiation 2009, 78, 223.

[64] S. Nam, R. Stowers, J. Lou, Y. Xia, O. Chaudhuri, Biomaterials 2019, 200, 15.

[65] J. Fang, P. Li, X. Lu, L. Fang, X. Lü, F. Ren, Acta Biomater. 2019, 88, 503.

[66] F. Liu, B. Wei, X. Xu, B. Ma, S. Zhang, J. Duan, Y. Kong, H. Yang, Y. Sang, S. Wang, W. Tang, C. Liu, H. Liu, Adv. Healthcare Mater. 2020, 10, 2001851.

[67] Y. Jiang, D. Zhou, B. Yang, J. Biomater. Appl. 2022, 37, 527.

[68] T. Komori, J. Cell. Biochem. 2011, 11, 2750.

[69] Y. Lei, Z. Xu, Q. Ke,W. Yin, Y. Chen, C. Zhang, Y. Guo, Mater. Sci. Eng., C 2017, 72, 134.

[70] Y. Zhang, C.Wu, S. Guo, J. Zhang, Nanotechnol. Rev. 2013, 2, 27.

[71] J. Zhang, F. Zhang, H. Yang, X. Huang, H. Liu, J. Zhang, S. Guo, Langmuir 2010, 26, 6083.

[72] C. K. Huang,W. Huang, P. Zuk, R. Jarrahy, G. H. Rudkin, K. Ishida, D. T. Yamaguchi, T. A. Miller, Plast. Reconstr. Surg. 2008, 121, 411.

[73] S.H.M.Wong, S. S. Lim, T. J. Tiong, P. L. Show,H. F.M. Zaid, H.-S. Loh, Int. J. Mol. Sci. 2020, 21, 5202.

Chapter 4

RESUMEN

Las técnicas de fabricación 3D surgieron entre los años 80 y 90 con la invención de la estereolitografía y la impresión 3D. Ambas técnicas tienen como objetivo la fabricación de estructuras 3D siguiendo meticulosamente un modelo previamente diseñado por ordenador (CAD). Concretamente, la impresión 3D se basa en el modelado por deposición fundida (FDM), que consiste en extruir capa por capa un material viscoso o semilíquido que irá creando objetos 3D. A este material se le denomina tinta.

Durante la década de 2000, esta tecnología se hizo popular y visible. Por un lado, debido a que el grupo dirigido por Athala et al. realizó el primer trasplante en un humano utilizando una vejiga fabricada por impresión 3D. Además, estas vejigas compuestas por colágeno y ácido poliglicólico seguirían siendo funcionales pasados 5 años desde la implantación. Por otro lado, debido al avance revolucionario que supuso esta tecnología en campo de la ortopedia, ya se patentó la primera prótesis de pierna funcional fabricada a tamaño real mediante impresión 3D.

Las siguientes décadas trajeron consigo la extinción de las patentes FDM, lo que dio lugar a la aparición de prototipos más accesibles y económicos. En consecuencia, esta tecnología de fabricación 3D se extendió a campos tan diversos como la arquitectura, la mecánica, la ingeniería, la industria alimentaria y la biomedicina. Fue en este último campo donde emergió la bioimpresión 3D. A diferencia de la impresión 3D, la bioimpresión 3D permite la adición de células vivas o componentes biológicos a la tinta, que pasó a llamarse biotinta. A partir de los 2010, tanto la impresión 3D como la bioimpresión 3D han ido evolucionando, creciendo y expandiéndose. Se han fundado nuevas empresas focalizadas en la bioimpresión, se han lanzado nuevos prototipos que son más asequibles y se ha incrementado la investigación basada en estas técnicas. La historia de las técnicas de manufacturación 3D se resumen en la Fig. 1.

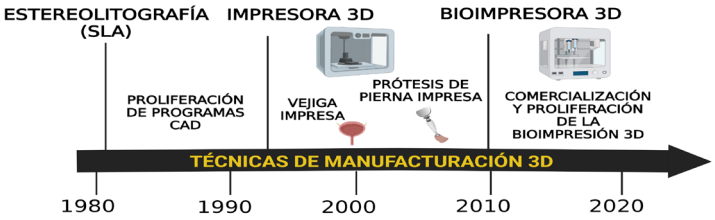

Figura 1. Historia de las técnicas de manufacturación 3D.

Estas técnicas han facilitado la fabricación de estructuras complejas con una alta resolución, por ello, han conseguido alcanzar la práctica clínica. Concretamente, la impresión 3D ha demostrado ser una tecnología eficaz para manufacturar diversos órganos anatómicamente funcionales como la piel, el hígado, el corazón o el riñón. Asimismo, ambas técnicas han demostrado una versatilidad plausible debido a su uso en la fabricación de estructuras para abordajes quirúrgicos, testeo y fabricación tanto de nuevos fármacos como de formas farmacéuticas, dispositivos médicos y productos ortopédicos y dentales (Fig.2).

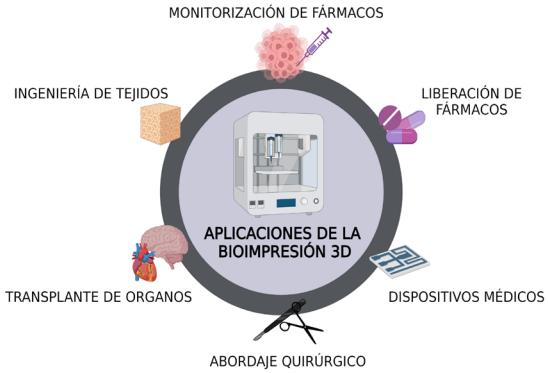

Figura 2. Aplicaciones de la bioimpresión 3D.

Con el surgimiento de la bioimpresión 3D, se ha intentado alcanzar el objetivo de fabricar órganos que no fueran solamente anatómicamente similares a los nativos, sino que también fuesen fisiológicamente funcionales. Sin embargo, la alta complejidad cito-histológica y fisiológica de los órganos hace difícil, por el momento, la fabricación de un órgano por bioimpresión. En consecuencia, la bioimpresión 3D se ha centrado principalmente en la rege-

neración tisular.

En el campo de la ingeniería de tejidos, la bioimpresión 3D ha desplazado a las técnicas convencionales de fabricación debido a su rapidez, reproducibilidad y automatización. Además, se aventaja del resto debido a que acepta un amplio rango de materiales y células. Dependiendo del método de extrusión y depósito de la biotinta, se pueden diferenciar tres tipos diferentes de bioimpresión 3D; la bioimpresión por extrusión, la basada en inyección de tinta y la asistida por láser (Fig.3).

La bioimpresión por extrusión consiste en la deposición continua de la biotinta a través de una aguja. La extrusión se produce mediante la aplicación de una presión que puede ser mecánica o neumática y tiene como resultado la obtención de estructuras 3D con una alta resolución. Es la técnica de bioimpresión más común ya que acepta el uso de altas densidades celulares, así como de materiales muy viscosos. La técnica de bioimpresión por inyección de tinta reside en la deposición de la biotinta en forma de gotas, que se producen tras la aplicación de una fuente electrostática o piezoeléctrica. Se diferencia del resto en ser simple y de bajo costo, pero las biotintas compuestas por materiales altamente viscosos y las densidades celulares altas pueden ser un factor limitante. Finalmente, en la bioimpresión asistida por láser, la estructura se fabrica al aplicar un haz de energía laser. A diferencia de las técnicas anteriores, en este método de bioimpresión las células dentro de la biotinta no se ven expuestas a fuerzas de extrusión que pueden comprometer su viabilidad. Sin embargo, es la técnica más costosa y tiene ciertas limitaciones al utilizar altas densidades celulares, así como con materiales que no se reticular con el láser.

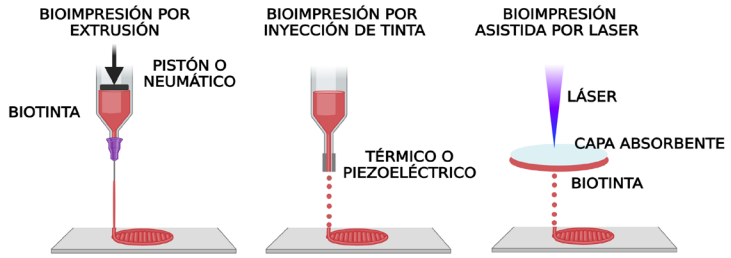

Figura 3. Técnicas de bioimpresión 3D: bioimpresión por extrusión, bioimpresión por inyección de tinta y bioimpresión asistida por laser.

Independientemente de la técnica de bioimpresión, el punto clave para lograr una bioimpresión adecuada es la biotinta, que, principalmente, debe contener dos propiedades; las mecánicas y las biológicas. Las primeras dictaminan como de imprimible es la biotinta, en otras palabras, la capacidad de la biotinta para fabricar estructuras 3D estables y con una buena resolución. Por el contrario, las propiedades biológicas reflejan como de compatible es la biotinta con las células, ya que, una buena biotinta debe favorecer la adhesión, proliferación y la maduración celular. Ambas propiedades vendrán determinadas por los materiales que componen la biotinta.

Los biomateriales sintéticos, entre los que se encuentran los termoplásticos como la policaprolactona (PCL), el alcohol polivinílico (PVA) o el ácido poliláctico (PLA), se han venido utilizando en la impresión 3D debido a sus propiedades mecánicas, ya que al modificar su temperatura transitan de sólido a un gel viscoso fácilmente imprimible. Sin embargo, la inclusión celular en la bioimpresión 3D obliga a una optimización de la biotinta para garantizar la máxima viabilidad celular. Esto se determinará por las propiedades biológicas de la biotinta. En este sentido, los biomateriales naturales han ido desplazando a los sintéticos ya que tienen la capacidad de formar hidrogeles muy acuosos que favorecen la viabilidad celular. Además, poseen ciertas propiedades mecánicas y pueden formar geles sólidos al exponerse a diferentes reticulantes. Por ejemplo, son biomateriales reticulables los sensibles a iones como el alginato, los termosensibles como la gelatina, los fotosensibles como el hialurónico metacrilado, los sensibles al pH como el quitosano o los sensi-

bles a enzimas como el fibrinógeno.

Otro factor determinante en la bioimpresión 3D es la esterilización de la biotinta, ya que puede influir tanto en sus propiedades mecánicas como biológicas. La biotinta debe estar esterilizada para evitar que cualquier microorganismo patógeno dañe a las células. Sin embargo, los biomateriales naturales tienden a ser más sensibles a los procesos físicos, mecánicos y químicos que conllevan las técnicas de esterilización.

Por lo tanto, para obtener una biotinta con un balance adecuado entre las propiedades mecánicas y biológicas, la elección del biomaterial es fundamental. Entre ellos, el alginato (Alg) destaca debido a que posee una excelente biocompatibilidad junto a un sencillo proceso de gelificación con cationes divalentes como el calcio. Además, ha demostrado su eficacia en diferentes aplicaciones como en la fabricación de sistemas de liberación de fármacos, en la encapsulación celular y en la bioimpresión 3D.

No obstante, la biotinta de Alg carece de las suficientes propiedades mecánicas, concretamente las reológicas, para conseguir fabricar estructuras 3D que tengan una alta resolución. En consecuencia, se le puede añadir modificadores reológicos como la nanocelulosa (NC). Aparte, se ha demostrado que la NC posee también propiedades biológicas, como el ser biocompatible y biodegradable.

Uno de los problemas que conlleva el uso de estos biomateriales derivados de plantas es que no se encuentran de forma natural en los tejidos humanos. En consecuencia, los materiales que derivan de la matriz extracelular (ECM) han ido ganando protagonismo como componentes de la biotinta. Entre ellos, se encuentra el ácido hialuronico (HA), que aparte de ser uno de los principales componentes del tejido conectivo, ha demostrado tener unas excelentes propiedades biológicas en cuanto a favorecer la adhesión, la proliferación y el crecimiento celular. Al igual que el HA, otros glucosaminoglicanos (GAGs) como el sulfato de condroitina (CS) y el sulfato de dermatán (DS) han demostrado ser una excelente opción para componer la biotinta. Especialmente, si el

objetivo es regenerar tejidos específicos como el cartílago, ya que tanto el CS y el DS, se encuentran de forma natural en la ECM de este tejido e intervienen en diversos procesos biológicos como en la diferenciación condrogénica, el metabolismo del cartílago y la maduración de los condrocitos.

Por lo tanto, otro factor importante a la hora de desarrollar una biotinta es el objetivo terapéutico. Así como las biotintas compuestas por los biomateriales ya mencionados pueden servir para regenerar tejidos como el cartílago, fallan en mimetizar la composición de tejidos más duros como el óseo. La adición a la biotinta de compuestos inorgánicos como la hidroxiapatita (HAP) o el óxido de grafeno (GO) podría ser la solución. La HAP es el mayor componente del hueso y ha demostrado tener propiedades biologicas como la bioactividad y la osteoinducción. Por otro lado, el GO ha ganado presencia en diversos campos científicos debido a sus magníficas propiedades fisicoquímicas y mecánicas. Además, se ha visto que aumenta la proliferación y capacidad de diferenciación osteogénica de las células mesenquimales (MSCs).

Teniendo en cuenta esta información, la biotinta se puede optimizar para crear estructuras 3D por bioimpresión para la regeneración tisular. Además, esta tecnología tiene la ventaja de que las estructuras bioimpresas pueden ajustarse a distintos tamaños, geometrías y porosidades que pueden ser muy útiles para tratar defectos óseos específicos del paciente. De la misma manera, la facilidad que da esta técnica a la hora de depositar la biotinta con un preciso control espacial podría lograr imitar tejidos que presentan una alta heterogeneidad composicional y estructural como el cartílago.

De hecho, las lesiones osteocondrales son muy prevalentes en la población general y se acentúan con la edad y el ejercicio físico intenso. Estas lesiones pueden derivar en enfermedades más graves como la osteoartritis (OA). Esta enfermedad se caracteriza por provocar dolor, inflamación y rigidez en las articulaciones junto a una disfunción de la misma (Fig.7). A pesar de la gravedad que presenta, el tratamiento farmacológico se vuelve ineficaz con el tiempo y el tratamiento quirúrgico tiene sus limitaciones.

Por ello, la bioimpresión 3D podría ser una solución eficaz para las lesiones

osteocondrales debido a que se podrían obtener estructuras 3D fabricadas por bioimpresión que regeneren ambos tejidos.

Teniendo en cuenta la información aportada, el objetivo de esta tesis doctoral es el desarrollar biotintas con las que se puedan fabricar estructuras 3D por bioimpresión para regenerar tejidos como el cartílago y el hueso. Para ello, la investigación se dividió en tres fases; pre-bioimpresión, bioimpresión y post-bioimpresión. En la primera fase se desarrollaron las biotintas, se caracterizaron y se estudió el proceso de esterilización. En la fase de bioimpresión se diseñó el modelo 3D y se fabricaron los constructos 3D optimizando los parámetros de bioimpresión. En la última fase, se realizó una caracterización de las estructuras bioimpresas y se evaluó, por un lado, la viabilidad como la funcionalidad celular dentro de los constructos, y, por otro lado, la capacidad de las células embebidas para diferenciarse a tejido cartilaginoso y óseo.

En la fase de pre-bioimpresión, primero se desarrollaron dos tipos de biotintas; la biotinta base compuesta por NC-Alg y la biotinta de hialurónico compuesta por NC-Alg-HA. Luego, se evaluaron las propiedades reológicas antes y después de la esterilización por autoclave, de ciclo corto y largo, la radiación-β y la radiación-γ. Los resultados mostraron que ambas biotintas tenían las propiedades reológicas adecuadas (adelgazamiento por cizallamiento, tixotropía y viscoelasticidad) para ser procesadas en una bioimpresora por extrusión. Sin embargo, la biotinta de hialurónico mostró un aumento en estas propiedades lo que podría resultar en una mejoría de su imprimibilidad y de la fabricación de las estructuras 3D. Asimismo, las propiedades reológicas de ambas biotintas se vieron afectadas por todos los procesos de esterilización, siendo el autoclave de ciclo corto la técnica de esterilización menos dañina.

Posteriormente, se desarrollaron las biotintas que estarían enfocadas a la regeneración de cartílago y hueso. Para ello, se añadió, por un lado, CS y DS a la biotinta base para formar las biotintas de cartílago NC-Alg-CS y NC-Alg-DS y, por otro lado, se añadió HAP y GO para formar las biotintas de hueso NC-Alg-HAP y NC-Alg-GO. Tras realizar la misma caracterización reológica se observó que las propiedades reológicas mejoraron tras la adición de CS y DS,

siendo la biotinta de condroitina la que mostró mejores propiedades. Además, al igual que con las anteriores biotintas, se observó una leve disminución de las propiedades reológicas tras la esterilización de autoclave por ciclo corto. Por el contrario, las propiedades reológicas de las biotintas de HAP y GO no se vieron disminuidas por el autoclave de ciclo corto, indicando una buena imprimibilidad. Sin embargo, el grafeno mostró signos de reducción química tras en el proceso de esterilización, aumentado así su toxicidad. Por ello, esta técnica se descartó para esterilizar la biotinta de grafeno y se opto por añadir el GO a la biotinta NC-Alg ya estéril.

Tras comprobar que todas las biotintas esterilizadas por autoclave de ciclo corto no fuesen citotóxicas, se procedió a incluir la parte biológica que consistía en células D1-MSCs, ya que tienen la habilidad de diferenciarse a tejidos como el cartílago y hueso. Además, para un mejor estudio de las biotintas de cartílago y hueso se usaron células D1-MSCs modificadas genéticamente para secretar EPO. Una vez formada la biotinta final con células se pasó a la fase de bioimpresión. En esta fase, se fabricaron estructuras 3D circulares en forma de malla con un diámetro de 15 mm. Los parámetros de bioimpresión como la presión, velocidad y diámetro de aguja se optimizaron para cada biotinta.

Primero, se realizó una bioimpresión acelular con cada biotinta y las estructuras 3D obtenidas se analizaron en términos de arquitectura, capacidad de hinchamiento, degradación. Los resultaros mostraron que los constructos que contenían HA, CS y DS mostraron una mejoría en la imprimibilidad ya que las estructuras se asemejaban al diseño CAD en mayor medida que con la biotinta base. La capacidad de hinchamiento se vio potenciada principalmente por el GO y HA, mientras que las estructuras compuestas por HAP, CS y DS obtuvieron valores mas bajos. La degradación fue similar para todos los tipos de constructos, siendo los que contenían HA, HAP y GO los que menor degradación sufrieron en los primeros días de estudio. Las estructuras enfocadas para regenerar cartílago y hueso fueron analizadas más en profundidad para evaluar sus propiedades biomecánicas. Los resultados mostraron, por un lado, un aumento de estas propiedades en los constructos que contenían CS en el caso de cartílago, y, por otro lado, un aumento de las propiedades mecánicas

con ambos componentes (HAP y GO) en los constructos de hueso. En este caso, el GO mostró una mejoría más significativa.

Por último, se evaluaron las propiedades biológicas de los constructos celulares. Las células mostraron una viabilidad alta y una actividad metabólica adecuada tras la bioimpresion en las estructuras fabricadas con la biotinta base y hialurónica. Sin embargo, en las estructuras que contenían HA se midieron unos valores mayores, indicando mejores propiedades biológicas. Asimismo, las células dentro de las estructuras manufacturadas por las biotintas de cartílago mostraron un aumento de los valores de viabilidad, metabolismo y funcionalidad en comparación con las estructuras NC-Alg. Además, la diferenciación condrogénica se vio potenciada en las estructuras que contenían CS y DS. Por otro lado, los constructos para la regeneración ósea ofrecieron una mejoría en la viabilidad, metabolismo y funcionalidad celular en comparación con las estructuras NC-Alg. En este caso, todas las células dentro de los contractos mostraron una diferenciación osteogénica, sin embargo, las estructuras de GO vieron esta capacidad de diferenciación ósea potenciada.

En conclusión, las biotintas a base de NC-Alg muestran una propiedades mecánicas y biológicas adecuadas para la fabricación de estructuras 3D por bioimpresión para la regeneración tisular. Además, la adición de HA potenció ambas propiedades. El enfoque para regenerar cartílago tras añadir CS y DS dio unos resultados prometedores pudiendo convertirse en una opción terapéutica para tratar las lesiones condrales. Por último, las biotintas que contenían HAP y GO han demostrado ser una opción excelente para simular las propiedades intrínsecas del hueso, pudiendo ser un enfoque terapéutico prometedor para tratar las lesiones óseas.